NOV 5 1997

SANDIA REPORT

SAND97–2518 • UC–700
Unlimited Release
Printed October 1997

SAND--97-2518

CTBT Integrated Verification System Evaluation Model

RECEIVED
NOV 10 1997
OSTI

Michael W. Edenburn, Marcus L. Bunting, Arthur C. Payne, Jr.,
Richard R. Preston, Jr., Lawrence C. Trost

Prepared by
Sandia National Laboratories
Albuquerque, New Mexico 87185 and Livermore, California 94550

Sandia is a multiprogram laboratory operated by Sandia Corporation, a Lockheed Martin Company, for the United States Department of Energy under Contract DE-AC04-94AL85000.

Approved for public release; further dissemination unlimited.

Sandia National Laboratories

MASTER

DISTRIBUTION OF THIS DOCUMENT IS UNLIMITED

Issued by Sandia National Laboratories, operated for the United States Department of Energy by Sandia Corporation.

NOTICE: This report was prepared as an account of work sponsored by an agency of the United States Government. Neither the United States Government nor any agency thereof, nor any of their employees, nor any of their contractors, subcontractors, or their employees, makes any warranty, express or implied, or assumes any legal liability or responsibility for the accuracy, completeness, or usefulness of any information, apparatus, product, or process disclosed, or represents that its use would not infringe privately owned rights. Reference herein to any specific commercial product, process, or service by trade name, trademark, manufacturer, or otherwise, does not necessarily constitute or imply its endorsement, recommendation, or favoring by the United States Government, any agency thereof, or any of their contractors or subcontractors. The views and opinions expressed herein do not necessarily state or reflect those of the United States Government, any agency thereof, or any of their contractors.

Printed in the United States of America. This report has been reproduced directly from the best available copy.

Available to DOE and DOE contractors from
Office of Scientific and Technical Information
P.O. Box 62
Oak Ridge, TN 37831

Prices available from (615) 576-8401, FTS 626-8401

Available to the public from
National Technical Information Service
U.S. Department of Commerce
5285 Port Royal Rd
Springfield, VA 22161

NTIS price codes
Printed copy: A05
Microfiche copy: A01

DISCLAIMER

Portions of this document may be illegible in electronic image products. Images are produced from the best available original document.

SAND97-2518
Unlimited Release
Printed October 1997

Distribution
Category UC-700

CTBT Integrated Verification System Evaluation Model

Michael W. Edenburn, Marcus L. Bunting, Arthur C. Payne, Jr.,
Richard R. Preston, Jr., Lawrence C. Trost
Arms Control Studies Department
Strategic Studies & Operational Analysis Center
Sandia National Laboratories
Albuquerque, New Mexico 87185-0425

ABSTRACT

Sandia National Laboratories has developed a computer based model called IVSEM (Integrated Verification System Evaluation Model) to estimate the performance of a nuclear detonation monitoring system. The IVSEM project was initiated in June 1994, by Sandia's Monitoring Systems and Technology Center and has been funded by the U.S. Department of Energy's Office of Nonproliferation and National Security (DOE/NN). IVSEM is a simple, "top-level," modeling tool which estimates the performance of a Comprehensive Nuclear Test Ban Treaty (CTBT) monitoring system and can help explore the impact of various sensor system concepts and technology advancements on CTBT monitoring. One of IVSEM's unique features is that it integrates results from the various CTBT sensor technologies (seismic, infrasound, radionuclide, and hydroacoustic) and allows the user to investigate synergy among the technologies. Specifically, IVSEM estimates the detection effectiveness (probability of detection) and location accuracy of the integrated system and of each technology subsystem individually. The model attempts to accurately estimate the monitoring system's performance at medium interfaces (air-land, air-water) and for some evasive testing methods such as seismic decoupling. This report describes version 1.2 of IVSEM.

Key Words: synergy, International Monitoring System, Comprehensive Nuclear Test Ban Treaty, CTBT, data fusion, sensor system integration, treaty verification, model

Acknowledgements

Many people have made significant contributions to this project. Tom Sellers (Director of Sandia's International Security Program Coordination) provided the vision and early funding for the project. Larry Walker (Sandia's CTBT Verification Research and Development Department) provided funding and direction and has been a key spokesman for the project. Bob Gough (Sandia's Policy and Analysis Research Department) supported model application, provided modeling ideas, and made valuable report editing comments. Dale Breding (Sandia's CTBT Verification Research and Development Department) provided program management. John Claassen (Sandia's Cooperative Monitoring Technology Department) was our chief source of seismic information. Luba Kmetyk (Sandia's Optics and Exploratory Technologies Department) and Rich Hunt (Sandia's Tester's and Experimental Ground Station Department) gave IVSEM a "face" by integrating the graphic user interface for input and output. Rod Whitaker (Los Alamos National Laboratories) was a significant contributor of infrasound information. Dave Harris (Lawrence Livermore National Laboratories) was a significant contributor of hydroacoustic information. Ray Warner and Dick Perkins (Pacific Northwest National Laboratory) provided information on radionuclide sensor capability and operation. Sumner Barr (Los Alamos National Laboratory) provided information on meteorological conditions which affect radionuclide dispersal. Kevin Anderson (Pacific Northwest Laboratory) helped with the statistical location accuracy algorithm. Bob Blandford (Air Force Technical Application Center) provided valuable critique of our seismic and location models. Leslie Casey and Lisa Evanson (DOE/NN) sponsored the work. We wish to thank these contributors and many others.

CONTENTS

Acronyms and Definitions

ACDA	Arms Control and Disarmament Agency
CTBT	Comprehensive Nuclear Test Ban Treaty
DOE	U.S. Department of Energy
FORTRAN	A computer programming language
IDL	Interactive Data Language software
IMS	International Monitoring System
LANL	Los Alamos National Laboratory
LLNL	Lawrence Livermore National Laboratories
NCDC	National Climatic Data Center
NDC	National Data Center
PC	Personal computer
PNNL	Pacific Northwest National Laboratory
SNL	Sandia National Laboratories

Attribution--Associating a nuclear explosion with a specific country or group

Auxiliary stations--Seismic stations not used for detection but used to help locate an event

Detection effectiveness--Ability of the monitoring system to detect a nuclear explosion, often called probability of detection

Hydroacoustic sensors--Sensors which measure low frequency sound (pressure) waves in the oceans

Identification effectiveness--Monitoring system's ability to distinguish nuclear detonations from other events

Infrasound sensors--Sensors which measure low frequency sound (pressure) waves in the atmosphere

Location accuracy--Area of location uncertainty measured in square kilometers, 90% confidence that true location is within the area

Primary stations--Seismic stations used to detect events

Radionuclide sensors--Sensors which detect gamma rays from the decay of nuclear fission products

Seismic sensors--Sensors which measure earth motion

σ--A symbol which represents the statistical standard deviation of a random variable

INTRODUCTION

The Integrated Verification System Evaluation Model (IVSEM) project was initiated in June, 1994 by Tom Sellers, who was then the director of Sandia's Monitoring Systems and Technology Center. The Arms Control Studies Department was asked to investigate the feasibility of developing a simple, "top-level," modeling tool which can help explore the impact of various sensor system concepts on CTBT monitoring and verification to be used by U.S. and international decision makers. The tool's main emphasis was to integrate results from the various sensor technologies and to investigate the synergy among the technologies. Comprehensive modeling, which had already been done for many of the individual technologies, was to be avoided in the interest of making the model fast and easy to use; however, the model was required to have acceptable fidelity to the more comprehensive models and to the true performance of monitoring technologies. The model was developed for application on a personal computer (PC) so that it can be easily transported to other work sites and used by a variety of analysts. It has also been adapted for use on computer workstations.

The Arms Control Studies Department developed a model architecture by July, 1994; demonstrated the feasibility of using simple models by September, 1994; and developed a technology integration methodology by December, 1994. In early 1995, the program was accelerated in an attempt to develop a useable model which could have an impact on the CTBT negotiations being conducted in Geneva. By June 1995 modules for the four international monitoring technologies--seismic, infrasound, radionuclide, and hydroacoustic--had been developed and incorporated into the model, and the model was given an internal critical review. In July, 1995, the model, supported by a graphics user interface developed in Sandia's Monitoring Systems and Technology Center was presented to and reviewed by personnel from DOE, and DOD. Since then the model has been briefed to personnel from DOE, DOD, the intelligence community, ACDA, and the U.S. CTBT delegation in Geneva and has been used to support the U.S. CTBT delegation in Geneva. Version 1.0, which estimated system detection effectiveness, was released to DOE labs and selected government contractors in November 1995. Version 1.1, which estimates system location accuracy as well as detection effectiveness, was released in July 1996. Version 1.2 has made adjustments to all areas of Version 1.1. The major changes are: 1) more input parameters are available to the user; 2) radionuclide precursors have been modeled; 3) location algorithms have been overhauled; 4) graphic output options have been added; and 5) a new color scheme is used for graphic output.

The project's objective has changed little since it started:

Objective:

Develop a basic, easy to use, fast running model which estimates the performance of a CTBT monitoring system, runs on a PC, and can aid in evaluating:

Monitoring system concepts and configurations;
Synergy among monitoring technologies; and
Technology improvements.

The model includes the four international monitoring technologies:

Seismic,

Infrasound,

Radionuclide, and

Hydroacoustic.

It can estimate the performance of each technology subsystem individually and it can estimate the performance of the integrated system with or without (a user option) accounting for synergy among the technologies. When we talk about monitoring system performance, we refer to four elements of performance:

Detection effectiveness;

Location accuracy;

Identification effectiveness; and

Attribution.

We define system detection effectiveness to be the measure of "how good" the system is at detecting an event. Due to the probabilistic nature of detection, the calculated value of system detection effectiveness can be characterized as a probability of detection or a weighted probability of detection. The model has been shown to make accurate estimates of system detection effectiveness by validation activities that we have completed to date. The model estimates monitoring system performance at medium interfaces (air-land, air-water) and for some evasive testing methods such as seismic decoupling.

The model estimates location accuracy in square kilometers. Location accuracy estimates take into account each station's detection probability and the station-to-event bearing angle errors or signal arrival time errors. The estimate uses a probabilistic or "Monte Carlo" model. Location accuracy estimates have been compared to those of more comprehensive models with good agreement.

The model does not include identification effectiveness in its present version. It will estimate the monitoring system's ability to distinguish among various kinds of events in a later version if funding permits. Attribution is beyond the model's scope and will not be addressed.

This report will cover IVSEM's estimation of system detection effectiveness and location accuracy.

Throughout this report, we present output products from IVSEM using CTBT-like examples. In every case, our intent is to illustrate IVSEM's capability rather than to estimate the International System's performance against a specific nuclear test scenario. For that reason, we do not reference scenario parameter values such as yield, height or depth of burst, or time of year. Many of the network configurations are hypothetical and do not represent actual IMS station locations or performance.

SUMMARY MODEL DESCRIPTION

The model has a FORTRAN core and an IDL graphics user interface. The IDL interface facilitates entering input data, runs the FORTRAN core, and provides output charts in a variety of forms. The model will run a single event application in a few seconds and a world coverage application in a few minutes. Specific run time depends on the particular application to be run and on the computer which is used.

Model operation consists of five sequential steps:

Model input--Input consists of model control parameters, event specification, technology parameters, station specification files, a detection effectiveness table, a world map file, and a wind data file.

Individual station detection responses--The model determines the probability of detection (the probability of a positive sensor response) for each individual station within each technology. The probability of a positive response depends on the signal strength reaching the station, the station's noise, the station's threshold setting, and statistical tests specific to the type of sensor technology.

System integration and detection effectiveness--Individual station detection probabilities are combined to find the probability that a specific number of stations within that technology respond. From these probabilities, we determine the probability that a specific combination of stations respond, for example, a specific system response might be that 1 seismic, 2 infrasound, 1 radionuclide, and 0 hydroacoustic stations respond with probability 0.23. The combination of all possible specific system responses with their associated probabilities is what we call the system detection response. Also associated with each specific system response is a detection effectiveness value for that response. If the detection effectiveness value for a response is 1.0, then that response constitutes a detection. If the detection effectiveness value is 0.0, then that response is not sufficient to constitute a detection. Values between 0.0 and 1.0 can be used to indicate levels of detection certainty. Detection effectiveness values are supplied by the user in the form of a detection effectiveness definition table. The detection effectiveness definition table defines how many responding stations from each technology or combination of technologies constitute a detection. System detection probability is calculated by multiplying response probability by response detection effectiveness for each specific response and adding the products over all specific responses. Using a similar process, individual subsystem detection probabilities are also estimated.

System location accuracy estimate--Stations with a detection probability greater than 0.2 are included in a 100 random trial probabilistic analysis to estimate the system's location accuracy, which is a 90% confidence area, in square kilometers. The probability that a station participates in any specific random location trial is equal to its detection probability. If a station participates in a trial, it is randomly assigned a "measured" signal arrival time or "measured" station-to-event bearing angle, or both, depending on the type

of station and on the station's statistical error distribution. Each station provides a bearing residual or arrival time residual (or both) to the location analysis for the trial. A location estimate is made for each random trial by minimizing the sum of the weighted residuals. The location estimates for the 100 random trials are used in a bivariate Gaussian analysis to find the elliptical area which has a 90% chance of including all location estimates. Location estimates are made for the integrated system and for each individual monitoring technology subsystem.

Model output--System and subsystem detection effectiveness and location accuracy results are written to tables which can be printed or to files which can be read by the graphics user interface and converted to charts showing graphical representations of effectiveness. Examples of global coverage output are shown in Figures 1 and 2. Different levels of detection effectiveness or location accuracy are represented by different colors on the contour plots.

Each of these steps is explained in more detail below.

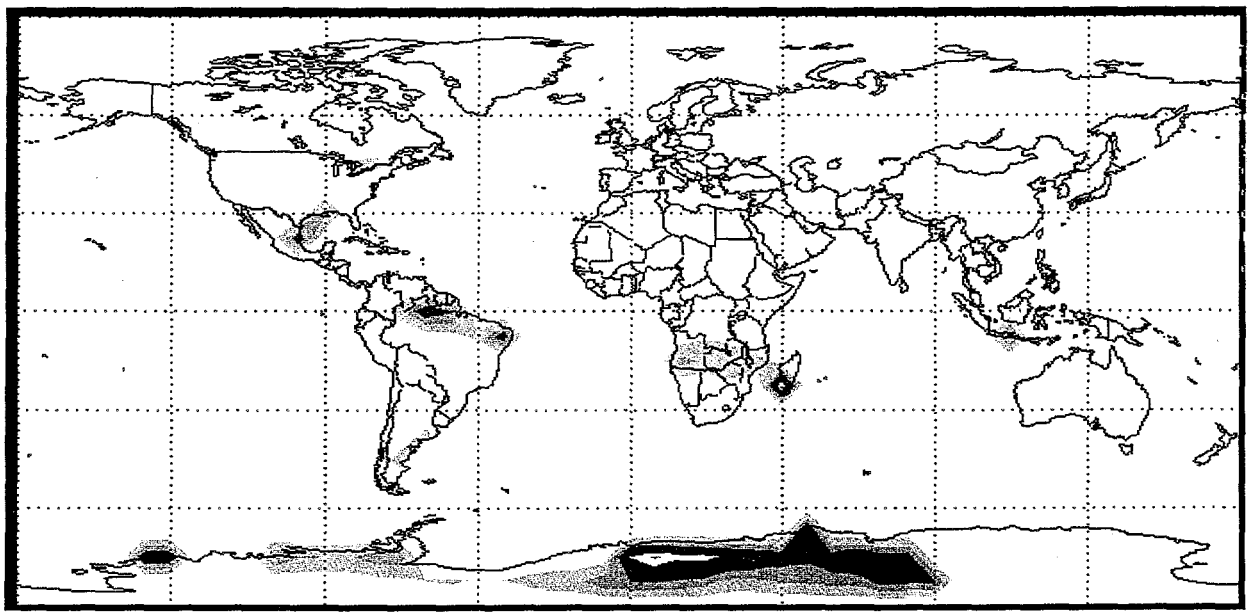

Figure 1. Typical Integrated System Global Detection Effectiveness

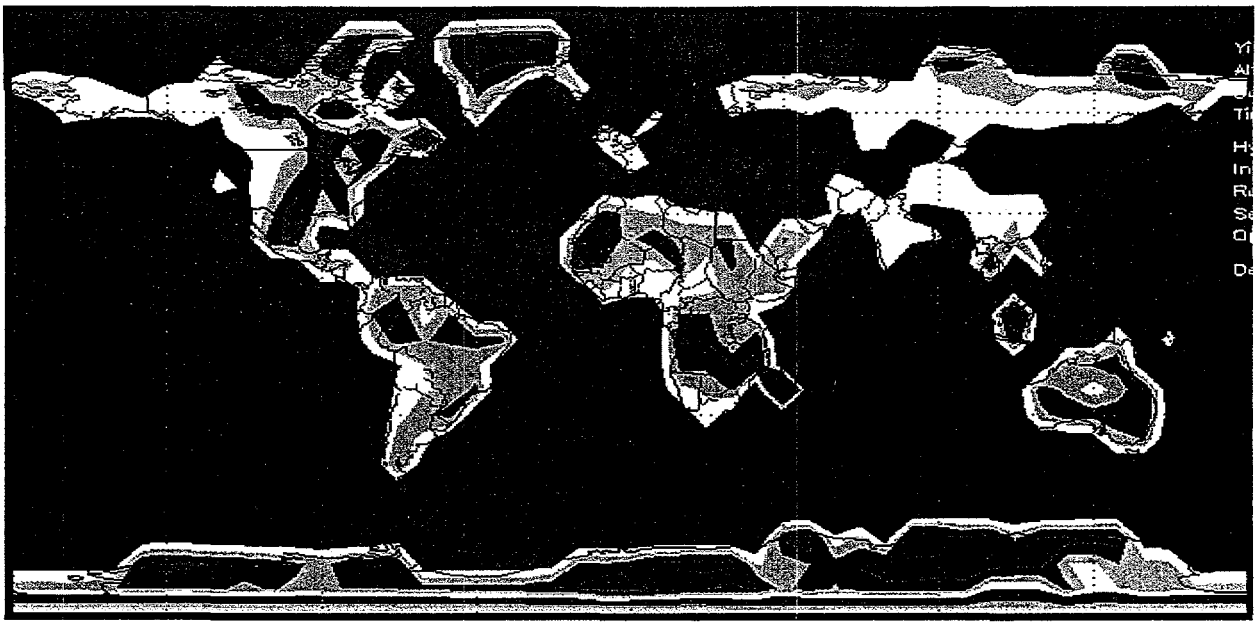

Figure 2. Typical Integrated System Global Location Accuracy

MODEL INPUT

Model input consists of ASCII files which contain data and parameter values used by the model:

a basic input parameter file,
station specification files,
a detection effectiveness table,
a wind data file, and
a world map file.

One basic input parameter file, one station specification file for each technology, and one detection effectiveness table file are copied from the model's library to the model's input file before the model runs. The resulting combined file can be altered to change any of the default parameter values before it is read into the model. This makes it possible to change parameter values for an application without changing files stored in the library. A basic input parameter file, several station specification files, and several detection effectiveness table files are stored in the model's library. A current listing of the files is shown in Table 1. The user can create additional library files containing data for special cases he desires to run. The world map file and wind data file cannot be modified by the user. They are read directly into the model.

The basic input parameter file--contains model control (single event vs. global coverage, switch to turn location accuracy on or off), event specification (size, time, location), and specific technology parameter values and descriptive text.

Station specification files--locate each station, specify the station type and number of elements, specify noise or background parameters, and possibly specify station sensitivity.

The detection effectiveness table--allows the user to specify which system responses constitute a system detection.

The model's world map file--LANDSEA2.DAT, divides the Earth's surface into 2.0 degrees in latitude by 2.0 degrees in longitude sections. Associated with each section is an integer which describes the surface:

0	seismically stable, unblocked ocean;
1	tectonic, unblocked ocean;
2	seismically stable, blocked (to hydroacoustic signals) ocean;
3	tectonic, blocked ocean;
4	seismically stable land, and
5	tectonic land.

This "map" is used in the following ways: 1) it determines whether an event is in the ocean or on the land for seismic coupling and radionuclide venting calculations; 2) it determines whether the

event and stations are in a seismically stable or tectonic region for seismic propagation calculations; and 3) it is used for signal blocking calculations in the hydroacoustic module.

The wind data file--divides the Earth's surface into 15 degrees in latitude by 15 degrees in longitude sections. For each section, the wind data file has monthly average wind data at the surface and at 14 altitudes up to about 40 km. Extracted from NCDC (1993), the data consist of average east and north wind vectors and east and north wind vector standard deviations. In the original file, altitudes were given in terms of millibar pressure. We converted altitude from millibars to kilometers using an approximate standard atmosphere algorithm.

Wind data are used in the infrasound module to find average monthly surface wind speeds and, from that, the noise at each station (the infrasound module does not use the wind data file to get 50 km wind velocity; it comes from another source which will be described later); and the radionuclide module uses average monthly wind velocity at the debris cloud's center point altitude to calculate the cloud's speed and path.

The basic input parameter file, station data files, and the detection effectiveness table are described in detail in appendix A.

Table 1. File Library

File Name **Description**

Basic Input Parameter Files

INP000 1 kt, - 35 m, Kansas, October, full seismic coupling, no rain

Seismic Station Files

SZM-P330 CTBT 50 Primary & 120 Auxiliary stations; CD/NTB/WP.330; 5/96
SZM-P335 CTBT 50 Primary & 120 Auxiliary stations; CD/NTB/WP.335; 6/96
SZM-330R CTBT 50 Primary & 120 Auxiliary stations; CD/NTB/WP.330 revised; 6/96

Infrasound Station Files

ISN-P330 CTBT 60 stations; CD/NTB/WP.330; 5/96
ISN-P335 CTBT 60 stations; CD/NTB/WP.335; 6/96
ISN-330R CTBT 60 stations; CD/NTB/WP.330 revised; 6/96

Radionuclide Station Files

RDN-P330 CTBT 80 stations; CD/NTB/WP.330; 5/96
RDN-P335 CTBT 80 stations; CD/NTB/WP.335; 6/96
RDN-330R CTBT 80 stations; CD/NTB/WP.330 revised; 6/96

Hydroacoustic Station Files

HYD-P330 CTBT 6 stations + 5 island T-phase; CD/NTB/WP.330; 5/96
HYD-P335 CTBT 6 stations + 5 island T-phase; CD/NTB/WP.335; 6/96
HYD-330R CTBT 6 stations + 5 island T-phase; CD/NTB/WP.330 revised; 6/96

Detection Effectiveness Tables

EFTAB001 Sandia version
EFTAB002 Location by a single technology is required for detection, no intertechnology synergy
EFTAB003 Three stations of any technology required for detection (1 radionuclide)

INDIVIDUAL STATION DETECTION RESPONSES

For each station within each technology subsystem, the model computes the probability that the station will register a response. These computations are done in separate modules for each subsystem. All of the technology subsystem modules follow the same computation sequence.

First, the source signal strength is computed for an event. The type of signal depends on the type of sensor being used.

Second, signal propagation effects and attenuation are estimated and signal strength at the station is computed.

Third, the station's noise characteristics are determined from background noise or wind (depending on the technology) data taken from the station specification file.

Fourth and last, signal and noise characteristics, threshold setting, and sensor sensitivity are combined in a statistical test to determine the station's probability of registering a positive response. The statistical test used depends on the type of technology.

These computations are described in more detail in the following appendices.

Seismic Detection--Appendix B

Infrasound Detection--Appendix C

Hydroacoustic Detection--Appendix D

Radionuclide Detection--Appendix E

SYSTEM INTEGRATION AND DETECTION EFFECTIVENESS

System Detection Response

The model estimates the probability that each station within each subsystem registers a positive response, and from these probability values the model computes a system response. Within each subsystem, we use the individual station response probabilities to compute the probability that exactly N (N is a positive integer) stations register a positive response. We call the probability that exactly N seismic stations respond P(NS). Note that this produces a set of probabilities: P(0S), P(1S), P(2S), P(3S), and etc. The probability that N (this N is not necessarily the same as the N for seismic, hydroacoustic, or radionuclide stations) infrasound stations respond is P(NI); the probability that N radionuclide stations respond is P(NR); and the probability that N hydroacoustic stations respond is P(NH). The system's response is the combination of subsystem responses; for example, 2 seismic plus 1 infrasound plus 1 radionuclide plus 0 hydroacoustic responses is a specific system response. We would designate this specific system detection response as (2S, 1I, 1R, 0H). The general system detection response (NS, NI, NR, NH) represents all possible system responses if we let NS, NI, NR, and NH include all numbers of stations up to the total number in their respective subsystems. The joint probability P(NS, NI, NR, NH) that we get system response (NS, NI, NR, and NH) is equal to the product of the individual subsystem response probabilities since the subsystems operate independently. This joint probability is given by the following equation:

$$P(NS, NI, NR, NH) = P(NS) \times P(NI) \times P(NR) \times P(NH) \quad (1)$$

P (NS, NI, NR, NH) is a four dimensional table or matrix which we call the system detection response table. This table is the model's description of a system's detection response to an event.

As an example, suppose the system consists of four seismic sensors and four infrasound sensors but no radionuclide or hydroacoustic sensors. Table 2 is a possible system detection response table where the numbers in the table correspond to the probability that a specific number of seismic and a specific number of infrasound stations responded to an event.

Table 2. Simplified (Two-Technology) Detection Response Table (Joint Probabilities)

Number of Responses Seismic Infrasound	0S	1S	2S	3S	4S
0I	.0001	.0015	.0039	.0025	.0000
1I	.0017	.0215	.0563	.0365	.0000
2I	.0067	.0821	.2153	.1399	.0000
3I	.0065	.0799	.2095	.1361	.0000
4I	.0000	.0000	.0000	.0000	.0000

System Detection Effectiveness

We define system detection effectiveness to be the measure of "how good" the system is at detecting an event. More specifically, it is a weighted probability of detection. The weights come from the detection effectiveness table and, in principle, reflect the "information content" in a detection by a specified number and combination of sensors.

The system detection response is denoted (NS, NI, NR, NH) where NS is the number of seismic stations which respond, NI is the number of infrasound stations which respond, NR is the number of radionuclide stations which respond, and NH is the number of hydroacoustic stations which respond. Associated with each possible system response is the probability of getting that response, P(NS, NI, NR, NH). Also associated with each possible system detection response is a system detection effectiveness E(NS, NI, NR, NH). This value, which we define to be between 0 and 1 inclusively, is a "goodness" of detection or a detection "figure of merit." It is represented by a four dimensional table or matrix and is currently specified in input by the user. It is a qualitative judgement, made by the user, which associates an effectiveness value with each possible system detection response. If the user gives a detection effectiveness value of either 1.00 or 0.00 to each specific system detection response, then he has defined some responses as detections and others as nondetections. In this case, the system detection effectiveness computed by the model will be the probability of detection. If values between 0.00 and 1.00 are used, detection effectiveness is a weighted probability of detection. A simplified, two-technology example detection effectiveness table is shown in Table 3.

Table 3. Simplified (Two-Technology) Detection Effectiveness Table Example ("Value" or "Information Content in a Specified Combination of Detecting Stations)

Number of Responses Seismic / Infrasound	0S	1S	2S	3S	4S
0I	.00	.00	.00	1.00	1.00
1I	.00	.00	.00	1.00	1.00
2I	1.00	1.00	1.00	1.00	1.00
3I	1.00	1.00	1.00	1.00	1.00
4I	1.00	1.00	1.00	1.00	1.00

The model combines the system detection response table with the system detection effectiveness table to get a system detection effectiveness value. It does this by multiplying the system response probability by the system response effectiveness for each possible system response and adding the results. This is expressed in the following algorithm:

$$\text{System Detection Effectiveness} = \Sigma\,[E\,(NS, NI, NR, NH) \times P\,(NS, NI, NR, NH)] \qquad (2)$$

The summation is done over all values of NS, NI, NR, and NH. The result is an expected value of detection effectiveness.

System detection effectiveness and system detection synergy are discussed more thoroughly in Appendix F.

SYSTEM LOCATION ACCURACY ESTIMATE

Statistical Location Accuracy Model Summary

IVSEM estimates the accuracy with which the overall IMS can locate an event. It also estimates the location accuracy which can be attained by each individual CTBT monitoring technology subsystem. When the operational IMS detects and estimates the location of an event, the estimated location will have an associated error. The size of the error will depend on where the event was located relative to the various types of sensors and which sensors responded. IVSEM estimates location accuracy employing a statistical location error. The statistical model considers two types of stations: bearing stations (infrasound) where each station estimates a station-to-event angular bearing; and signal arrival time stations (infrasound, seismic, and hydroacoustic) where each station records a signal arrival time. Each infrasound station records both bearing angle and signal arrival time. IVSEM does not make a location error estimate for radionuclide sensor detections because associated location accuracies are extremely variable.

Based on geometric considerations, a minimum number of detecting stations is required to obtain a location estimate. The IVSEM location estimate does not include altitude or depth; thus, the estimate is for a surface location. Bearing information from at least two stations or arrival time information from at least three stations is required to make a location estimate.

IVSEM estimates location accuracy using the following process. This process is described in more detail later in Appendix G. Location estimates are made for the integrated system and for each individual subsystem.

IVSEM Implementation of the Statistical Location Accuracy Model

IVSEM estimates the probability that each station will respond to an event; thus, unless all probabilities are equal to 1, the set of stations used to locate an event will be random. If an event could be repeated a large number of times, a different set of stations might respond each time. To account for random station selection and implement the statistical location error model, IVSEM uses the following six-step process.

1. **All stations with detection probability below 0.2 are eliminated.** The practice of the seismic community is to eliminate all stations with detection probability below 0.2. This practice has been extended to all technologies in IVSEM. Auxiliary seismic stations are allowed to participate in the location process if at least three primary stations detect the event. The maximum number of stations from each technology which may participate in location is limited to 40 seismic, 20 infrasound, and 10 hydroacoustic stations. This is done to reduce computation time and space and will be important only for relatively large yields. If the number of stations with detection probability above 0.2 exceeds the limit, the stations are ordered from "best to worst," and the limiting number is selected. Ordering is based heavily on detection probability and lightly on station-to-event

distance. The idea is to chose those stations most likely to be included in the location set, but give preference to the nearest stations when probabilities are similar in value. The rationale is that, when the number of stations in the location set is large, the more distant stations will probably make a relatively small contribution to location accuracy.

2. **Station parameters are calculated.** Based on event and station latitudes and longitudes, an azimuth angle, α, from the event to each station is calculated with east being angle 0.0. The east, X+, and north, Y+, distances from the event to each station are calculated ($X_i = D_i \cos(\alpha_i)$; $Y_i = D_i \sin(\alpha_i)$; where D_i is event to station distance). Although the location error model uses Cartesian instead of spherical coordinates, the angular orientation and distance from the event to each station are correct.

   A mean arrival time or mean station-to-event bearing angle (or both) is calculated for each station. Mean arrival time is simply distance divided by speed for infrasound and hydroacoustic stations. Infrasound signal speed is assumed to be 0.3 km/s, and hydroacoustic signal speed is assumed to be 1.5 km/sec. Seismic signal arrival time is found using a table which gives signal travel time as a function of angle in one degree increments with linear interpolation between. Mean bearing angles for infrasound stations are assumed to be the true bearing angle.

   Bearing angle and arrival time standard deviations are calculated using algorithms built into the model:

$$\text{Seismic:} \quad \sigma = \{0.75^2 + [.15/(\text{snr}-1)]^2\}^{1/2} \text{ sec}$$

$$\text{Hydroacoustic:} \quad \sigma = \{1^2 + .02^2 D_i\}^{1/2} \text{ sec}$$

$$\text{Hydroacoustic "T-Phase:} \quad \sigma = \{5^2 + .02^2 D_i\}^{1/2} \text{ sec}$$

$$\text{Infrasound arrival time:} \quad \sigma = 2\% \text{ of signal travel time}$$

$$\text{Infrasound bearing:} \quad \sigma = 1.8^\circ \text{ from 0 to 3000 km;}$$
$$\text{increasing to } 7^\circ \text{ at 4000 km;}$$
$$7^\circ \text{ from 4000 to 10,000 km;}$$
$$\text{increasing to } 27.5^\circ \text{ at 15,000 km;}$$
$$27.5^\circ \text{ beyond 15,000 km.}$$

   The seismic standard deviation was suggested by John Claassen (SNL, April 1996) for a well calibrated network. It consists of a 0.75 second "arrival time" error and a "model" error which depends on signal-to-noise ratio. Hydroacoustic standard deviations were suggested by Dave Harris (LLNL, May 1996) as very preliminary rough estimates. They include "pick" errors of 1 second for hydroacoustic stations and 5 seconds for island "T-

phase" stations and travel time errors for both station types of $0.02(D_i)^{1/2}$. A "pick" error is the error associated with selecting the signal's arrival time from a signal profile. The infrasound arrival time standard deviation was suggested by Rod Whitaker (LANL, April 1996) as having some sketchy, historical basis from the Nevada Test Site. The infrasound bearing standard deviation was suggested by Dean Clauter (NDC, April 1996).

Weights for each station are calculated. For all stations the weight is $1/\sigma_i^2$.

3. **Stations are randomly selected to participate in a location trial.** For each station selected in step #1, a random number is chosen from a uniform distribution. If the station's detection probability exceeds the random number, it is included in the location trial. Each station participating in the trial is assigned a randomly selected bearing or arrival time and it provides one or two residual equations to the trial.

4. **A location estimate (x,y) is computed for the location trial.** This is done by finding the event time and location (x,y) which minimize the sum of the weighted, squared residuals.

5. **Steps 3 and 4 are repeated 100 times to get 100 location estimate values.** We tried up to 10,000 trials and compared results for several station sets. 100 trials is not as reliable as 10,000, but it gets fairly consistent results when the random seed is varied. When we varied the random seed 5 times, the standard deviation in distance error was about 15% for the fairly challenging case being considered. Using 200 repetitions would improve reliability but it would roughly double location accuracy computation time which is now between 5 and 10 minutes for a world coverage run. We believe that a 15% standard deviation is adequate considering IVSEM's philosophy of being a basic model which seeks minimum computation time.

6. **The 90% confidence area is estimated as IVSEM's location error estimate.** The 100 x,y location coordinate estimates computed in step 5 are used in a covariance analysis which assumes that the location estimates have a bivariate Gaussian distribution. The area of an ellipse which contains 90% of the location estimates is computed. Even though we made 100 trials, we may not get 100 errors because the random process may have selected fewer than three stations, and location for that trial is not possible. In this case, the 90% confidence area is based on the remaining trials. Thus, the error we estimate is the error one would get given there are enough stations for location. Using the 90% confidence area means that the location estimate will fall within the 90% confidence ellipse 90% of the time.

The location accuracy model is described in more detail in Appendix G

IVSEM location accuracy results have been compared to results from more comprehensive models. The results agree very well. Location accuracy validation is covered in Appendix H.

MODEL OUTPUT

The model estimates system detection effectiveness (probability of detection or weighted probability of detection) and location accuracy in square kilometers for a specified event. The model operates in one of two modes. The first mode is estimating subsystem and system effectiveness for a single event. In this mode, details of system performance are saved in an output file. The second mode is world coverage for which the model estimates system effectiveness values for events at 1225 points located on a 7.5 degree in latitude by 7.5 degree in longitude grid. Subsystem and system effectiveness values for each event point are saved in an output file which is used for making contour plots. Detailed system performance information for each event point is not saved in the world coverage mode. With the exception of SVSEM.OUT, output files have been designed to interface with the graphics user interface to produce various types of charts.

Single Event Mode

When the model operates in the single event mode, three output tables are generated: SVSEM.OUT, SPLOTSTA.OUT, and SPLOTEFF.OUT.

SVSEM.OUT is a table organized into four sections. The first section summarizes model input. The second section presents tables of subsystem performance parameters for each sensor subsystem (technology). Typical output parameters include information for each station: station location, distance to the event, signal strength, noise parameters, threshold values, and station probability of detection. The third section gives location accuracy information: stations which participated and their parameter values; location distance error statistics; and the log of location area error for each subsystem and for the system. The fourth section summarizes system response: the probability that N stations within each subsystem respond to the event, and effectiveness values for each subsystem and for the system. This is a very good diagnostic table to use when trying to determine why the system responded as it did to a specific event.

SPLOTSTA.OUT is a table which gives each station's location in longitude and latitude and its probability of detection. The table starts with a five line header that reflects model input. The table's body consists of four columns: longitude in degrees, latitude in degrees, a station type tag such as SZM for seismic, and the probability of detection. The file is used to draw station location response maps by the graphics user interface.

SPLOTEFF.OUT is a table which gives subsystem and system detection effectiveness and location error. The table starts with a five line header that reflects model input. The table's body consists of columns of data which give the probability that exactly N stations responded within each subsystem. One column for each subsystem is given in the following order: seismic: infrasound, radionuclide, and hydroacoustic. Following the table, one line of data contains seismic subsystem effectiveness; infrasound subsystem effectiveness, radionuclide subsystem effectiveness, hydroacoustic subsystem effectiveness, and integrated system detection effectiveness, and a second line of data contains location accuracy. This table is used to provide

data for making subsystem and system effectiveness histograms (bar charts) by the graphics user interface.

World Coverage Mode

When the model operates in the world coverage mode, three output tables are generated: CVSEM.OUT, CPLOTSTA.OUT, and CPLOTEFF.DAT.

CVSEM.OUT summarizes model input. It does not provide detailed computations as did SVSEM.OUT because providing detailed computations for each of the 1225 coverage cases is not practical. If you would like to see detailed computations, pick a specific event location and run the model in the single event mode (see Appendix A).

SPLOTSTA.OUT is a table which gives each station's location in longitude and latitude. The table starts with a five line header that reflects model input. The table's body consists of three columns: longitude in degrees, latitude in degrees, and a station type tag such as SZM for seismic. The file is used to draw station location maps by the graphics user interface.

SPLOTEFF.OUT is a table which gives subsystem and system detection effectiveness in tabular form for each event location on a 7.5 degree in longitude by 7.5 degree in latitude grid. There are 1225 line entries in the table's body. The table starts with a five line header which reflects model input. The table's body consists of 12 columns. The first seven are event latitude, event longitude, seismic subsystem effectiveness, infrasound subsystem effectiveness, radionuclide subsystem effectiveness, hydroacoustic subsystem effectiveness, and integrated system detection effectiveness. The last five columns contain corresponding location accuracy values in the form of the log of location area error for each subsystem and for the system. This table is used to provide data for making subsystem and system effectiveness contour plots by the graphics user interface.

SUMMARY

IVSEM has a FORTRAN core and an IDL graphics user interface. The IDL interface facilitates entering input data, runs the FORTRAN core, and provides output charts in a variety of forms. The model will run a single event application in a few seconds and a world coverage application in a few minutes.

Model operation consists of five sequential steps:

Model input--Input consists of model control parameters, event specification, technology parameters, station specification files, a detection effectiveness table, a world map file, and a wind data file.

Individual station detection responses--The model determines the probability of detection (the probability of a positive sensor response) for each individual station within each technology.

System integration and detection effectiveness--Individual station detection probabilities are combined to find the probability that a specific number of stations within that technology respond. From these probabilities, IVSEM determines the joint probability that a specific combination of stations respond. Multiplying response joint probability by response detection effectiveness (detection effectiveness values are supplied by the user in the form of a detection effectiveness definition table) for each specific response and adding the products over all specific responses results in the system's weighted detection probability. Using a similar process, individual subsystem detection probabilities are also estimated.

System location accuracy estimate--Individual station detection responses are used in a probabilistic analysis to estimate the system's location error in square kilometers. Location errors are also estimated for each individual subsystem.

Model output--System and subsystem detection effectiveness and location accuracy results are written to tables which can be printed or to files which can be read by the graphics user interface and converted to charts showing graphical representations of effectiveness.

The model has been briefed to DOE, ACIS, ACDA, and the U.S. CTBT delegation in Geneva and has been used extensively to support the U.S. CTBT delegation in Geneva.

REFERENCES

NCDC, 1993: Global Upper Air Climatic Atlas Ver 1.0, a 2 CD-Rom Set, National Climatic Data Center and Naval Oceanography Command Detachment Asheville, National Oceanic and Atmospheric Administration, April 1993.

APPENDIX A. MODEL INPUT

Basic Input Parameter File

Figure A1 shows a basic input file for the model. It contains model control, event specification, and specific technology parameter values and descriptive text. Recommended values for some parameters are given in the descriptive text. The first line gives a description of the case which the file represents. This example is one basic input files contained in the model's library. Default basic input files are typically named INPXXX.DAT where XXX is a specific descriptor like 003 or PDQ.

Model Control Parameters

The first model control parameter determines whether the run will be a single event application or a world coverage application. If a value of 1 is entered, a single nuclear event will be "detonated" at a specific location and the system response to that event will be estimated. If a value of 2 is entered, a nuclear event will be "detonated" on a 7.5 by 7.5 degree latitude-longitude grid on the earth. The system's estimated detection effectiveness for each event will be written to an output file.

The second parameter is a location accuracy option switch. If the switch is set to 0, IVSEM will skip the location accuracy computation. If it is set to 1, IVSEM will do the location accuracy computation with full synergy; that is, system location accuracy will integrate stations from all technology subsystems. If it is set to 2, IVSEM will do the location accuracy without synergy; that is, system location accuracy will equal the location accuracy of the best individual subsystem.

The third parameter is a model progress tracking parameter. The default value is 0, but if set to 1, the model will tell which subroutine is executing, and (for a coverage application) the event location for which computations are being made. This option helps locate errors.

Figure A1. Typical Basic Input Parameter File

```
DEFAULT INPUT DATA; SCENARIO #0, 1 kt, -20 m, KANSAS

MODEL CONTROL
         1  1 for single event, 2 for contour plot
         1  location accuracy switch (0 for no location, 1 for location with
            synergy, 2 for location without synergy)
         0  progress tracking parameter (0 for no tracking, 1 for tracking)

EVENT SPECIFICATION
      1996  year
        10  month
         1  day
         0  hour
         0  minute
       40.  latitude
     -100.  longitude
     -.020  altitude
        1.  yield in kt

SEISMIC TECHNOLOGY SPECIFICATION
         1  include index (1 for include, 0 for leave out)
        1.  cavity decoupling factor (typically 1 to 70)
        1.  medium decoupling factor for land (1. for rock, 6.3 for alluvium)
       .16  medium decoupling factor for water (recommend .16)
        3.  threshold to noise ratio (recommend 3.)
        1.  location accuracy toa error multiplication factor (recommend 1.)

INFRASOUND TECHNOLOGY SPECIFICATION
         1  include index (1 for include, 0 for leave out)
       1.5  threshold (number of noise standard deviations)
        1.  location accuracy bearing err multiplication factor (recommend 1.)
        1.  location accuracy toa error multiplication factor (recommend 1.)

RADIONUCLIDE TECHNOLOGY SPECIFICATION
         1  include index (1 for include, 0 for leave out)
       240  maximum allowed detection time from the event in hours (>24)
        1.  fission fraction
        2.  earth vent fraction (use 0.-1. or >1. for built-in computation)
       2.6  threshold (number of background standard deviations)
       0.0  rain intensity in mm/hr
         0  rain duration in hr

HYDROACOUSTIC TECHNOLOGY SPECIFICATION
         1  include index (1 for include, 0 for leave out)
        1.  location accuracy toa error multiplication factor (recommend 1.)
```

toa means signal time-of-arrival

Event Specification Parameters

These parameters give the event's time, its location, its altitude, and its yield. The only critical time parameter is the month number. The month determines which wind data are used to determine infrasound attenuation, infrasound noise, and radionuclide cloud movement. We have determined that, averaged over the earth, October is the worst month for infrasound detection, March is the worst month for radionuclide detection, and October is the worst month for a synergistic combination of infrasound and radionuclide. Wind conditions do not affect seismic or hydroacoustic computations. We use October (month 10) as the default month.

Event location is specified by latitude and longitude, both in degrees. When the world coverage option is used, the model picks its own event locations.

The event's altitude is specified in kilometers. Positive values imply an atmospheric detonation, and negative values imply a subsurface detonation. The model's map does not contain topographical information; thus, the world's surface is assumed to have a uniform altitude.

Yield is specified in kilotons.

Specific Technology Parameters

Seismic sensor technology parameters--consist of the "include index," decoupling parameters, a threshold parameter, and a location accuracy parameter.

The first parameter is the "include index." If set to 0, the seismic technology is turned off and excluded from the application. A value of 1 activates the technology.

The second parameter is a cavity decoupling factor. The seismic signal's amplitude can be reduced by this factor if the detonation is in a cavity. A default value of 1 should be used for full coupling. Seismologists believe that the maximum possible decoupling value is around 70 for a cavern which has been designed especially for that purpose.

The third parameter is a medium decoupling factor for a detonation in earth or rock. A value of 1, the default, should be used if the device is detonated in solid rock. A value of 6.3 should be used for alluvium.

The fourth parameter is the decoupling factor for an underwater detonation. MRC (1994) specified that the magnitude for a detonation in water is 0.8 higher than for one in granite. This results in a decoupling factor of 0.16 for a water detonation. This decoupling factor is less than 1 which says that the signal for a water detonation is greater than that for a detonation in solid rock by a factor of 6.3 (0.8 in magnitude units).

The fifth parameter is the threshold-to-noise ratio which the signal-to-noise ratio must exceed to get a station detection. Seismologists currently use a value of 3 which we have adopted as our default value. If the signal-to-noise ratio is equal to this threshold, the response probability is 0.5.

The sixth parameter is a location accuracy parameter. The signal arrival time error built into the model is multiplied by this parameter. If the input parameter is given a value of 1.0, the built-in error will be used; if it is given a value of 1.7, the built-in error will be multiplied by 1.7. The built-in error is an rms arrival time error and is the square root of the sum of two squared errors. The first error is a constant error of 0.75 seconds. The second error is 0.15 seconds divided by signal-to-noise ratio minus 1. The default value for the location accuracy parameter is 1.0 which does not alter the built-in error.

The model does not use the cavity decoupling factor if the detonation is in air or water; and it determines whether the detonation is in air, land, or water using the altitude parameter and a world map of land and sea locations. For a world coverage application, the medium decoupling factor for land is constant for all land detonations. The model's map does not distinguish between solid rock and alluvium locations.

Infrasound technology parameters--consist of the "include index," a threshold value, and two location accuracy parameters.

The first parameter is the "include index." If set to 0, the infrasound technology is turned off and excluded from the application. A value of 1 activates the technology.

The second parameter is the threshold value which the signal-to-noise ratio must exceed to get a station detection. If the signal-to-noise ratio is equal to the threshold value, the probability of a station response to the event is 0.5. The threshold's default value is 1.5.

The third parameter is a location accuracy parameter for bearing errors. The bearing error built into the model is multiplied by this parameter. The built-in error is an rms bearing error, and it is equal to 1.8 degrees for station-to-event distances between 0 and 3000 km; it increases linearly to 7.0 degrees for distances between 3000 and 10,000 km; it increases linearly to 20 degrees for distances between 10,000 and 15,000 km; and it is 20 degrees beyond 15,000 km. The default value of the input parameter is 1.0 which does not alter the built-in error.

The fourth parameter is a location accuracy parameter for arrival time errors. The arrival time error built into the model is multiplied by this parameter. The built-in error is an rms arrival time error which is assumed to be 2% of signal travel time. The default value of the input parameter is 1.0 which does not alter the built in error.

Radionuclide technology parameters--consist of the "include index," the maximum allowed detection time, a fission fraction, a vent fraction, a threshold, and two rain parameters.

The first parameter is the "include index." If set to 0, the radionuclide technology is turned off and excluded from the application. A value of 1 activates the technology.

The second parameter is the maximum allowed detection time which is the length of time (in hours) after an event in which the radionuclide subsystem is allowed to get a detection. The default is 240 hours (10 days). For this default value, a detection occurs if radiation from any 24 hour sample within the 10 day period exceeds the specified threshold value. Smaller or larger values can be used, and execution time is directly dependent on maximum allowed detection time.

The third parameter is the fission fraction which specifies the fraction of fissions generated from fission neutrons in contrast to the fraction generated from fusion neutrons. This parameter has a small effect on the source term. We use a default value of 1.0 to indicate a fission weapon.

The fourth parameter is the vent fraction which is the fraction of fission product material assumed to vent immediately from an underground or underwater detonation. If a value greater than 1 (2 is the default) is specified, the model computes a value which depends on scaled depth of burst. If a value between 0 and 1 is specified, the model uses that value as the vent fraction. Radionuclides which are assumed to vent immediately become a part of the elevated debris cloud which may ultimately trigger sensors. Radionuclides which vent slowly are assumed to become part of a diffuse, low concentration, ground cloud which does not trigger sensors because ground winds have low speed and the cloud will probably not reach a sensor before the radionuclides decay.

The fifth parameter is a threshold which the sample activity must exceed to get a station detection. Every station site is given an average and a standard deviation of preexisting background radiation for each radionuclide. The default threshold of 2.6 specifies that the signal (which includes background radiation) must be 2.6 standard deviations above the average background radiation to get a sensor response probability of 0.5. The default value of 2.6 gives roughly 1.7 false alarms per year (for a 24 hour sample period).

The sixth parameter is rain intensity in mm/hr. Our default value is 0. A heavy rain might be 40 mm/hr. Rain removes aerosols from the atmosphere. A long, light rain will remove aerosols more effectively than a short, heavy rain if the total rainfall is the same for both.

The seventh parameter is rainfall duration in hours. Our default value is 0.

Hydroacoustic technology parameters-- consist of the "include index," a threshold, and a location accuracy parameter.

The first parameter is the "include index." If set to 0, the hydroacoustic technology is turned off and excluded from the application. A value of 1 activates the technology.

The second parameter is a location accuracy parameter. The built-in rms signal arrival time error is multiplied by this parameter. The built-in rms arrival time error is the square root of the sum of two squared errors. The first error is a constant pick-time error of 1 sec. for hydroacoustic stations and 5 sec. for island T-phase stations. Pick-time error is the error associated with selecting an arrival time from a signal profile. The second error is a travel time error and is assumed to be 0.02 times the square root of station-to-event distance. The input parameter's default value is 1.0 which does not alter the built in error.

Station Specification Files

All station specification files consist of a header line which describes the file and station data lines which specify station parameters. The first 15 characters of the header line is a short description of the file and is used in the model's output. The remaining characters in the header line give a more complete description of the file. Following the header line there is one station specification line for each station. The model counts the number of station lines to determine the number of stations. At present, the model restricts the maximum number of stations for a single technology to 200 for seismic stations, 100 for infrasound stations, 150 for radionuclide stations, and 50 for hydroacoustic stations; thus, the number of stations listed in a single file must not exceed these numbers.

A typical (but truncated) seismic station data file is shown in Figure A2. All seismic library files are named SZM-XXXX.DAT where XXXX is a unique descriptor of the file.

The first parameter is each station specification line is a station on-off parameter. If set to 1, the station is on in the IVSEM analysis. If set to 0, the station is off.

The second and third parameters in each station specification line are station latitude and longitude in degrees.

The fourth parameter specifies whether the station is primary or auxiliary. A value of 1 means the station is primary. A value of 0 means it is auxiliary. Only primary stations are used for event detection. Both primary and secondary stations are used for location accuracy estimation if the verification system detects the event.

The fifth parameter is the number of elements used at the station. If the number of elements exceeds one, the station is called an array.

The sixth, seventh, and eighth parameters are noise values in nanometers for teleseismic distances for seismic magnitudes greater than 4.5, between 3.5 and 4.5, and less than 3.5 respectively. Different stations will have different noise values; however, in the absence of specific station data, we use uniform noise values.

The ninth and tenth parameters are noise values for intermediate distances (1111 to 2500 km for stable regions, 500 to 2000 km for tectonic regions) and regional distances (less than 1111 km for stable regions, less than 500 km for tectonic regions) respectively.

The last parameter is a station description which is not used by the model.

Figure A2. A Typical, but Truncated, Seismic Station File

```
SZM-P330rn170   seismic  CD/NTB/WP.330r+tbd added; 8/24/96 Low Noise
  1  -40.73   -70.55   1   1   10.167   2.689   0.810   0.1794   0.1142  Argentina  Paso Flores
  1  -19.94   134.34   1  20    6.073   1.713   0.585   0.0764   0.0245  Australia  Warramunga
  1  -23.67   133.90   1  19    2.717   1.0     0.398   0.1966   0.1197  Australia  Alice Spring
  1  -31.88   141.59   1   1    7.588   2.452   0.877   0.4253   0.2408  Australia  Stephens
  1  -67.60    62.87   1   1   21.525   4.226   1.284   0.3231   0.2673  Australia  Mawson
  1  -16.29   -68.13   1   1    1.949   0.780   0.386   0.2132   0.1174  Bolivia    La Paz
  1  -15.64   -48.01   1   1   10.280   2.685   0.966   0.4420   0.2575  Brazil     Brazilia
  1   50.25   -95.88   1   1   10.235   4.755   1.925   0.7293   0.3793  Canada     Lac du Bonett
  1   62.49  -114.61   1  20    6.461   3.877   1.553   0.2452   0.0547  Canada     Yellowknife
  1   54.82   -66.78   1   1   69.005  29.802  13.997   6.5247   5.2439  Canada     Schefferville
  1    5.18    18.42   1   1    3.212   0.913   0.270   0.1355   0.1161  CAR        Bangui
  1   49.27   119.74   1   9    1.170   0.587   0.507   0.4516   0.3713  China      Hailar
  1   36.09   103.84   1   9    2.723   2.252   3.052   2.2440   1.2902  China      Lanzhou
  1    4.86   -74.33   1   1    2.717   1.0     0.398   0.1966   0.1197  Colombia   El Rosal
  1    6.67    -4.86   1   1    2.717   1.0     0.398   0.1966   0.1197  Coast Ivory Dimbroko
  1   26.00    33.00   1  10    2.717   1.0     0.398   0.1966   0.1197  Egypt      Luxor
  1   61.44    26.08   1   9  116.33   32.444   8.564   0.8898   0.4585  Finland    Lahti
  1  -17.57  -149.57   1   1    2.717   1.0     0.398   0.1966   0.1197  France     Tahiti
  1   48.85    13.70   1  25    3.136   1.900   1.437   0.5349   0.3185  Germany    Freyung
  1   38.52    51.39   1   1    2.717   1.0     0.398   0.1966   0.1197  Iran       Tehran
  1   36.54   138.21   1   9    9.927   5.882   3.106   2.0078   1.3257  Japan      Matsushiro
  1   46.80    82.00   1   9    2.717   1.0     0.398   0.1966   0.1197  Kazakhstan Makanchi
  1   -1.27    36.80   1   1    2.717   1.0     0.398   0.1966   0.1197  Kenya      Kilima Mbogo
  1  -31.61   -68.24   0   1    8.592   3.162   1.259   0.6217   0.3785  Argentina  Coronel Fontana
  1  -55.00   -68.00   0   1    8.592   3.162   1.259   0.6217   0.3785  Argentina  Ushuaia
  1   40.05    44.72   0   1    6.389   4.262   4.016   2.5486   1.1465  Armenia    Garni
  1  -20.09   146.25   0   1   12.368   3.376   0.904   0.2066   0.1463  Australia  Charters towers
  1  -18.10   125.64   0   1    8.592   3.162   1.259   0.6217   0.3785  Australia  Fitzroy Crossing
  1  -32.93   117.23   0   1   17.405   8.022   1.736   0.2098   0.1149  Australia  Narrogin
  1   22.4     91.8    0   1    1.654   0.777   0.518   0.3846   0.1843  Bangladesh Chinagong
  1  -15.99   -61.07   0   1    8.592   3.162   1.259   0.6217   0.3785  Bolivia    San Ignacio
  1  -25.01    25.60   0   1    7.114   2.338   0.549   0.2145   0.1449  Botswana   Lobatse
  1   -0.73   -59.97   0   1    8.592   3.162   1.259   0.6217   0.3785  Brazil     Pitinga
```

A typical, but truncated, infrasound station data file is shown in Figure A3. All infrasound station files are named ISN-XXXX.DAT where XXXX is a unique file descriptor.

The first parameter is each station specification line is a station on-off parameter. If set to 1, the station is on in the IVSEM analysis. If set to 0, the station is off.

The second and third parameters in each station data line are station latitude and longitude in degrees.

The fourth parameter is the number of elements used at the station. A greater number of elements will result in a larger signal. We use four elements as a default.

The fifth parameter is a noise reduction factor for the station. Noise reduction may be accomplished by a "spider" or hoses. The default noise reduction is 4.0.

The sixth parameter is the average wind speed at the site in m/s. The average wind speed is used to calculate the station's noise. If the wind speed is set to 99.0, the infrasound module computes average monthly wind speed from surface wind data in the wind data file based on the station's regional location. The average monthly surface wind speed computed from the wind data file may or may not be the best average wind speed to use because careful location may result in an average local wind speed which is significantly lower than the average regional wind speed.

The last parameter is a description of the station and is not used by the model.

Figure A3. A Typical but Truncated Infrasound Station File

```
ISN-P330r-59    60 STATIONS WP.330r+COLOMBO 8/26/96
  1  -40.73   -70.55  4  4.0    3.76  Argentina       PASO FLORES, PLCA
  1  -55.0    -68.0   4  4.0    6.64  Argentina       USHUAIA
  1  -68.4     77.6   4  4.0   11.3   Australia       Davis Base, ANT MAW
  1  -42.07   147.21  4  4.0    3.55  Australia       HOBART, HOBA
  1  -32.93   117.23  4  4.0    3.34  Australia       NARROGIN, NWAO
  1  -12.30    97.00  4  4.0    7.41  Australia       COCOS IS COCO
  1  -19.93   134.33  4  4.0    2.62  Australia       WARRAMUNGA, WRA
  1  -16.29   -68.13  4  4.0    2.42  Bolivia         LA PAZ, LPAZ
  1  -15.64   -48.01  4  4.0    2.33  Brasil          BRASILIA, BDFB
  1   50.25   -95.88  4  4.0    4.68  Canada          LAC DU BONNET, ULM
  1   16.00   -24.00  4  4.0    7.00  CAPE VERDE IS   Cape Verde VERDE
  1    5.18    18.42  4  4.0    1.61  CAR             BANGUI, BGCA
  1  -27.00  -109.20  4  4.0    4.43  Chile           EASTER ISLAND EAST
  1  -33.80   -80.70  4  4.0    3.49  Chile           JUAN FERNANDEZ, JFRN
  1   40.00   116.00  4  4.0    2.52  China           BEIJING, BEI
  1   25.00   102.80  4  4.0    2.52  China           KUNMING, KUNM
  1    6.67    -4.86  4  4.0    2.36  Cote d'Ivoire   DIMBROKO, IVOR
  1   76.53   -68.67  4  4.0    2.77  Denmark         THULE, GREENLAND, THUL
  1   11.30    43.50  4  4.0    3.29  DJIBOUTI        DJIBOUTI DJIB
  1    0.00   -91.70  4  4.0    4.63  Ecuador         GALAPAGOS IS, GALA
  1  -22.10   166.30  4  4.0    3.98  France          PORT LAGUERRE,  NOUC
  1  -49.15    69.10  4  4.0   11.83  France          KERGUELEN IS, KERG
  1    5.21   -52.73  4  4.0    2.47  France          KOUROU, FR GUIANA KOG
  1  -10.00  -140.00  4  4.0    9.35  France          MARQUESAS MARQ
```

A typical (but truncated) radionuclide station data file is shown in Figure A4. Radionuclide station data files are named RDN-XXXX.DAT where XXXX is a unique file descriptor.

The first parameter in each station specification line is a station on-off parameter. If set to 1, the station is on in the IVSEM analysis. If set to 0, the station is off. For the radionuclide subsystem this parameter also switches the xenon and barium sensors on or off independently:

0 -- both sensors are off (the station is off);
1 -- both sensors are on;
2 -- the barium sensor is on and the xenon sensor is off; and
3 -- the barium sensor is off and the xenon sensor is on.

The second and third parameters in each station data line are station latitude and longitude in degrees.

The fourth, fifth, and sixth parameters are the average and standard deviation of local background radiation levels and the minimum detectable activity, respectively, for each station in Bq/m^3 for Xe-133g. Notice that the background values are higher in the northern hemisphere that in the southern hemisphere, a result of nuclear power generation and fuel processing site locations.

The seventh, eighth, and ninth parameters are the average and standard deviation of local background radiation levels and the minimum detectable activity, respectively, for each station in Bq/m^3 for Ba-140. (To date, we have used Ba-140 background levels of 0.0 for all stations.)

The last parameter describes the station and is not used by the model.

Figure A4. A Typical but Truncated Radionuclide Station File

```
RDN-330rn80      CTBT 80 Radionuclide; CD/NTB/WP.330r +tbds added; 8/24/96
1  -34.00   -58.00  2.50E-06  1.25E-06  1.00E-03  0.00E+00  0.00E+00  3.00E-05  Argentina
1  -41.01   -71.25  2.50E-06  1.25E-06  1.00E-03  0.00E+00  0.00E+00  3.00E-05  Argentina
1  -24.00   -65.00  5.00E-06  2.50E-06  1.00E-03  0.00E+00  0.00E+00  3.00E-05  Argentina
1  -37.45   144.58  2.50E-06  1.25E-06  1.00E-03  0.00E+00  0.00E+00  3.00E-05  Australia
1  -31.90   116.00  2.50E-06  1.25E-06  1.00E-03  0.00E+00  0.00E+00  3.00E-05  Australia
1  -12.40   130.70  5.00E-06  2.50E-06  1.00E-03  0.00E+00  0.00E+00  3.00E-05  Australia
1  -19.20   146.80  5.00E-06  2.50E-06  1.00E-03  0.00E+00  0.00E+00  3.00E-05  Australia
1  -12.00    97.00  5.00E-06  2.50E-06  1.00E-03  0.00E+00  0.00E+00  3.00E-05  Australia
1  -54.00   159.00  2.50E-06  1.25E-06  1.00E-03  0.00E+00  0.00E+00  3.00E-05  Australia
1  -67.60    62.50  5.00E-07  2.50E-07  1.00E-03  0.00E+00  0.00E+00  3.00E-05  Australia
1  -22.54   -43.10  5.00E-06  2.50E-06  1.00E-03  0.00E+00  0.00E+00  3.00E-05  Brazil
1   -8.00   -35.00  5.00E-06  2.50E-06  1.00E-03  0.00E+00  0.00E+00  3.00E-05  Brazil
1    4.20     9.90  1.00E-05  5.00E-06  1.00E-03  0.00E+00  0.00E+00  3.00E-05  Cameroon
1   49.25  -123.17  2.00E-03  1.00E-03  1.00E-03  0.00E+00  0.00E+00  3.00E-05  Canada
1   74.70   -94.90  2.50E-05  1.25E-05  1.00E-03  0.00E+00  0.00E+00  3.00E-05  Canada
1   62.45  -114.48  2.50E-05  1.25E-05  1.00E-03  0.00E+00  0.00E+00  3.00E-05  Canada
1   47.00   -53.00  2.00E-03  1.00E-03  1.00E-03  0.00E+00  0.00E+00  3.00E-05  Canada
1  -53.08   -70.55  2.50E-06  1.25E-06  1.00E-03  0.00E+00  0.00E+00  3.00E-05  Chile
```

A typical hydroacoustic station data file is shown in Figure A5. Hydroacoustic station data files are named HYD-XXXX.DAT where XXXX is a unique file descriptor.

The first parameter in each station specification line is a station on-off parameter. If set to 1, the station is on in the IVSEM analysis. If set to 0, the station is off.

The second and third parameters in each station data line are station latitude and longitude in degrees.

The fourth parameter specifies whether the station is a hydroacoustic station or an island "T-phase" station. A value of 0 denotes a hydroacoustic station, and 1 denotes a "T-phase" station. Island "T-phase" stations are seismic stations which measure seismic P waves induced by hydroacoustic waves at the ocean-island interface. Both types of stations participate in both detection and location.

The fifth parameter is a local noise parameter: a value of 1 implies high noise; 2 implies medium noise; and 3 implies low noise. This parameter should depend on the station's distance from shipping lanes and other sources of low frequency (roughly 1 to 100 Hz) noise.

The final parameter is a station description which is not used by the model.

Figure A5. A Typical Hydroacoustic Station File

```
HYD-P330-6+5T  CTBT 6 Hydro +5 T stations;  CD/NTB/WP.330; 5/28/96
  1  -34.40   115.10  0  2.   Australia  Cape Leeuwin
  1  -33.70   -78.80  0  2.   Chile      Fernandez
  1  -46.50    52.20  0  3.   France     Crozet
  1   -7.30    72.40  0  1.   UK         BIOT/Chagos
  1   -8.00   -14.40  0  1.   USA        Ascension
  1   19.30   166.60  0  2.   USA        Wake
  1   16.30   -61.10  1  1.   France     Guadeloupe
  1   52.10  -131.50  1  1.   Canada     Queen Charlotte Is.
  1   18.20  -114.60  1  2.   Mexico     Clarion Is.
  1   39.30   -31.30  1  1.   Poprtugal  Flores Is.
  1  -37.20   -12.50  1  3.   UK         Tristan da Cunha
```

Detection Effectiveness Table

A typical detection effectiveness table is shown in Figure A6. Detection effectiveness table files are named EFTABXXX.DAT in the library where XXX is a unique file descriptor. The table has four dimensions, one for each technology, but it is easier to explain if we start with a two dimensional table, Table A1. The table below shows the number of seismic and infrasound stations which respond in combination to an event and the associated, subjectively determined, detection effectiveness value for each response combination. We call the response combination the system response. For example, three seismic responses plus two infrasound responses (highlighted cell) is a system response.

Table A1. A Two-Technology Detection Effectiveness Table Example

Number of Responses					
Seismic / Infrasound	**0**	**1**	**2**	**3**	**4**
0	.00	.00	.00	1.00	1.00
1	.00	.00	.00	1.00	1.00
2	1.00	1.00	1.00	1.00	1.00
3	1.00	1.00	1.00	1.00	1.00
4	1.00	1.00	1.00	1.00	1.00

The values in the table represent the user's judgement as to which system responses (i.e., combination of sensors for each technology responding to an event) should constitute a detection. The user can fill out the table to meet his needs. In this table, for 1 seismic and 1 infrasound station responses, the effectiveness value 0.00 indicates that this system response is not considered to be a detection. In this table we used a detection effectiveness value of 0.00 to indicate that the system response is not a detection, and we used a detection effectiveness value of 1.0 to indicate that a system response is a detection. For 3 seismic and 0 infrasound or 2 infrasound and 0 seismic responses, the effectiveness value is 1.00 and we call these system responses a detection. Thus, the user can specify which combination of station responses are considered to be detections and which responses are not considered to be detections by entering values of 1 or 0 into the table for the appropriate system responses. This table is expanded into four dimensions in Figure A6.

Each of the twelve subtables in Figure A6 shows a cross-section of the four dimensional table. The first subtable, in the upper left hand corner, is the one we started with above and represents 0 hydroacoustic and 0 radionuclide responses. The header for each subtable specifies the number of hydroacoustic and radionuclide station responses for that subtable. The number of seismic responses correspond to columns and the number of infrasound responses correspond to rows in

each of the subtables just like in the table above. For all system responses beyond the range of this table, the detection effectiveness value is assumed to be 1.00.

Figure A6. A Typical Detection Effectiveness Table

```
EFT #3: 3 Seismic, 3 Hydroacoustic, 2 Infrasound, or 1 Radionuclide required
*
*                              Infrasound(col)/Seismic(row)
*      0 hydroacoustic                0 hydroacoustic                0 hydroacoustic
*      0 radionuclide                 1 radionuclide                 2 radionuclide
*   0    1    2    3    4      0    1    2    3    4      0    1    2    3    4
0  .00  .00  .00 1.00 1.00   1.00 1.00 1.00 1.00 1.00   1.00 1.00 1.00 1.00 1.00
1  .00  .00  .00 1.00 1.00   1.00 1.00 1.00 1.00 1.00   1.00 1.00 1.00 1.00 1.00
2 1.00 1.00 1.00 1.00 1.00   1.00 1.00 1.00 1.00 1.00   1.00 1.00 1.00 1.00 1.00
3 1.00 1.00 1.00 1.00 1.00   1.00 1.00 1.00 1.00 1.00   1.00 1.00 1.00 1.00 1.00
4 1.00 1.00 1.00 1.00 1.00   1.00 1.00 1.00 1.00 1.00   1.00 1.00 1.00 1.00 1.00
*
*      1 hydroacoustic                1 hydroacoustic                1 hydroacoustic
*      0 radionuclide                 1 radionuclide                 2 radionuclide
0  .00  .00  .00 1.00 1.00   1.00 1.00 1.00 1.00 1.00   1.00 1.00 1.00 1.00 1.00
1  .00  .00  .00 1.00 1.00   1.00 1.00 1.00 1.00 1.00   1.00 1.00 1.00 1.00 1.00
2 1.00 1.00 1.00 1.00 1.00   1.00 1.00 1.00 1.00 1.00   1.00 1.00 1.00 1.00 1.00
3 1.00 1.00 1.00 1.00 1.00   1.00 1.00 1.00 1.00 1.00   1.00 1.00 1.00 1.00 1.00
4 1.00 1.00 1.00 1.00 1.00   1.00 1.00 1.00 1.00 1.00   1.00 1.00 1.00 1.00 1.00
*
*      2 hydroacoustic                2 hydroacoustic                2 hydroacoustic
*      0 radionuclide                 1 radionuclide                 2 radionuclide
0  .00  .00  .00 1.00 1.00   1.00 1.00 1.00 1.00 1.00   1.00 1.00 1.00 1.00 1.00
1  .00  .00  .00 1.00 1.00   1.00 1.00 1.00 1.00 1.00   1.00 1.00 1.00 1.00 1.00
2 1.00 1.00 1.00 1.00 1.00   1.00 1.00 1.00 1.00 1.00   1.00 1.00 1.00 1.00 1.00
3 1.00 1.00 1.00 1.00 1.00   1.00 1.00 1.00 1.00 1.00   1.00 1.00 1.00 1.00 1.00
4 1.00 1.00 1.00 1.00 1.00   1.00 1.00 1.00 1.00 1.00   1.00 1.00 1.00 1.00 1.00
*
*      3 hydroacoustic                3 hydroacoustic                3 hydroacoustic
*      0 radionuclide                 1 radionuclide                 2 radionuclide
0 1.00 1.00 1.00 1.00 1.00   1.00 1.00 1.00 1.00 1.00   1.00 1.00 1.00 1.00 1.00
1 1.00 1.00 1.00 1.00 1.00   1.00 1.00 1.00 1.00 1.00   1.00 1.00 1.00 1.00 1.00
2 1.00 1.00 1.00 1.00 1.00   1.00 1.00 1.00 1.00 1.00   1.00 1.00 1.00 1.00 1.00
3 1.00 1.00 1.00 1.00 1.00   1.00 1.00 1.00 1.00 1.00   1.00 1.00 1.00 1.00 1.00
4 1.00 1.00 1.00 1.00 1.00   1.00 1.00 1.00 1.00 1.00   1.00 1.00 1.00 1.00 1.00
*
*      4 hydroacoustic                4 hydroacoustic                4 hydroacoustic
*      0 radionuclide                 1 radionuclide                 2 radionuclide
0 1.00 1.00 1.00 1.00 1.00   1.00 1.00 1.00 1.00 1.00   1.00 1.00 1.00 1.00 1.00
1 1.00 1.00 1.00 1.00 1.00   1.00 1.00 1.00 1.00 1.00   1.00 1.00 1.00 1.00 1.00
2 1.00 1.00 1.00 1.00 1.00   1.00 1.00 1.00 1.00 1.00   1.00 1.00 1.00 1.00 1.00
3 1.00 1.00 1.00 1.00 1.00   1.00 1.00 1.00 1.00 1.00   1.00 1.00 1.00 1.00 1.00
4 1.00 1.00 1.00 1.00 1.00   1.00 1.00 1.00 1.00 1.00   1.00 1.00 1.00 1.00 1.00
```

An alternate way of filling out the table is shown in Figure A7. Instead of only using values of 1.00 and 0.00, we can assign fractional values to indicate "how good" a particular response is in terms of detection. For example, a system response of 1 hydroacoustic, 0 radionuclide, 1 seismic, and 1 infrasound response gets a detection effectiveness value of 0.85. We interpret that this is not quite good enough to be an unquestionable detection, but it is close.

Both philosophies for filling out the table can reflect the user's ideas of synergy among technologies. The idea of synergy will be discussed in the integration section of this report.

Figure A7. An Alternate Detection Effectiveness Table

```
EFT #1: Fractional Values with Synergy
*
*                                Infrasound(col)/Seismic(row)
*      0 hydroacoustic                 0 hydroacoustic                 0 hydroacoustic
*      0 radionuclide                  1 radionuclide                  2 radionulcide
*   0    1    2    3    4      0    1    2    3    4      0    1    2    3    4
0  .00  .10  .30  .70  .90    .70  .88 1.00 1.00 1.00    .90 1.00 1.00 1.00 1.00
1  .10  .33  .77  .99 1.00    .88 1.00 1.00 1.00 1.00   1.00 1.00 1.00 1.00 1.00
2  .30  .77 1.00 1.00 1.00   1.00 1.00 1.00 1.00 1.00   1.00 1.00 1.00 1.00 1.00
3  .70  .99 1.00 1.00 1.00   1.00 1.00 1.00 1.00 1.00   1.00 1.00 1.00 1.00 1.00
4  .90 1.00 1.00 1.00 1.00   1.00 1.00 1.00 1.00 1.00   1.00 1.00 1.00 1.00 1.00
*
*      1 hydroacoustic                 1 hydroacoustic                 1 hydroacoustic
*      0 radionuclide                  1 radionuclide                  2 radionulcide
0  .10  .33  .77  .99 1.00    .88 1.00 1.00 1.00 1.00   1.00 1.00 1.00 1.00 1.00
1  .33  .85 1.00 1.00 1.00   1.00 1.00 1.00 1.00 1.00   1.00 1.00 1.00 1.00 1.00
2  .77 1.00 1.00 1.00 1.00   1.00 1.00 1.00 1.00 1.00   1.00 1.00 1.00 1.00 1.00
3  .99 1.00 1.00 1.00 1.00   1.00 1.00 1.00 1.00 1.00   1.00 1.00 1.00 1.00 1.00
4 1.00 1.00 1.00 1.00 1.00   1.00 1.00 1.00 1.00 1.00   1.00 1.00 1.00 1.00 1.00
*
*      2 hydroacoustic                 2 hydroacoustic                 2 hydroacoustic
*      0 radionuclide                  1 radionuclide                  2 radionulcide
0  .30  .77 1.00 1.00 1.00   1.00 1.00 1.00 1.00 1.00   1.00 1.00 1.00 1.00 1.00
1  .77 1.00 1.00 1.00 1.00   1.00 1.00 1.00 1.00 1.00   1.00 1.00 1.00 1.00 1.00
2 1.00 1.00 1.00 1.00 1.00   1.00 1.00 1.00 1.00 1.00   1.00 1.00 1.00 1.00 1.00
3 1.00 1.00 1.00 1.00 1.00   1.00 1.00 1.00 1.00 1.00   1.00 1.00 1.00 1.00 1.00
4 1.00 1.00 1.00 1.00 1.00   1.00 1.00 1.00 1.00 1.00   1.00 1.00 1.00 1.00 1.00
*
*      3 hydroacoustic                 3 hydroacoustic                 3 hydroacoustic
*      0 radionuclide                  1 radionuclide                  2 radionulcide
0  .70  .99 1.00 1.00 1.00   1.00 1.00 1.00 1.00 1.00   1.00 1.00 1.00 1.00 1.00
1  .99 1.00 1.00 1.00 1.00   1.00 1.00 1.00 1.00 1.00   1.00 1.00 1.00 1.00 1.00
2 1.00 1.00 1.00 1.00 1.00   1.00 1.00 1.00 1.00 1.00   1.00 1.00 1.00 1.00 1.00
3 1.00 1.00 1.00 1.00 1.00   1.00 1.00 1.00 1.00 1.00   1.00 1.00 1.00 1.00 1.00
4 1.00 1.00 1.00 1.00 1.00   1.00 1.00 1.00 1.00 1.00   1.00 1.00 1.00 1.00 1.00
*
*      4 hydroacoustic                 4 hydroacoustic                 4 hydroacoustic
*      0 radionuclide                  1 radionuclide                  2 radionulcide
0  .90 1.00 1.00 1.00 1.00   1.00 1.00 1.00 1.00 1.00   1.00 1.00 1.00 1.00 1.00
1 1.00 1.00 1.00 1.00 1.00   1.00 1.00 1.00 1.00 1.00   1.00 1.00 1.00 1.00 1.00
2 1.00 1.00 1.00 1.00 1.00   1.00 1.00 1.00 1.00 1.00   1.00 1.00 1.00 1.00 1.00
3 1.00 1.00 1.00 1.00 1.00   1.00 1.00 1.00 1.00 1.00   1.00 1.00 1.00 1.00 1.00
4 1.00 1.00 1.00 1.00 1.00   1.00 1.00 1.00 1.00 1.00   1.00 1.00 1.00 1.00 1.00
```

References

MRC, 1994: Assessment of Techniques for Nuclear Testing that Evade Detection, MRC/WDC-R-340, November 1994.

APPENDIX B. SEISMIC DETECTION

Introduction

The purpose of the seismic module in IVSEM is to provide a simple, fast-running detection and location model that can be used to generate a first-order analysis of seismic network detection and location performance. Identification and yield estimation are not included in the present version of IVSEM. This effort was undertaken by Organization 5415, Sandia National Laboratories Albuquerque (SNLA), with support by Organization 5700, SNLA for use by US government agencies and their contractors supporting the Comprehensive Test Ban Treaty (CTBT) negotiations and the ratification process. This work was started in August 1994.

Seismic monitoring of nuclear explosions is based on the fact that underground explosions generate various types of seismic waves. These waves can travel for large distances (thousands of kilometers) from the explosion. These waves can be detected at monitoring stations as very small movements of the Earth, on the order of nanometers. There are various types of seismic waves and propagation modes for these waves. There are two principal classes of waves, based upon their propagation modes. Some waves travel along the surface of the earth and are called surface waves. Others travel deep within the earth and are called body waves. At short distances the body waves travel through the crust. At somewhat longer distances, the waves can move along the interfaces between the crust and the mantle. At large distances, called teleseismic distances, the waves move through the mantle and the core. As these waves move at predictable speeds through the earth, the arrival times of these waves at several stations can be used to provide location estimates for the event. Figure B1 shows some of the travel modes of these waves.

Seismic monitoring is based upon the detection of those waves produced in the Earth by explosive events. This is a favored method of detecting underground tests (UGTs) because it is the only reliable method of detecting these tests at long ranges (1000s of kilometers) in a prompt manner and determining their location and size. Seismic waves are unaffected by weather, and while evasion efforts may be successful, they require much effort on the part of the evader. For these reasons, seismic detection is one of the four technologies selected for the International Monitoring System (IMS).

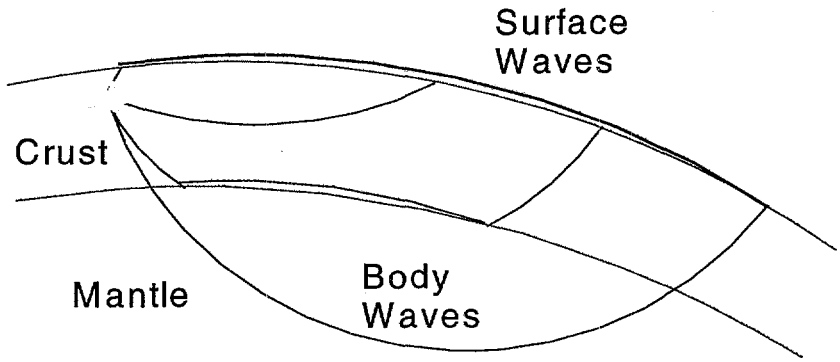

Figure B1. Seismic Wave Propagation Modes

Explosions primarily generate body waves with relatively short periods of 1 second or less. These waves, called P waves, are compression waves. In the IVSEM model seismic detection is based upon the P wave envelope amplitude. Earthquakes generate P waves as well, but also generate strong shear waves, S waves, with periods of 10 sec or more. These are not compression waves, but have a circular motion. Nuclear explosions, on the other hand, are relatively weak sources of these long period waves. This difference is a means of discrimination between earthquakes and explosions. However, chemical explosions also exhibit this pattern of strong P waves and weak S waves. As a result, nuclear explosions cannot be discriminated from large chemical explosions on this basis at the present time. Currently, IVSEM does not model the discrimination process. Figure B2 shows examples of seismic waves generated by an earthquake and an explosion.

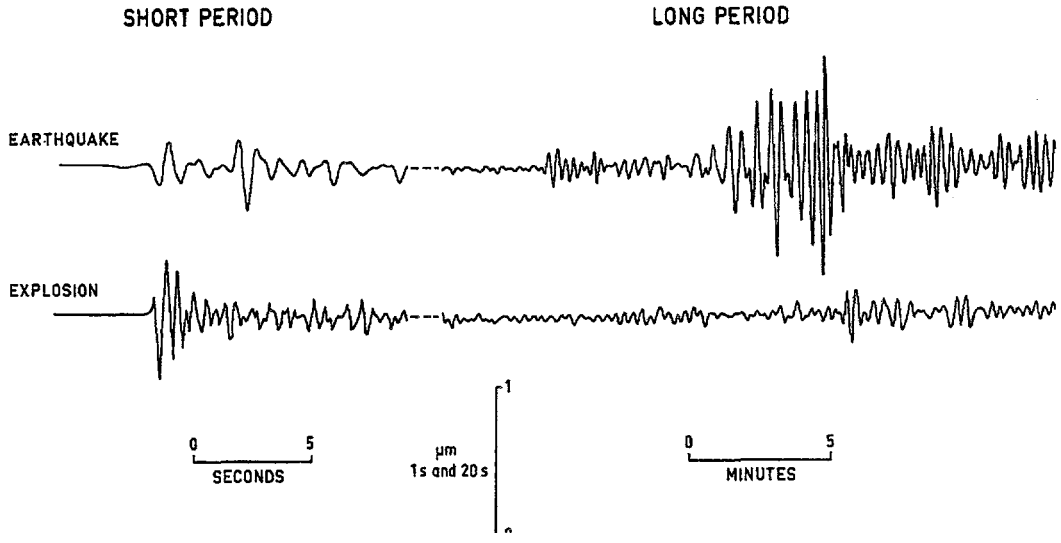

Figure B2. Explosion and Earthquake Generated Wave Trains

Overall Process

The approach used in the model is based upon empirical equations. A seismic magnitude is generated, based upon the device yield, the depth of burial, the medium of burial, and the effects of any evasion attempts. The seismic magnitude is a dimensionless number that is a measure of the energy that has been coupled into the earth to produce seismic waves. There are various magnitude numbers, based upon the production of different types of seismic waves. The magnitude used in this model is the M_b, or body wave magnitude. This is the measure of the energy that goes into the production of P waves. P waves are used for detection in this model because they travel the fastest and are the first arrivals at a monitoring stations. In addition, for an explosion, they have the greatest amplitude. This magnitude and the great circle distance from the event epicenter to the receiving station are entered into a series of equations in order to find the signal amplitude at the receiving station. The detection probability is then calculated using this signal and the station noise characteristics. The types of waves modeled in IVSEM are the P waves at frequencies of from .8 to 5 Hz, and the detection process is based upon the detection of the amplitude envelope at the optimum frequency for detection which varies according to whether the stations are at regional (less than 2000 km from the event), or teleseismic distances (greater than 2000 km).

Source Terms

The equation used for estimating magnitude from explosion yield is based upon empirical data from numerous underground nuclear explosions collected over many years. The equation currently used for estimating the magnitude is shown here:

$$Mb = 4.0+.9\log(Y)$$

M_b is the seismic magnitude
Y is the explosive yield in kilotons.

This equation is based upon data from the US Nevada Test Site provided by John Claassen (SNL, 1994). As a result, it accurately models a condition where the event is in a seismically unstable region. The stations that collected the data used to formulate the equation were mostly in seismically stable regions. Data collected from tests conducted in other regions (principally Russian and Chinese tests), indicate that events conducted in stable regions produce a greater seismic magnitude (Adushkin, 1995; Marshall, 1979). This is because seismically stable crustal regions propagate the seismic waves with a smaller loss than do unstable regions. In order to approximate this affect, a seismic map of the world is incorporated into IVSEM. This map, which is a separate input file, divides the world into regions that are 2 x 2 degrees in latitude and longitude. Each region is given a number that indicates whether the region is seismically stable or unstable. During the detection process, for each potential seismic receiving station, stability numbers for both the source region and the region in which the station falls are examined. If both the event and station are in stable regions, a factor of .3 is added to the M_b. If both fall in

unstable regions, a factor of .3 is subtracted. If one is stable and the other is unstable, the M_b equation is used without modification.

Coupling

The extent to which the energy of the explosion is converted to seismic waves is called coupling. The M_b equation above assumes that the event takes place in a hard rock medium like granite at a depth sufficient to produce good coupling. For explosions at shallow depths and in materials other than hard rock, the M_b equation must be modified. Modifications to the seismic magnitude based upon the depth or height of burst are produced internally in the IVSEM code. Currently, information based upon hydrocode results is used to model these effects. Figure B3 shows the decoupling magnitude, caused by height or depth of burst, relative to a fully coupled event. This decoupling magnitude is subtracted from the M_b equation described earlier.

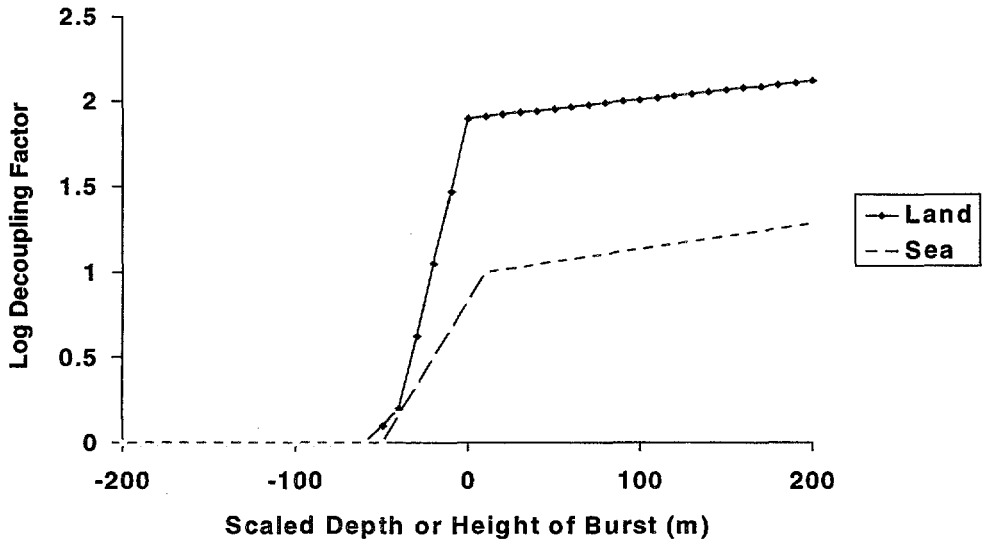

Figure B3. Decoupling Magnitude with Depth or Height of Burst

This is based upon work done by several organizations. (Day, 1986; Wortman, 1994). Some work has been done that indicates that seismic magnitude will decrease for large depths of burial, as a result of increasing overburden pressure. To date this effect is not modeled in IVSEM, which assumes that deeply overburied events will not occur.

In addition to the effects of the height or depth of burst, other factors affect the coupling as well. The medium in which the event takes place affects the coupling. In general, the harder the medium, the greater the coupling. Not only does the medium in which the device is buried affect the coupling, but there may be deliberate attempts to minimize the energy converted into seismic

waves. These efforts, called decoupling techniques, may be part of an attempt to evade seismic detection. In the model, these effects are accounted for by three input decoupling factors. The log of these factors are directly subtracted from the seismic magnitude. These three decoupling factors are, first, a land decoupling factor, which accounts for the effect of the local geology at the event location. Typical values are 1 for a hard rock site and 6.3 for alluvium. The second factor accounts for the effects of decoupling if the event takes place in a cavity. Typical values vary from one, for no cavity, to 70, for a large cavity producing full decoupling. The final factor accounts for events in water, and its current value is .16. The effect of this factor is to add 0.8 to the magnitude for a fully coupled event, due to better energy coupling into water than into granite (Wortman, 1994). IVSEM does not have a separate set of decoupling factors for events in the seabed. For seabed events, the user must enter a "water" decoupling factor which accounts for all decoupling. For underground detonations, the burst altitude factor is added to the geology factor and compared to the cavity decoupling factor. The larger of these two values is used . For example, if a 6.3 decoupling factor for medium is input, but a cavity decoupling factor of 70 is also used, then the total decoupling factor for both medium and cavity is 70, not 76.3. For events in the ocean, cavity decoupling is not used.

Propagation

In the seismic model, detection is modeled upon the amplitude of the compressive body or P waves. Empirical equations model the relationship between the seismic magnitude, the distance to the sensor site, and the body wave amplitude; that is, they account for the signal attenuation. In equations currently used by the seismic community for magnitude calculations at seismometer stations, an empirical station correction factor is used. These correction factors are not yet included in this model because a different station correction factor would have to be entered for each station as part of the input, and these are not yet known for many stations.

Different equations are used to account for different propagation conditions: stable versus unstable geology, and regional versus teleseismic propagation. These equations are explained below.

A = seismic amplitude in nanometers
M_b = seismic magnitude
T = period in seconds
(The wave periods used for these equations correspond to the optimum propagation frequencies.)
D = distance in kilometers

The following set of equations is used to model propagation for regional distances (less than 3000 km), for unstable (Western US-like), geologies, based upon event location (Evernden, 1967).

D < 1000 km

$$\log A/T = [M_b + 7.55\text{-}3.68\log(D)]/1.21$$

T = .25 sec

1000 km < D < 2000 km

$$\log A/T = M_b + 3.27\text{-}2\log(D)$$

T = .33 sec

2000 km < D < 3000 km

$$\log A/T = M_b + 10.35\text{-}4\log(D)$$

T = 1.25 sec, for $M_b > 4.5$

T = .5 sec, for $3.5 < M_b < 4.5$

T = .23 sec, for $M_b < 3.5$

The following equations are used for regional distances up to 200 km for stable regions (Eastern US-like), based upon event location (Evernden, 1967).

D < 1100 km

$$\log A/T = M_b + 3.27\text{-}2\log(D)$$

T = .25 sec

1100 km < D < 2200 km

$$\log A/T = M_b + 3.27\text{-}2\log(D)$$

T = .33 sec

The amplitude equation for teleseismic distances (greater than 3000 km for unstable regions, or greater than 2200 km for stable regions) is based upon work done for the National Data Center (NDC) (Veith, 1972). The equation has this form:

$$\log(A/T) = M_b - P$$

T = 1.25 sec, for $M_b > 4.5$

T = .5 sec, for $3.5 < M_b < 4.5$

T = .23 sec, for $M_b < 3.5$

P is an empirical attenuation factor that is a function of the event-receiver distance in degrees. It accounts for geometrical spreading of the signal and attenuation by the signal medium .

In IVSEM, these equations are solved for the signal amplitude A.

Detection

A statistical process is used to model detection. Figure B4 shows the basic nature of the process. Both the signal and the noise are assumed to be log-normal distributed, based upon the results of numerous seismic observations. The mean signal value is given by A in the preceding equations. The mean noise value is specified in the station input files for each of the cases described above. Separate noise levels are used for each of the amplitude-distance curves, based upon the noise at that particular frequency which the curve deals with. The standard deviations of the signal and noise are based upon data from the seismic community (Claassen, 1994), and are shown in the following tables:

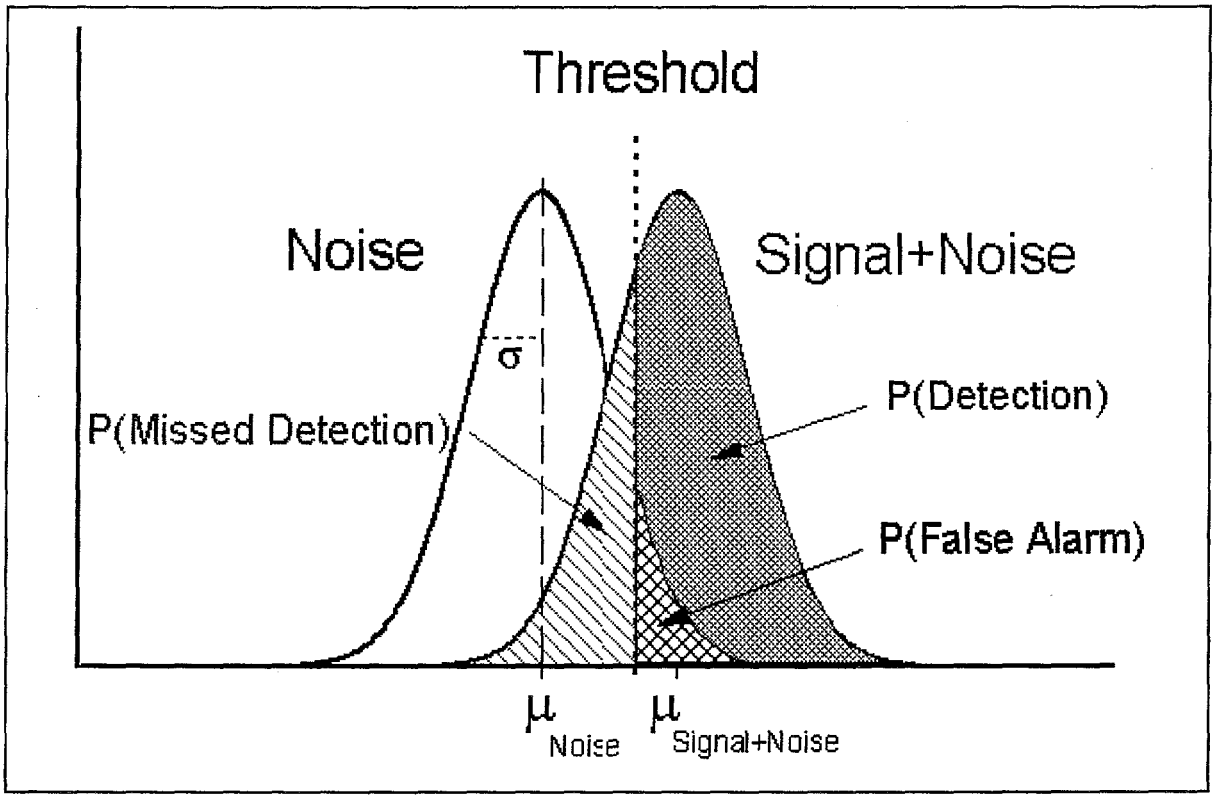

Figure B4. The Detection Process

Signal and Noise Standard Deviations, Unstable Geology

	D <1000 km	1000 < D < 2000 km	2000 < D < 3000 km
σ_{signal}	.38	.38	.38
σ_{noise}	.35	.30	.25, $M_b > 3.5$ .30, $M_b < 3.5$

Signal and Noise Standard Deviations, Unstable Geology

	D <1100 km	1100 < D < 2200 km
σ_{signal}	.26	.26
σ_{noise}	.35	.30

Signal and Noise Standard Deviations, Teleseismic Distances

σ_{signal}	.365, geologically stable source region .38, geologically unstable source region
σ_{noise}	.25, $M_b > 3.5$ .30, $M_b < 3.5$

Based upon the signal received at the station and the local noise, which is contained in the station data file, a signal-to-noise ratio is generated, which is also log-normal. Array gain, which is assumed to be equal to the square root of the number of station array elements, is used to increase the signal-to-noise ratio. The standard deviation of the signal-to-noise ratio is found by taking the square root of the sum of the squares of the signal and noise standard deviations. The probability of detection is found by integrating the signal-to-noise probability density function from a lower bound, which is the threshold signal-to-noise ratio, to an upper bound approximating infinity. The threshold is an input value. The final step in the process is to multiply the probability of detection by a station reliability value. The current value is assumed to be .95 for primary stations which will be maintained at a high operational readiness rate. A station can also be an auxiliary station, in which case it will have a .85 reliability. The type (primary or auxiliary) of each particular station is set by the user in the station input file.

Network Detection Criteria

A detection by a single seismic station is usually considered insufficient to declare an event, due to the high false alarm rate experienced by seismic stations. Usually detections by three or more stations are needed. This is because a location estimate is considered necessary to form an event. If the event cannot be located, then the signals may be no more than random false alarms with no

time or location correlation. The time-of-arrival analysis used to estimate event location needs at least three stations.

IVSEM takes the individual station detection probabilities and generates the probability of each specific number of stations detecting the event. These probabilities are used with a detection effectiveness table to give the probability of the network declaring a detection as a function of the number of stations which detect an event. The final output is a network effectiveness figure, which can be considered as the probability that at least N stations detect the event, the value N being in the input tables.

Location

The location of events is computed by using signal time-of-arrival data. Given detections at several stations, and good characterization of the velocities of the waves in the surrounding media (called travel time curves), a series of equations in several unknowns can be solved to determine the most probable location for an event, based upon the distance the wave has traveled from the source to each station. The result is an approximation of the location of the event. The process used to model this is complex, involving repeated iterations to minimize the sum of residuals in the system of equations.

The errors in the travel times are internally generated in the model. They are assumed to be a 0.75 sec model time error, and an arrival time error equal to 0.15/(signal-to-noise ratio-1). Both are rms errors. An input scale factor can be used as a multiplier to modify the internal travel time errors, to make a network either more or less accurate than the default values would indicate.

Identification

Identification is not currently modeled in IVSEM. Only the short period P waves from .8 to 5 Hz are modeled. None of the regional phases, which have frequencies up to 10 Hz, or the S waves, which are below 1 Hz, are included. In order to perform identification analysis, these waves would need to be modeled. A future version of IVSEM may include identification.

Inputs

The inputs for the seismic module of IVSEM are contained in three files. The first file, VSEMINP.INP, contains data to control the code and information pertaining to the event. A list of the inputs in this file that pertain to the seismic model follows.

1. A switch to control whether a single event is to be modeled or if a global contour map is to be generated

2. Yield of the event in kilotons
3. Location of the event: latitude, longitude, and depth or height of burst in kilometers
4. A flag to control whether the seismic model is to be used in this particular run
5. The input decoupling factors, which are:
   a. The medium factor(hard rock, soft rock, etc.)
   b. The ocean factor. This is a medium factor to be used if the position of the event is in an ocean area
   c. The decoupling factor due to evasive attempts
6. The threshold signal-to-noise ratio.
7. The scaling factor for location accuracy

The second file is the station network file. Its name is VSEMSZM.INP. It contains information on the seismic station network. The top line contains identifying information for the particular network contained in the file. A separate line for each station contains the following data:

1. A switch to turn that particular station on or off for the run
2. The location in latitude and longitude coordinates
3. A switch to indicate whether the station is primary or auxiliary. Primary stations are used for detection and location. Auxiliary stations are not used for detection, but only for location determination. In addition, the reliability factors for the two types of stations are different, as indicated earlier.
4. The number of array elements
5. The noise factors for the five regional and teleseismic amplitude-distance equations
6. The station name and/or identification code

The final file is called LANDSEA.DAT. This is basically a world map in two degree latitude and longitude blocks. For each block, an integer between 0 and 5 is associated. The meaning of the integer value is thus:

0 = Stable ocean
1 = Unstable ocean
2 = Stable ocean (blocked for hydroacoustic transmission)
3 = Unstable ocean (blocked for hydroacoustic transmission)
4 = Stable land
5 = Unstable land

Four numbers are used for the ocean because LANDSEA.DAT is also used for the IVSEM hydroacoustic model, and the value of the integer also indicates if a hydroacoustic path exists in this block. Numbers two through five indicate that the hydroacoustic paths are blocked in that region.

Example Results

For the global contour map option in IVSEM, events are laid down worldwide on a grid 7.5 degrees apart in latitude and longitude. Probabilities of a network declaring a detection are shown as colored contours. Figure B5 shows an example of a simulation producing detection contours for a small partially decoupled explosion. The station network, which is purely hypothetical, is shown in Figure B6. The network is similar to the International Monitoring System seismic network, which is composed of primary and auxiliary stations. Only the primary stations function to detect an event. Once an event is detected, the auxiliary stations are called in to refine the location estimate. The primary station locations are shown as green dots in Figure B6, while the auxiliary stations are red dots.

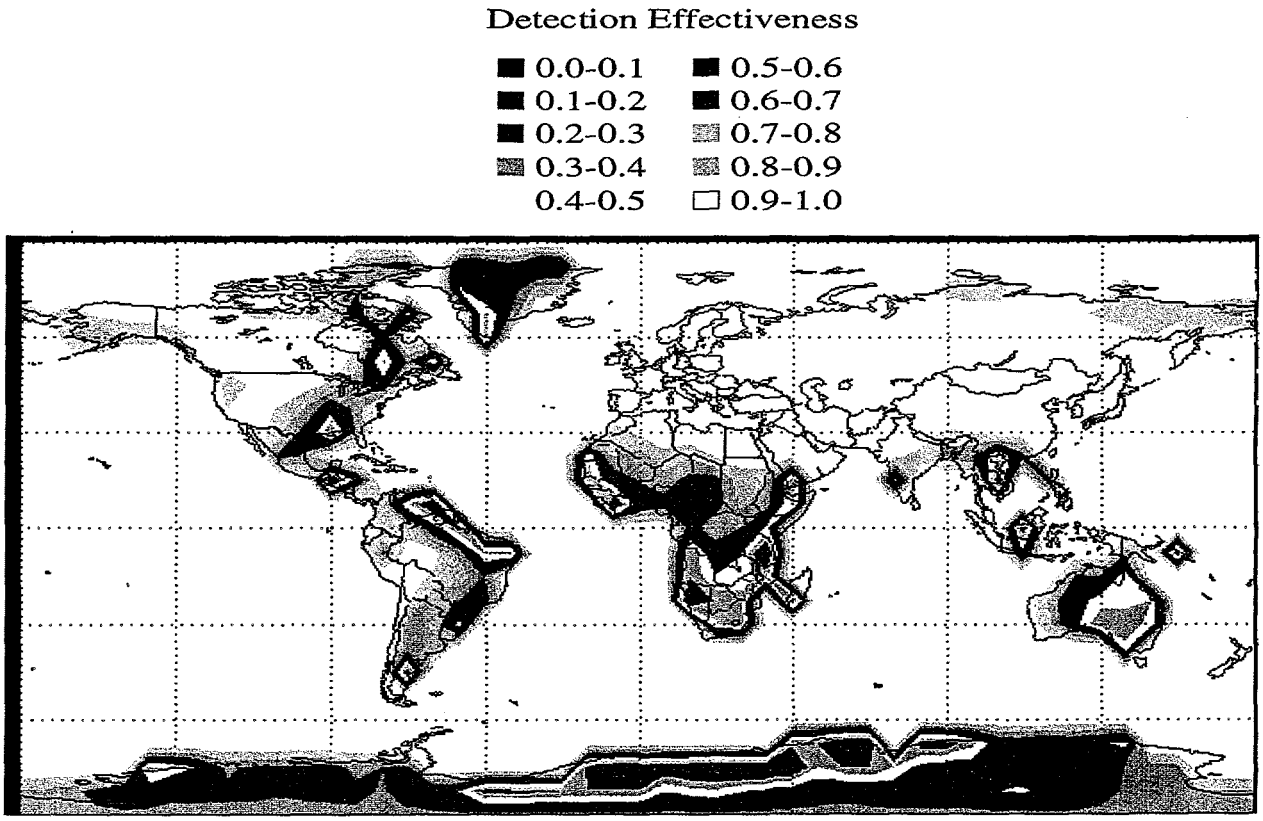

Figure B5. Sample Seismic Detection Contours

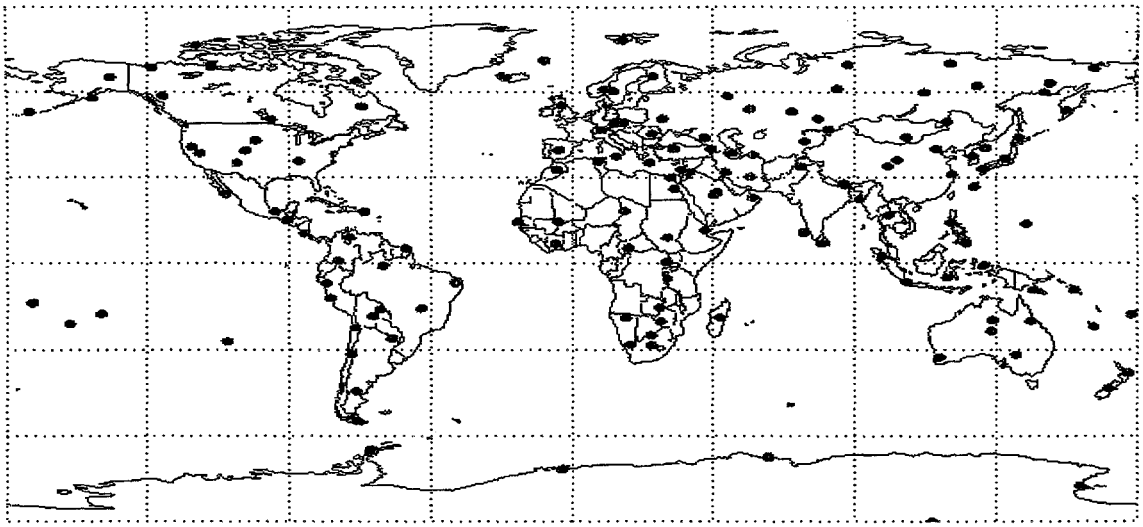

Figure B6. Seismic Station Locations

When the contour map option is selected, the results of the location accuracy analysis are shown as contours that indicate the size of 90% confidence intervals. That is, they show the size, in square kilometers, of an ellipsoid around the estimated event location in which there is a 90% probability that the actual event took place. Figure B7 shows the location accuracy contours for the same simulation run that generated the detection probabilities in Figure B5.

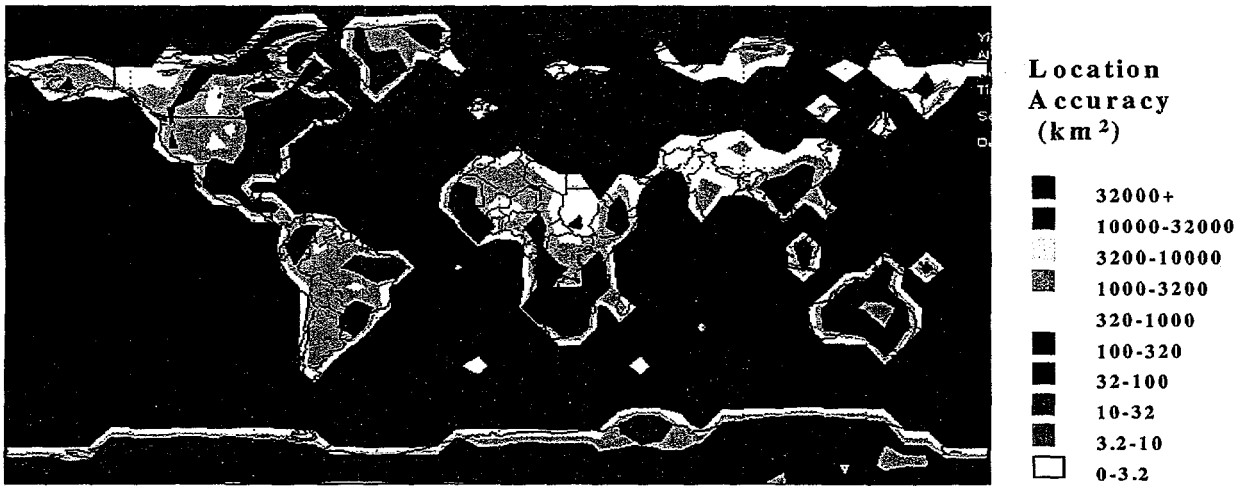

Figure B7. Sample Location Accuracy Contours

Validation

In order to perform validation upon the model, the results were compared to results obtained from the NETSIM model, a validated, generally accepted seismic network model. The NETSIM results from the same frequency regions that are modeled in IVSEM were examined.

Figure B8 presents detection results of a single event against a single receiving station. The event has a seismic magnitude of 4. The event is in an unstable region and the receiving station is in a geologically stable region. A low noise situation is present, characteristic of a well designed and sited seismic station. In this run the stations are characterized as three-axis stations, not arrays.

In the close in region, detection probability is very high. A steep drop in the detection probability occurs at about 2500 km. This is where the transition from regional to teleseismic effects occur. Several P wave propagation modes which are effective at shorter ranges cease to work at this distance, and only the deep body waves are transmitted. There is a dip in the probability of detection at 3200 km. The signal strength is dependent upon the geological properties of the path that the signal takes. According to the data of Veith and Clawson, there is poor transmission at the 800-1000 km depth. This strongly affects signals received at a distance of 28-29 degrees, or approximately 3200 km. Finally, in the region between 15,000 and 20,000 km, a large rise in detection probability occurs, due to the phenomenon of the PkP waves. These are waves that are reflected by the earth's core and are focused at the surface in this region.

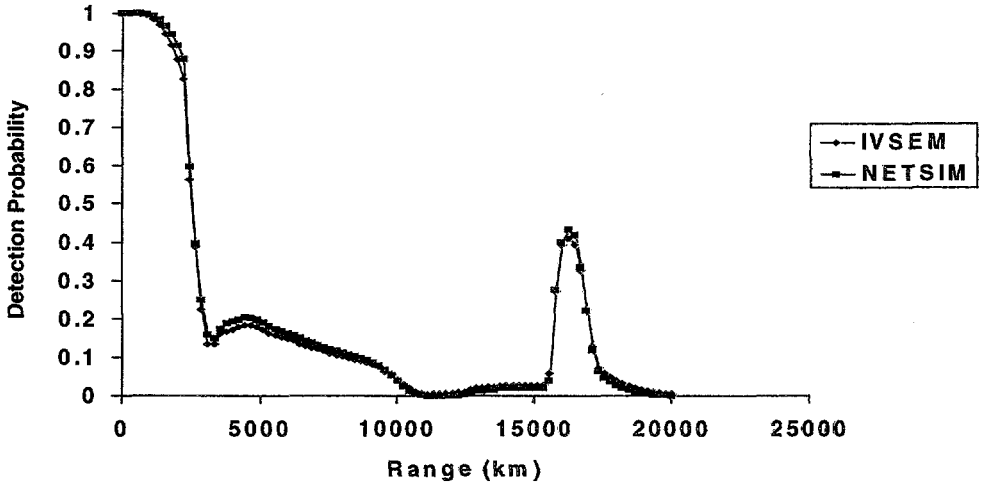

Figure B8. Detection Probability Versus Range for a Magnitude 4 Event with Low Noise

As a step in the validation process, these results were compared with results from the validated NETSIM seismic network model. As can be seen, there is excellent agreement between the two models.

Figure B9 presents detection probabilities for a case where the noise at the receiving stations is 10 dB higher than in the preceding case. It can be seen that the detection probabilities fall off much more rapidly and the PkP phenomenon is nearly totally suppressed.

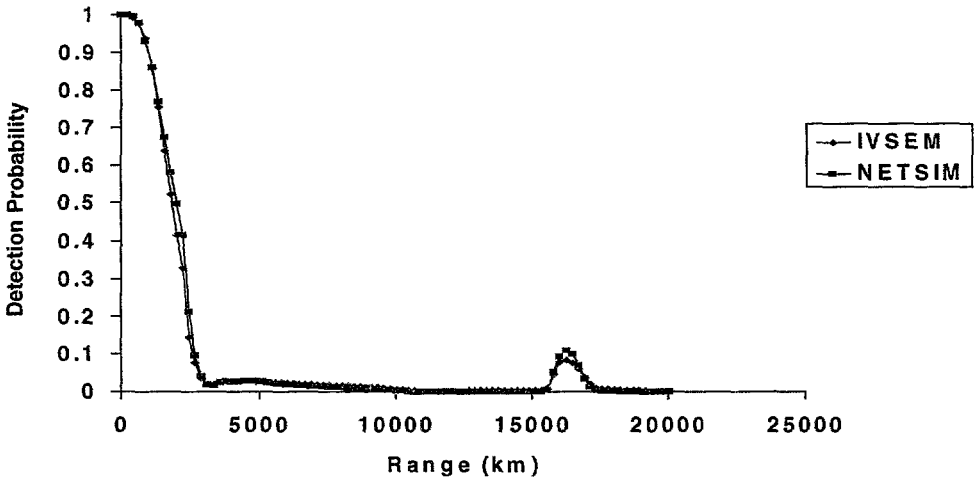

Figure B9. Detection Probability Versus Range for Magnitude 4 Event with High Noise

Figure B10 shows detection probabilities for a magnitude 5 event. As expected, the detection probabilities are much greater than for the magnitude 4 event at the same range.

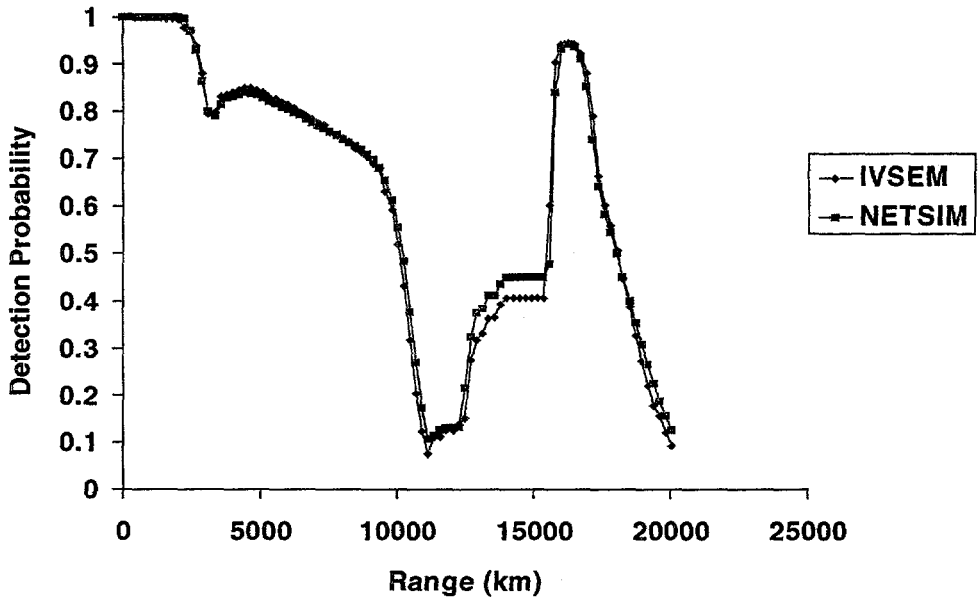

Figure B10. Detection Probability Versus Range, Magnitude 5 Event

Figure B11 presents the detection probabilities for magnitude 5, high noise event with a high decoupling factor. It can be seen that the probability of detection beyond about 2000 kilometers is essentially zero.

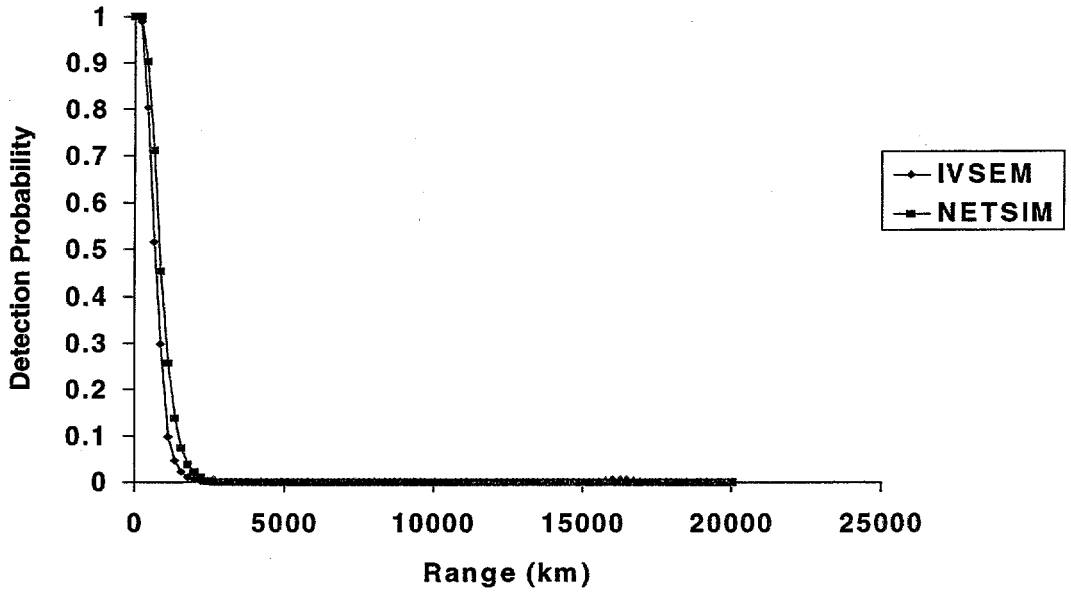

Figure B11. Detection Probability Versus Range, Decoupled Event

As can be seen in Figures B8 through B11, excellent agreement was obtained for single event cases.

Figures B12 and B13 show NETSIM detection contours compared to IVSEM contours for the same inputs. It can be seen that in general there is good agreement between the results. IVSEM yields slightly higher probabilities of detection in some areas, especially in parts of the Pacific. Limitations in the plotting routine of NETSIM make the differences look greater than they actually are. The NETSI plot above presents all detection probabilities less than .30 appear as the same shade. Thus the oceans show little detail.

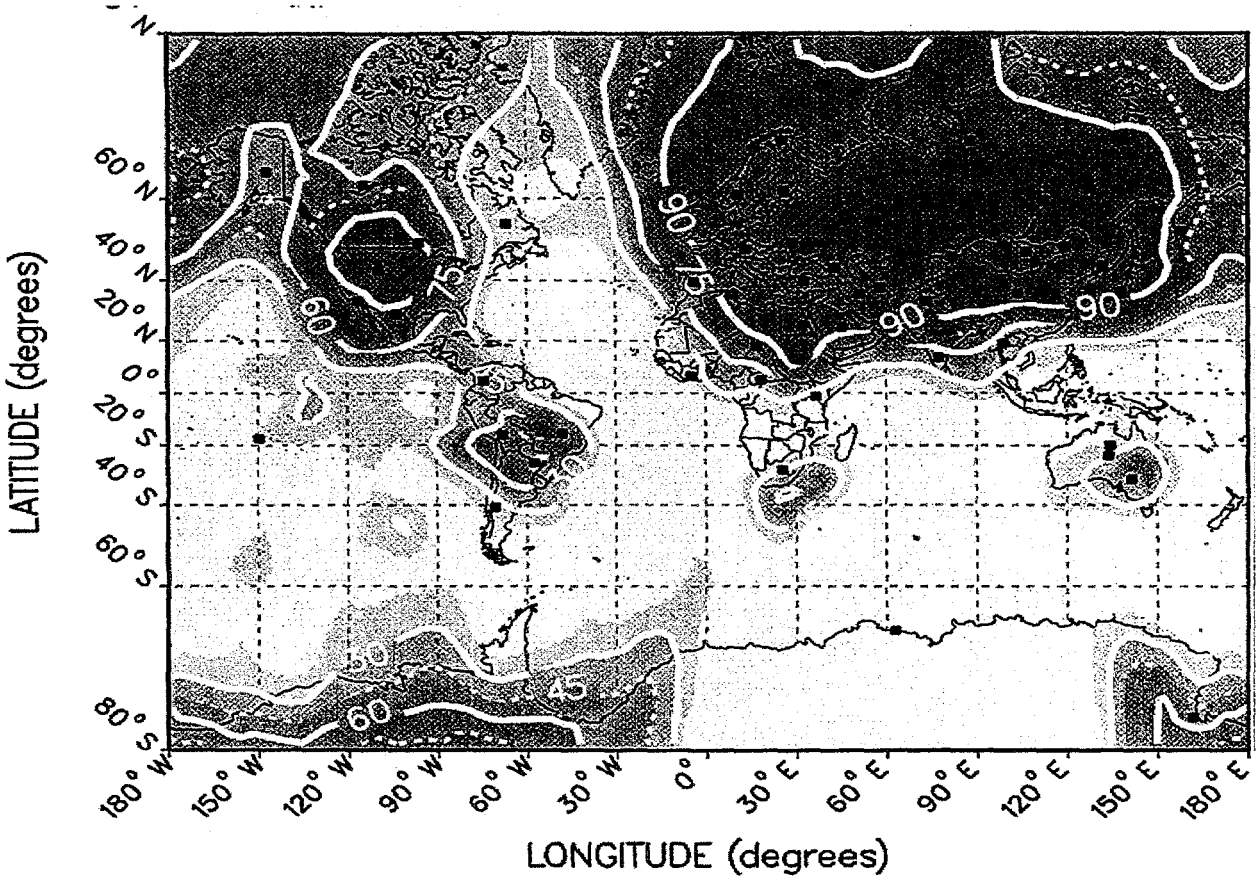

Figure B12. NETSIM Detection Contours for Magnitude 3.5 Event, WP.330 Network

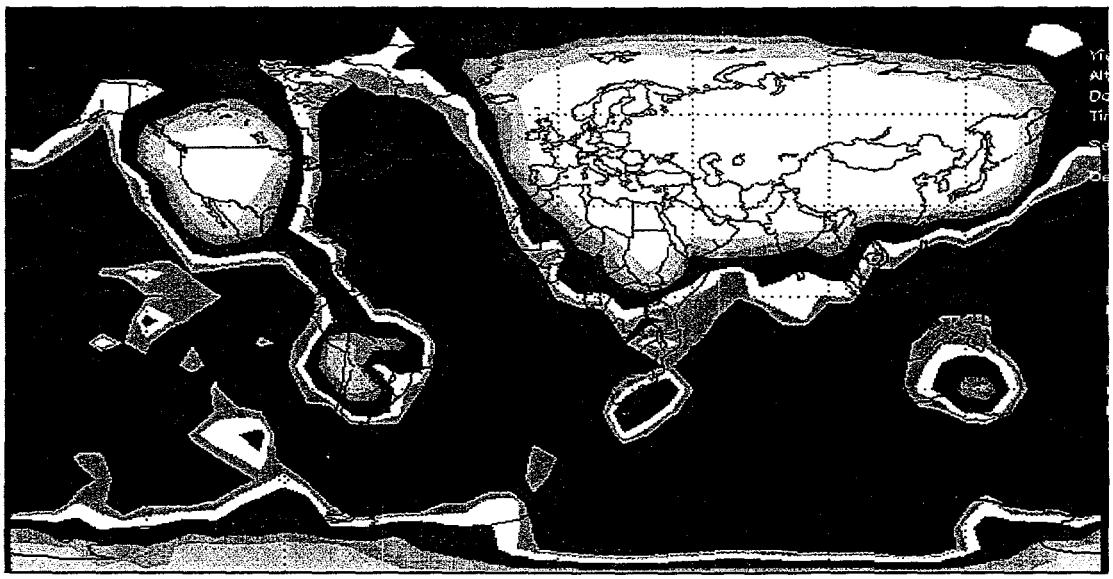

Figure B13. IVSEM Detection Contours for Magnitude 3.5 Event, WP.330 Network

Limitations

As this model is intended to be a simple, top-level simulation, there are certain limitations. In this model, only the P waves in the 1-5 Hz region are used for detection. Regional phases in the 5 to 10 Hz range are not used. In addition, seismic stations can use S waves for detection of actual events. Since IVSEM does not model S waves, the effect of this is to produce conservative detection results. Except for depth of burial effects coupling is not computed in the model but is left for the user as an input. This places the responsibility upon the user to input the most correct values possible. The model divides the earth into two geologies - stable and unstable. Except for this, regional propagation characteristics due to geology are not treated. Yield estimation is not modeled. Depth determination is not performed by this model, so the location output is the epicenter only. Finally, as stated above, IVSEM version 1.2 does not perform identification. This would require IVSEM to model signals at multiple frequencies, in place of the optimum frequency envelope approach currently used.

Summary

This code will perform a good first-level simulation of the seismic detection process, sufficient to perform tradeoff studies and preliminary network evaluations. We anticipate that later versions of IVSEM will model the identification process. Detection validation of this model against the more detailed NETSIM simulation has been performed, and good agreement has been obtained. As described above, there are some limitations to the model. It does demand a knowledgeable intelligent user, as careless use can result in misleading results.

References

Adushkin, 1995. V.V. Adushkin, "Monitoring of Underground Nuclear Test by Seismic Stations in the Former Soviet Union (FSU)", Monitoring a Comprehensive Test Ban Treaty, NATO ASI Series, Vol. 303, 1995.

Bache, 1982. T. C. Bache, "Estimating the Yield of Underground Nuclear Explosions", Bulletin of the Seismological Society of America, Vol. 72, NO. 6, pp. S231-S168, 1982.

Day, 1986. S. M. Day, N. Rimer, T. G. Barker, E. J. Halda, and B. Shkoller, "Numerical Study of Depth of Burial Effects on the Seismic Signature of Underground Explosions", S-Cubed, DNA-TR-86-114, 1986.

Evernden, 1967. Evernden, J. F. , "Magnitude Determination at Regional and Near-Regional Distances in the United States", Bulletin of the Seismological Society of America, Vol. 57, No. 4, August, 1967, 591-639.

Marshall, 1979. P. D. Marshall, D. L. Springer and H. C. Rodean, "Magnitude Corrections for Attenuation in the Upper Mantle", Geophysics Journal of the Royal Astronomical Society, Vol. 57, pp 609-638, 1979.

Wortman, 1994. W. Wortman, T. McCarter, C. Longmire, L. J. Nichish, S Chavin, T Barker, and J Murphy, "Assessment of Techniques for Nuclear Testing That Evade Detection", Mission Research Corporation, MRC/WDC-R-340, 1994.

Veith, 1972. K. F. Veith, and G. E. Clawson (1972), "Magnitude from Short-Period P-Wave Data", Bulletin of the Seismological Society of America, Vol.52, No. 2 April 1972, pp 435-452.

APPENDIX C. INFRASOUND DETECTION

Introduction

The purpose of the infrasound module in IVSEM is to provide a simple, fast-running detection and location model of an infrasound network that can be used to perform first order analysis of network effectiveness. This effort was undertaken by Organization 5415, Sandia National Laboratories Albuquerque (SNLA), with support by Organization 5700, SNLA for use by US government agencies and their contractors supporting the Comprehensive Test Ban Treaty (CTBT) negotiations and the ratification process. This work was started in August 1994.

Infrasound monitoring is based upon the detection of low frequency sound waves from nuclear events. These waves, which have frequencies of 10 Hz and below, are the extremely attenuated remnants of the shock waves produced by events. These waves travel by refraction of the upper atmosphere, and are detected by low frequency microphones or microbarographs. Infrasound signals are a good means of detection for atmospheric nuclear events, because the waves can travel thousands of kilometers through the atmosphere and be detected. Bearing and signal arrival time analysis can be used with a network of stations to produce an estimate of event location as well

Figure C1 is an example of infrasonic signals detected from a large HE explosion. Note that the frequency of the waves is about 1 Hz. This data was collected by LANL at a series of stations from the Misty Picture event in 1987. This was a DNA high explosive event conducted at White Sands. The charge weight was 4800 tons of ammonium nitrate and fuel oil. This has an explosive yield equivalent to 7.7 kilotons. The stations were at Los Alamos, New Mexico; St. George, Utah; Bishop, California; and Bakersfield, California. The distances from the event were approximately 260 km, 750 km, 1160 km, and 1160 km, respectively.

In the late 1950s and the 1960s, infrasonic detection stations were a major part of the US nuclear detection network. Stations were located in a world wide network of more than 15 stations. When satellite-based detection systems became available, and testing largely moved underground, the infrasonic network was discontinued. Infrasonic monitoring has become of interest recently because of the CTBT negotiations. Infrasound detection is one of the four technologies included in the International Monitoring System. It was included because it offers a relatively cheap, reliable means of detecting atmospheric tests. It is believed to be cheaper than satellite-based systems and it offers more prompt detection means than radionuclide detection, as well as being able to perform location estimation. It is also believed to be relatively resistant to evasive attempts.

Directly propagated infrasonic waves attenuate too rapidly to be detected beyond a few hundred km. Long distance propagation of infrasonic waves in this model is based upon their refraction from high altitudes. High altitude winds produce a turnaround at altitudes of 50 km. The waves traveling upward are turned around and travel back to the ground. The refracted waves descend and reflect from the earth to return to high altitude and are refracted again. This process can be

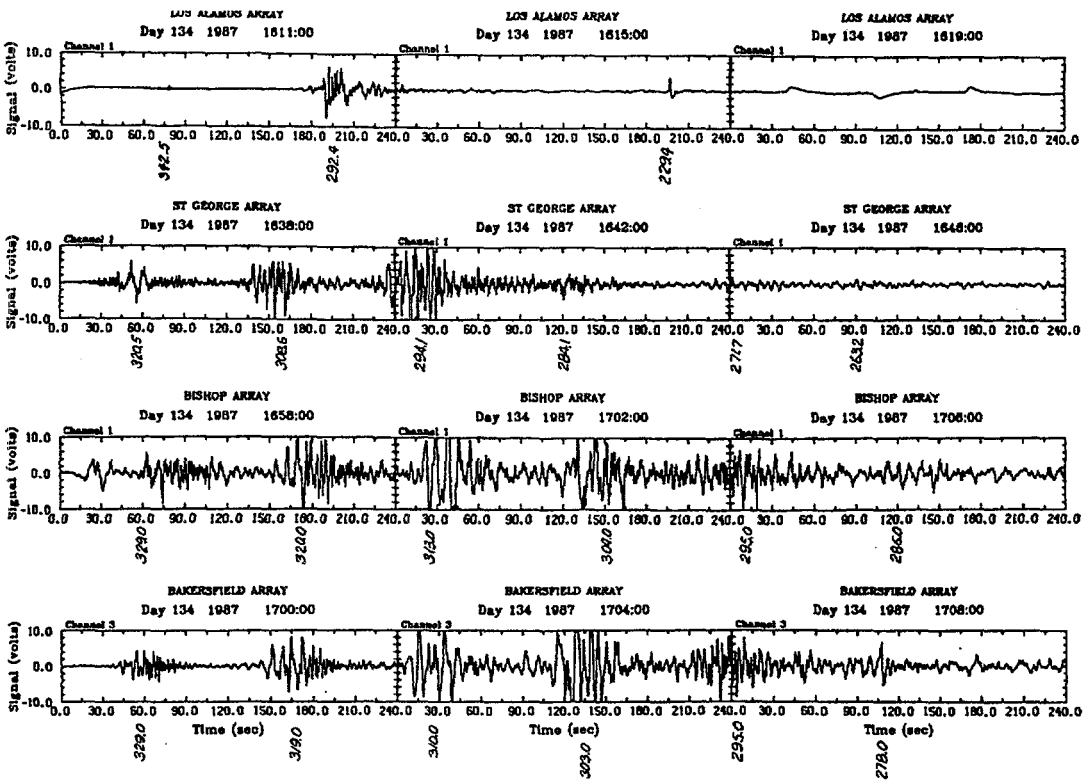

Figure C1. Sample Infrasound Data

repeated several times over distances of thousands of km. In addition, the temperature profile of the atmosphere produces a refraction effect that results in a total turnaround of upwardly directed infrasonic waves at an altitude of 90-110 km. The infrasonic waves can be detected by very sensitive microphones or microbarographs. Figure C2 shows different propagation modes that infrasound signals can use. Data from LANL indicates that the 50 km signal is stronger for explosion-produced waves than the 100 km signal, and this signal type is used in IVSEM.

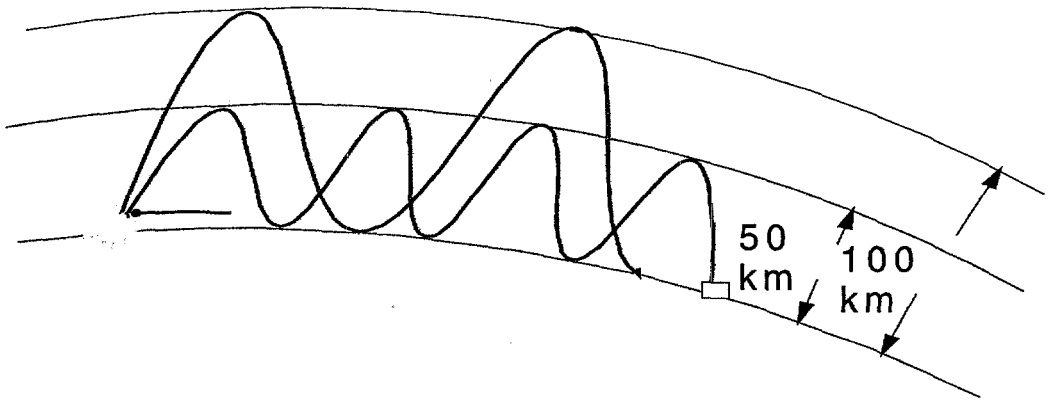

Figure C2. Infrasound Signal Propagation Modes

Overall Process

The basic approach taken in the model is empirical. Data obtained from observations of nuclear and large high explosive events have been scaled to find the signal amplitude as a function of distance from a standard one kt atmospheric burst. The signal pressure is then multiplied by the square root of the effective yield of the event, a standard method of pressure scaling for blast waves.

Effective Yield

The effective yield is the true yield as input, modified by height of burst effects. The shock wave from an atmospheric event will be reflected from the ground. The reflected shock wave can combine with the upward traveling shock wave to form a single stronger shock. This reflection effect can be modeled as an increased effective yield. Figure C3 shows effective yield as a function of height of burst. The data used for above ground bursts was taken from Reed, 1969. Note that shallow underground bursts can be input for simulation runs. The data used for effective yield from underground events was obtained by the use of the DWSA code NEMESIS (DNA, 1995). The overpressure at 1 km from 1 kt events at increasing depths was used to obtain a curve for effective yield versus depth of burial.

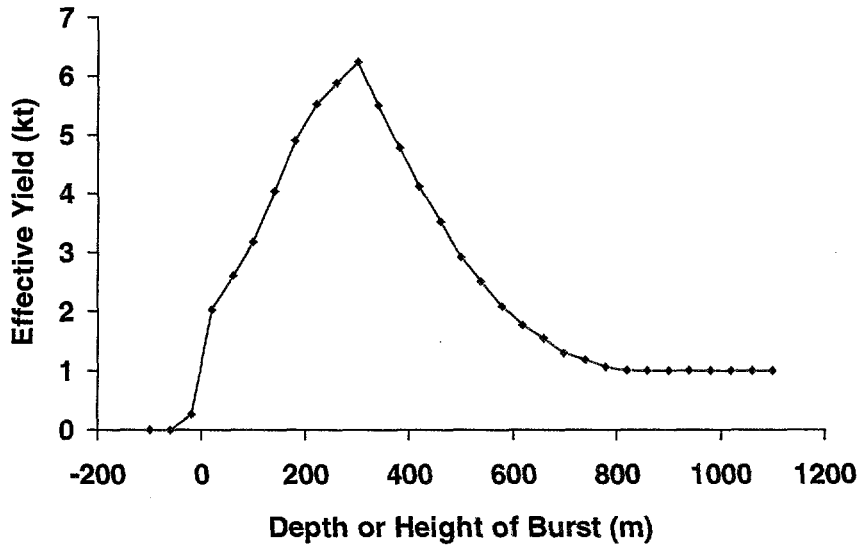

Figure C3. Effective Yield of a 1 kt Event as a Function of Height of Burst

Propagation

Figure C4 shows the data that was used to generate the basic empirical relationship used to calculate the signal strength as a function of effective yield and distance. This is a combination of data taken from numerous reports.

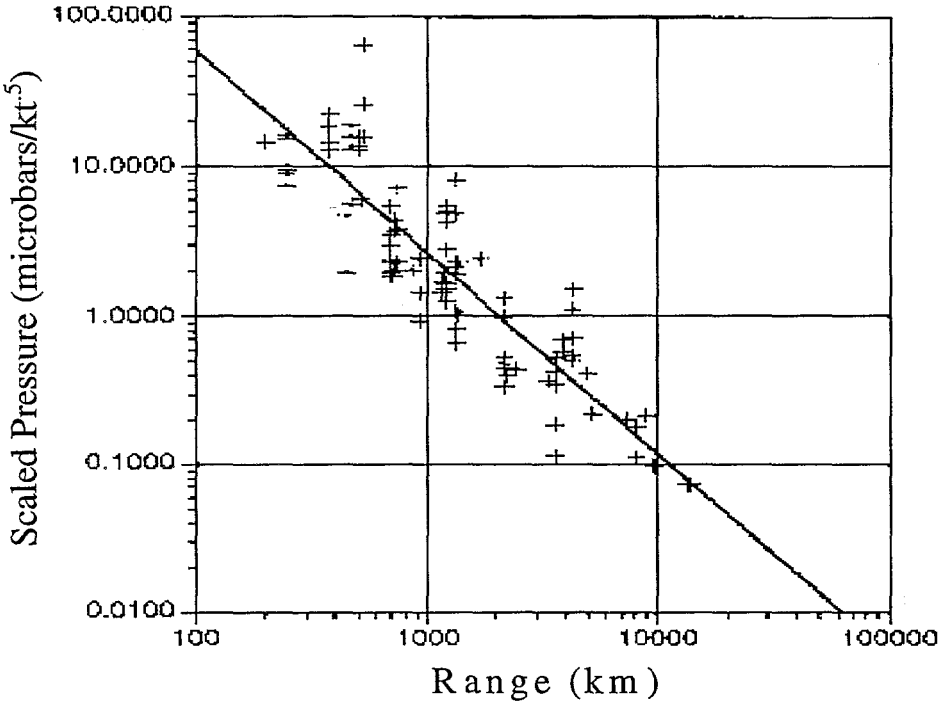

Figure C4. Signal Amplitude Versus Range Data

An equation was fit to the data and is shown by the line in Figure C4. It is shown here:

$$P = (29374)(Y^{.5})(R^{-1.349}) \qquad \text{(C1}$$

P = pressure in microbars
Y = effective event yield in kilotons
R = distance from the source in kilometers

The data was collected from early nuclear atmospheric tests and later high explosive tests. The equation was fit to the data at a model review meeting in October 1995. This equation is believed to represent the return from the 50 km region, which predominates.

High Altitude Wind Effects

A phenomenon that has been observed in connection with infrasound observations of nuclear and large high explosive events is that the signal strength is dependent upon the event-to-station geometry, and this dependence varies with the season. The source of this effect is the strength and direction of the winds in the 50 km refraction zone. In simple terms, a signal propagating upwind is weaker than a signal propagated crosswind at the same distance, and a signal propagating downwind is stronger than the crosswind signal. The predominant winds in the 50 km altitude band are the east-west winds, called the zonal winds. The north-south winds, called the meridional winds, are of much smaller magnitude, averaging 10% or less the strength of the zonal winds. These winds vary according to season and latitude. Figure C5 shows monthly averages for zonal winds at the Equator, 30 degrees North Latitude, and 30 degrees South Latitude as a function of the time of year. Positive values indicate a west to east wind, while negative numbers indicate an east to west wind.

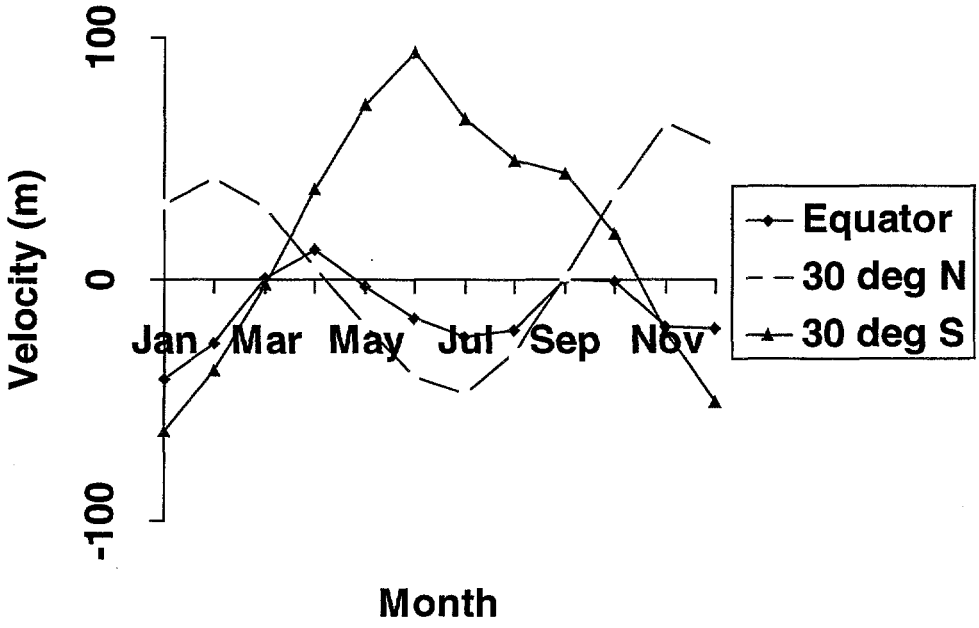

Figure C5. Zonal Wind Velocities

Note that the data for the Southern Hemisphere are not symmetric with respect to the Northern Hemisphere data. This may be due to the greater ocean surface area in the Southern Hemisphere. The data used in the model were obtained from data published by the Committee on Space Research of the International Astronautical Federation (COSPAR, 1972), and W. L. Webb (Webb, 1967). The data is incorporated in the model as monthly averages in 10 degree latitude zones.

A correction for upper atmospheric winds is applied to the basic signal amplitude, Equation C1, derived from the data in Figure C4. An average wind velocity is found along the path between the event and the receiving station. The projection of this average velocity vector along the signal propagation path furnishes a value that is input into the following equation:

$$W = 10^{(.173V)} \qquad \text{(C2}$$

V = wind velocity along the path from the event to the station in meters /sec
W = dimensionless signal amplitude correction factor

This equation is derived from data collected by LANL (Mutschlecner 1990). The signal amplitude derived from the empirical signal amplitude equation is multiplied by this factor to find the wind corrected amplitude at the infrasound receiving station.

Figure C6 shows the effect on the signal amplitude as a function of the wind velocity. The event is a 1 kt, free air event. The event-to-station distance is 1000 km. Positive wind values indicate that the direction of the wind is from the event to the station, while negative wind values indicate that the signal is traveling upwind. The signal strength obtained from the amplitude-distance equation is the value at 0 meters per second. It can be seen that the signal strength will vary greatly, depending upon the strength of the wind.

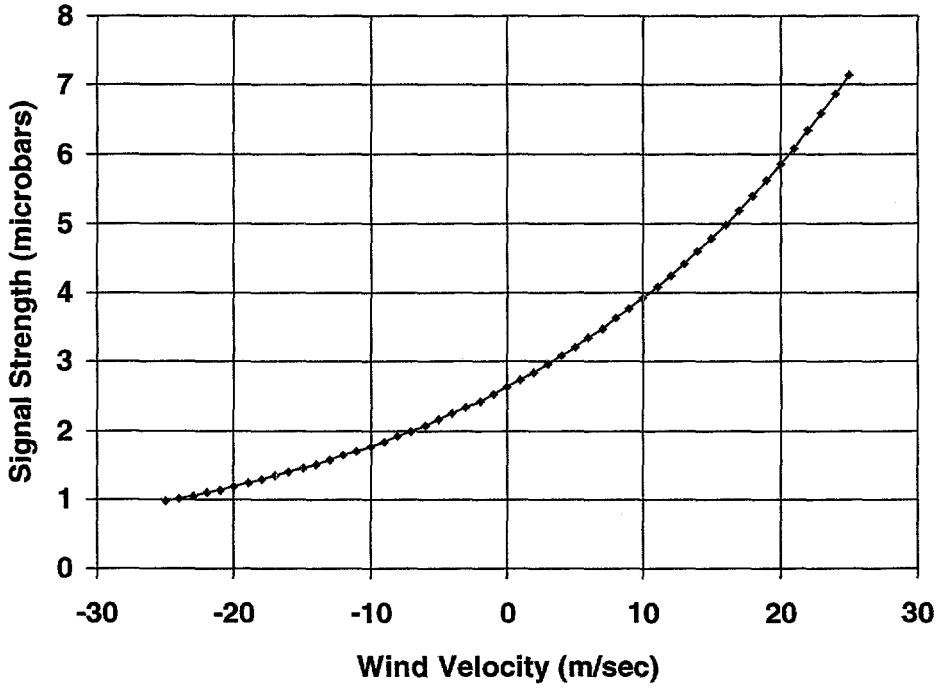

Figure C6. Signal Strength as a Function of 50 km Winds

Detection

The former US network was used to monitor early Soviet atmospheric tests. Many of these were in the multiple megaton range, and were very easily detectable. (For example, the Soviet 58 megaton test in 1960 produced three signals at one station: the signal arriving directly at the station, the signal that traveled around the world in the opposite direction, and the direct signal after it had traveled around the world again.) Recent US work has concerned large HE tests at White Sands and most of the stations were located within 1500, km of the events. With this emphasis on large events, not much work has been done to model the effect of and collect statistics for local station noise.

For the IVSEM model, it is currently assumed that the signal and noise for infrasonic detection are normally distributed. The signal mean value is calculated using equations C1 and C2, and we assume it has a standard deviation of 60% of its mean value.

The noise is a function of the local wind velocity. Wind blowing over a microphone or a microbarograph will apply a pressure to the instrument. Because of turbulence and wind fluctuations, the pressure is constantly changing, but the pressure and its fluctuations can be related to average wind speed. The instrument nulls out the average pressure and only measures fluctuations in pressure; thus, the mean value of the noise is 0. The values for noise standard deviation currently used in IVSEM are calculated from the local wind velocity according to equation C3:

$$N = \begin{cases} .4V, & V < 5.00 \text{ m/s} \\ .035V^{2.5}, & V > 5.00 \text{ m/s} \end{cases} \qquad \text{(C3}$$

V = local wind speed in meters per second
N = standard deviation of wind noise in microbars

This equation is based on work performed at NOAA and LANL (Bedard, 1992). The noise equation for low wind speeds is the Bedard linear relationship. The equation for high wind speeds was developed to furnish values midway between the Bedard square and cube relationships. For IVSEM runs, the local surface wind velocity for each station is based either on user supplied inputs for each station or global wind data which supplies monthly wind velocity statistics based upon the station latitude and longitude.

An infrasound station may use a system of porous hoses or pipes to decrease the local noise. This results in a reduction of the noise by a factor that may be four or higher. The exact value is a function of the type of hose system used. The noise reduction factor is a user-defined input.

A standard signal processing approach is used to model the detection process. Figure C7 shows this process. Gaussian signal and noise statistics are assumed. A gaussian signal plus noise curve is computed, and the area under the curve is integrated to determine the probability of

detection. The threshold is set to a multiple of the noise sigma. The exact multiple is a user input.

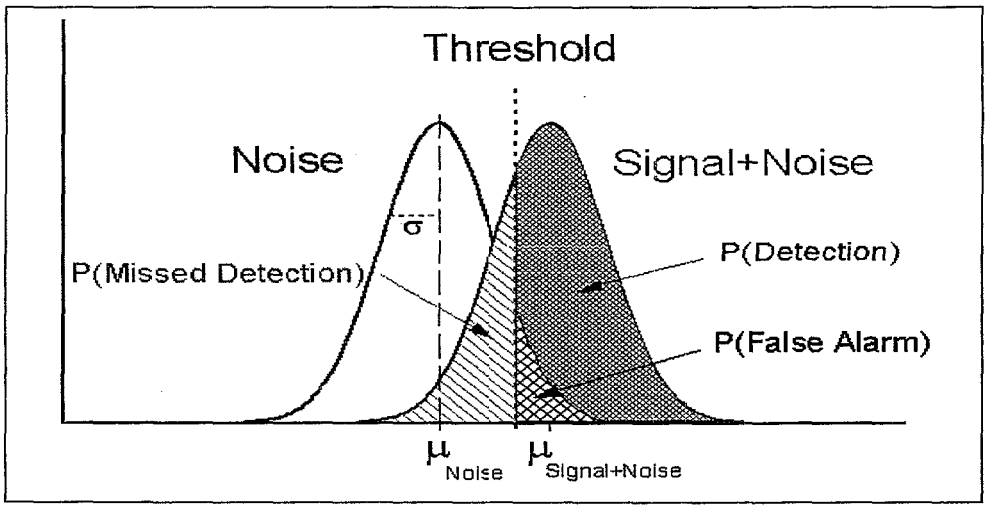

Figure C7. Signal Detection Process

Network Detection Criteria

A detection by a single station is usually considered insufficient to declare an event. Usually, detections by several stations are needed to factor out single station anomalies and because a location estimate is considered necessary to form an event. The time-of-arrival analysis used to estimate event location needs at least three stations to form an event. Infrasound stations can produce bearing estimates as well as time-of-arrival estimates. Two or more bearing estimates can be used for triangulation to estimate event location and form an event.

IVSEM takes the individual station detection probabilities and generates the probability of set numbers of stations detecting the event. These probabilities are then modified by the use of detection effectiveness tables, which give the probability of the network declaring a detection as a function of the number of stations which detect an event. The final output is a network effectiveness figure, which can be considered as the probability that at least N stations detect the event.

Location

Location estimation is based upon both time-of-arrival analysis and triangulation from bearing estimates. In IVSEM, each infrasound station is treated as two stations for location accuracy determination purposes. One station participates in time-of-arrival analysis and the other participates in triangulation. A series of Monte Carlo trials is performed where an estimated

event location is found which minimizes the sum of arrival time and bearing residuals. This estimate is compared to the true event location. The area in which 90% of the estimated locations fall is the figure of merit for location accuracy analysis.

The bearing and time-of-arrival standard deviations are integral to the model. For infrasound, the rms bearing errors are as follows: 1.8 degrees, for event-to-station distances less than 3000 km. For 3000 km to 4000 km, the bearing sigma increases linearly up to 7.1 degrees. For 4000 to 10000 km station to event distances, the error is 7.1 degrees. From 10000 to 15000 km, the error increases from 7.1 to 27.5 degrees. Above 15000 km, it remains at 27.5 degrees. The arrival time error is 2 percent of the travel time.

Identification

Identification is currently not treated in the IVSEM model.

Inputs

The inputs for the infrasound module of IVSEM are contained in three files. The first file, VSEMINP.INP contains data to control the code and information pertaining to the event. A list of the inputs in this file that pertain to the infrasound model follows.

1. A switch to control whether a single event is to be modeled or if a global contour map is to be generated
2. Yield of the event in kilotons
3. Location of the event: latitude, longitude, and depth or height of burst in kilometers
4. A flag to control whether the infrasound model is to be used in this particular run
5. The detection threshold value
6. Scaling factors for location accuracy
7. The time of year

The second file is named VSEMISN.DAT and contains the station network data. The top line in the file contains identification data. The rest of the file contains one data line for each station. Each entry has the following information:

1. An on-off switch for each station
2. The station latitude and longitude
3. The number of elements in each station array
4. The noise reduction factor produced by a noise reduction system
5. The local wind velocity in meters per second (If the value is 999, the local wind speed is read from the model's wind data file)
6. The station name or station code for identification

The third file is named WIND.DAT. This contains wind data for use in generating station noise levels..

Examples Of Results

Single Event Detection

Figure C8 shows detection probabilities as a function of range for a small air burst. The event takes place at 0 degrees longitude and 0 degrees latitude at an altitude of 1000 m. A series of stations was placed due north, south, east, and west of the event. July high altitude wind conditions were assumed. A 6 km/hr surface wind speed at each station was input. It can be seen that the detection range differs greatly between east and west, but not between north and south. This is a result of the high altitude east winds that prevail in July.

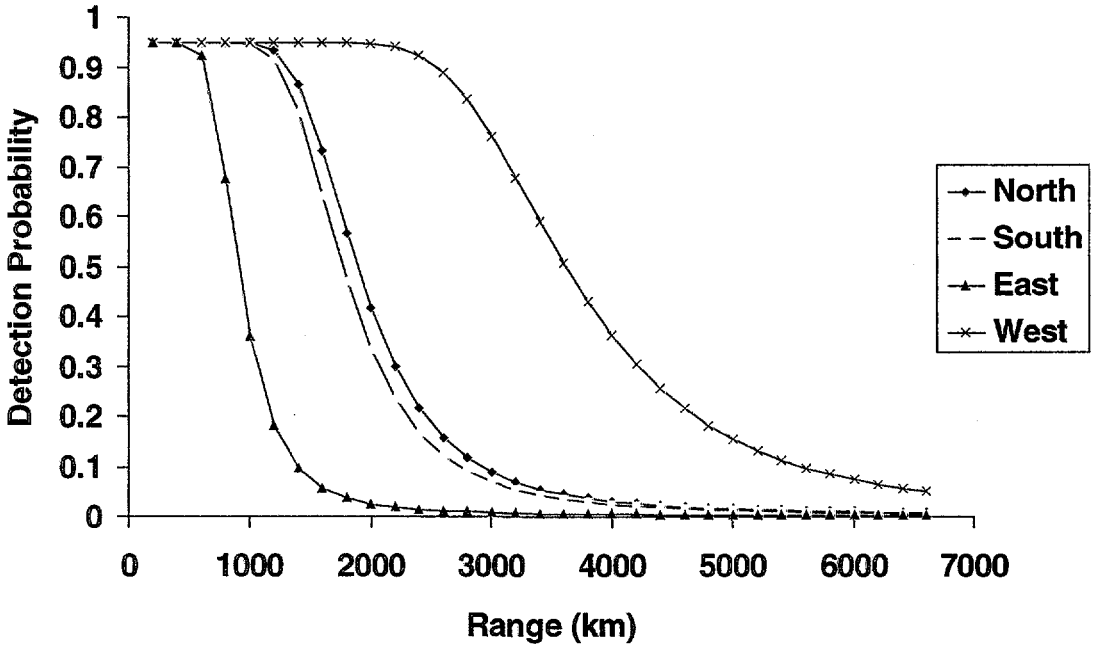

Figure C8. Detection Probability Versus Range for a Small Event

Detection Contours

If the proper switch is set in VSEMINP.INP, a single event is not modeled. Rather, events are laid down on a worldwide grid 7.5 degrees apart in latitude and longitude. Probabilities of the network declaring a detection are shown as colored contours. Figure C9 shows an example of

IVSEM detection contours for a small atmospheric event in a particular month. The legend above the contour map explains the color code used.

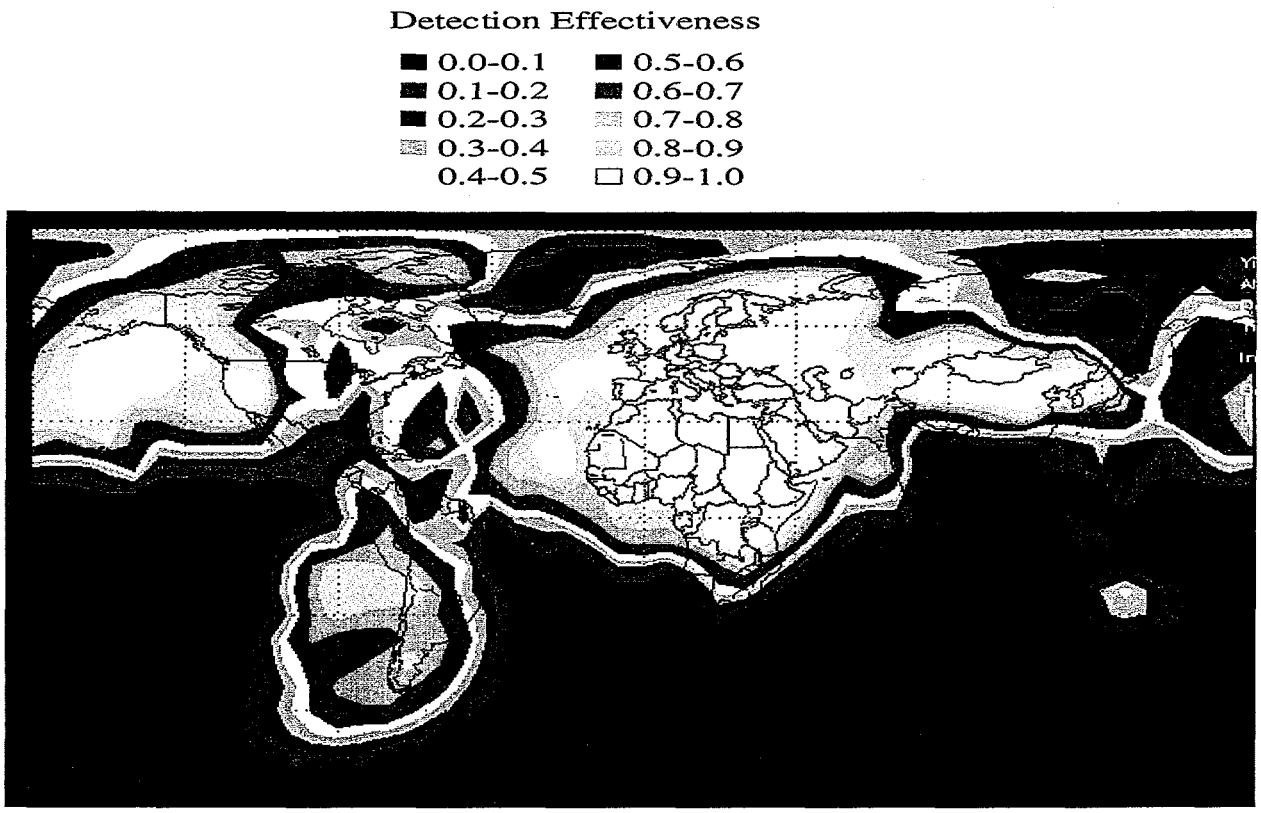

Figure C9. Sample Detection Contours, Small Atmospheric Event

The station network, which is purely hypothetical, is shown in Figure C10. The station locations are shown as green dots.

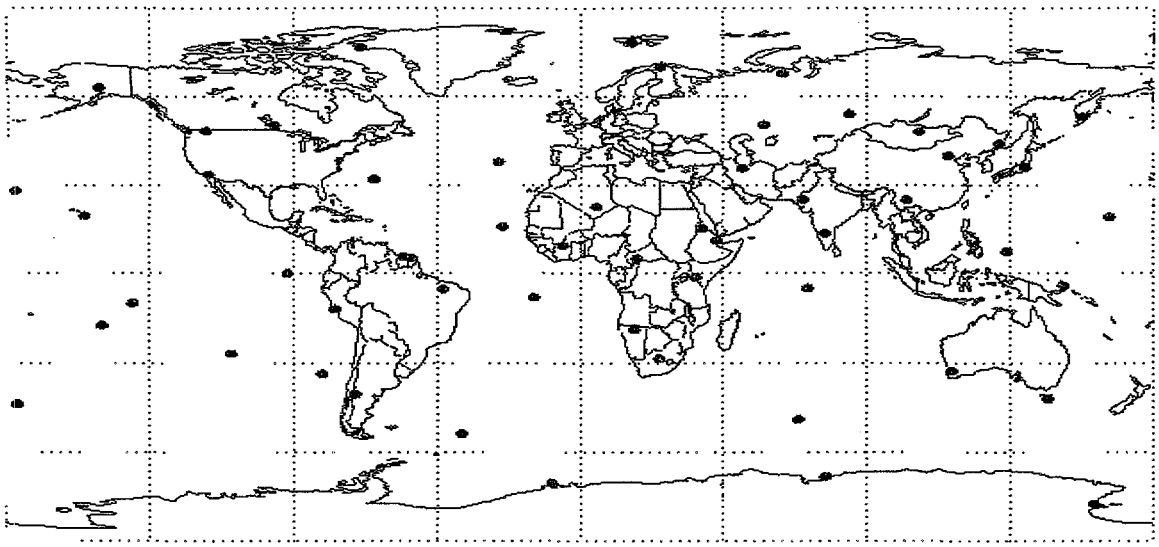

Figure C10. Infrasound Station Locations

Location Contours

Figure C11 shows contours of location accuracy for the same simulation that produced the detection contours in Figure C9. It can be seen that there are large areas where location accuracy is very poor for this network. As explained earlier, the location performance is based upon the historical performance of the former US national network. It is possible that newer technology could improve that performance.

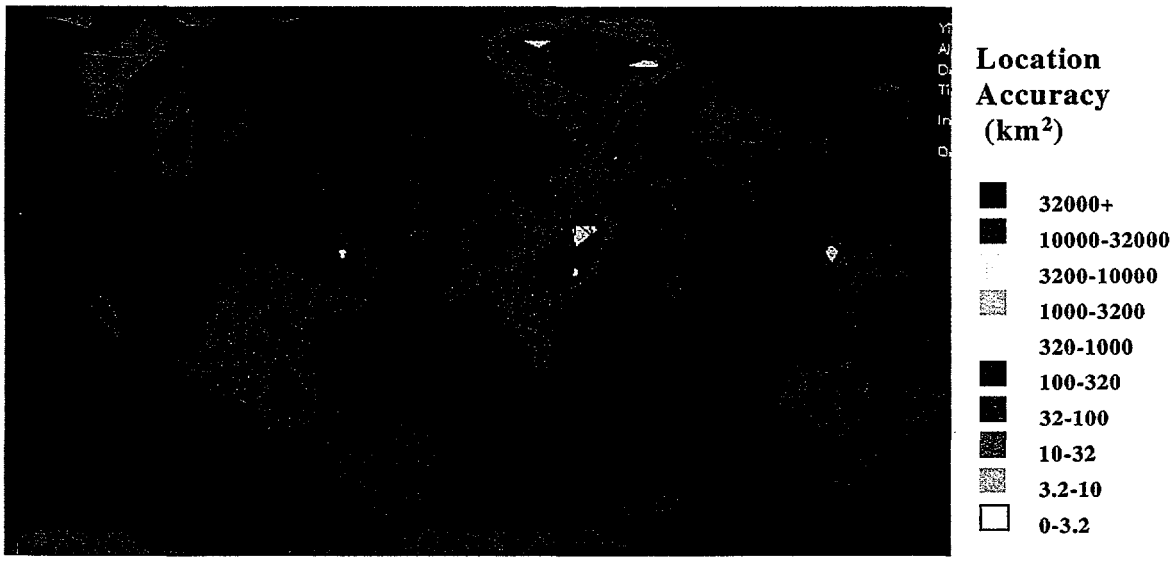

Figure C11. Sample Location Accuracy Contours, Small Atmospheric Event

Validation

To date, there is no generally accepted infrasound model against which to validate the IVSEM infrasound module. The basic signal amplitude versus distance equation is derived from experimental data, as are the equations governing high altitude wind effects and surface wind noise. Limited validation against NTS events has been accomplished, and is shown in Figures C11 and C12. These figures compare the signal strength, as predicted from the model, with test data recorded for NTS atmospheric explosions (Reed, 1969), at two stations, one located east of the NTS, and one located west.

The data shown in Figure C11 was taken at a station at Bishop, Cal., due west of the events. It can be seen that the station recorded higher amplitudes in the summer and lower amplitudes in the winter. This is due to the nature of the winds in the 50 km region. During the summer, they blow in an east-to-west direction, while the opposite is true in the winter. The signal is attenuated to a lessor or greater degree. The heavy black line with crosses represents results of the IVSEM simulation. The model results fall well within the spread of the data. The spread in the data can be explained by a number of factors. First, the uncertainty in the yield estimates would affect the

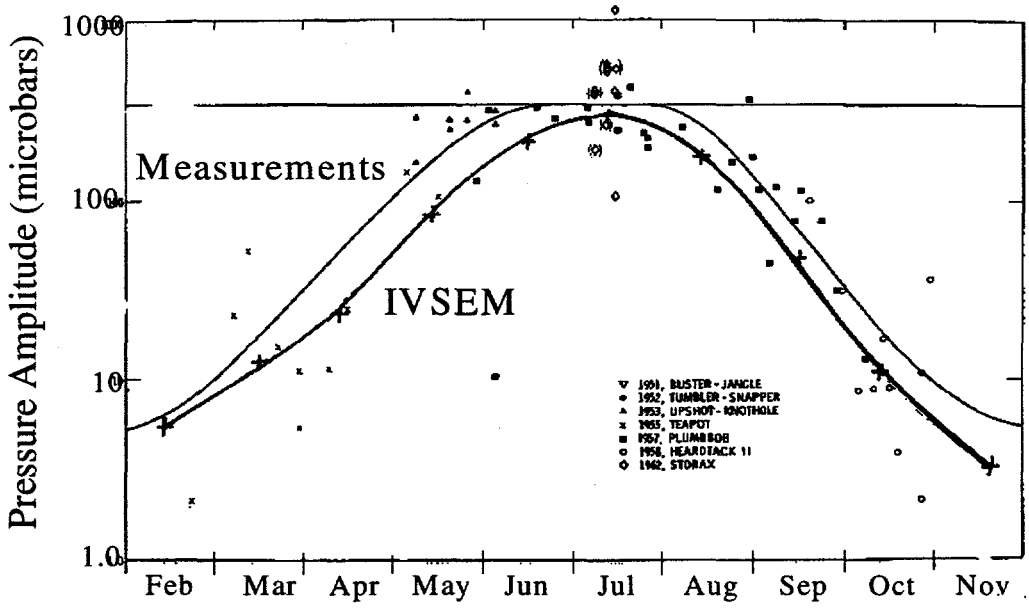

Figure C11. Infrasound Amplitude Variance with Season, Station West of Event

scaling. Second, the upper atmosphere winds exhibit considerable variability. Fluctuations in wind strength of over 10 meters per sec in a period of a day are possible. The IVSEM model uses monthly average data for the wind model. It must be noted that these data are for relatively small distances and large yields and extrapolation to greater distances and smaller yields is controversial.

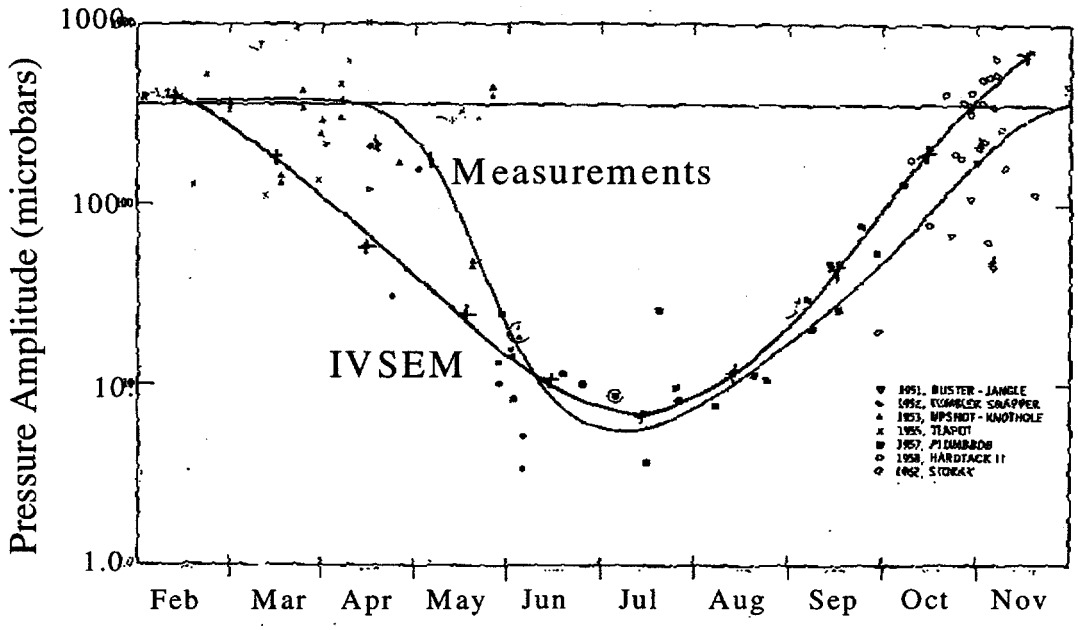

Figure C12. Infrasound Amplitude Variance with Season, Station East of Event

Figure C12 shows atmospheric test data taken at St George, Utah, due east of the NTS. It can be seen that the seasonal trend is the opposite of that for the western station. From this data, it can be concluded that the region of possible detection for an event will not be circular, rather that it will be elongated, with detection of events possible at a much greater distance if the high altitude winds are blowing from the event to the station. The shape of this region will vary according to the high altitude winds which vary with season. The heavy black curve shows IVSEM results. Again, the fit is quite close, except for the March - April region. This may be a result of rapid change in the 50 km zonal winds. The monthly averages used in the model may not reflect precisely the actual wind levels that were present during the tests.

Limitations

There are several limitations of IVSEM's infrasound module. The state of knowledge of infrasound propagation and detection is not as well developed as that of seismic signals. The zonal winds are based upon monthly averages, while the variance of the winds is known to be large. There are some gaps in meridional wind data, which had to be filled by interpolation. The state of knowledge of noise statistics is still limited. A Gaussian distribution was chosen as a reasonable first estimate. A stringent examination of more data might change the distribution. The primary effect of these factors is to produce some uncertainty in the detection estimates.

The bearing and time-of-arrival errors used in the location accuracy determination are based upon historical monitoring data. It may be possible to improve the accuracy using modern equipment, but no rigorous studies of the location performance of modern infrasound equipment have been performed.

The whole area of identification in infrasonic monitoring is at an early state. The model uses the frequency range from .01 to 10 Hz, where natural phenomena which generate explosion-like signals are infrequent. LANL has reported that explosions can be identified from earthquake noise by examining the length of the signal. Explosion signals are quite short in duration (not wave period), while earthquake signals last for considerably longer time. Another means of identification is to use the period of the signal. The period is proportional to the fourth root of the explosive yield. This can be used to estimate the yield of the event. At the present time, there has been no work done upon distinguishing between nuclear and large chemical explosions.

Summary

When verified against experimental data, the model has close agreement in amplitude. Comparison with other infrasonic detection models has not been possible, so far, as no generally accepted, validated infrasound model is available. Location accuracy has also been modeled. Validation against experimental data is still in progress. Future versions may include identification features.

References

Bedard, 1992. A. J. Bedard, R. W. Whitaker, G. E. Greene, P. Mutschlecner, R. T Nishiyama, and M. Davidson, "Measurements of Pressure Fluctuations Near the Surface of the Earth", Tenth Symposium on Turbulence and Diffusion, American Meteorological Society, 1992.

COSPAR, 1972. Committee on Space Research, COSPAR International Reference Atmosphere 1972, Berlin, Akademie-Verlag, 1972.

DNA, 1995. "NEMESIS: Nuclear Effects Models for Estimating Sensitivities to Input Scenarios", DNA, 1995.

Mutschlecner 1990. J. P. Mutschlecner and R. W. Whitaker, "The Correction of Infrasound Signals for Upper Atmospheric Winds. Fourth International Symposium on Long Range Sound Propagation, ASA Cp-3101, 1990.

Reed 1969. J. Reed., "Climatology of Airblast Propagation From Nevada Test Nuclear Airbursts", Sandia National Laboratories, SC-RR-69-572, 1969.

Webb 1966. W. L. Webb, Structure of the Stratosphere and Mesosphere. Academic Press, 1966.

APPENDIX D. HYDROACOUSTIC DETECTION

Hydroacoustic Modeling: Introduction

This appendix documents the hydroacoustic monitoring section of the Integrated Verification System Evaluation Model (IVSEM). This model simulates acoustic signal generation, the coupling and the transmission losses, the background noise environment, and the detection processes associated with explosions in the ocean or low air burst above the ocean. This effort was undertaken by Organization 5415, Sandia National Laboratories, Albuquerque (SNLA).

To predict the capability of proposed hydroacoustic networks to detect underwater explosions or air bursts in proximity to the ocean surface, a model was developed and incorporated into IVSEM. However, ongoing efforts at LLNL, NRL, and BBN to develop a much more comprehensive, community-accepted, validated simulation dictate that the present hydroacoustic model be considered more an interim effort than a final product. At that time when the more comprehensive simulation results become available and the data can be assimilated, it will then be incorporated into IVSEM.

The methods used in this model rely heavily on the use of text books and journal articles for both analytical estimates and test results of hydroacoustic effects. When necessary, the relevant information was extrapolated to approximate the conditions of a nuclear event. Because of the nature of the IVSEM model, two constraints were placed upon the hydroacoustic model. First, the model must be simple and second, the model must be fast running on a PC. Clearly, this model will not supply exact answers in terms of the absolute precision. Rather it is intended to show relative trends as the parameters are varied.

It is well known that the ocean is a very easy medium through which to propagate sound. Pressure waves from explosions will propagate to very great distances (10,000 km) assuming there is not some form of blockage present. As will be shown, the model successfully handles the propagation, attenuation, and detection functions associated with this yield burst, however, the model does not consider the larger question of what to do about natural occurring and man-made false alarms.

Background

The transmission of acoustic energy to very long ranges in the ocean is made possible by the presence of the Deep Sound Channel (DSC) or as it is sometimes called the SOFAR duct, for SOund Fixing And Ranging. Low-frequency sound is preferentially favored for long distance propagation via the DSC. For example, in 1960 a 150 kg charge of TNT was detonated in the sound channel off Perth, Australia and was clearly recorded on hydrophones located in the DSC off Bermuda, a distance of nearly 20000 km. The DSC is a consequence of the deep ocean sound velocity profile. This profile has a minimum at a depth which varies from about 0.75 km to 1.25 km in the midlatitudes to near the surface in the polar regions. This minimum sound speed depth is called the axis of the deep sound channel. This velocity minimum causes the ocean to act like

a lens continually bending the sound rays toward the depth of minimum velocity. Thus, for a source in the DSC, a portion of the acoustic energy remains within the channel and is assumed to encounter minimal losses aside from geometric spreading and attenuation. This is an idealization which greatly simplifies the calculation of the sound attenuation as it propagates across the oceans. Neglected are the interaction with the bottom, including attenuation due to a variety of bottom materials, surface interactions, and propagation losses through shallow water regions.

Figure D1 from Urick 1983 is a pictorial of the DSC with the channel axis located at the sound velocity minimum. The scale at the right of the figure shows the ocean sound velocity profile. The sound speed minimum is created by the existence of a balance between the effects of ocean temperature and hydrostatic pressure. Sound speed increases upward from the axis because the water temperature increases; it increases downward from the axis because of the increasing hydrostatic pressure. DSC thickness is typically on the order of 1-2 km. Observe the manner in which acoustic energy, originating from a source on the axis, is refracted towards the axis from both above and below the minimum.

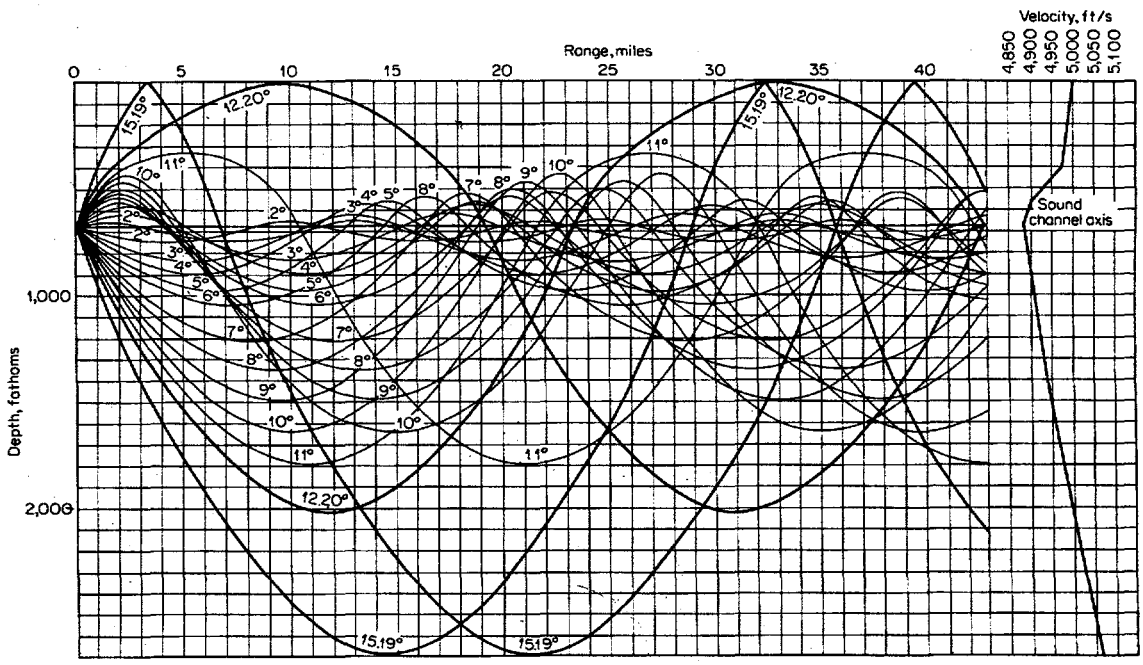

Figure D1. Acoustic Ray Path for Deep Sound Channel

Figure D2 illustrates a idealized sound profile for the deep ocean. Beneath the DSC axis, here shown to be at 1000 meters depth, the temperature of the oceans is fairly uniform and the sound speed increases with depth at a rate of 0.0173 m/sec per meter. Above the axis the sound speed increases with higher temperatures. In the actual case there would be considerable variability, especially as one nears the ocean surface. For this particular example, the sound speed gradient above the axis is observed to be -.0744 m/sec per meter.

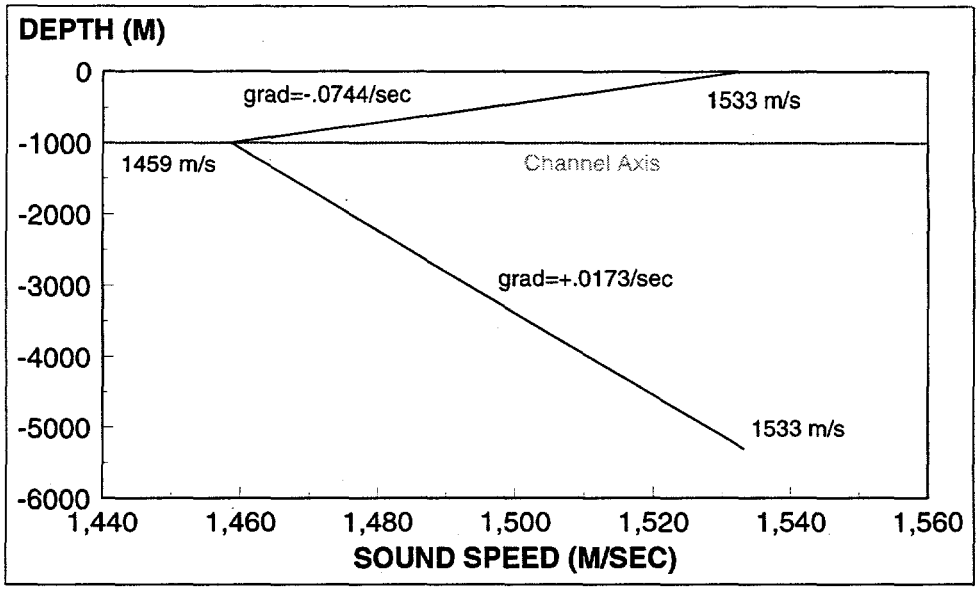

Figure D2. Idealized Sound Velocity Profile

Model Design

The hydroacoustic problem can be partitioned into several broad functional areas which can be investigated separately in developing a model for evaluating the detection probability of a particular sensor given a sensor-event separation distance, an event yield, and an event burst depth. These areas may be classified as: source, coupling, axis-loss, long-range transmission, and noise. The relationships which will be developed for each of these different areas will then be combined to provide an estimate of the probability the event will be detected by a given sensor.

The first area, denoted as the source parameter, relates to defining the acoustic strength of a particular explosion. To obtain a source term, one must have a means of associating a point-source acoustic signal intensity with an input explosion yield. This signal intensity will also be a function of the position of the burst with respect to the ocean surface as well as frequency. As is common in underwater acoustic systems analysis, the source term, as well as all of the other parameter values, will be expressed in terms of decibel levels.

The next functional area, denoted as the coupling parameter, represents that fraction of the acoustic intensity which couples into the water. This is to account for bursts occurring near to or above the ocean surface where significant amounts of source energy may not participate in the generation of an acoustic signal. This parameter is a function of the burst yield and its altitude above or below the ocean surface.

Axis-loss accounts for the reduction in signal intensity caused by a burst not being located on the DSC axis. Variables which affect this parameter include the distance the burst is off the DSC axis and the local ocean sound velocity profile.

A critical parameter when considering sensor-event distances of many thousands of kilometers is the loss of signal intensity due to such transmission loss factors as geometric spreading, attenuation, or signal blockage. The transmission parameter will be a function of the range and of several variables dependent upon the specific sensor-event path.

The final input parameter which is necessary in evaluating the likelihood of detection is that of the ambient ocean noise. It is this noise background that complicates the task of being able to detect the presence of the desired source signal. Because the ambient ocean noise is due to a variety of different sources such as surface perturbations, turbulence, distant shipping and storms, molecular motion, and seismic disturbances, it is observed to have different characteristics at different frequencies.

All of the above parameters define relationships which will be combined in the model with the specifics of the explosion location and yield to determine the probability of the explosion being detected by a given sensor or set of sensors. This probability that if a burst signal is actually present, the correct decision, "burst present," is made is called the detection probability P(D). The probability that if no detonation has actually taken place, the incorrect decision, namely "burst present" is made is called the false-alarm probability P(FA). Once all of the above parameter values are calculated, an overall signal-to-noise ratio can be derived. This signal-to-noise ratio will be used, in conjunction with the signal duration, signal bandwidth, and assumed knowledge of signal shape, to determine P(D) at some preassigned level of false-alarm probability.

Hydroacoustic Source Term Scaling

The aspect of the hydroacoustic modeling effort that is most difficult to quantify concerns the determination of the source term magnitude. Methods presented in such text books as Urick 1983 are empirical; based largely upon measurements of relatively small point-source charges of high explosive. Correspondingly, if one compares the peak pressure equation of Urick with that for nuclear yields given in EM1 (DNA 1991), the results are equivalent. This suggests the possibility of extrapolating peak pressure, and hopefully such derived terms as the energy density from small HE bursts to yields on the order of nuclear devices. Prior to deriving the source term used in IVSEM, we will first discuss some basic hydroacoustic concepts and definitions.

Urick 1983 details how, within a propagating sound wave, there exists certain amounts of kinetic energy of particle motion and potential energy of stresses in the medium. The amount of energy per second crossing a unit area of surface is called the *intensity* of the wave. The reference unit of intensity is the intensity of a plane wave having an rms pressure equal to 1 micropascal. To define the *level* of a sound wave, one takes the ratio of the intensity of that wave to the reference

intensity of a plane wave of pressure equal to 1 micropascal and expresses it in decibels (dB) units. This gives us the notation "dB re 1 μPa".

An underwater high-explosive generated shock wave propagates out in all direction in the medium. This shock wave initially exhibits a very steep rise to a high pressure followed by a rapid decay. In addition to the generation of the direct shock, there also exists a series of pressure pulses called bubble pulses caused by the oscillation of the mass of gaseous materials created by the explosion. At minimum volume of the oscillating gas globe, a positive pressure pulse is generated where each subsequent pulse is weaker than the preceding one. Hence, the explosive shock wave energy spectrum is a complex combination of the shock wave spectrum and the bubble pulse spectrum.

In defining the source term for an underwater explosion, it is necessary to introduce the energy flux density of an acoustic wave as the time integral of the instantaneous intensity. This quantity can also be defined relative to the energy flux density of a plane wave of pressure 1 micropascal and expressed in decibels. From this basis, the curves shown in Figure D3 as taken from Urick 1971 and Urick 1983 are used to define the source energy density levels of HE charges and are extrapolated to nuclear-level yields. Spectrum level refers to the level of a sound wave in a frequency band 1 Hz wide. Included on the chart is a simple example of how the explosive spectrum chart is used.

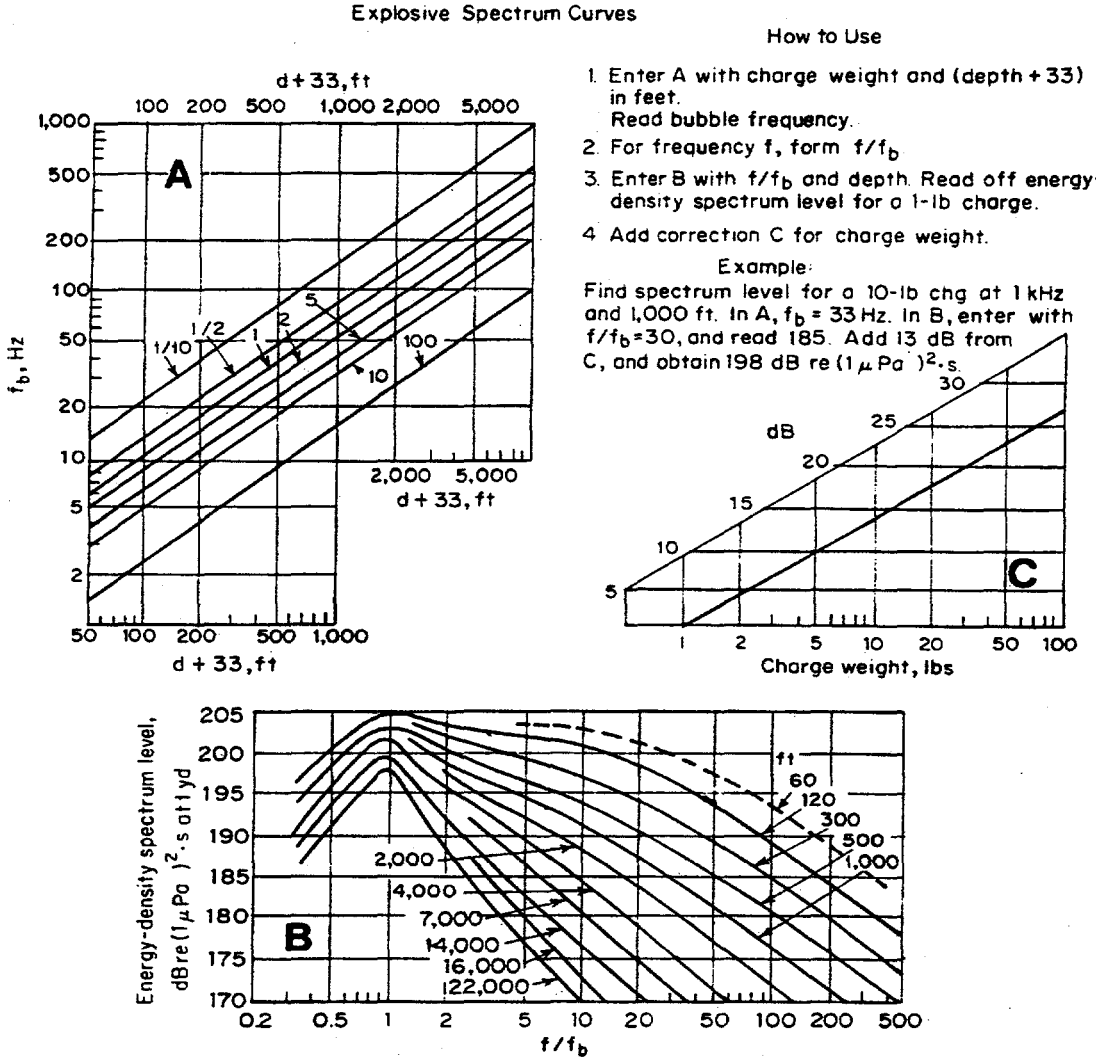

Figure D3. Source Term Definition Graphs

From extrapolation of energy density spectrum level data presented in Figure D3, the source level can be calculated for desired yields, burst depths within the ocean, and frequency. For bursts occurring in the ocean, the signal band is assumed to extend from 2 Hz up to a maximum of 100 Hz. Bursts occurring above the ocean surface were assumed to have a source bandwidth from 3 Hz to 50 Hz. The duration of the signal is assumed to be on the order of 10 seconds for nuclear yields. Because the other measures of acoustic wave characteristics such as transmission losses and noise values are given in intensity level units, it is necessary to adjust the source energy flux density in the following manner to produce an intensity source level:

$$\mathbf{SL = 10 \log \mathit{E} - 10 \log \mathit{T}}$$

where SL = source level (dB)

E = energy flux density (dB over 1 second) at a given frequency, and

T = signal duration (sec).

The source level is found to be only weakly dependent on burst depth, variations being usually less than one or two decibels. For a 1 kt burst at 1 km depth, the total integrated source level is approximately equal to 279 dB for a 10 second signal duration or 289 dB for a 1 second signal duration.

Energy Coupling into the Water

For bursts which occur deep in the ocean, practically all the available energy will be coupled into the water. As the burst depth is raised near to and above the water surface, the explosive energy can be significantly decoupled from the ocean. Considerable work has been done at Lawrence Livermore National Laboratory (LLNL) to look at this question of source term coupling. A series of computer simulations were run of the early stages of signal propagation, roughly out to a distance of 10 km, for a 1 kt explosion. These runs characterize the signal as a function of explosion location with respect to the ocean surface. All simulations were run at explosive yields of 1 kt. Clarke 1995, obtained from D. B. Harris, details the results of the LLNL analysis.

The LLNL calculations vary burst heights from 1 km deep in the ocean to 1 km above the ocean surface. The strong-shock very-early time calculations are done on the CALE hydrodynamics computer code. These early time calculations are carried out on a grid to a radius of approximately 300 meters. At this point, the weak shock calculations are then transferred from CALE to the weak-shock code NPE. This code then propagates the shock out to a range of 10 km. From this point, linear models can be employed to extend the solution to distances of several thousand kilometers.

Assuming complete coupling at a burst depth of 1 km, all other energy values at depths less than 1 km were then normalized by dividing by the energy value for 1 km. The resultant values were then transformed into decibel levels and are plotted in Figure D4. Note the gradual falloff in coupling as the depth-of-burst approaches the surface followed by the extremely sharp decrease in coupling near the ocean surface. The coupling then continues to decrease as the burst point is raised to 1 km above the surface but at a much reduced rate.

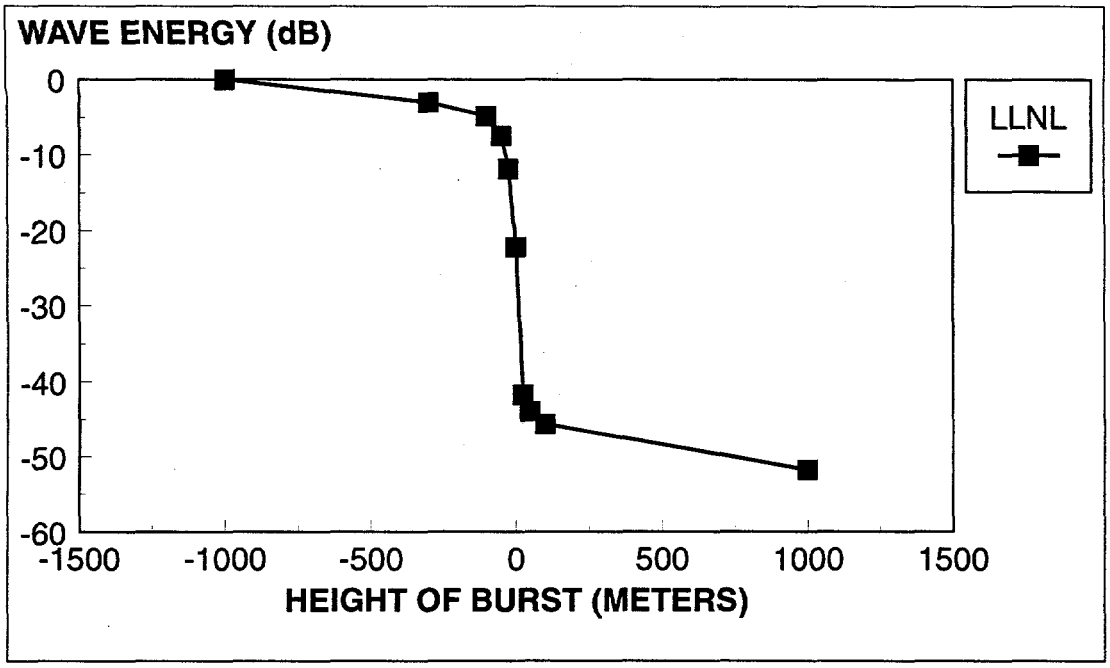

Figure D4. Explosive Energy Coupling into Water as a Function of HOB

Loss Used for Events Not Located on the Deep Sound Channel Axis

If the source is not on the DSC axis, then there is a reduction in the signal intensity, denoted as "axis-loss", that propagates in the channel. For the IVSEM study, no off-axis loss was included unless the burst took place below the axis depth. Any reduction in source strength from the sound axis to the ocean surface was assumed to be accounted for in the energy coupling curve of Figure D4. For an assumed axis depth of 1000 meters and employing the information from Bryan 1963, Figure D5 presents the derived loss curve. Note that for most reasonable depths of burst, the loss in signal intensity on the order of 5-8 dB is fairly small when compared to the source level.

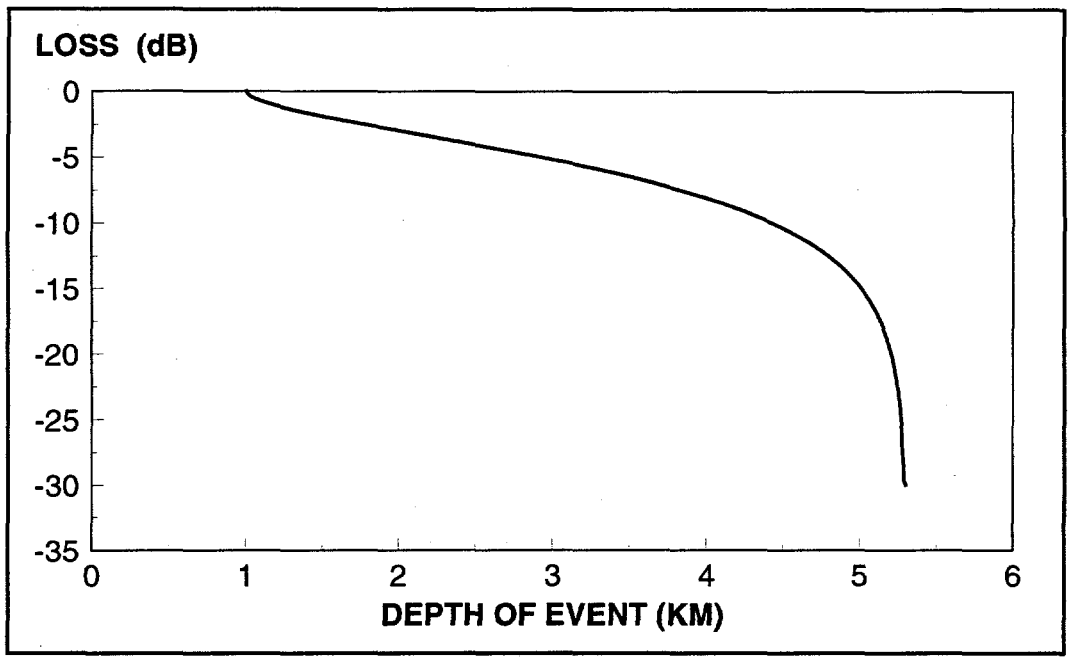

Figure D5. Loss Used for Events Below the Sound Channel Axis

IVSEM Hydroacoustic Blockage

The principal reason an ocean acoustic signal may not reach a distant sensor is that the path from the event to the sensor is intersected by a land mass. This obstruction of the event signal prior to reaching a sensor is denoted as blockage. Land masses which extend above the ocean surface are primary in defining blockage. Further, underwater obstacles such as seamounts which rise above the DSC axis by at least one-third of the distance to the ocean surface, are also counted as blockage. One of the aspects which determines whether a clear ocean path exists is the fidelity of the land and ocean maps used in the blockage analysis. Clearly the finer the map gradation, the more detailed the results. However, the amount of data storage and the time required to do calculations are both adversely affected as map resolution increases. The earth surface elevation and bathymetry values come from the ETOPO (Earth TOPOgraphy) data base set while the DSC-axis depth information comes from a data base derived by Dave Harris at LLNL.

For each burst event and proposed network of sensors, the great-circle path from the burst to each sensor is checked to see if any land mass intervenes. Although acoustic waves may, to some extent, be able to refract around certain obstacles, this hydroacoustic model as employed in IVSEM assumes complete signal blockage if there does not exist an unobstructed ocean path between the burst and the sensor.

The accompanying Figure D6 illustrates a 1.0^{o} by 1.0^{o} resolution land-ocean plus derived blockage data set used to generate the map employed in evaluating signal travel between ocean bursts and hydroacoustic sensors. Land masses are shown in gray, the oceans in white, and the

underwater blockages in black. Due to computer memory storage constraints, the actual map resolution presently used in IVSEM is 2.0° by 2.0°. Although this is a significant improvement over the earlier 7.5° by 7.5° IVSEM land/ocean map, still, many land and underwater obstructions may be missed.

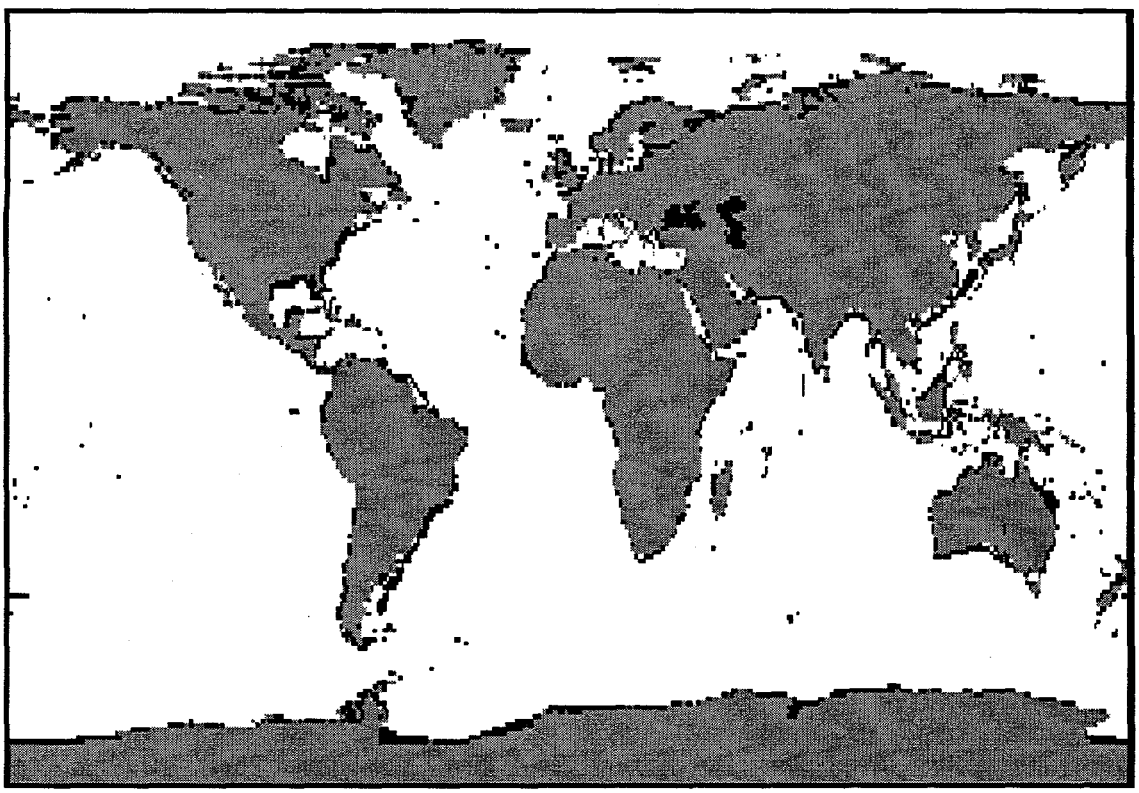

Figure D6. IVSEM Land-Ocean Blockage Map

Long-Distance Hydroacoustic Transmission Loss

Open-Ocean Transmission Loss

Transmission loss may be considered to be a sum of a loss due to spreading and a loss due to attenuation. Spreading is the geometrical effect representing the regular weakening of a signal as it spreads outward from its source. Spreading loss varies with range according to the log of the range. Attenuation loss, which varies linearly with range, includes the effects of absorption, scattering, and leakage out of the sound channel.

Sound travels long distances in the ocean, in general, by some form of ducted propagation. When traveling in a duct, sound is thus prevented from spreading in all directions resulting in less loss than non-ducted propagation. The associated transmission loss out to some range r can be viewed as the result of spherical spreading out to a transition range r_o followed by cylindrical

spreading from r_o to r. An expression for this type of ducted transmission loss as given Urick 1983 is:

$$\mathbf{TL = 10 \log r_o + 10 \log r + \alpha r \times 10^{-3}} \quad \text{(Cylindrical Spreading)}$$

where TL is the transmission loss in dB, r_o is the transition range in yards, r is the range in yards, and α is the attenuation coefficient in dB per kiloyard.

If it is the case that the sound transmission is better represented by spherical spreading, then the representative equation is of the form:

$$\mathbf{TL = 20 \log r + \alpha r \times 10^{-3}} \quad \text{(Spherical Spreading)}$$

where again r is the range in yards and α is the attenuation coefficient in dB per kiloyard.

There appears to be much controversy as to what is the best relationship to account for attenuation as a function of the acoustic frequency. Thorp 1965 suggests a fairly low attenuation value for frequency values below approximately a hundred Hz. Urick 1966 and Urick 1983 seem to indicate that there may be less reduction in the attenuation constant as frequency decreases. IVSEM follows the later references, as does Farrell 1996, of using a fixed value for the attenuation constant. This will be conservative in terms of producing significantly lower signal levels at long ranges from an explosion. Specifically, IVSEM uses the value suggested in Urick 1983 (kyd denotes thousands of yards):

$$\mathbf{\alpha\ (dB/kyd) = 0.003}$$

In order to determine which form of transmission loss to use in IVSEM and what constants are most appropriate, we will use experimental data from the well-known Heard Island Hydroacoustic Experiment.

Heard Island Hydroacoustic Experiment

A multi-nation well-documented (see Baggeroer 1992, Munk 1994, and Collins 1995) long-distance acoustic experiment, the Heard Island Feasibility Test, was conducted in January 1991. It is from the propagation data that was generated by this test that a measure of the reduction in acoustic signal strength at long ranges is derived. The following describes the rationale behind the basic experiment and the relevant results.

To understand and predict global warming, it is important to measure changes in the ocean heat content. To overcome the difficulty of local variations obscuring the detection of the much-larger-scale warming, one needs a method of measuring average temperature changes over large ocean ranges. Because sound speed increases by 4.6 m/sec per centigrade degree, travel time is shorter for a warmer ocean. A test was conducted off Heard Island (an uninhabited Australian Island discovered in 1853) in the southern Indian Ocean which demonstrated that low-frequency

underwater acoustic signals can be received at distance of up to 18,000 km or halfway around the Earth. Hence, year-to-year variation in acoustic travel time between distant sources and receivers can provide a measure of possible ocean warming.

An acoustic transmitter array was positioned off Heard Island at a depth of 175 meters, the depth of the local deep sound channel axis. The total array acoustic power was estimated to be 220 dB. The carrier frequency was selected to be 57 Hz. The signal was monitored by 16 stations with a maximum travel time of approximately 3.5 hours.

Figure D7 from Baggeroer 1992 illustrates the various paths taken by the Heard Island acoustic signals. Observe the location of Heard Island and the accessibility through several oceans to various sensor locations. Below the global picture are time-amplitude plots of the transmitted and received acoustic signal (57-Hz carrier). This particular receiver was located at Ascension Island, a distance of approximately 9000 km. The 57-Hz carrier is obvious in both the time-amplitude and the spectrum plots.

Figure D8 presents the transmission loss as a function of the source-to-receiver range. The stars represent various stations which received the Heard Island acoustic signal. The more optimistic cylindrical spreading relationship as previously defined is plotted in Figure D8 with the 10 log r_o term corresponding to the loss in excess of cylindrical spreading incurred during the initial divergence and insonification of the SOFAR channel set equal to 36.0 based upon the Heard Island and Urick 1983 data. This curve closely matches the losses of several of the Heard Island receiving stations. The spherical spreading curve represents a more conservative worst-case transmission loss alternative. Although both the cylindrical and the spherical equations are available in IVSEM, the cylindrical spreading transmission loss equation appears a better match to the data and is therefore presently used for all open-ocean long-range transmission loss calculations.

Transmission Loss in the Arctic Ocean

To include the possibility of either a nuclear burst or a sensor being located in the Arctic Ocean, the transmission loss must be corrected to account for the deep sound channel being at or near the surface and for the ice covering. Sound propagates to long ranges in the Arctic by repeated reflections from the undersurface of the ice and by repeated refraction from below. A number of measurements of the transmission loss, using explosive sources detonated at ranges out to several hundred miles from a receiving hydrophone, are summarized in Figure D9 as given in Urick 1983 from the original work in Buck 1968. The transmission loss is given for several frequencies. For comparison, the dashed line corresponds to spherical spreading. Note the under-ice curves are better than, i.e. have lower losses, than spherical spreading out to some distance and then become much poorer beyond. At the nearer ranges, sound ducting results in improved transmission over simple spherical spreading while at the long ranges, repeated reflections off the under-ice surface degrades transmission.

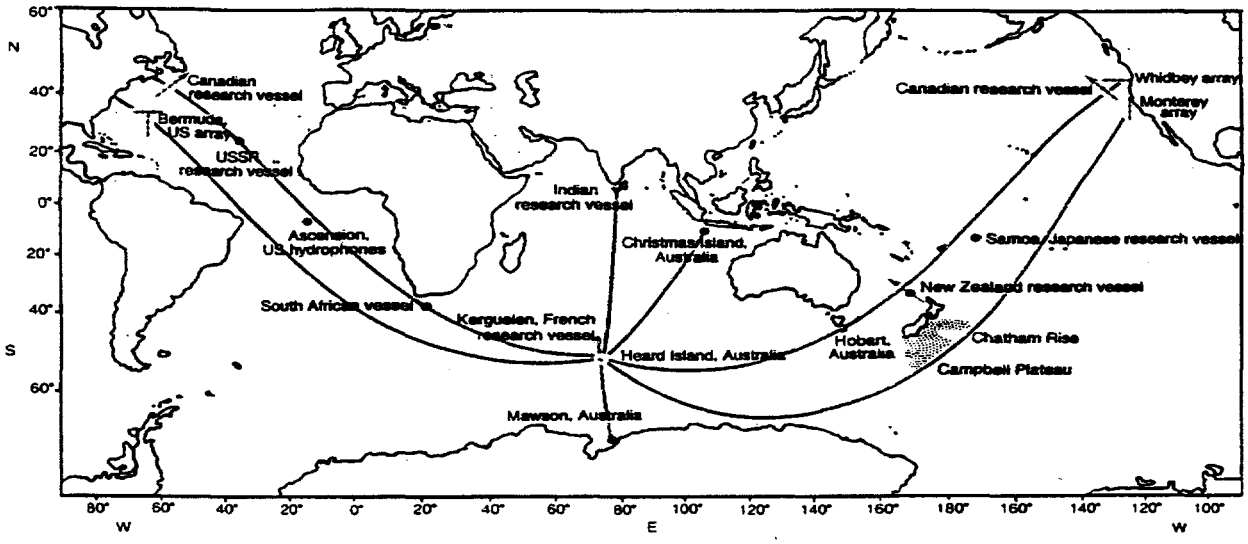

Paths taken by sound in the Heard Island feasibility test. The sources were suspended from the center well of the R/V Cory Chouest 50 km southeast of Heard Island. Black circles indicate receiver sites. Horizontal lines represent horizontal receiver arrays off the American west coast and off Bermuda. Vertical lines designate vertical arrays off Monterey and Bermuda. Lines with arrows off California and Newfoundland indicate Canadian towed arrays. Ray paths from the source to receivers are along refracted geodesics, which would be great circles but for the Earth's nonspherical shape and the ocean's horizontal sound speed gradients. Signals were received at all sites except the vertical array at Bermuda, which sank, and the Japanese station off Samoa.

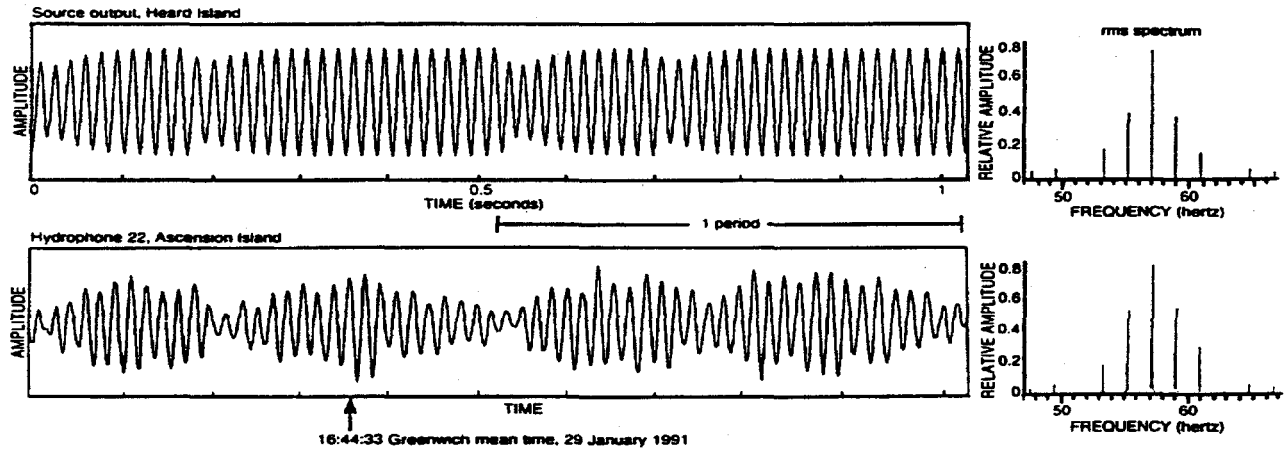

Transmitted and received signals and their spectra. Top: Transmitted signal and its spectrum as recorded at the source near Heard Island. Bottom: Signal received at Ascension Island, about 9000 km away, and its spectrum. The spectrum consists of the five strong lines of the pentaline code; half the power is in the 57-Hz carrier. (Figure courtesy of David Palmer, Atlantic Oceanographic Marine Laboratory, National Oceanic and Atmospheric Administration.)

Figure D7. Heard Island Feasibility Test

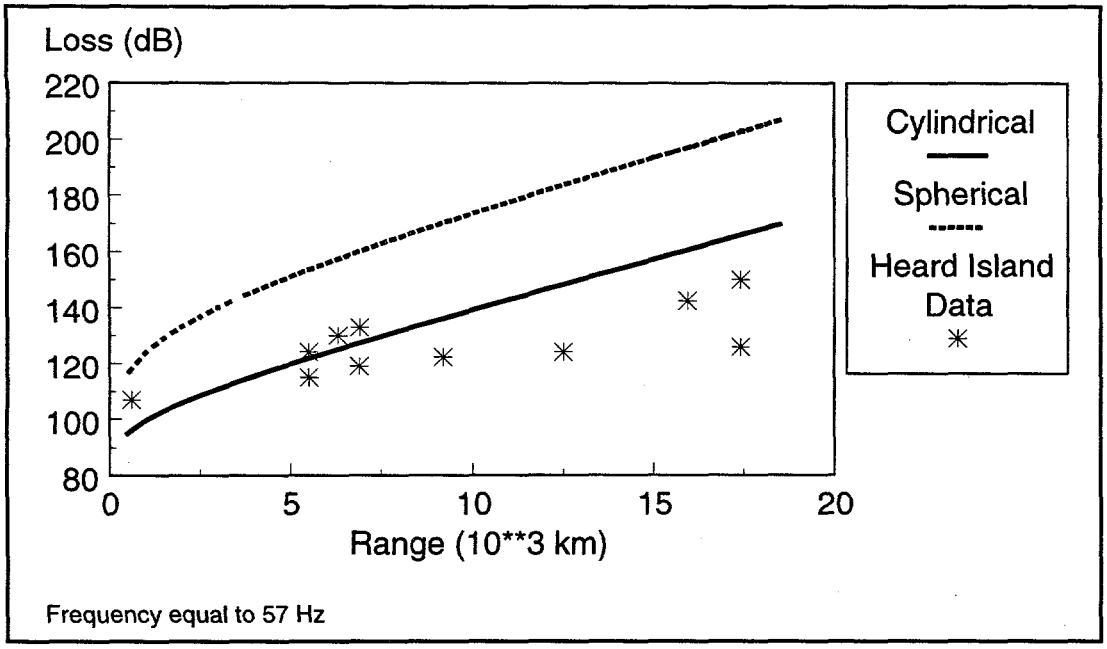

Figure D8. Transmission Loss Based upon Heard Island 57 Hz Data

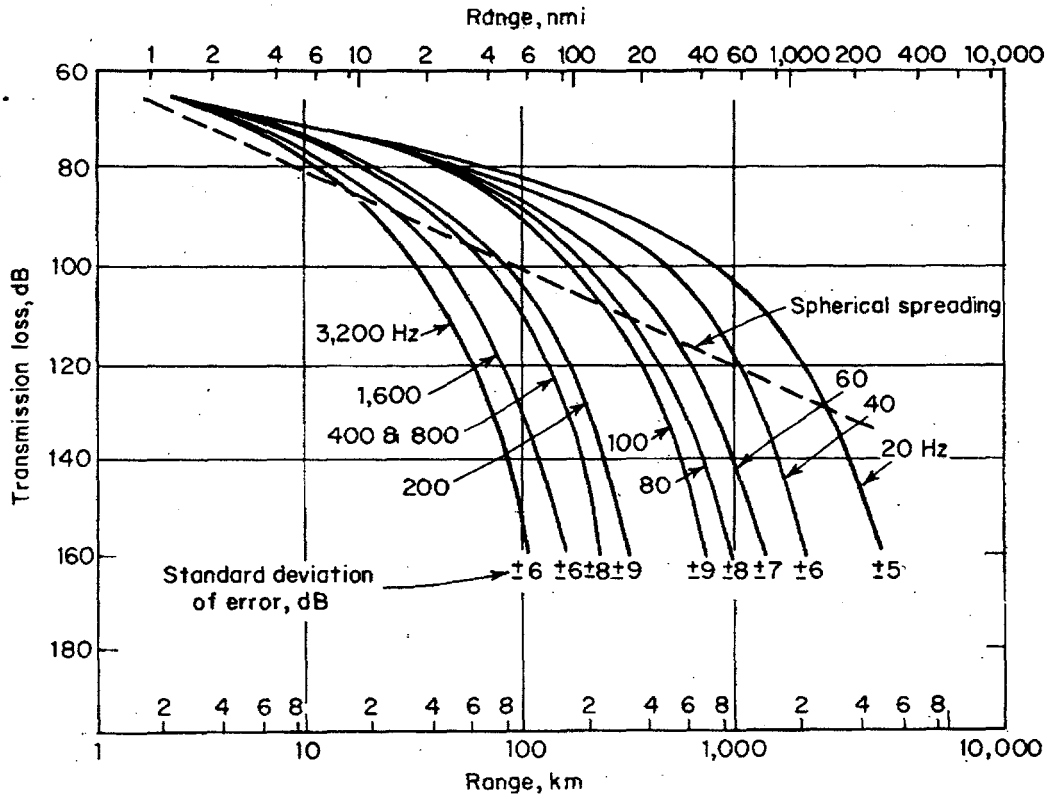

Figure D9. Average Transmission Loss in the Arctic

For use in the hydroacoustic module of IVSEM, the information in Figure D9 must be extrapolated and then simplified so that for a given frequency and range, the transmission loss can be quickly and easily calculated. Figure D10 illustrates the transmission loss for Arctic Ocean propagation for several frequencies. For cases in which either the explosion or the receiver is in an ice-covered area and the other is in open ocean, the total transmission loss is determined by simply scaling based upon the proportion of the path under ice to that under open ocean.

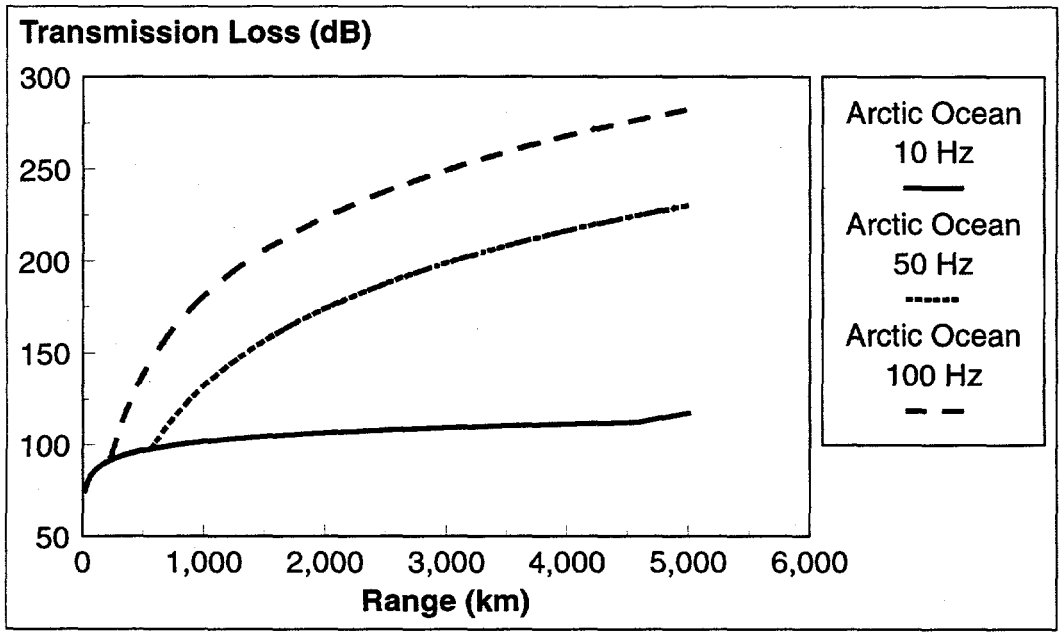

Figure D10. Arctic Transmission Loss Approximations

Deep-Water Ambient Noise Spectrum

Figure D11 presents the average deep-water ambient-noise spectra for different conditions as given in Urick 1983. The single curve from 1 Hz to 50 Hz with a spectral slope of -8 to -10 dB/octave is most probably the result of ocean turbulence. The ambient-noise spectrum flattens out to the right of the single curve where now the noise appears to be dominated by distant ship traffic. Three curves are used to differentiate between the shipping-related spectrum levels. The heavy shipping curve is appropriate for sensors located near North Atlantic shipping lanes while the light shipping curve is more appropriate for locations remote from the shipping traffic. At still higher frequencies, the noise source appears to be located at the ocean surface in proximity to the sensor. Observe the strong dependence on wind speed for this set of curves. The final high frequency noise curve, which has a noticeable positive spectrum slope, is characteristic of the thermal noise originating in the molecular motion of the ocean. The values observed in this figure in general either bound or are consistent with those levels described in Birdsall 1994,

Baggeroer 1994, Brundrit 1994, Cato 1980, Cato 1976, and Burdic 1984.

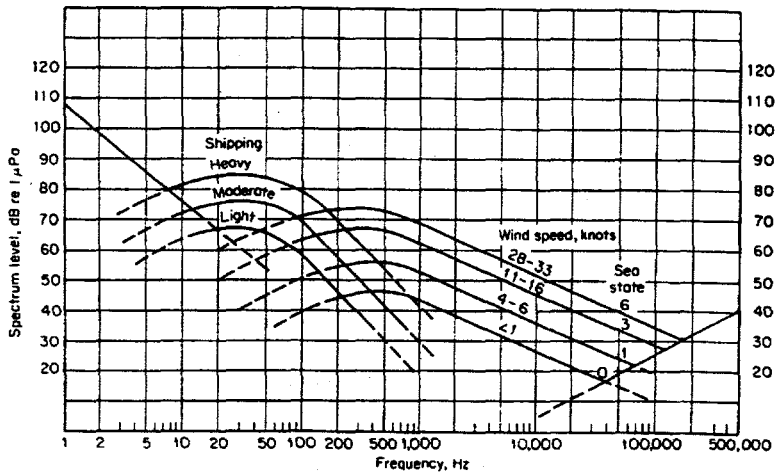

Average deep-water ambient-noise spectra.

Figure D11. Deep-Water Ambient Noise Spectrum

Simplifying Figure D11 to something more usable, Figure D12 illustrates the three ambient noise spectrum levels which can be selected for use in the IVSEM hydroacoustic model. Notice there exists a maximum of about 17 dB difference between the "high" and the "low" levels. Depending upon the location of each individual hydroacoustic sensor, in particular how close is it to shipping lanes, the most appropriate level can be selected as representing the ambient ocean noise for that sensor.

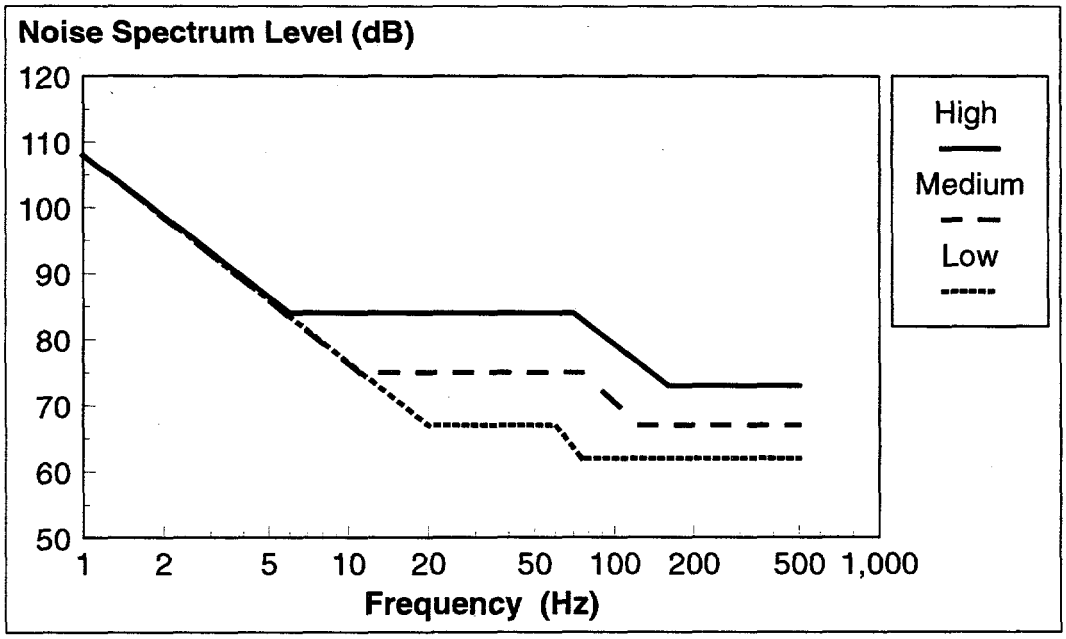

Figure D12. IVSEM Ambient Ocean Noise Level Approximations

Probability-Density Distributions of Noise and Signal+Noise

In relating the previously defined source level, the transmission loss, and the ambient ocean noise to the probability of a "Detection", Urick 1962 and Urick 1983 define the passive-sonar equation as:

$$\mathbf{SL - TL = NL + DT}$$

where SL= Source Level (dB)
TL= Transmission Loss (dB)
NL= Noise Level (dB)
and DT= Detection Threshold (dB).

Prior to examining the relationship between the detection threshold and specific probability values, we will first define just what is meant by "Detection". A general description is presented on how the probabilities of detection and false-alarm are related and how they are calculated.

Figure D13 illustrates the probability density functions P(a) plotted against amplitude a for noise only and for signal plus noise. The mean amplitude of noise is given by μ_{Noise} and the mean amplitude of the signal plus noise is $\mu_{Signal+Noise}$. Both distributions are assumed to be gaussian with equal variances σ^2. For an given threshold value of amplitude, the area under the signal-plus-noise density function to the right of the threshold is equal to the probability that an amplitude in excess of the threshold is due to signal plus noise and is equal to the probability of detection P(D). Likewise, if only noise is present, the area under the noise density function curve to the right of the threshold will be equal to the probability of a false alarm P(FA). As the threshold is swept through all values of amplitude a, a functional relationship between P(D) and P(FA) will be generated. The form of the P(D) versus P(FA) will be dependent upon the specific values of μ_{Noise} , $\mu_{Signal+Noise}$, and σ^2.

A parameter relating the signal and noise characteristics as defined in the Figure D13 is called the detection index and is defined as:

$$d = [\mu_{Signal+Noise} - \mu_{Noise}]^2 / \sigma^2$$

For any given value of the detection index d, a curve will be defined relating P(D) and P(FA) as the threshold is varied across all values of amplitude. A family of these curves, obtained from Urick 1983 and called receiver-operating-characteristic (ROC) curves, is illustrated in the Figure D14. These ROC curves, plotted on probability coordinates so as to be linear functions, have d values ranging from 0 to 36. Recall that it was assumed that the noise and the signal-plus-noise distributions were gaussian and the functional form of d is given by the equation shown.

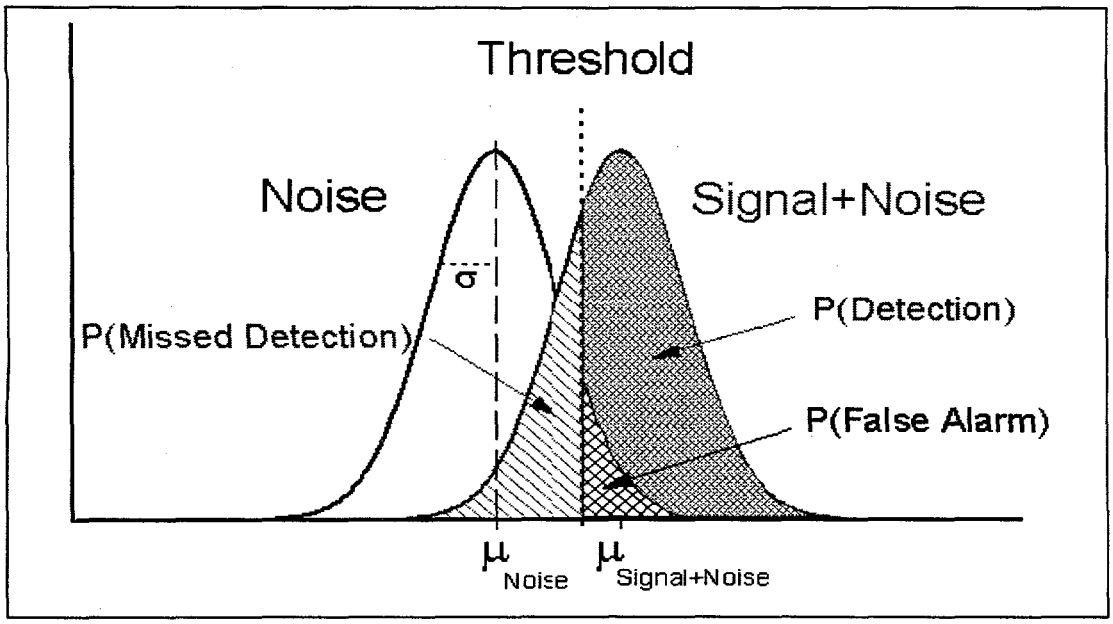

Figure D13. Distributions of Noise and Signal+Noise

Noise and Signal+Noise assumed Gaussian with equal σ^2
Detection Index $d = [\mu_{N+S} - \mu_N]^2 / \sigma^2$

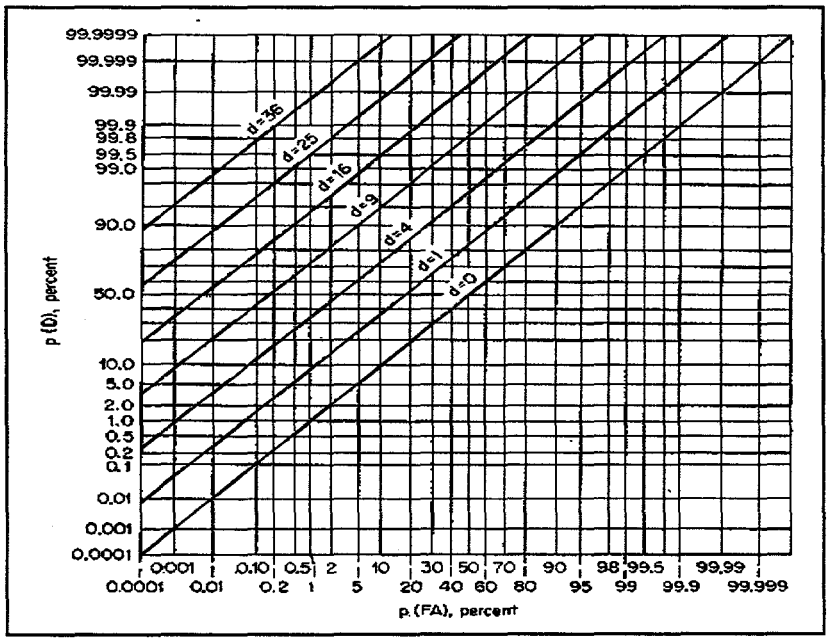

Figure D14. ROC Curves of P(Detection) vs P(False Alarm) for Detection Index d

As shown in Figure D14, the probability of detection of an event is closely tied to the probability of a false alarm and hence to the rate of false alarms that one is willing to live with. The specific costs associated with making a decision error, either in missing an actual event or in generating a false alarm, may be quite complex and is likely dependent upon many operational, political, and/or fiscal factors. For the problem at hand, let us assume that it is desired to have three or less false alarms a year from a given hydroacoustic sensor. If the assumed signal length is approximately 10 seconds, this results in a probability of false alarm of 10^{-6}. For this fixed P(FA), we can obtain P(D) as a function of the detection index value *d*, from the previous figure. Fortunately, the detection index *d* can also be related to the detection threshold and signal-to-noise, our measure of sensor performance, by the following equation given in Urick 1983:

$$\mathbf{DT = 10 \log S/No = 5 \log } d \, \beta / \, T$$

where DT = detection threshold,
S = total signal power in the receiver band,
No = noise power in a 1 Hz bandwidth,
d = detection index,
β = signal bandwidth, and
T = signal length in seconds.

This equation assumes a completely unknown signal in a background of gaussian noise. From this relation between *d* and signal-to-noise, we can now obtain the P(D) versus signal-to-noise ratio relationship as show in Figure D15.

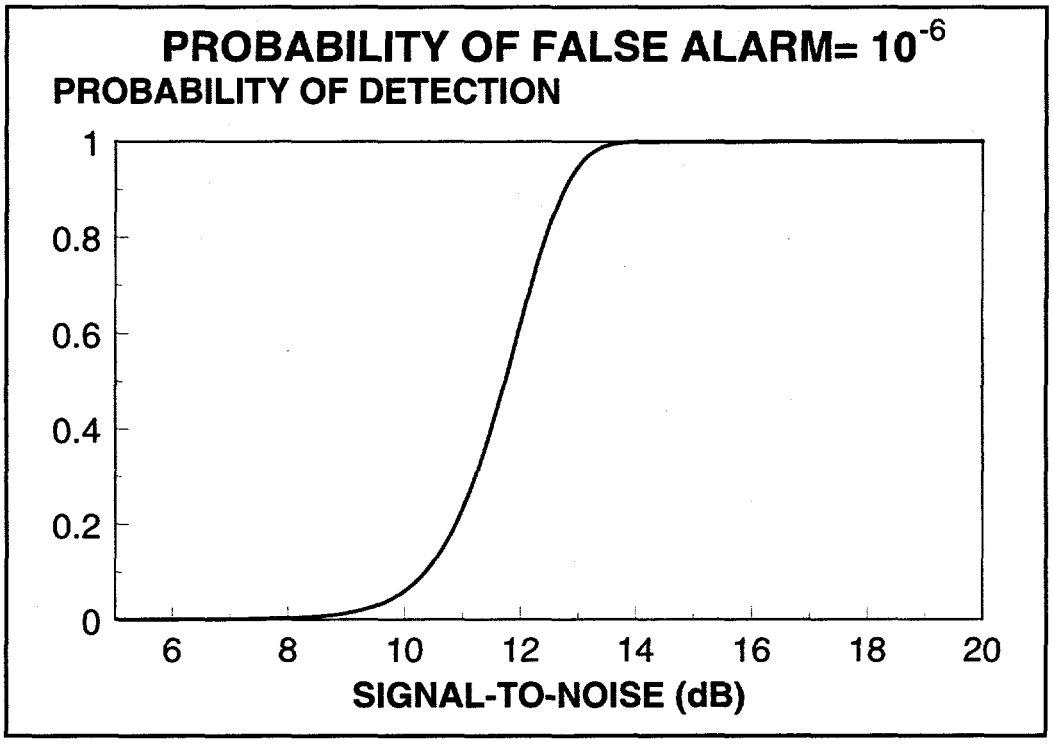

Figure D15. IVSEM Hydroacoustic Example Detection Performance

T-Phase Island Stations

There are two type of stations proposed for the hydroacoustic network: in-ocean fixed-cable hydrophone stations and tertiary- or T-phase island/coastal stations. T-phases are the seismic signals created by ocean acoustic signals hitting steep shorelines and recorded by a seismometer. At this time there is insufficient data available to reliably model the T-phase station response for a given nuclear burst in or above the ocean. As observed by Dave Harris of LLNL, the very limited information which seems applicable indicates a T-phase sensor signal-to-noise level would be 20 dB or more below that of a corresponding hydroacoustic in-ocean station.

To model T-phase station performance, the hydroacoustic module in IVSEM has been modified to allow for several changes in the received signal level and in the determination of the probability of detection of that signal. The first change was the reduction of the signal upper frequency limit, from 100 Hz for an in-ocean hydrophone station, to a value of 20 Hz which appears more characteristic of a T-phase station. Secondly, a simple means of reducing the received signal level, in general from 20 dB to 40 dB, was included in the program. Finally, because the actual detection instrument is now a seismometer instead of a hydrophone, it might be reasonable to use a probability-of-detection vs signal-to-noise relationship more typical of seismic stations than that used for hydroacoustic in-ocean stations. These modifications, either individually or in combination, may be employed to simulate possible T-phase station performance. Once new data is developed which better defines actual T-phase station capability, these parameters can easily be modified.

Figure D16 illustrates the relationship of probability of detection versus event-to-sensor range for an in-ocean station and for a T-phase station. The event is a 1 kt burst occurring at the ocean surface in conjunction with high ambient noise. The hydroacoustic in-ocean station has a probability of detection of near 1.0 for all ranges out to approximately 14,000 km. The T-phase station is modeled by simply taking the ocean acoustic signal at a given range then reducing the subsequently calculated signal-to-noise value by 40 dB as suggested Ted Farrell of BBN. Using this reduced signal-to-noise ratio to generate a probability of detection using the standard ocean detection relationship given in Figure D15, the T-phase curve in Figure D16 is defined. This is the manner in which IVSEM presently determines probability of detection for a T-phase station. Observe that the T-phase detection ranges for a fixed probability of detection are significantly reduced, on the order of 10,000 km, compared to the in-ocean hydroacoustic station.

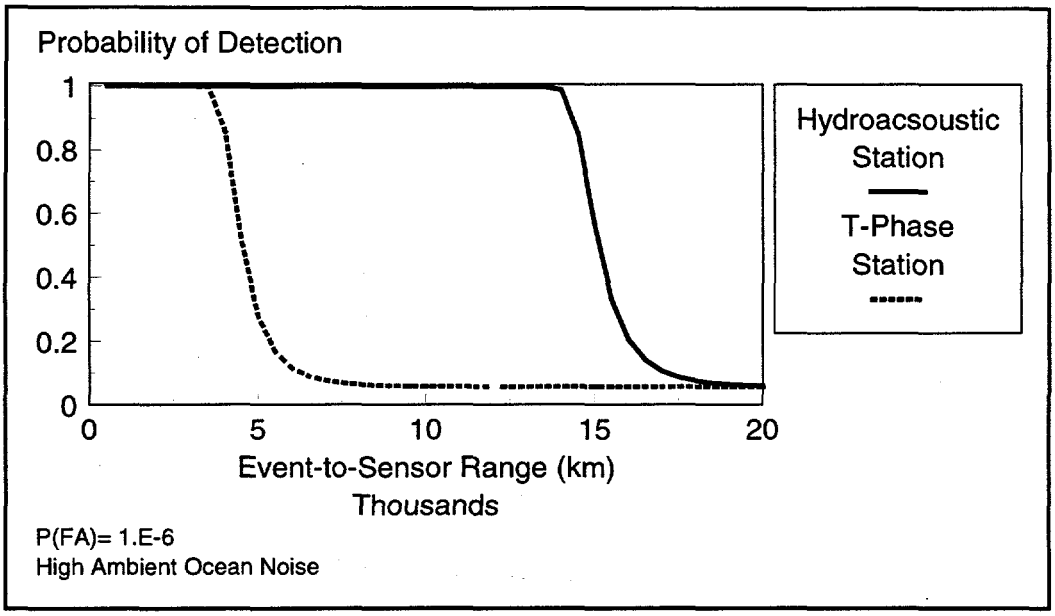

Figure D16. T-Phase Station Detection Comparison with In-Ocean Station : 1 kt Surface Burst

Single-Station Detection Performance

For a given source level, coupling and transmission loss values, and ambient noise level a signal-to-noise ratio can be generated. This signal-to-noise value can then be related to a probability of detection for a fixed probability of false alarm from which the performance of an individual sensor can be evaluated. Figure D17 illustrates the ranges associated with detecting an event occurring on the sound channel axis at 1 km depth-of-burst, at the water surface, and at 1 km height-of-burst as a function of the event yield. A detection probability at the hydroacoustic sensor of at least 50% is required. The probability of false alarm is set at 10^{-6} and the ambient ocean noise is chosen to be high. Observe that in-ocean bursts of yield from 0.1kt to 1 kt are detected with the required probability out to nearly the maximum considered range of 20000 km. Only as the yield falls below 0.2 kt does the detection range reduce to under 20,000 km. As the burst location is raised to the ocean surface, the useful event-to-sensor separations now fall to the 13,000-15,000 km range while the 1 km airburst explosion further reduces detection ranges to 3,500-7,500 km. This strong dependence on burst distance above the ocean surface is driven by the LLNL HOB-decoupling data shown in Figure D4.

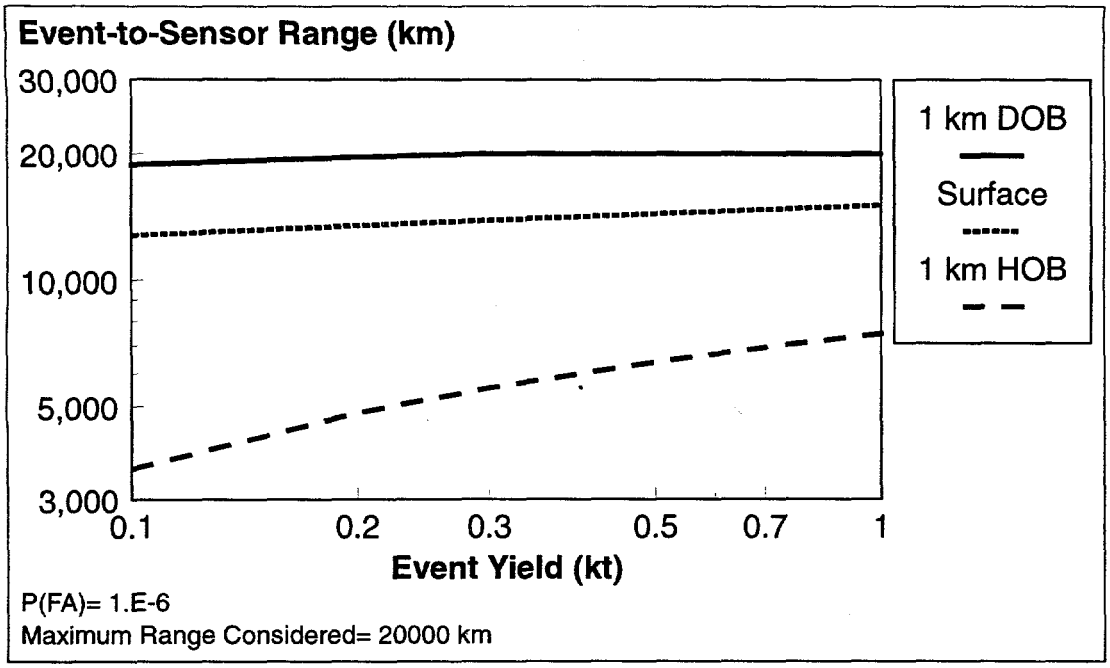

Figure D17. Single-Station Performance as a Function of Event Yield and Height-of-Burst: Probability of Detection > 0.50 (High Noise Case)

Hydroacoustic Model Summary

The presented hydroacoustic model as implemented in IVSEM is based largely upon elementary empirical and analytical methods, including abundant extrapolations, to develop estimates of source, coupling, transmission, and noise parameters. This results in hydroacoustic sensor performance evaluations that can be performed both simply and quickly. The model-generated sample cases display trends in detection performance as a function of event-to-sensor range, burst HOB, yield variations, and ambient noise levels which appear consistent with the relatively small amounts of relevant data examined to date.

Validation

Introduction

Due to the lack of calibrated data on hydroacoustic detection of in-ocean and above-ocean nuclear shots, rigorous validation of the IVSEM hydroacoustic module is difficult. What has been done in terms of insuring maximum module utility involves comparisons with smaller magnitude source level data. In particular, data from HE explosions in water and long-range tests of acoustic tonal generators has been compared to IVSEM calculations. In addition, the recent acquisition of an excellent hydroacoustic simulation, Farrell 1996, also provides results which can be compared to those generated by IVSEM.

Specifically, the Hydroacoustic Coverage Assessment Model (HydroCAM) was developed under U.S. Department of Energy funding for predicting the detection and localization performance of global hydroacoustic monitoring networks. This is a very detailed model which is run on UNIX workstations and contains a large assortment of oceanographic databases, acoustic propagation models, network performance models, and software for visualizing and interpreting the results. HydroCAM accounts for such factors affecting global-scale acoustic propagation as horizontal refraction from bathymetric features and horizontal changes in sound speed, travel time variability due to spatial and temporal fluctuations in the ocean, and detailed characteristics of the source. This computer simulation was developed by Ted Farrell of BBN Systems and Technologies. Limited runs of HydroCAM were used to compare source and noise levels, propagation losses, and signal-to-noise ratios with those used in and derived by IVSEM.

Source Term

The source term defines the initial starting conditions for a particular case of interest. IVSEM uses the energy spectral density relationships presented in Urick 1971 and Urick 1983 with extrapolation to nuclear yields. The source term is dependent upon the yield, the burst location, as well as the frequency bandwidth of interest. Because the exact source relationship is seldom explicitly defined, few examples were found where direct comparisons with IVSEM could be made. This is also the case when trying to compare the IVSEM energy spectral density with that used in HydroCAM. What can be done, however, is to compare the total source energy, integrated over all relevant frequencies for a 1 kt nuclear explosion, employed in HydroCAM and in IVSEM. This total source energy value or source level is illustrated in Figure D18 as a function of the depth or height of burst for a 1 kt yield. Note that there exists only a small difference in the source level between IVSEM and HydroCAM at the defining 1 km depth-of-burst point. Over the rest of the burst regime, the source level values are quite close. It should be noted that the general shape of the data for both HydroCAM and IVSEM as a function of the event height is based upon the LLNL computer analysis of a 1 kt hydroacoustic source as presented in Clarke 1995.

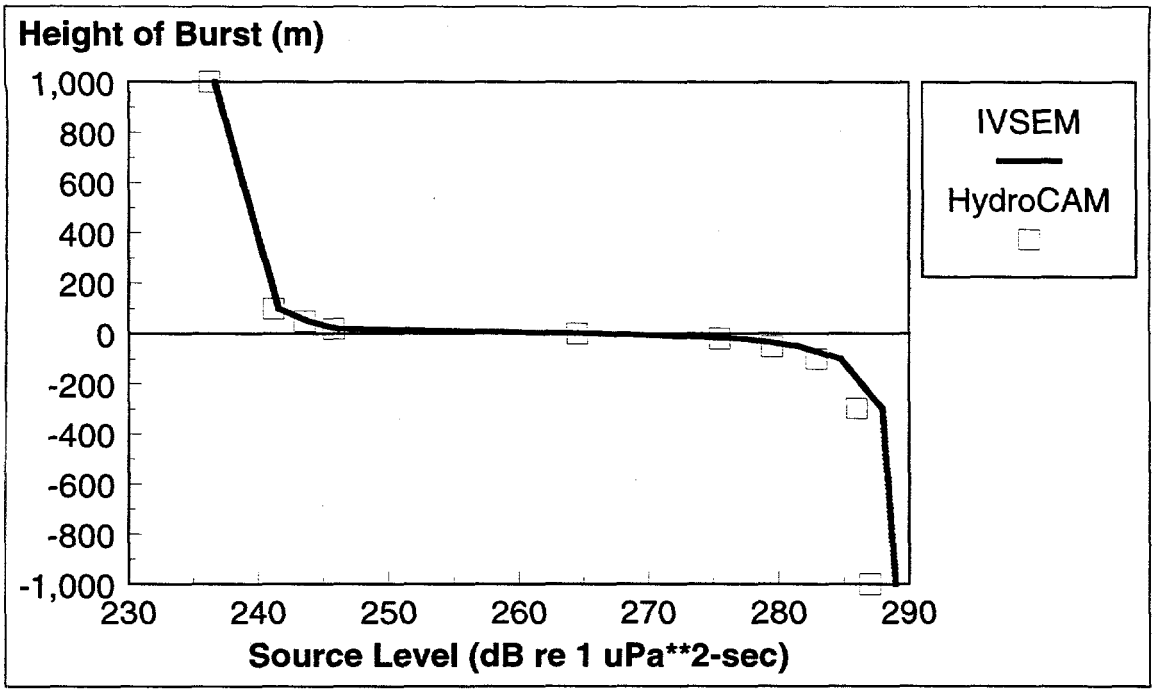

Figure D18. Comparison of IVSEM and HydroCAM Source Levels vs HOB for a 1 kt Explosion

Transmission Loss

The long range transmission loss model used in IVSEM was based upon the Heard Island Feasibility Experiment. Agreement with the transmission loss obtain from the Heard Island, as detailed in Birdsall 1994, is illustrated in Figure D8. While matching well for the short and medium range values, IVSEM transmission loss is more conservative at ranges beyond 10,000 km than that represented by the Heard Island data. This excess loss at long ranges is due to the selected constant attenuation value used in the transmission loss equation. Figure D19 compares the Heard Island data with the baseline IVSEM constant attenuation transmission loss and with an identical transmission loss term which now contains a frequency-dependent attenuation term based upon data from Thorp 1965. Observe that this new transmission loss formulation now underestimates the Heard Island loss data. One could manipulate the initial spherical spreading 10 log r_o transition term from its value of 36.0 to obtain better agreement for either of the illustrated curves or one could devise a new attenuation relationship based solely upon the Heard Island data. Instead, because of the large uncertainty and variability inherent in ocean attenuation determination, it was decided to continue to use the derived transmission loss formulation employing the constant attenuation term. The effect is that the IVSEM transmission loss will be higher than that observed in the Heard Island data resulting in a more conservative estimate of the capability of a station to detect a given explosion.

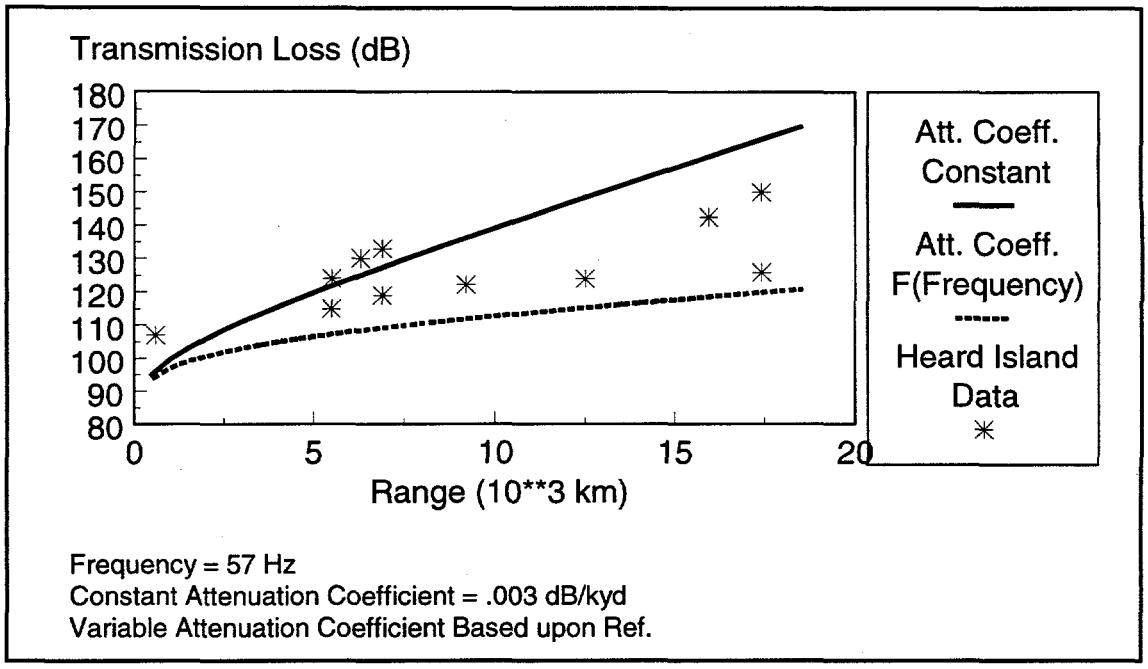

Figure D19. Comparison of Transmission Losses for Baseline Constant Attenuation Coefficient Versus Frequency-Dependent Attenuation Coefficient Based Upon Data in Thorp 1965

The default transmission loss module in HydroCAM has the basic form:

$$\mathbf{TL\ (dB) = 60. + 10\ log\ r\ (km) + .0033\ r\ (km)}$$

In addition to this loss term, HydroCAM also has the option to include losses due to bottom bounce of the hydroacoustic wave, For the number of open-ocean cases which were run on HydroCAM, however, the transmission loss for most of the receiving stations (excluding those were significant blockage or shadowing occurred) closely approximated the above basic equation. Converting the IVSEM equation for transmission loss from yards and kiloyards into kilometers gives:

$$\mathbf{TL\ (dB) = 66.4 + 10\ log\ r\ (km) + .0033\ r\ (km)}$$

Hence, the HydroCAM and resultant IVSEM transmission loss equations are quite similar, differing only by 6.4 dB.

Ambient Ocean Noise

The IVESM ambient ocean noise level approximations shown in Figure D12 resulted in values of 84, 75, and 67 dB across the plateau portions of the respective curves. For the Heard Island Feasibility Test, the ambient ocean noise was estimated to be, depending upon the receiving station, 89 dB (Baggeroer 1994), or from 70-75 (Brundrit 1994). Birdsall 1994 gave an

expected range of 65-90 dB for the expected noise spectral density at 57 Hz set by shipping traffic.

A comparison of the IVSEM noise model given in Figure D12 is illustrated with the default receiver noise model used in HydroCAM in Figure D20. The HydroCAM noise model is much more detailed than the simplified IVSEM approximation. Observe that in the region of primary interest from several hertz to a hundred hertz, the HydroCAM noise values are contained between the IVSEM medium to low cases.

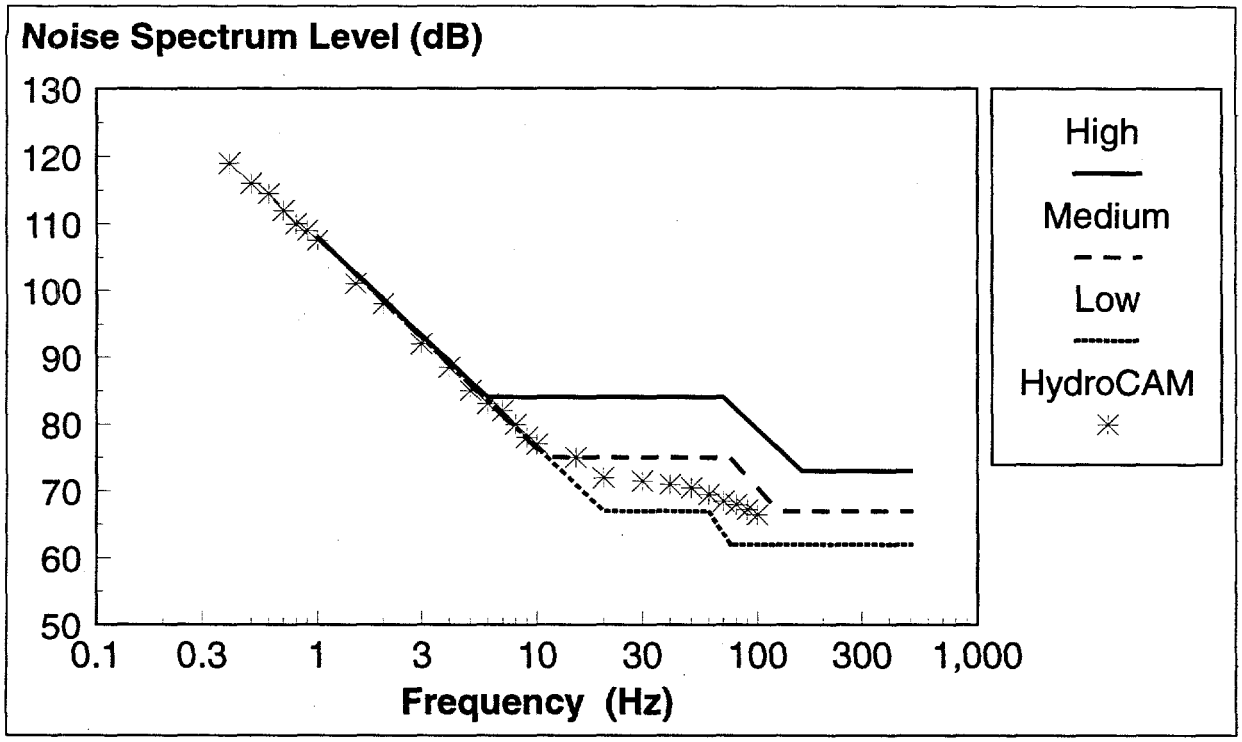

Figure D20. Comparison of IVSEM and HydroCAM Ambient Ocean Noise Levels

Signal Intensity and Signal-to-Noise-Ratio

Urick 1963 provides data on a number of 4 lb HE charges fired at depths of 0.5 km or 1.1 km which is near the local SOFAR axis. Shown is the peak signal intensities in the 50 to 150 Hz bandwidth for various ranges. Figure D21 presents this data in the units given in the reference. Also included in Figure D21 are curves illustrating the results of IVSEM runs for 4 lb charges on the SOFAR axis as a function of range for both the baseline cylindrical and the spherical transmission loss formulations. Note that the IVSEM cylindrical transmission loss curve somewhat overpredicts the received signal intensities and does not give the rapid falloff of signal at ranges beyond 1500 miles. Further, the data illustrates an approximate 10 dB reduction in signal for the charges off the SOFAR axis. IVSEM gives only about a 3 dB reduction in signal for these off-axis charges. The IVSEM spherical transmission loss curve was also shown to

indicate that, at least for this case, the two transmission options available in IVSEM would bound the observed data.

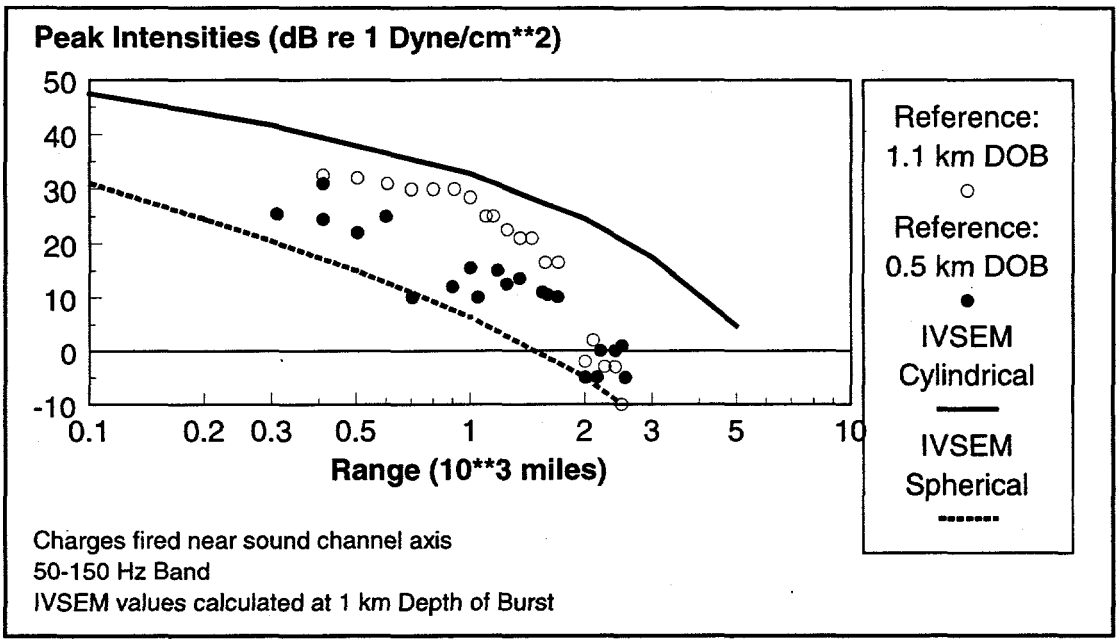

Figure D21. Comparison of IVSEM and Urick 1963 Signal Levels as a Function of Range for 4 lb HE Charges

Bryan 1963 presents data pertaining to 48 lb HE charges detonated near the sound channel axis and the resultant signal received at two hydrophones located near the sound axis at the SOFAR station on Fernando de Noronha. Figure D22 presents this data in the units given in the reference. Also included is the baseline IVSEM signal intensity as a function of range for the yield and depth-of-burst for this case. The scatter in the data was felt to be due largely to the variability of the shot depth relative to the channel axis. Regardless, the IVSEM prediction appears to be quite acceptable.

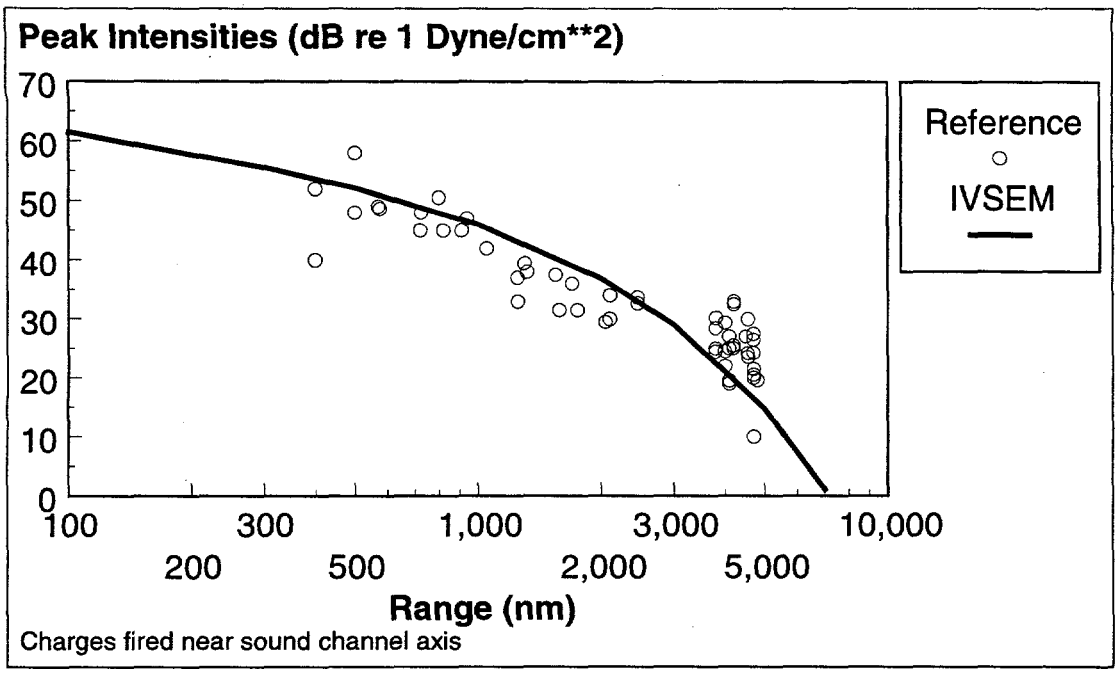

Figure D22. Comparison of IVSEM and Bryan 1963 Signal Levels as a Function of Range for 48 lb HE Charges

A final test case involved making a number of HydroCAM runs assuming a 1 kt burst at a 1000 m depth. Several receiving stations were assumed in the Pacific Ocean as the location of the burst was varied. The resulting signal-to-noise ratios at these stations were compiled and are shown on Figure D23. A number of IVSEM runs were then made for various ranges from a 1 kt source on the sound channel axis. Both the HydroCAM runs and the IVSEM runs were made at a single frequency equal to 30 Hz. Because HydroCAM assumes that the total source energy of the explosion resides at the 30 Hz frequency, a correction to the IVSEM source term of +24.1 dB was included to account for this simulation construct. Further, the HydroCAM signal integration default value is equal to 1 second. Although this could have been changed in the setup files to some other value, it was felt easier to reset the IVSEM signal length from 10 seconds to 1 second. Finally, the default noise level at 30 Hz in HydroCAM is equal to approximately 72 dB while that of IVSEM (for the high noise case) was 84 dB. Hence, an additional 12 dB was then added to the IVSEM signal-to-noise ratio. The resultant corrected IVSEM signal-to-noise versus range relationship was plotted on Figure D23. Observe that for the majority of the points, there is quite good agreement between the HydroCAM and IVSEM results. However, there exist a number of HydroCAM points which fall some distance below the IVSEM curve. These points are likely the result of poor propagation paths between the explosion and the receiver. Shadowing by undersea land masses or island shielding of the receiving hydrophone from the direct hydroacoustic wave appears a likely cause in the reduced signal-to-noise ratio data. This points up the difference between detailed, fine-grained simulations such as HydroCAM with their massive data bases and advanced propagation path determination tools and the fast and easy to run systems-level models such as IVSEM.

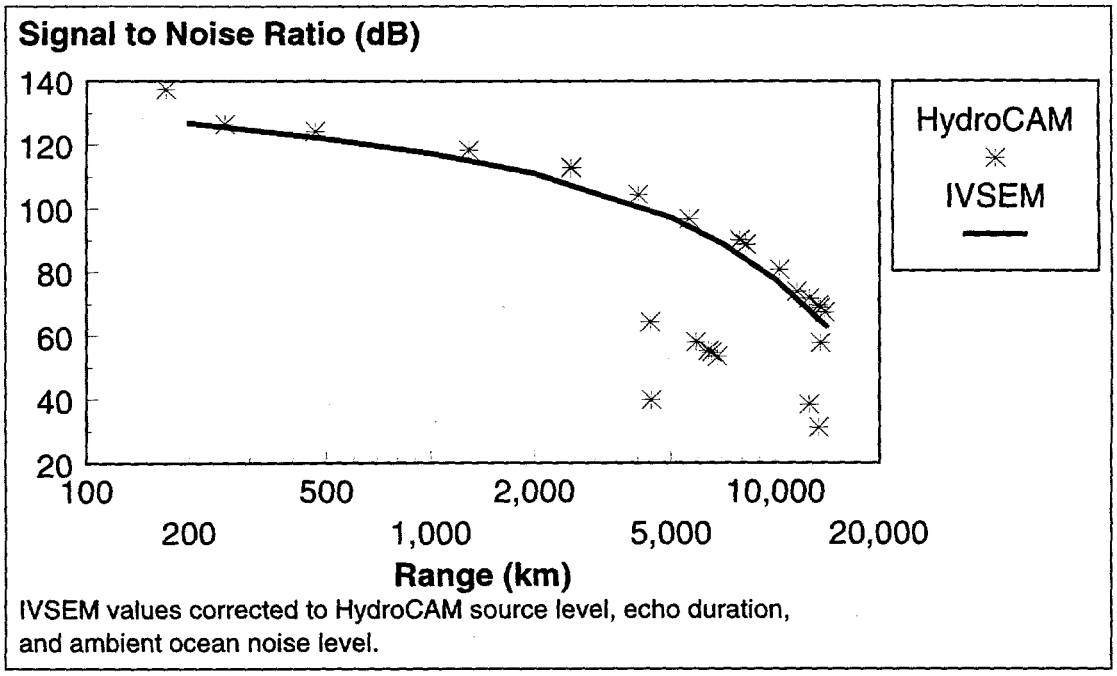

Figure D23. Comparison of IVSEM and HydroCAM Signal-to-Noise Ratio versus Range for a 1 kt Explosion

In addition to the above HE and simulation comparisons, a classified source was found which had limited data pertaining to an underwater nuclear shot. Although there were calibration problems and receiver saturation events, some data was usable for deriving signal levels at various ranges from the burst. Comparison of IVSEM runs made assuming, as closely as possible, the same yield, DOB, and bandwidth, resulted in signal levels which appeared to be reasonable consistent to the actual data. Further comparisons with other HE, nuclear, or simulation sources are planned in the future.

References

Baggeroer 1992. Arthur Baggeroer, Walter Munk, "The Heard Island Feasibility Test," Physics Today, pg. 22-30, September 1992.

Baggeroer 1994. Arthur Baggeroer, Brian Sperry, Khosrow Lashkari, Ching-Sang Chiu, James Miller, Peter Mikhalevsky, Keith von der Heydt, "Vertical Array Receptions of the Heard Island Transmissions," J. Acoust. Soc. Am., Volume 96, Number 4, pg. 2395-2413, October 1994.

Birdsall 1994. Theodore G. Birdsall, Kurt Metzger, Matthew A. Dzieciuch, "Signals, Signal Processing, and General Results," J. Acoust. Soc. Am., Volume 96, Number 4, pg. 2343-2352, October 1994.

Brundrit 1994. G. B. Brundrit, L. Krige, "Heard Island Signals Through the Agulhas Retroflection Region," J. Acoust. Soc. Am., Volume 96, Number 4, pg. 2464-2468, October 1994.

Bryan 1963. George M. Bryan, Marek Truchan, John I. Ewing, "Long-Range SOFAR Studies in the South Atlantic Ocean," J. Acoust. Soc. Am., Volume 35, Number 3, pg. 273-278, March 1963.

Buck 1968. N. M. Buck, "Arctic Acoustic Transmission Loss and Ambient Noise, " in J. E. Sater (ed.), "Arctic Drifting Stations," Arctic Institute of North America, 1968.

Burdic 1984. William S. Burdic, Underwater Acoustic System Analysis, Prentice-Hall Inc., Englewood Cliffs, NJ, 1984.

Cato 1976. Douglas H. Cato, "Ambient Sea Noise in Waters Near Australia," J. Acoust. Soc. Am., Volume 60, Number 2, pg. 320-328, August 1976.

Cato 1980. Douglas H. Cato, "Some Unusual Sounds of Apparent Biological Origin Responsible for Sustained Background Noise in the Timor Sea," J. Acoust. Soc. Am., Volume 68, Number 4, pg. 1056-1060, October 1980.

Clarke 1995. D. B. Clarke, J. W. White, D. B. Harris, "Hydroacoustic Coupling Calculations for Underwater and Near-Surface Explosions," Lawrence Livermore National Laboratory, UCRL-ID- 122098, September 1995.

Collins 1995. Michael D. Collins, "Three-Dimensional Effects in Global Acoustics," J. Acoust. Soc. Am., Volume 97, Number 3, pg. 1567-1575, March 1995.

DNA 1991. EM-1, "Capabilities of Nuclear Weapons: Chapter 5-Underwater Explosions (U)," DNA-EM-1-CH-5, Naval Surface Warfare Center White Oak, Silver Spring, MD, September 1991, Confidential.

Farrell 1996. Ted Farrell, Kevin LePage, Chris Barclay, "Users Guide for the Hydroacoustic Coverage Assessment Model (HydroCAM) Version 1.0," BBN Systems and Technologies, Arlington, VA 22209, BBN Tech. Memo. W1273, August 1996.

Munk 1994. Walter Munk, Robert Spindel, Arthur Baggeroer, Theodore Birdsall, "The Heard Island Feasibility Test," J. Acoust. Soc. Am., Volume 96, Number 4, pg. 2330-2342, October 1994.

Thorp 1965. William H. Thorp, "Deep-Ocean Sound Attenuation in the Sub-and Low-Kilocycle-per-Second Region," J. Acoust. Soc. Am., Volume 38, pg. 648-654, 1965.

Urick 1062. R. J. Urick, "Generalized Form of the Sonar Equation," J. Acoust. Soc. Am., Volume 34, Number 5, pg. 547-550, May 1962.

Urick 1963. R. J. Urick, "Low-Frequency Sound Attenuation in the Deep Ocean," J. Acoust. Soc. Am., Volume 35, Number 9, pg. 1413-1422, September 1963.

Urick 1966. R. J. Urick, "Long-Range Deep-Sea Attenuation Measurement," J. Acoust. Soc. Am., Volume 39, Number 5 (Part 1), pg. 904-906, 1966.

Urick 1971. R. J. Urick, "Handy Curves for Finding the Source Level of an Explosive Charge Fired at a Depth in the Sea," J. Acoust. Soc. Am., Volume 49, Number 3 (Part 2), pg. 935-936, 1971.

Urick 1983. R. J. Urick, Principles of Underwater Sound, 3rd Edition, McGraw-Hill Book Company, New York, 1983.

APPENDIX E. RADIONUCLIDE DETECTION

Introduction

In this section we will discuss the radionuclide sensor subsystem model. The discussion will follow the model's computational sequence:

1. **User input**. The input is used to initialize the calculations.
2. **Source term**. This is divided into four parts: 1) the calculation of the number of atoms of a particular nuclide produced directly from the nuclear explosion, 2) the number of atoms of that nuclide retained in the underground cavity for subsurface bursts, 3) the number of atoms removed by direct deposition in the near field as a result of incorporation into heavy particles from upsweep of surface debris (for both subsurface and near surface detonations), and 4) for each nuclide under consideration, the determination of the final number of atoms and their activity that are assessed to be in the initial cloud.
3. **Initial debris cloud elevation**. This determines the wind field used to calculate the motion of the cloud.
4. **Debris cloud motion**. The wind field determines the motion of the center of the cloud.
5. **Dry deposition and rain effects**. These processes remove aerosols from the cloud.
6. **Radioactive debris cloud diffusion**. Here we calculate the atmospheric concentration of a particular radionuclide at each sensor taking into account cloud diffusion and all of the previously discussed effects.
7. **Radioactive decay and detection**. Here the algorithm accounts for radioactive decay and determines if a detection has occurred at a particular sensor.
8. **Model validation**. The various parts of the model have been validated using the general literature and the whole model has been validated by comparing its results to those of HY-SPLIT.
9. **Important limitations.** These must be kept in mind when evaluating the results.

Overall Process

Figure E1 shows the various steps in the process that we are trying to model. First, the explosion and the production of the nuclides. Second, the release of those nuclides from the underground cavity, if the explosion is underground. Third, the early fallout and development of the initial cloud. Fourth, the transport of the debris cloud to the sensor taking into account the expansion of the cloud due to atmospheric turbulence, dry deposition and rainout of the aerosols, and radioactive decay and finally, the probability of detection by the sensor.

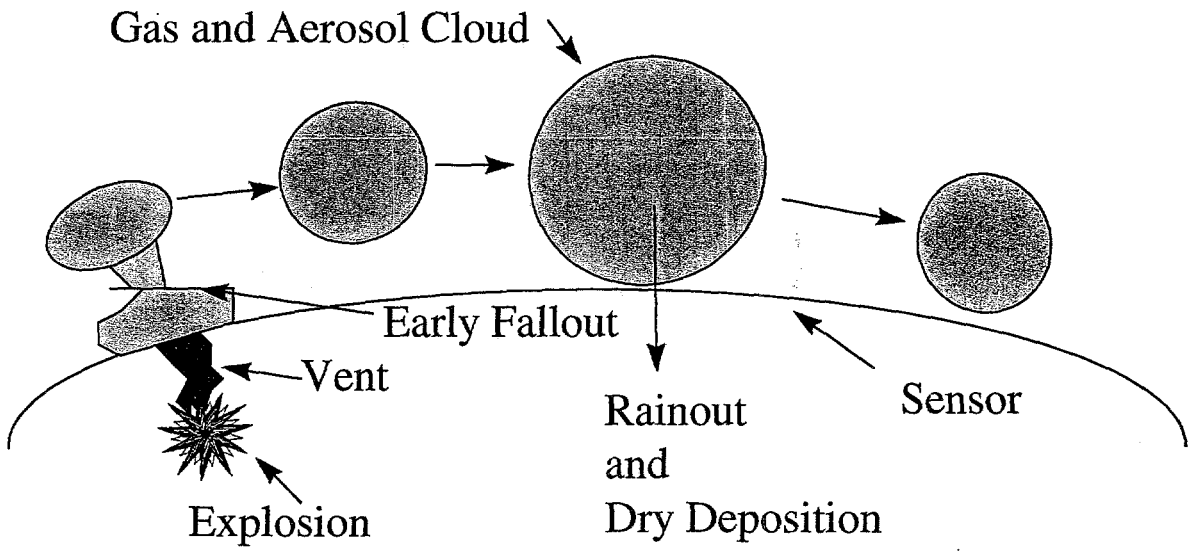

Figure E1. Overall Process

System Initialization

The first step in evaluating a network is to define the characteristics of the network we wish to evaluate. In order to define a network one needs to specify the location of each sensor in the network, the local background concentration of the nuclides being evaluated, the standard deviation in these backgrounds, and the sensitivity of the sensors. All of this information is incorporated into the station data file "**VSEMRDN.INP.**" In addition a flag indicating whether or not the station has only aerosol or Xenon sensors or both is included.

The file consists of a header line with a 15-character label for the file and a 75-character description. Each line in the file represents the characteristics of an individual station in the network. First, the flag setting the status of the sensors: 0 = no sensors, 1 = both Xenon and aerosols, 2 = aerosols only, and 3 = Xenon only. Then the latitude and longitude as decimal numbers from -90 to +90 and -180 to +180, respectively. Next the mean background of Xe-133g, the background standard deviation of Xe-133g, the sensitivity of the sensor to Xe-133g, the mean background of Ba-140, the background standard deviation of Ba-140, and the sensitivity of the sensor to Ba-140 all in Bq/m^3. This is usually followed by text describing the station location, number, etc. A typical, but truncated file is shown below:

```
RDN-IMS 79 CURRENT IMS 1/13/97
1  -41.01  -71.25 2.50E-06 1.25E-06 1.00E-03 0.00E+00 0.00E+00 3.00E-05 Argentina Beriloche
1  -34.00  -58.00 2.50E-06 1.25E-06 1.00E-03 0.00E+00 0.00E+00 3.00E-05 Argentina Buenos Aires
1  -24.00  -65.00 5.00E-06 2.50E-06 1.00E-03 0.00E+00 0.00E+00 3.00E-05 Argentina Salta
1  -12.00   97.00 5.00E-06 2.50E-06 1.00E-03 0.00E+00 0.00E+00 3.00E-05 Australia Cocos Is.
1  -12.40  130.70 5.00E-06 2.50E-06 1.00E-03 0.00E+00 0.00E+00 3.00E-05 Australia Darwin
  .....
```

Second, one must define the event and calculation characteristics that can be divided into:

1) Model Control - single location or 7.5^{O} world-wide grid of detonation points,

2) Event Specification - time of burst: year, month, day, hour, minute (the radionuclide calculation uses only the month in order to select monthly wind patterns), event latitude and longitude (used for single event calculation, ignored for contour plot), event altitude in km, and total yield in kt, and

3) Radionuclide Technology Specifications - inclusion flag: 0 = no radionuclide calculation, 1 = perform a radionuclide calculation; number of hours from detonation to end of detection calculation; fission fraction - the fraction of the energy produced from fission vs. total yield (this is used to determine the actual production of the different nuclides for the different neutron energies characteristic of fission and fusion events); venting fraction - specify a vent fraction for aerosols used to override the default calculation in the code or use a value greater than 1.0 for the default calculation; detection threshold - the number of standard deviations over mean background the signal must be to call a detection; and rainout effects - this represents the intensity of the rain in mm/hr. and the duration of the rain in hours.

These are entered into the "**VSEMINP.INP**" file that is the general user input file. These user inputs combined with the defaults allow the user to tailor the calculation for a wide variety of events and conditions.

MODEL CONTROL

1 1 for single event, 2 for contour plot
1 location accuracy parameter (0 no location, 1 with synergy, 2 no synergy)
0 progress tracking parameter (0 for no tracking, 1 for tracking)

EVENT SPECIFICATION

1996 year
10 month
1 day
0 hour
0 minute
40. latitude
-100. longitude
-0.035 altitude (km)
1 yield in kt

RADIONUCLIDE TECHNOLOGY SPECIFICATION

1 include index (1 for include, 0 for leave out)
240 maximum allowed detection time from the event in hours (>24)
1. fission fraction
2. earth vent fraction (use 0. to1., or use >1. for built-in computation)
2.6 threshold (number of background standard deviations)
0.0 rain intensity in mm/hr
0.0 rain duration in hr.

Figure E2 shows an example network of 80 sensor sites selected as part of a study to maximize worldwide coverage with a 10 day detection time. This is an example, and does not represent any real or proposed network.

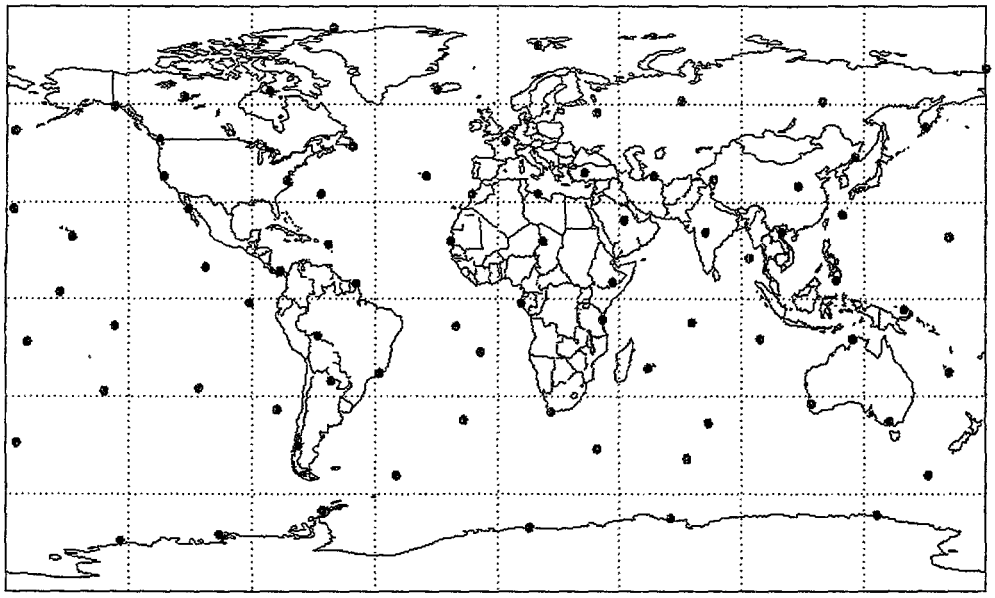

Figure E2. Example Sensor Network

In addition to these two user files, two data files are used in the radionuclide calculation and are included with the code. The first is a 2^{O} Land-Sea map which is used to determine if a subsurface detonation is underground or underwater (this is modified from etopo5, a 5 min topographical map of the world) and the second is a wind file which contains 15^{O} gridded average monthly weather data (NOAA, 1993) (N/S and E/W wind speed and standard deviations from surface to 10 mbar) used to determine debris cloud transport.

Source Term Calculation

In this section, we will discuss the calculation of the initial number of atoms of a particular nuclide produced in the nuclear explosion from first principles. The model currently evaluates weapons fueled with U-235 only (results for U-238 and PU-239 will be slightly different, but should not change the overall model results significantly).

The number of atoms of a particular nuclide produced depends on the energy of the neutron responsible for the fission. Fission yields are available in the general literature (GE 1974) for fission's produced by thermal neutrons, fast neutrons produced from fission, and very fast neutrons (14 Mev) produced from thermonuclear reactions (fusion). These yields are for both the total chain yield of mass number A and the independent yield of each nuclide in the chain (Broom 1962, Wahl 1955, Cuninghame 1957, Strom 1966, Norris 1966, Wahl 1962, Katcoff 1960, Vandenbosch 1973). The number of atoms is calculated by first calculating the total number of fissions, then determining the fraction of fissions caused by neutrons in each energy

range, and finally weighting the fission yields for each energy range. The user specifies the total yield of the device and the fraction of energy resulting from fission reactions. The code then determines the amount of energy resulting from fission as: [total yield • fraction from fission] and the energy resulting from fusion as: [total yield • (1- fraction from fission)]. The code then calculates the total number of neutrons produced in each process and the fraction of the total number of neutrons from each process. Fissions are assumed to be equally likely by any neutron and the total number of fissions from fast neutrons or 14 Mev neutrons is calculated (This is not really correct since in a two stage weapon the fissions in the first stage are primarily from fast neutrons and in the second stage the fissions are not all from 14 Mev neutrons; however, the user can adjust these parameters to create the source term he wants and it gives the right behavior in the relative number of nuclides).

The code currently tracks two nuclides: Ba-140 and Xe-133g. For Ba-140, we assume that all atoms of 140 mass number above Ba in the fission fragment decay chain decay immediately to the nuclide of interest because of their very short half-lives. For Xe-133g; however, its aerosol precursor I-133g has a half-life of 21 hr. which is significant in terms of the transport time of the debris cloud and the time over which chemical (retention of Iodine in aerosol particles) and mechanical effects operate (rainout and gravitational settling are included in this analysis). We simplify the Xenon decay chain by first assuming all aerosol precursors decay immediately to I-133g, and that the I-133g all decays directly to Xe-133g (i.e., none going to Xe-133m). Because of the long half-life of Xe-133m (2.193 days) and the fact that the independent yield of Xe-133m is about 4 times that of Xe-133g, we account for the decay of the independent yield of Xe-133m to Xe133g separately and add it to the final Xe-133g concentration. The neglect of the fractional decay of I-133g to Xe-133m introduces about a 3% error into the calculations and does not impact the results significantly. The code then calculates the total number of atoms and total activity of each nuclide using a weighted average of the fission yields for the different energy ranges.

Decay Chain For Atomic Mass Number 140

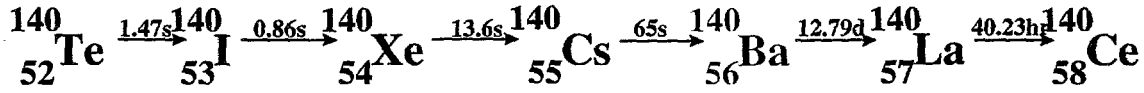

Decay Chain For Atomic Mass Number 133

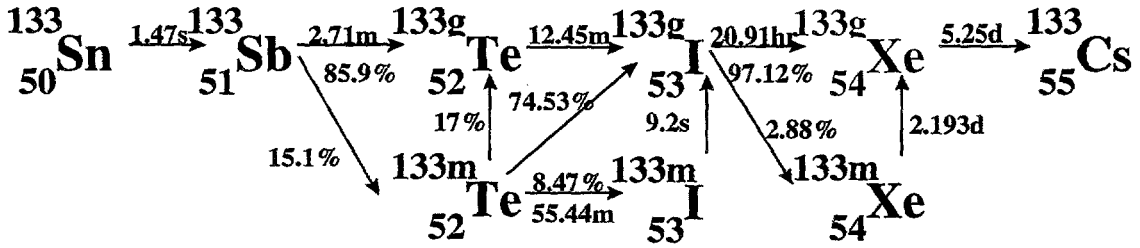

Figure E3. Fission Product Decay Chains

For a pure fission weapon fueled with U-235, the fission yield of mass number 133 (not including Cs) is approximately = 0.065; while for mass number 140 (not including La and Ce) it is approximately = 0.060. For a 1 kt weapon, the total number of fissions is = $1.45139 \cdot 10^{23}$ and the total number of atoms of mass 133 is, therefore, = $9.38366 \cdot 10^{21}$ which is apportioned as: aerosol precursors (i.e., I-133g) = $9.37533 \cdot 10^{21}$, Xe133m = $6.87683 \cdot 10^{18}$, and Xe133g = $1.45719 \cdot 10^{18}$. The independent yield of Xe-133m is, therefore, about 4.7 times that of Xe-133g. The total number of atoms of mass 140 is = $8.75646 \cdot 10^{21}$.

Corrections For Venting

If the burst is at or above ground level, all radionuclides are immediately free to participate in the atmospheric transport; however, for underground or underwater bursts some fraction of the aerosols produced is retained in the detonation medium and some fraction is released over an extended period of time. For this analysis, we consider only immediate releases of fission products and this is assumed to include all materials released within the first 12 hrs. of the detonation. Also, for noble gas nuclides, the precursors in the fission fragment decay chain are aerosols and so can be trapped by the same process.

For aerosols and aerosol precursors, we use correlations found in the KDFOC3 code (Harvey 1994) and in EM-1 (DNA 1990) to estimate the fraction of the aerosols that are retained in the medium. The code first calculates a scaled depth of burst (SDOB) which is a function of the actual depth (HOB, height of burst) and the yield of the device ($SDOB=HOB/Y^{1/3.4}$). It sets the vent fraction (fv) for the noble gases produced directly from fission equal to 1.0. It then calculates for aerosols the vent fraction appropriate for wet (water or ocean) and dry (dry rock or land) medium using correlations from the KDFOC3 code. The assumption that the correlation for wet medium can be used for water is very weak and is in the process of being revised but it is used in the current version to give the correct behavior in water (i.e., that the release from an equivalent depth of water is greater than the same depth of land).

The vent fraction computation depends on the user specified vent fraction in the following manner:

1) If the user specifies a vent fraction greater than 1.0, the code uses the default calculations contained in the code.

2) If the user specified vent fraction is greater than $1 \cdot 10^{-20}$ but less than or equal to one, the code assumes the user wishes to override the default calculation for underground bursts only and sets the aerosol vent fraction for those cases to the user specified value; however, the gas vent fraction is still set to 1.0. Detonations in the ocean always use the default calculation even though a vent fraction between 0 and 1 is specified by the user.

3) If the user specifies a vent fraction that is less than $1 \cdot 10^{-20}$ then the code assumes that the user does not want any radionuclide venting for this scenario and sets all

underground vent fractions to zero including that for the direct yield of noble gases. Underwater detonations are not affected.

Figure E4 shows a plot of the KDFOC3 correlations used to determine the default vent fractions for underground or under water bursts versus scaled depth of burst.

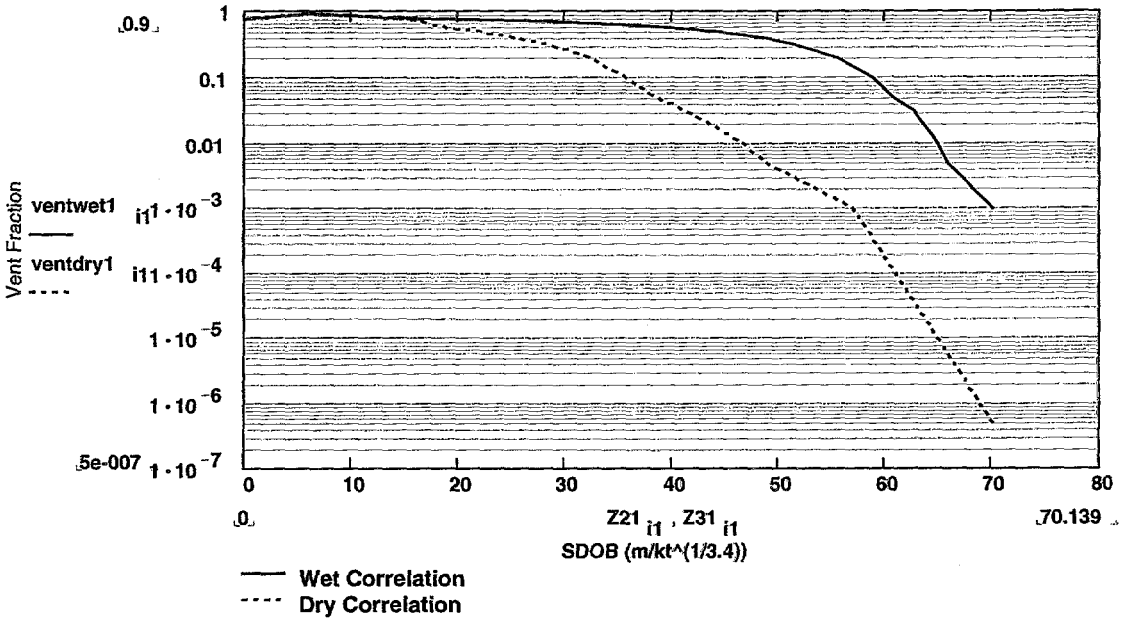

Figure E4 Vent Fractions vs. Scaled Depth of Burst

Early Deposition

Early fallout results from the fact that for bursts near the earth's surface some of the radionuclides produced are entrained in large aerosol particles produced from the material swept up from the surface during the explosion. Some of these particles are so large that they immediately fall back to the surface and any material trapped in them can not participate in the formation of the initial cloud; although, they may be released later over a long period of time at the surface. For this calculation, these nuclides are assumed not to participate in the general motion of the cloud and so can not be detected at a distance. We subtract, therefore, any nuclides trapped in these particles from the source term. This process only affects aerosols and the aerosol precursors of the noble gases at the time of the explosion. The fraction deposited is estimated from correlations in EM-1 and is a function of the total yield of the device and the distance from the surface or height of burst. If the HOB is greater than $\mathbf{55 \cdot yield^{0.4}\ m}$ then the burst is far enough from the surface that no direct fallout is produced. If the burst is on or below the surface, then about 1/2 is deposited. (This is assumed true for both land and water in this calculation but clearly the deposition in or over water will be different since the entrainment medium, water, is very different than soil. This is currently under investigation and will be improved in subsequent

model versions). From the surface to the maximum height, the amount remaining in the cloud increases according to the formula:

$$fd = 1 - fdep = 1 - 0.5 \cdot 0.453^{HOB/(Y^{1/3} \cdot 20\,m)}$$

Figure E5 shows a plot of the fraction deposited as early fallout for a 1 kt burst at various altitudes. Notice that the function is discontinuous at the maximum height. This effect is small and does not affect the results significantly.

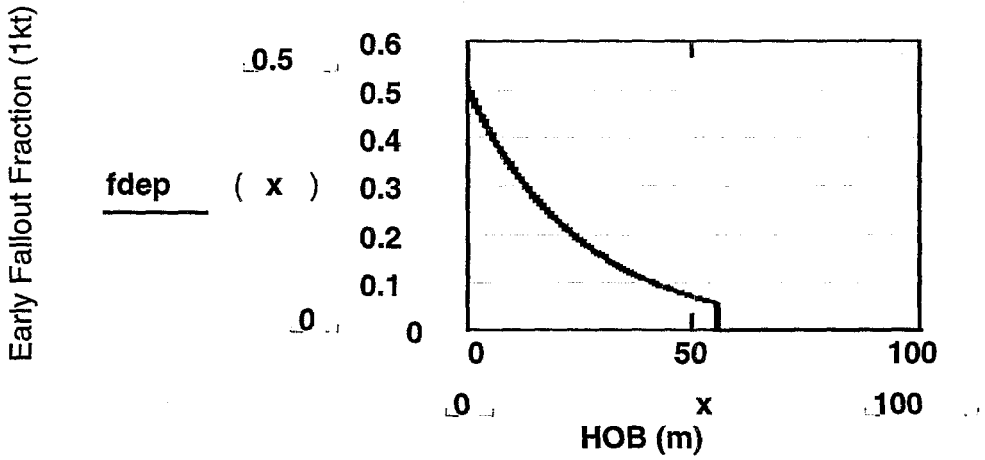

Figure E5. Early Fallout Fraction vs. Detonation Altitude For 1 Kt

Initial Cloud Configuration

Once the source terms are calculated, the initial configuration of the cloud that contains these nuclides must be determined. Descriptions of the evolution of the initial cloud from a nuclear detonation are given in EM-1 and the KDFOC3 manual. These descriptions show how the cloud can be represented by a base cloud and stem for deeply buried bursts; base cloud, stem and main cloud for near surface bursts, and stem and main cloud for high altitude bursts. For this analysis, all of the radionuclides released at the time of detonation are assumed to be in a single cloud that is the sum of the base, stem, and main cloud. For surface or atmospheric bursts, correlations given in EM-1 are used to determine the top and bottom height of the final stabilized cloud produced from the explosion and are given in Figure E8.

For underground or underwater bursts, we must first calculate an equivalent yield and then use the same correlations. The equivalent yield is determined by summing the energy released to the base and main clouds using other correlations given in EM-1 that show the fraction of the energy of the device released to the main and base cloud from subsurface explosions versus the scaled depth of burst.

Equivalent Yield for Main Cloud for Underground bursts

Figure E6 shows the correlations from EM-1 for the fraction of energy released to the main cloud for both wet and dry medium as a function of scaled depth of burst.

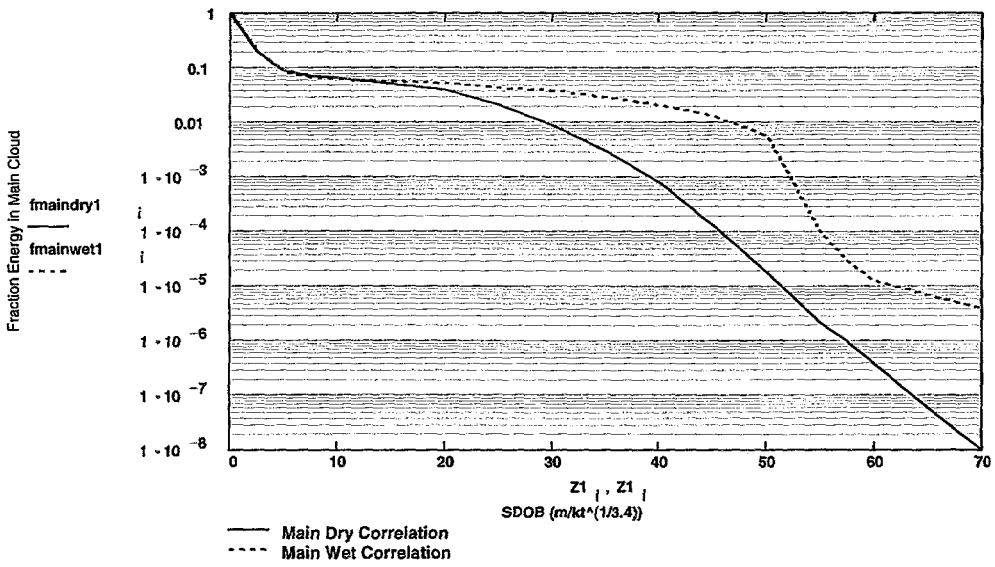

Figure E6. Fraction of Energy Released to Main Cloud

Equivalent Yield for Base Cloud for Underground bursts

Figure E7 shows the correlations from EM-1 for the fraction of energy released to the base cloud for both wet and dry medium as a function of scaled depth of burst.

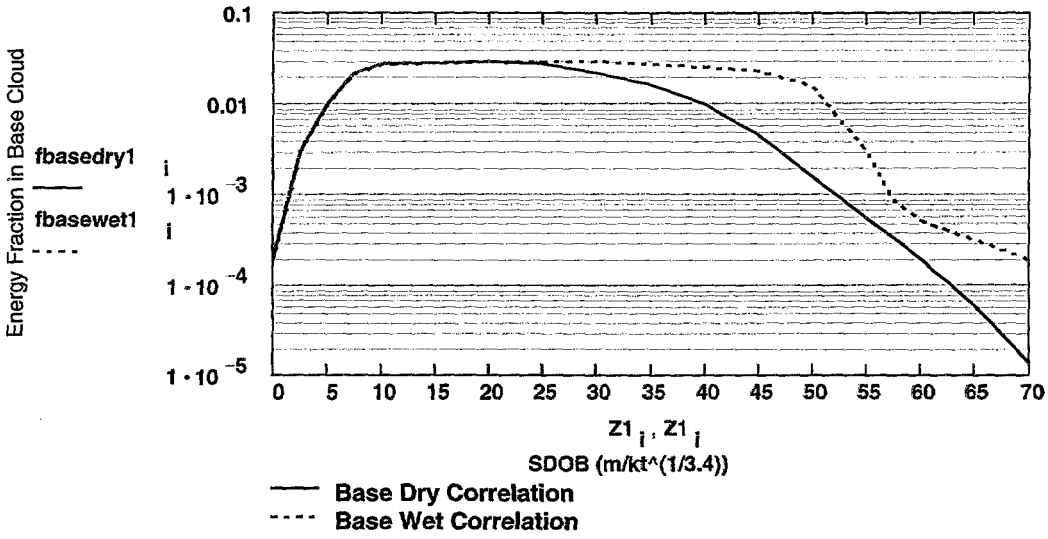

Figure E7. Fraction of Energy Released to Base Cloud

Cloud Top and Bottom Heights

Figure E8 shows the correlations from EM-1 that give the top and bottom heights of the final stabilized cloud versus the yield of the device. These values are averaged to give a center altitude for the cloud that is used to determine the wind field used for cloud transport. The three curves represent the data, a cubic spline interpolation, and a linear interpolation on the log of the yield.

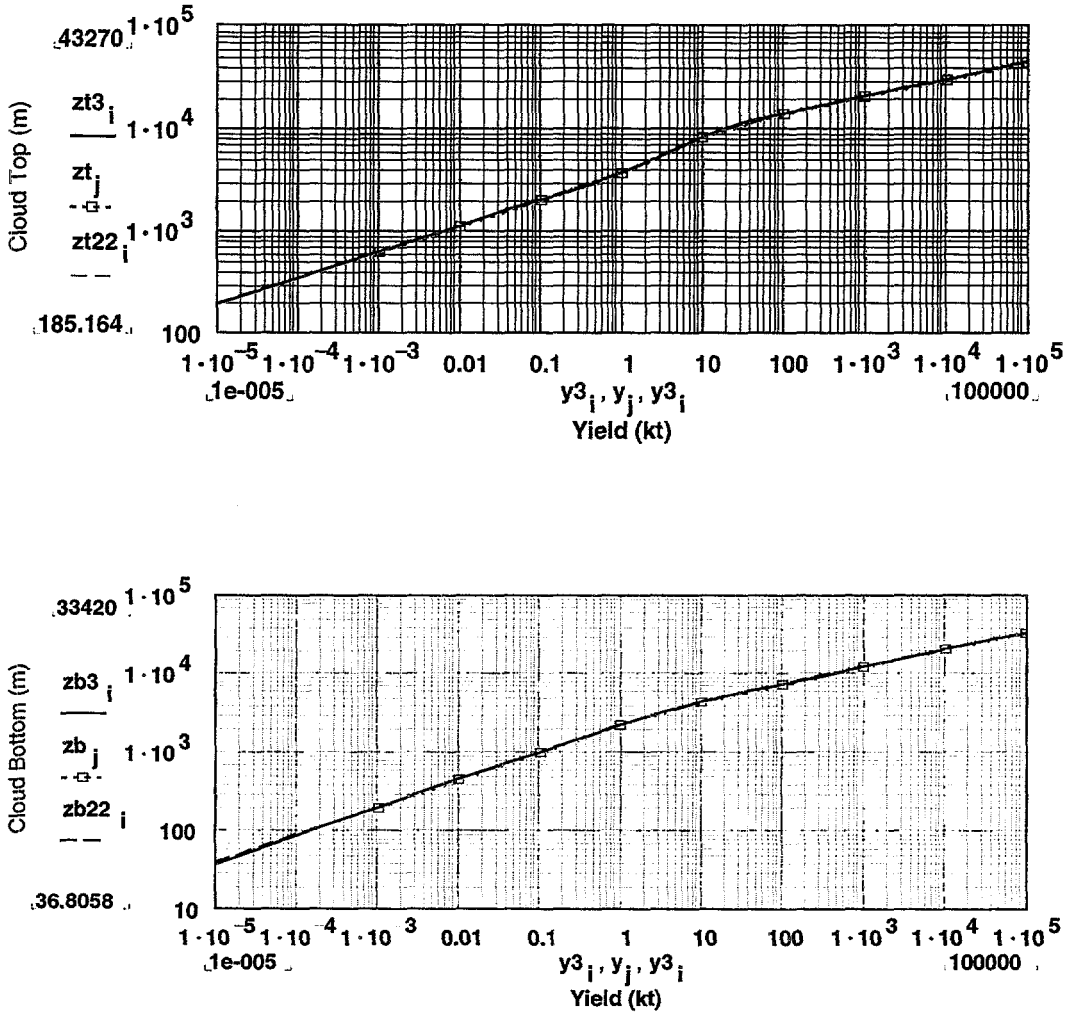

Figure E8. Cloud Top and Bottom Altitudes vs. Yield

Wind Field and Cloud Trajectories

In order to construct a trajectory for the cloud and to account for the different wind fields at different times of the year and at different altitudes, we have used a world-wide data base from NOAA (NOAA 1993). This data base has, for a 2.5^{O} grid spacing and for each month of the year (Period of Record = 1985-1991), mean wind speed and standard deviation for the North-South and East-West wind components at 15 different heights from the surface to 10 mbar. We have

reduced these data to a 15^{O} grid but retained the month and altitude dependence and converted from mbar to km using a standard atmosphere. In order to simulate the trajectory of the cloud, we use simplified versions of the methods found in atmospheric simulation studies (Charles 1959, Djuric 1961, Veerabhadra 1993, Ley 1982, Smith 1968, McNider 1988). First, using the initial location of the burst, we determine the mean wind components for the grid square in which it falls at the height of the center of the cloud; then, using a random number and standard deviation for each component, we determine a correction to the wind speed components. Every hour we repeat this process and create a trajectory for the cloud center that is used to determine the distance of the cloud from each sensor site.

Figure E9 shows an example of the 15° wind pattern for surface winds in the month of January.

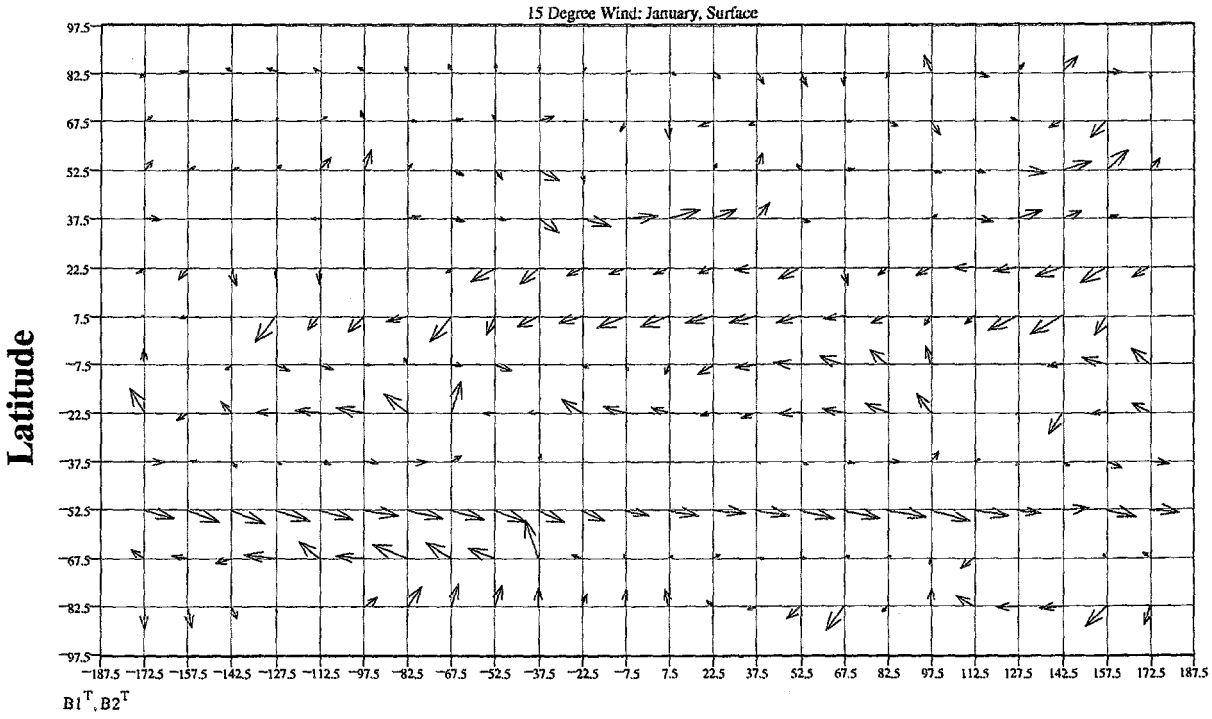

Figure E9. Surface Wind Pattern For January

Dry Deposition

For aerosol and the aerosol precursors of the noble gas nuclides, two additional effects operate to reduce the size of the source term as the material is transported in the cloud. The first of these is dry deposition. Even though the aerosol particles are small enough that they do not precipitate immediately as in the case for the early fallout, the particles do settle slowly to the ground due to gravitational settling. In order to account for this effect, we use a standard dry deposition model such as found in the MACCS code (MACCS 1990). This model is an exponential reduction in the fraction of aerosols remaining in the air as a function of the dry deposition velocity (vd,

selected for this analysis as 1 cm/sec or 36 m/hr), the elapsed time (t), and inversely proportional to the center height of the cloud (zc):

$$drydep = e^{-vd \cdot t/zc} = e^{-s \cdot t}$$

where s = vd•t/zc is defined to be the settling rate.

Rainout

The rainout model is a standard model found in the literature for use with Gaussian models (MACCS 1990, Watson 1977, Brenk 1981). It is a function of the rain intensity (I) in mm/hr and the duration of the rain (t_r) in hours. Rainout is accounted for starting at the time of burst and extending for the rainstorm's duration. The debris cloud is assumed to be completely in the rain cloud for the duration of the rain. The Iodine aerosol precursor of Xenon that is removed from the cloud as a result of these mechanisms is not allowed to contribute to the Xenon concentration used to determine detection probability.

$$rainout = e^{-(a \cdot I^b \cdot t_r)} = e^{-r \cdot t_r}$$

where $r = a \bullet I^b$ is defined to be the washout coefficient, t_r is either the transport time or the rain duration whichever is smaller, a is 0.342/hr ($9.5 \bullet 10^{-5}$/sec), and b is a dimensionless constant = 0.8.

Diffusion

As the cloud moves in the wind field, we account for turbulent diffusion using the standard Gaussian model used in meteorological modeling of environmental pollutants (Sutton 1932, Overcamp 1982, Palazzi 1982, Wilson 1981, Dvore 1982, Overcamp 1990, Wilson 1982) and in the MACCS (MACCS 1990) code for radiological releases from reactor accidents. These models in various forms and complexity have been used in the atmospheric sciences for modeling continuous and transient releases of material of all kinds, and estimates of the appropriate parameter values have been determined by comparison to experimental results from the release of materials into the atmosphere and from attempting to model actual releases from mining activity and dust storms (Gifford 1987, Gifford 1982, Carras 1988, Haagenson 1990, Barr 1987, Fowler 1983, Kristensen 1981, Gifford 1991, Rodriguez 1995, Lupini 1981, McNider 1988). The model used in IVSEM represents the initial cloud as an instantaneous release. The expansion of the cloud proceeds independently in both the horizontal and vertical directions using Fickian diffusion coefficients (i.e., the coefficients increase linearly with time). Terms to account for reflection of the portion of the cloud that hits the ground are included. We determine the concentration of each radionuclide at some distance (R) from the center of the cloud at ground level every hour. The final equation for the concentration at the surface from a cloud at height zc, neglecting radioactive decay, dry deposition, and rainout terms, is given by:

$$D(R(t),t) = \frac{e^{-\frac{1}{4\cdot t}\cdot\left(\frac{r^2}{kr}\right)} \cdot 2 \cdot e^{-\frac{zc^2}{4\cdot t\cdot kz}}}{8\cdot(\pi\cdot t)^{1.5}\cdot(kr\cdot kr\cdot kz)^{.5}}$$

where: D(R(t), t) is the relative concentration of any nuclide in the cloud (per m^3), R(t) is the radial distance from the center of the cloud to the sampling point at the time the sample is taken (m), and t is the time the sample is taken measured from the time of the detonation (hr), zc is the center height of the cloud (m), kr is the radial diffusion coefficient ($3.6\bullet10^8$ m^2/hr or $1\bullet10^5$ m^2/sec), and kz is the vertical diffusion coefficient ($1.8\bullet10^4$ m^2/hr or 5 m^2/sec).

Sampled Independent Xenon 133g

The final Xenon source term is divided into two parts: the "dependent" Xenon resulting from decay of its aerosol precursors and the "independent" Xenon produced directly from fission as Xe-133g and Xe-133m. The direct production is 0.09% of the total number of atoms of mass number 133 so most of the Xenon results from the decay of its aerosol precursors of which I-133 with a half-life of 20.8 hours is the dominant nuclide. IVSEM tracks the dependent and independent Xenon separately because of the different physical process that the aerosol precursors are subject to. In this section, we will discuss how IVSEM handles the independent Xenon. Dependent Xenon will be discussed in the following section.

At any time after the event, the total number of independent Xe-133g atoms in the cloud depends only on the number of Xe-133g and Xe-133m atoms originally vented to the atmosphere and the radioactive decay of Xe133m into Xe-133g and the decay of Xe-133g into Cs-133. Because both isotopes are noble gases, the same physical processes act on each and, for our purposes, they behave exactly the same. At any time t (in hours), measured from the event, the number of independent atoms of Xe-133g in a one hour sample taken at time $t_s < t$ at a station can be represented using the following model:

$$gind(t) = Gind(t)\cdot D(R(t_s),t_s)\cdot VG$$

where Gind(t) is the total number of independent Xe-133g atoms remaining in the cloud accounting for radioactive decay up to time t (this includes the decay of independent Xe-133m to Xe-133g), $D(R(t_s),t_s)$ is the relative concentration of any radionuclide in the cloud as a result of diffusion as described in Section E.11 at the time the sample is taken, and VG is the sampling volume flow rate for gases in m^3/hr. Since independent Xe-133g and Xe-133m are captured in the sample in the same ratio that they exist in the cloud at the time the sample was taken, they continue to decay just as they did in the cloud; therefore,

$$Gind(t) = 0.0009\cdot N_{133}\cdot fvxe\cdot\{A\cdot e^{-\lambda_g\cdot t} + B\cdot e^{-\lambda_m\cdot t}\}$$

where: A = 0.17-B, B = 0.83• $\lambda_m/(\lambda_g-\lambda_m)$, λ_m is the decay constant for Xe-133m, λ_g is the decay constant for Xe-133g, fvxe is the vent fraction of the independent Xenon that is in the cloud (the default model assumes that all the independent Xenon always escapes (fvxe = 1) except if the user sets the aerosol vent fraction to less than 1E-20 when the model assumes the user does not want any radionuclide release (fvxe = 0)), and $0.0009 \bullet N_{133}$ is the total number of Xenon atoms of mass number 133 produced directly from the nuclear detonation . The activity of Xe-133g in a one hour sample taken at time t_s at time t is, therefore, $\lambda_g \bullet$ gind(t).

Sampled Xenon 133g From Precursor Aerosols

Because the aerosol precursors of the dependent Xenon are removed from the sample at the time it is collected and because the aerosol precursors are subject to significantly different physical processes than the noble gases, the behavior in the number of dependent Xenon atoms in the sample is more complicated.

The number of dependent atoms of Xe-133g in a one hour sample taken at time t_s at a station is:

$$gdep'(t_s) = Gdep(t_s) \cdot D(R(t_s),t_s) \cdot VG$$

where Gdep(t_s) is the total number of Xe-133g atoms produced from decay of Iodine in the cloud at the time the sample is taken, D(R(t_s),t_s) is the relative concentration of any radionuclide in the cloud at the time of the sample, and VG is the sampling volume flow rate for gases in m^3/hr. When Xe-133g from precursors is captured in a sample, the decay process changes since I-133g is removed from the sample and dry deposition and rainout no longer apply. Also, we neglect the fact that Xe-133m is also being produced from the decay of I-133g (only 2.88% of the I-133g decays to Xe-133m). The reason for this is that, if none or only a very small amount of aerosols escape, the source term is dominated by the independent yield where we account for the Xe-133m; but, if significant aerosols escape, the source term will be dominated by the I-133g decay and neglecting Xe-133m will introduce only a 2.88% error.

If $t_r \geq t_s$

$$Gdep(t_s) = 0.9991 \cdot N_{133} \cdot fv \cdot fd \cdot \{A \cdot e^{-\lambda_g \cdot t_s} + B \cdot e^{-(\lambda_I + s + r) \cdot t_s}\}$$

If $t_r < t_s$

$$Gdep(t_s) = 0.9991 \cdot N_{133} \cdot fv \cdot fd \cdot \{C \cdot e^{-\lambda_g \cdot t_s} + D \cdot e^{-r \cdot t_r} \cdot e^{-(\lambda_I + s) \cdot t_s}\}$$

where: A = -B, B = $\lambda_I/(\lambda_g-(\lambda_I + s + r))$, D = $\lambda_I/(\lambda_g-(\lambda_I+ s))$, C = A + (B-D) •exp($(\lambda_g-(\lambda_I+ s + r))$ •t_r), λ_I is the decay constant for I-133g, λ_g is the decay constant for Xe-133g, s is the dry deposition rate, r is the rainout rate, t_r is the rainout time, fv is the aerosol vent fraction, fd is the

aerosol immediate deposition fraction and 0.9991 • N_{133} is the total number of aerosol precursor atoms of mass number 133 produced in the nuclear detonation.

The Xe-133g captured in a sample continues to decay and at any future time t:

$$gdep(t) = gdep'(t_s) \cdot e^{-\lambda_g \cdot (t - t_s)}$$

where gdep(t) is the number of atoms of Xe-133g at time t in the one hour sample taken at time t_s. The activity for a one hour sample is λ_g• gdep(t).

Sampled Barium 140

For the mass number 140 decay chain, all of the Ba-140 precursors have half-lives of less than 1 minute. The only precursor in the mass number 140 decay chain that is a gas is Xe-140 with a half-life of 13.7 sec. Because of this, we assume in this model that all the precursors immediately decay to Ba-140.

The number of atoms of Ba-140 in a one hour sample taken at time t_s at a station is:

$$gba'(t_s) = Gba(t_s) \cdot D(R(t_s), t_s) \cdot VA$$

where $Gba(t_s)$ is the total number of Ba-140 atoms in the cloud at time t_s, $D(R(t_s),t_s)$ is the relative concentration of any radionuclide in the cloud, and VA is the sampling volume flow rate for aerosols in m^3/hr. When Ba140 is captured in a sample, dry deposition and rainout no longer apply.

If $t_r \geq t_s$

$$Gba(t_s) = N_{140} \cdot fv \cdot fd \cdot e^{-(\lambda_B + s + r) \cdot t_s}\}$$

If $t_r < t_s$

$$Gba(t_s) = N_{140} \cdot fv \cdot fd \cdot e^{-r \cdot t_r} \cdot e^{-(\lambda_B + s) \cdot t_s}\}$$

where: λ_B is the decay constant for Ba-140, s is the dry deposition rate, r is the rainout rate, and t_r is the rainout time, fv is the vent fraction, fd is the early deposition, and N_{140} is the number of mass number 140 atoms produced in the detonation.

The Ba-140 captured in a sample continues to decay and at any future time t:

$$gba(t) = gba'(t_s) \cdot e^{-\lambda_B \cdot (t - t_s)}$$

where gba(t) is the number of atoms of Ba-140 at time t in the one hour sample taken at time ts. The activity for a one hour sample is $\lambda_B \bullet g(t)$.

Sampling Times, Cool Down Times, and Count Times

In order to determine if a particular sensor can detect the presence of a particular radionuclide, we must determine the concentration of that nuclide in a sample of air collected at the site over some period of time. For Xenon, only the amount of Xenon in gaseous form at the time the sample is collected is counted and all of it is assumed to be free. (Dependent Xenon is assumed to have escaped from the aerosol particles in which its parent I-133g may have been imbedded. Depending on the precise nature of the mixing of the nuclear debris with the rock or water for underground or underwater detonations, respectively, the Iodine could be homogeneously mixed or preferentially on the surface of the particles and the particles themselves could be either porous or non-porous. Therefore, the Xenon could be retained to some extent in the aerosol particles and not be free to be sampled by the Xenon sensor and the source term could be overestimated.)

The sample activity is calculated in the following fashion. First, we calculate the amount of each radionuclide in the volume of air collected for each hour of the sampling interval by multiplying the concentration at the beginning of the hour by the volume of air collected in that hour. Second, we add a decay factor to time shift each one hour sample comprising the total sample to the end of the sample interval. Third, we allow for a cool-down time, to reduce unwanted background radiation, and apply an appropriate decay factor and; finally, we calculate the mean activity in the sample by averaging over a counting interval to account for the radioactive decay occurring during that interval.

For this calculation, we assume that aerosol samples are taken over a 24 hour interval and Xenon samples over a 8 hour interval. A cool-down time of 24 hours for aerosols and 4 hours for Xenon is used and a counting interval of 24 hours for aerosols and 24 hours for Xenon is used.

Since we do not know when the sample will be taken relative to the passage of the cloud over the sensor site, we compute the activity for samples ending each hour after the detonation out to the maximum detection time entered by the user in the input file. We then chose the sample with the largest activity for the detection calculation.

Probability of Detection

Next we calculate the probability of recognizing the signal against the background radiation for the nuclides being detected. For purposes of this analysis, we assume that the Minimum Detectable Amount (MDA) for each sensor is known and determined based on the standard method given in Currie 1968 and Brodsky 1986. We also assume that the amount of each nuclide that exists in the atmosphere is known (The station data file contains nominal background concentrations of Xe-133g and Xe-133m from nuclear fuel cycle related activities

which are highest in the reactor belt, $+30^{O}$ to $+60^{O}$ latitude, and decrease towards the north and the south pole. The Ba-140 background is set to zero. These values are user input and when local measurements become available, after stations are installed, then the real values can be entered.).

The problem for this analysis is to be able to differentiate the presence of nuclides from a nuclear detonation from any existing background of these nuclides. In order to do this, we first calculate the total mean activity from the background and add that to the activity from the signal to get the total mean activity in the sample. We calculate a threshold level as the mean background plus n times the standard deviation of the background where n is specified by the user in the initial input. If this threshold is less than the MDA, we set the threshold equal to the MDA. We then compare the threshold to the total signal (i.e., signal plus background) assuming that the signal has a normal distribution with standard deviation equal to the square root of the sum of the squares of the standard deviations of the signal and background (The standard deviation of the signal is assumed to be 10% of the signal amplitude). We calculate the probability of detection by integrating the signal's normal distribution above the threshold.

Sample Output

Figure E10 shows a sample output of the detection effectiveness contour map for Xe-133g only generated by the model for a small underground detonation in a particular month for the example 80 station network shown before. The Xenon sensors are assumed to have a 20 $\mu Bq/m^3$ sensitivity for Xe-133g and the detection time is from 0 to 5 days.

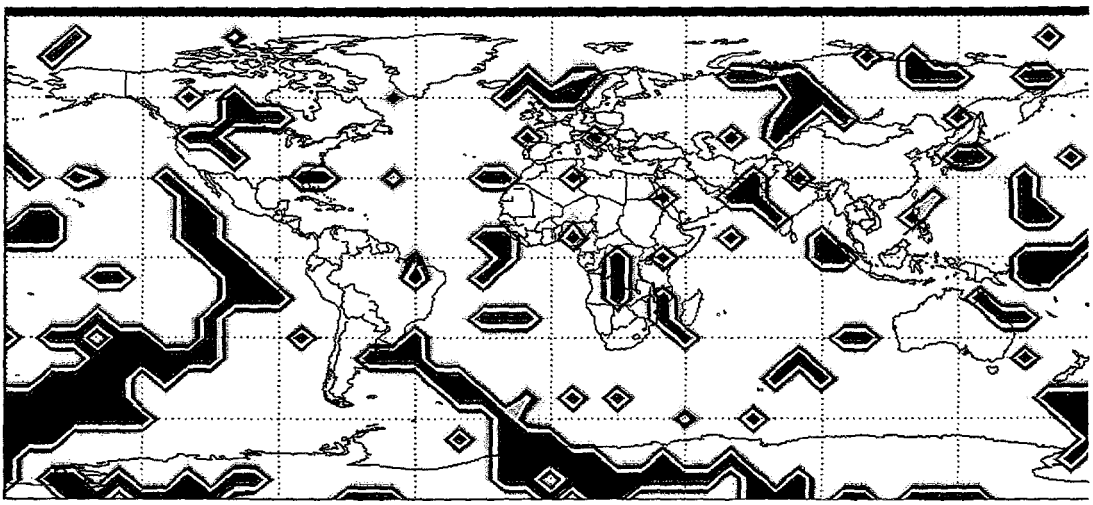

Figure E10. Detection Effectiveness at 5 Days

Model Validation

We have attempted to validate the model in several different ways. First, as described in previous sections, we have used standard submodels and parameter values determined from comparison of the models in the literature with actual and experimental observations. For example: standard radioactive decay models, fission yields from experimental data, releases from underground explosions based on correlations obtained from US test data, early deposition and initial cloud configuration models also from US test data, trajectory simulation model used in meteorological analysis, dry deposition and rainout models used in environmental impact codes and based on experimental data from artificial releases, standard diffusion model used in numerous environmental studies comparing theoretical and measured results, and a detection model based on standard signal detection theory.

Second, we have performed numerous parametric sensitivity calculations, both singly and in combination, to confirm that the model behaves in the way one would expect based on fundamental physical principles (Payne 1995).

Third, we have made some comparisons with the results of the HY-SPLIT code (Draxler 1992) being used by the Defense Advanced Research Projects Agency (DARPA) subcontractor Pacific Sierra Research (PSR). These calculations were done as identically as possible. They used the same two sensor networks, with identical sensor locations and sensitivities, the results were both averaged over a one year period with multiple weather scenarios representing the different wind conditions at different times of the year, and they used identical source terms. However, there are still major differences in the models used by the two codes, the data processing, and the way in which the results are presented. These differences are enumerated in Table E1. The comparisons were made for Ba-140 only. Table E2 shows the differences between the two networks used in the calculations. Two slightly different networks were used to see if the two codes would show similar changes in network performance for small/large differences in station location. Some stations were moved from one location to another and one station was added.

Table E1. Major Differences Between IVSEM and HY-SPLIT

IVSEM	HY-SPLIT
Single Cloud moving contiguously depending on mean altitude	Multiple levels and rings with wind depending on altitude
Simulated weather scenarios based on average monthly data	Historical weather scenarios based on 6 hr trajectory data
Yearly average: 48 runs -- 4 per month	Yearly average: 40 runs -- 10 per season
No data smoothing	Averaging over nearest neighbor points
Equal angle points (1224)	Equal distance points (1000), none on equator
Lofts cloud to equilibrium height	Release at surface

Table E2. Differences Between Net 1 and Net 2

Net 1	Net 2
Ashland, Kansas	Farmington, New Mexico
Nordvik, Russia	Noril'sk, Russia
Pt. A Pitre, Guadeloupe	Santiago De Cuba, Cuba
-	Mururoa
Nagpur, India	Allahabad, India
Bangkok, Thailand	Rahimyar Kahn, Pakistan

Figures E11-E16 show the comparisons of HY-SPLIT and IVSEM calculations at 3, 7, and 14 days for the two networks. The contours are different for the two sets of plots and Table E3 shows the correspondence.

Table E3. Contour Levels

HY-SPLIT	IVSEM
0.0 -0.25 Red	0.0-0.1 Black 0.1-0.2 Brown 0.2-0.3 Red
0.25-0.5 Orange	0.2-0.3 Red 0.3-0.4 Orange 0.4-0.5 Yellow
0.5 -0.75 Yellow	0.5-0.6 Green 0.6-0.7 Blue 0.7-0.8 Pink
0.75-0.9 Blue	0.7-0.8 Pink 0.8-0.9 Gray
0.9 - 1.0 Green	0.9-1.0 White

Even with all the differences between the two codes, time dependent coverage was very similar from short times (3 days) to long times (14 days). The weak areas were in roughly the same locations and coverage developed over time eliminating the various weak areas in roughly the same time frame. IVSEM predicts coverage developing slightly faster than HY-SPLIT. This is probably due to the differences resulting from the fact that IVSEM lofts the cloud to equilibrium altitude where winds have higher speeds while in the HY-SPLIT calculations the release is at ground level. This results in slower winds for the bulk of the cloud in the HY-SPLIT case, particularly in the equatorial region. The differences between the two networks can also be seen to have similar effects on network coverage, so both models are responding to the changes in station locations in the same way. The results of this comparison are discussed in detail in the following paragraphs.

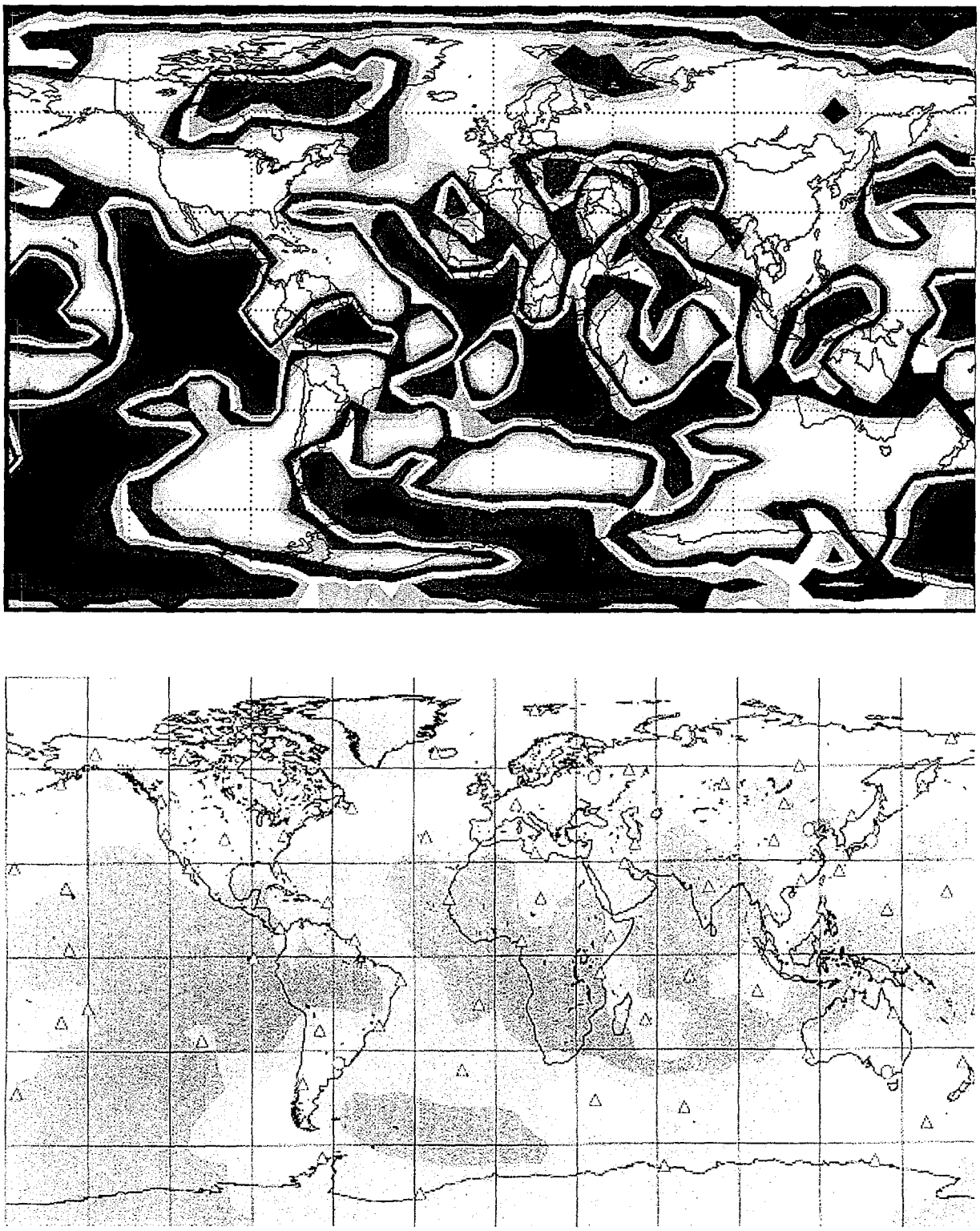

Figure E11. 3 Day Coverage, Ba-140, Net 1. Top IVSEM, Bottom HY-SPLIT

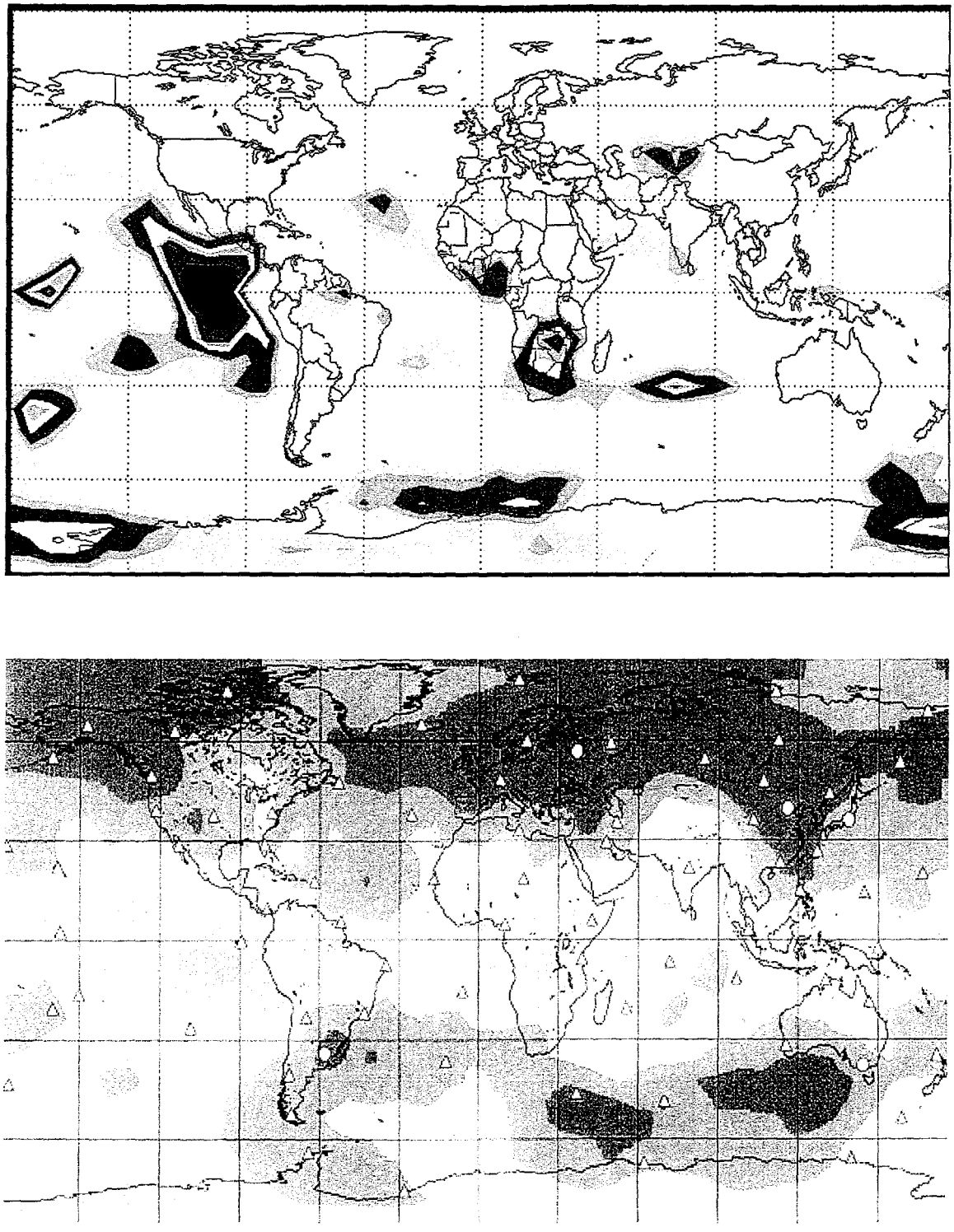

Figure E12. 7 Day Coverage, Ba-140, Net 1. Top IVSEM, Bottom HY-SPLIT

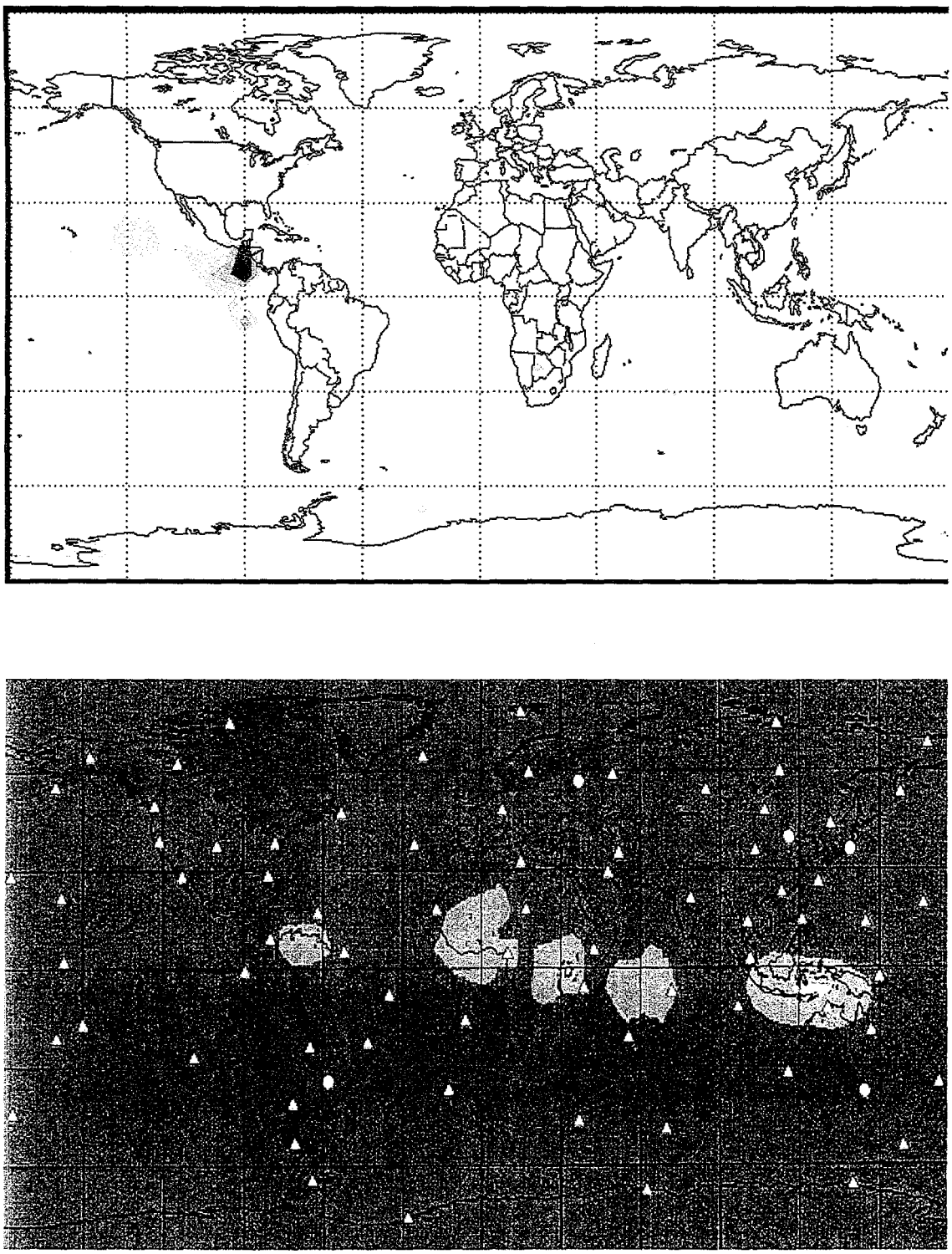

Figure E13. 14 Day Coverage, Ba-140, Net 1. Top IVSEM, Bottom HY-SPLIT

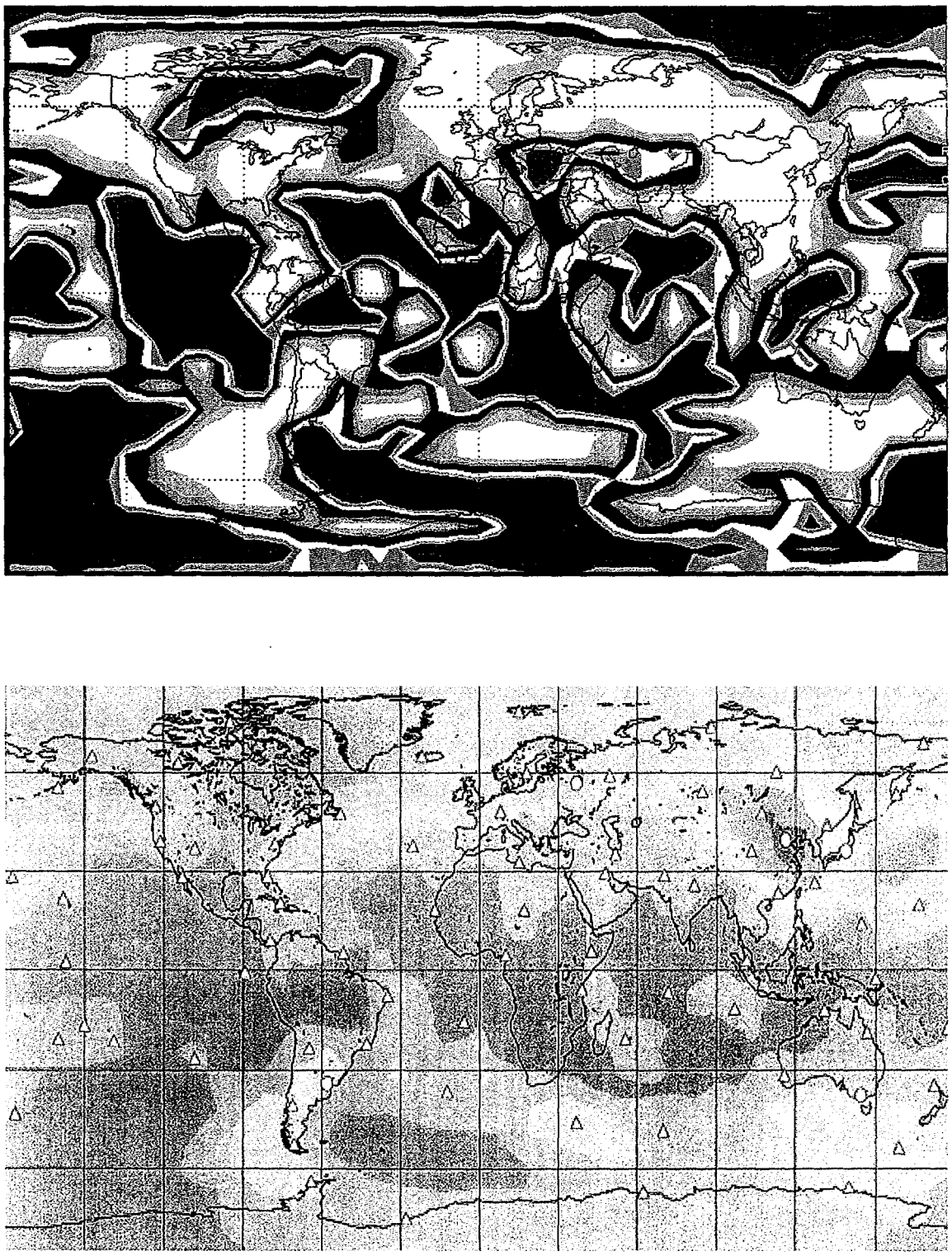

Figure E14. 3 Day Coverage, Ba-140, Net 2. Top IVSEM, Bottom HY-SPLIT

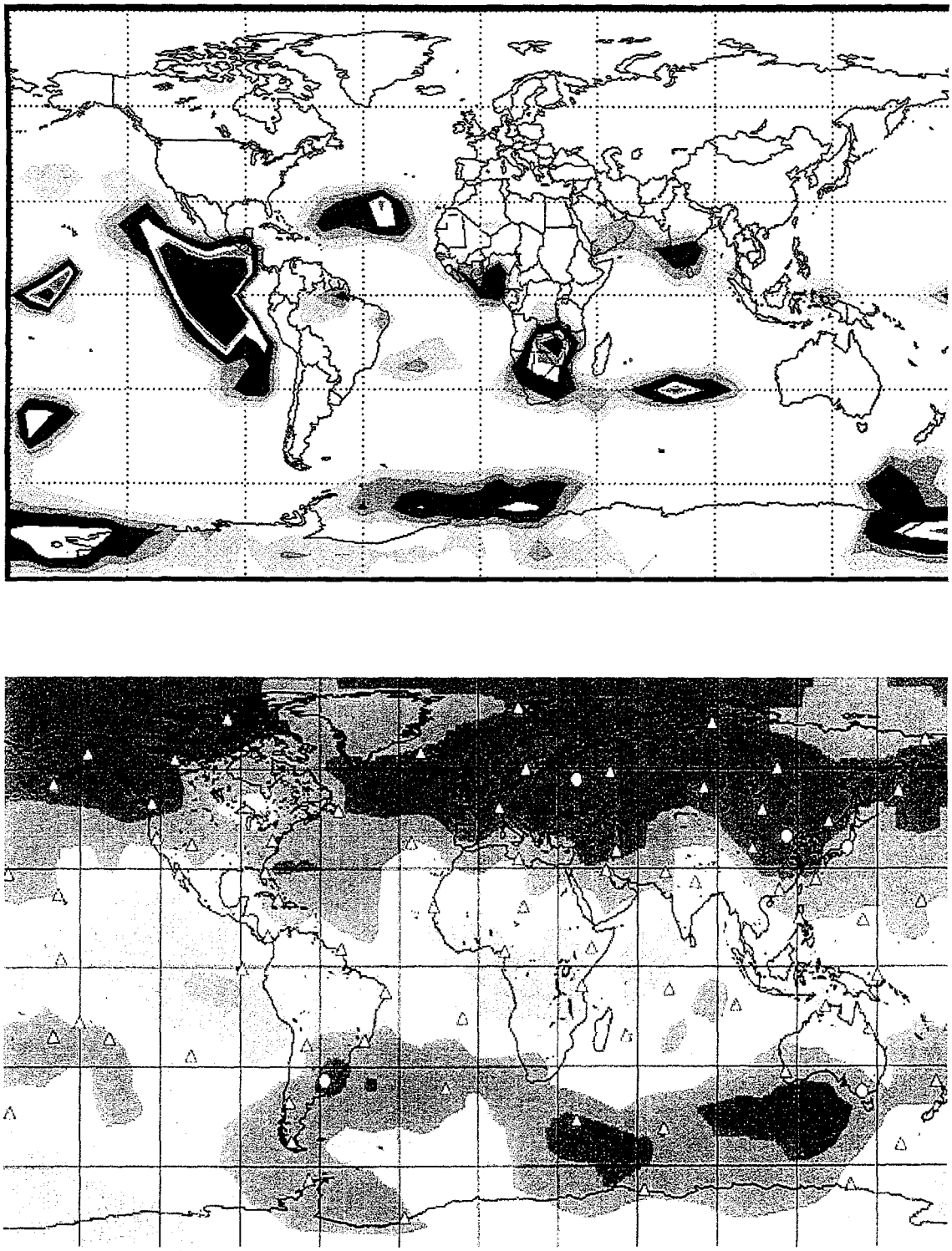

Figure E15. 7 Day Coverage, Ba-140, Net 2. Top IVSEM, Bottom HY-SPLIT

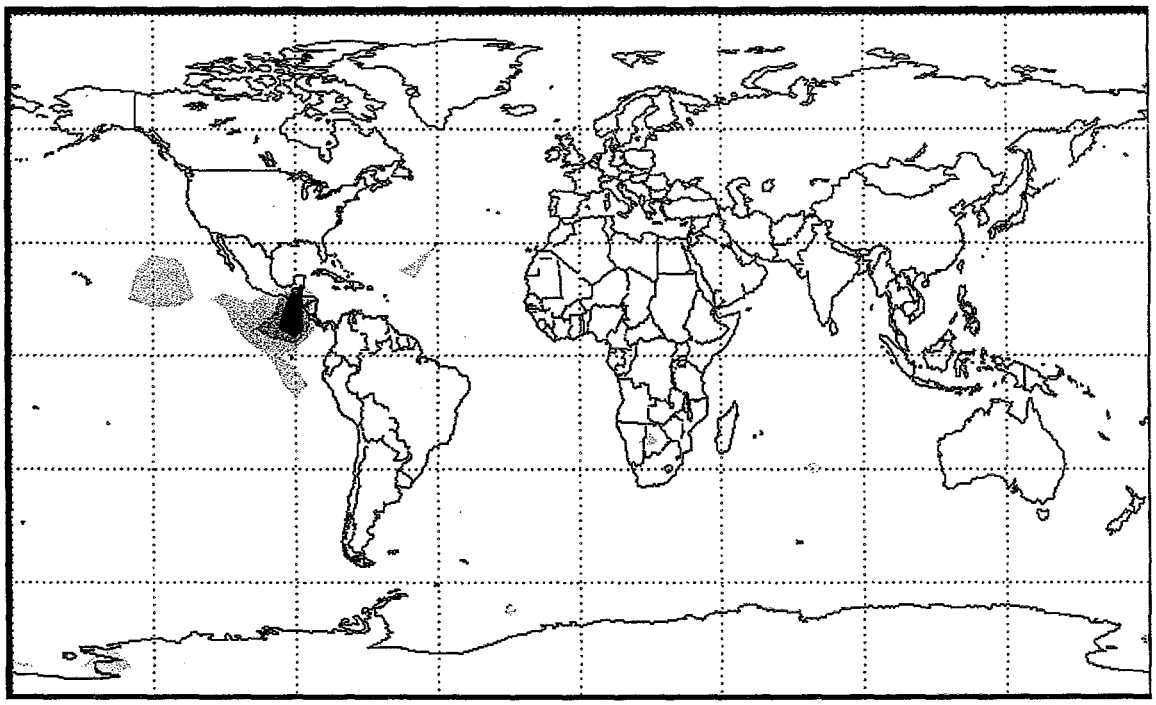

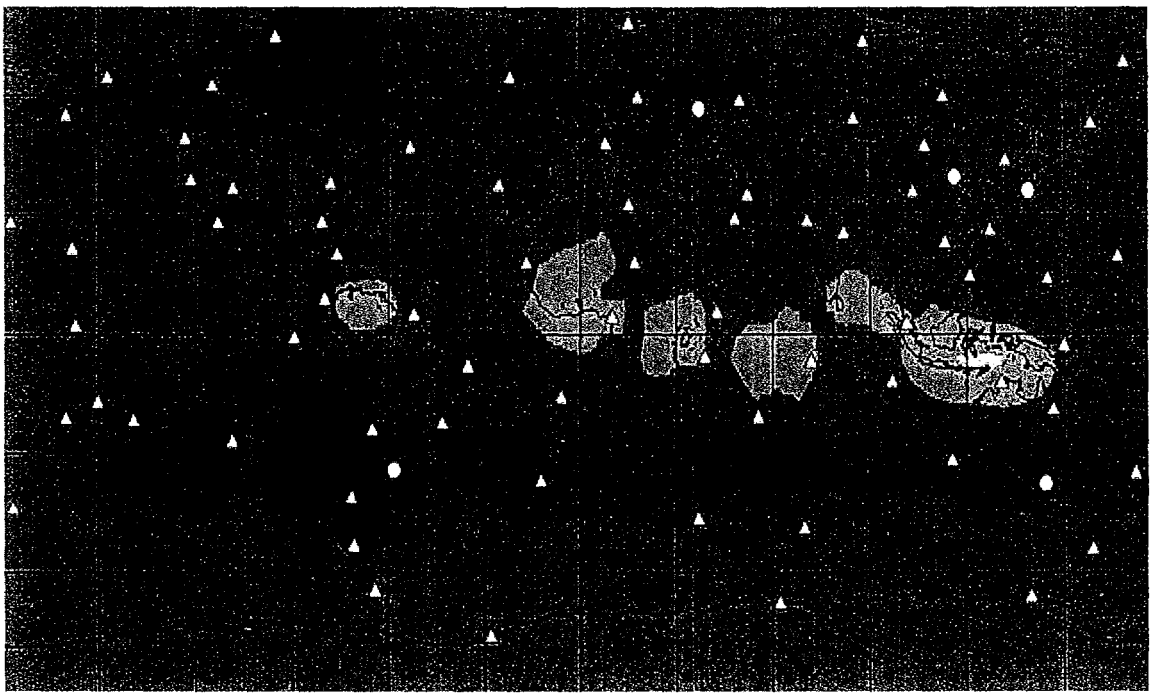

Figure E16. 14 Day Coverage, Ba-140, Net 2. Top IVSEM, Bottom HY-SPLIT

In Figure E11, the 3 day coverage of Net 1 is compared. Examining the maps one can see that the areas of weak coverage are almost the same. The weak area extending from the southern Pacific up and to the east to merge with the weak area in the eastern Pacific is virtually identical in both analyses. In both models, this area extends on eastward over central Brazil, south-eastward near the Peruvian coast, and westward along the equator towards New Guinea. A weak area is predicted in both models over the Hudson Bay area of Canada and extending eastward to lower Greenland. Both models predict a weak area over the south Atlantic extending from the Argentine coast to Queen Maude Land in Antarctica with a lesser weakness extending over the whole Antarctic continent. A weak area is predicted in the north-western Pacific east of Japan by both models. Another weak area is predicted by both models over Indonesia extending south-westward to the south-central Indian ocean. A weak area is predicted by both models over southern India, the Arabian sea, and up into Pakistan and over Tibet. Southern Africa extending north to the Sudan and north-west into the central Atlantic ocean is predicted to be weak in both models. The main differences are the slight weakness predicted by IVSEM north of Finland and the weak area predicted in the Arctic above north-western Russia. In HY-SPLIT the area north of Finland is weak but not any more so than other nearby regions. HY-SPLIT does predict a weak area over western Russia north of the Sea of Okhotsk which is similar to a weakness predicted by IVSEM slightly further to the east but does not show the general weakness over the north pole shown by IVSEM.

In Figure E12, the 7 day coverage maps for Net 1 are shown. By 7 days most of the world is very well covered and only a few really weak areas remain. Both models still predict the very weak area over the eastern Pacific. Less weak areas are predicted by both models over the southern Pacific near the Antarctic coast, Indonesia, the Arabian sea, and south central Africa. Mildly weak areas are predicted by both models over the south Atlantic near Antarctica, south-central Atlantic between Africa and Brazil, the Pacific ocean connecting the very weak area in the south to the very weak area in the east-central Pacific, and the south-central Indian ocean below Raratonga. Notice, in particular, the slight weakness predicted by both models in the central Atlantic (at 30^{O}N, 40^{O}W in IVSEM and 30^{O}N, 50^{O}W in HY-SPLIT). In both models coverage is almost complete over the northern hemispheric above 30^{O} latitude and in the band between 30-60^{O} in the southern hemisphere. The most significant differences are: IVSEM predicts a weak area north of India that does not explicitly show up in the HY-SPLIT analysis, the weak area in Africa predicted by IVSEM is further south than the corresponding area predicted by HY-SPLIT, and central India is shown to be particularly weak in the HY-SPLIT calculations but not by IVSEM.

In Figure E13, the 14 day coverage maps for Net 1 are shown. Both models are predicting almost complete global coverage by aerosols for surface bursts by 14 days. IVSEM is still showing some slight weakness in the eastern Pacific while HY-SPLIT is predicting slight weakness along the equatorial belt from Columbia to Indonesia.

Figures E14-E16 for Net 2 show a similar correspondence between the IVSEM and HY-SPLIT results so we will not discuss them; however, we will compare the differences in the network coverages predicted by the two models at equivalent times.

At 3 days, if we compare Figure E11 and E14, we see that the two models predict very similar effects on network performance from moving stations or adding stations. Moving the station at Ashland, Kansas to Farmington, NM results in decreased coverage over the central US with the weak area in Canada expanding south and the weak area over Mexico expanding north. Moving the station from Guadeloupe to Santiago De Cuba results in similar shifts in coverage over the central Atlantic ocean with the weak area off of the African coast near Senegal expanding further westward. The addition of a station at Mururoa in the central Pacific improves coverage in the weak area linking the weakness in the southern Pacific with the weak area in the eastern Pacific. Moving Nagpur, India to Allahabad, India and Bangkok, Thailand to Rahimyar Kahn, Pakistan results in similar shifts in coverage over the Indian subcontinent; that is, improved coverage over northern India and central Asia and weaker coverage over southeast Asia. The only difference in performance predicted by the two models comes from the movement of the station at Nordvik to Noril'sk. IVSEM predicts significantly worse coverage over western Russia as a result of moving the station eastward and improved coverage over the Barents sea region. While HY-SPLIT predicts no improvement in the coverage over the Barents sea and almost no difference in the coverage over western Russia (if one looks closely one can see a slight expansion of the weak area over western Russia further north-westward but not eastward as would be expected). Some of the difference here can be explained by the large contour intervals being used in the HY-SPLIT results compared to the IVSEM results; however, IVSEM is predicting changes sufficiently large that they should be seen in the HY-SPLIT results.

At 7 days, if we compare Figures E12 and E15, we again see that the models predict similar results. The effect of moving the station at Ashland, Kansas to Farmington, NM is almost washed out by this time. IVSEM shows essentially no difference and HY-SPLIT again shows a slight decrease in coverage over Nevada/Utah. Moving the station from Guadeloupe to Santiago De Cuba again results in similar shifts in coverage over the central Atlantic ocean with the weak area off of the African coast near Senegal still deepening and expanding further westward. The addition of a station at Mururoa in the central Pacific still results in improved coverage in the weak area linking the weakness in the southern Pacific with the weak area in the eastern Pacific. Moving Nagpur, India to Allahabad, India and Bangkok, Thailand to Rahimyar Kahn, Pakistan again results in similar shifts in coverage over the Indian subcontinent; that is, improved coverage over northern India and central Asia and weaker coverage over southeast Asia and southern India. In this time frame, there is essentially no difference in coverage predicted by the two models from the movement of the station at Nordvik to Noril'sk.

At 14 days, if we compare Figures E13 and E16, we again see that the models predict similar results. The effect of moving the station at Ashland, Kansas to Farmington, NM is completely washed out by this time. Moving the station from Guadeloupe to Santiago De Cuba still results in a very slight decrease in coverage over the central Atlantic ocean in IVSEM but no difference in HY-SPLIT. The addition of a station at Mururoa in the central Pacific results in no difference in this time frame. In this time frame moving Nagpur, India to Allahabad, India and Bangkok, Thailand to Rahimyar Kahn, Pakistan still results in some differences between IVSEM and HY-SPLIT predictions. HY-SPLIT predicts a slight decreases in coverage over the Bay of Bengal while IVSEM predicts no difference. We believe that this difference results for two reasons: 1) IVSEM elevates the bulk of the cloud to higher elevations than HY-SPLIT and, therefore, into

faster wind fields so the cloud will travel further in the same time frame and coverage should improve faster in IVSEM than in HY-SPLIT; and 2) HY-SPLIT does not have detonation points along the equator so there are fewer chances that a detonation will be detected along the equator because there are fewer scenarios being evaluated in that region. In this time frame, there is no difference in coverage predicted by the two models from the movement of the station at Nordvik to Noril'sk.

In summary, we believe that this comparison shows very clearly that IVSEM and HY-SPLIT predict very similar network performance both spatially and as it evolves over time.

Model Limitations

At the moment there are four principal limitations to the radionuclide portion of IVSEM. First, we treat the cloud as a single coherent whole. In actuality, the cloud will breakup into smaller segments that will act independently of each other and this fragmentation will continue in time to smaller and smaller scales. Each piece of the cloud will be at different altitudes and travel in different wind fields. The actual concentration of debris in the atmosphere, therefore, will be very inhomogeneous. Real measurements taken from release experiments show that the concentration of some tracer material from a sensor in the cloud can vary widely from one sample to the next. No code, therefore, can come close to modeling the actual development of the debris cloud; however, the Gaussian model used here has been shown to be adequate to model the aggregate time-averaged behavior of such clouds and is useful at a system level. Such a model would not be adequate, for example, to model the details necessary for specific siting calculations to determine the effects of local topology.

Second, in IVSEM, we use one simulated trajectory that is different for each detonation point for a particular month of the year. The random seed for this calculation is changed in the model, but not by the user. This has both positive and negative implications. On the positive side, the results show the coverage for one particular realization of the global weather patterns and clearly show how the strong and weak areas of coverage vary with changing global wind patterns as the seasons change. On the negative side, this obviously results in the need to do a lot of calculations to see all of the potential variations and does not allow one to directly see areas of continual weakness. A more comprehensive model, described later, allows the calculation of monthly, seasonal, and yearly averages. Since the real weather on any day is not the same from year to year, it is also important to understand how the potential variability in the weather patterns on any day can effect network performance. This allows the analyst to see the effects of observed statistical variation in monthly, seasonal, or yearly weather patterns on network coverage directly and to determine areas that are weak under all weather conditions.

Thirdly, we are uncertain about the effects of venting, dry deposition, and rainout on the aerosol precursors of Xenon. For underground detonations, in particular; the nuclides can be embedded in other aerosol particles and significant amounts of the Xenon decay product may not be able to escape to the atmosphere. Currently we are assuming that all Xenon produced from decay of iodine in aerosols which are not removed from the cloud is released immediately to the

atmosphere and can be detected by the gas sensors but we could be overestimating the source term. Los Alamos is looking into this for us.

Fourth, the default modeling of the source term for underwater explosions is only approximated using wet medium results for soil. This is true for both the vent fraction and the energy released to the cloud. This gives the right trends in expected behavior compared to the underground explosions but must be taken into account when evaluating the results. Doing two single event calculations, one on land and one in the ocean, will allow the user to examine the source terms in detail and determine if they are acceptable. If not, then the user can adjust various parameters until he obtains the source terms he wants.

In addition to the radionuclide model in IVSEM, we have a similar but more comprehensive model with many additional features such as: 1) allowing the user to independently specify the vent fractions for gases and aerosols in land or water, 2) retaining the Xe-133m decay, 3) alternate fuels Pu-238 for primary and U-238 for secondary, 4) user specified fission and fusion fractions in both primary and secondary allowing the user to precisely tailor the source term, 5) user specified wind correlations for inducing inertia into the cloud trajectory calculations, 6) allowing the user to run monthly, seasonal, or yearly average calculations (4 wind trajectories/month), 7) calculating the additional isotopes: Mo-99, Xe-133m, Xe-135g, and Xe-135m, 8) a 1^{O} Land-Sea map, 9) 2.5, 5, and 10^{O} wind data files, 10) 1, 2, 2.5, and 5^{O} detonation grids, 11) user specified volume flow rates, collection times, cool down times, and count times for both gases and aerosols for each station individually, 12) user specified parameter values for diffusion rates, 13) time dependent output (daily), and 14) user specified fraction of Xenon produced by iodine decay retained in aerosol particles and not available for detection.

Summary

In conclusion, we feel that IVSEM allows the user sufficient flexibility to model a large number of interesting scenarios and get a reasonable estimate of system performance in an interactive environment. This allows the user to quickly investigate a large number of cases and identify important cases.

References

Barr 1987. S. Barr and F. A. Gifford, "The Random Force Theory Applied To Regional Scale Tropospheric Diffusion," pg. 1737-1741, Volume 21, Number 8, Atmospheric Environment, 1987.

Brenk 1981. H. D. Brenk and K. J. Vogt, "The Calculation of Wet Deposition from Radioactive Plumes," pg. 362-371, Volume 22, Number 3, Nuclear Safety, May-June 1981.

Brodsky 1986. A. Brodsky, "Accuracy and Detection Limits for Bioassay Measurements in Radiation Protection: Statistical Considerations," NUREG-1156, US Nuclear Regulatory Commission, Washington, DC, February 1986.

Broom 1962. K. M. Broom, "14.7-Mev Neutron-Induced Fission of U-238," pg. 627-631, Volume 126, Number 2, Physical Review, April 15, 1962.

Carras 1988. J. N. Carras and D. J. Williams, "Measurements of Relative sy Up to 1800 KM From a Single Source," Atmospheric Environment, Vol. 22, No. 6, pp. 1061-1069, 1988.

Charles 1959. B. N. Charles, "Empirical Models of Interlevel Correlation of Winds," pg. 581-585, Volume 16, Journal of Meteorology, October 1959.

Cuninghame 1957. J. G. Cuninghame, "The Mass-Yield Curve For Fission of Natural Uranium by 14-Mev Neutrons," pg. 1-5, Volume 5, J. Inorg. Nucl. Chem., 1957.

Currie 1968. L. A. Currie, "Limits for Qualitative Detection and Quantitative Determination: Application to Radiochemistry," pg. 586-593, Volume 40, Number 3, Analytical Chemistry, March 1968.

Djuric 1961. D. Djuric, "On the Accuracy of Air Trajectory Computations," pg. 597-605, Volume 18, Journal of Meteorology, October 1961.

DNA 1990. EM-1, "Capabilities of Nuclear Weapons, Radiation phenomena, Chapter 8 Nuclear Radiation/Fallout (U)," Kaman Sciences, Defense Nuclear Agency, March 1990. (Report is SRD, sections on stabilized cloud height, energy of release, and vent fractions are unclassified).

Draxler 1992. R. R. Draxler, "Hybrid Single-Particle Lagrangian Integrated Trajectories (HY-SPLIT): Version 3.0 - User's Guide and Model Description," NOAA Technical Memorandum ERL ARL-195, Air Resources Laboratory, June 1992.

Dvore 1982. D. S. Dvore and R. Vaglio-Laurin, "Atmospheric Diffusion of Small Instantaneous Point Releases Near the Ground," pg. 2791-2798, Volume 16, Number 12, Atmospheric Environment, 1982.

Fowler 1983. M. M. Fowler, "A Long-Range Atmospheric Tracer Field Test," pg. 1677-1685, Volume 17, Number 9, Atmospheric Environment, 1983.

GE 1974. M. E. Meek, B. F. Rider, "Compilation of Fission Product Yields Vallecitos Nuclear Center 1974,", January 26, 1974, NEDO-12154-1, Boiling Water Reactor Systems Department, General Electric Company, Vallecitos Nuclear Center, Pleasanton CA 94566.

Gifford 1982. F. A. Gifford, "Horizontal Diffusion in the Atmosphere: A Lagrangian-Dynamical Theory," Atmospheric Environment, Vol. 16, No. 3, pp. 505-512, 1982.

Gifford 1987. F. A. Gifford, "A Note on the Nature of Atmospheric Diffusion at Very Large, Regional to Global Scales," 15 March 1987.

Gifford 1991. F. A. Gifford, "The Structure of Atmospheric Diffusion At Regional Scales," U.S. Army Research Office, January 31, 1991.

Harvey 1994. T. Harvey, F. Serduke, and L. Peters, "KDFOC3: A Nuclear Fallout Assessment Capability," September 13, 1994, UCRL-52338, Lawrence Livermore National Laboratory, Livermore, CA.

Haagenson 1990. P. L. Haagenson, K. Gao, and Y. Kuo, "Evaluation of Meteorological Analyses, Simulations, and Long-Range Transport Calculations Using ANATEX Surface Tracer Data," pg. 1268-1283, Volume 29, Journal of Applied Meteorology, December 1990.

Katcoff 1960. S. Katcoff, "Fission-Product Yields from Neutron-Induced Fission," pg. 201-208, Nucleonics, November 1960.

Kotamarthi 1993. V. R. Kotamarthi and G. R. Carmichael, "A Modeling Study of the Long-Range Transport of Kosa Using Particle Trajectory Methods," pg. 426-441, 45B, Tellus, 1993.

Kristensen 1981. L. Kristensen, N. O. Jensen, and E. L. Petersen, "Lateral Dispersion of Pollutants In a Very Stable Atmosphere - The Effect of Meandering," pg. 838-844, Volume 15, Number 5, Atmospheric Environment, 1981.

Ley 1982. A. J. Ley, "A Random Walk Simulation of Two-Dimensional Turbulent Diffusion in the Neutral Surface Layer," Atmospheric Environment, Vol.16, No. 12, pp. 2799-2808, 1982.

Lupini 1981. R. Lupini and P. Malguzzi, "A Contribution To the Problem of Modeling the Dispersion of Pollutants In a Time-Varying, Height-Structured Atmospheric boundary Layer," pg. 363-369, Volume 15, Atmospheric Environment, 1981.

MACCS 1990. H-N Jow, J. L. Sprung, J. A. Rollstin, L. T. Ritchie, and D. I. Chanin, "MELCOR Accident Consequence Code System (MACCS): Model Description," NUREG/CR-4691 Vol. 2, SAND86-1562, Sandia National Laboratories, Albuquerque, NM, February 1990.

McNider 1988. R. T. McNider, M. D. Moran, and R. A. Pielke, " Influence of Diurnal and Inertial boundary-Layer Oscillations on Long-Range Dispersion," pg. 2445-2462, Volume 22, Number 11, Atmospheric Environment, 1988.

NOAA 1993. Global Upper Air Climatic Atlas Ver 1.0, 2 CD-Rom Set, National Climatic Data Center and Naval Oceanography Command Detachment Asheville, National Oceanic and Atmospheric Administration, April 1993.

Norris 1966. A. E. Norris, and A. C. Wahl, "Nuclear Charge Distribution in Fission: Y^{92}, Y^{93}, Y^{94}, and Y^{95} Independent Yields," pg. 926-931, Volume 146, Number 3, Physical Review, June 17, 1966.

Overcamp 1982. T. J. Overcamp, "A Statistical Plume Model with First-Order Decay," pg. 1589-1593, Volume 21, Number 11, Journal of Applied Meteorology, November 1982.

Overcamp 1990. T. J. Overcamp, "Diffusion Models for Transient Releases," Journal of Applied Meteorology, Vol. 29, page 1307, December 1990.

Palazzi 1982. E. Palazzi, M. De Faveri, G. Fumarola, and G. Ferraiolo, "Diffusion From a Steady Source of Short Duration," pg. 2785-2790, Volume 16, Number 12, Atmospheric Environment, 1982.

Payne 1995. A. C. Payne Jr., Letter report to Leslie Casey DOE/NN-20 summarizing radionuclide model sensitivity calculations related to IMS radionuclide network design, Unclassified Controlled Access Information/Official Use Only,1995.

Rodriguez 1995. D. Rodriguez, H. Walker, N. Klepikova, A. Kostrikov, and Y. Zhuk, "Evaluation of Two Pollutant Dispersion Models Over Continental Scales," pg. 799-812, Volume 29, Number 7, Atmospheric Environment, 1995.

Smith 1968. F. B. Smith, "Conditioned Particle motion In a Homogeneous Turbulent Field," pg. 491-508, Volume 2, Atmospheric Environment, 1968.

Strom 1966. P. O. Strom, D. L. Love, A. E. Greendale, A. A. Delucchi, D. Sam, and N. E. Ballou, "Nuclear-Charge Distribution of Fission-Product Chains of Mass Numbers 131-133," pg. 984-993, Volume 144, Number 3, Physical Review, April 22, 1966.

Sutton 1932. O. G. Sutton, "A Theory of Eddy Diffusion in the Atmosphere," pg. 143-165, Proc. Roy. Soc., Series A, Vol. CXXXV, London, England, April 1932.

Vandenbosch 1973. R. Vandenbosch and J. R. Huizenga, "Nuclear Fission," Academic Press, New York, NY, 1973.

Wahl 1955. A. C. Wahl, "Fission of U-235 by 14-Mev Neutrons: Nuclear Charge Distribution and Yield Fine Structure," pg. 730-739, Volume 99, Number 3, Physical Review, August 1, 1955.

Wahl 1962. A. C. Wahl, R. L. Ferguson, D. R. Nethaway, D. E. Troutner, and K. Wolfsberg, "Nuclear-Charge Distribution in Low-Energy Fission," pg. 1112-1127, Volume 126, Number 3, Physical Review, May 1 1962.

Watson 1977. C. W. Watson, S. Barr, and R. E. Allanson, "Rainout Assessment: The ACRA System and Summaries of Simulation Results," LA-6763, Los Alamos Scientific Laboratory, Los Alamos, New Mexico, September 1977.

Wilson 1981. D. J. Wilson, "Along-Wind Diffusion of Source Transients," pg. 489-495, Volume 15, Atmospheric Environment, 1981.

Wilson 1982. D. J. Wilson, "Concentration Fluctuations in an Elevated Plume: A Diffusion-Dissipation Approximation," pg. 2581-2589, Volume 16, Number 11, Atmospheric Environment, 1982.

APPENDIX F. SYSTEM DETECTION EFFECTIVENESS AND SYNERGY

System Detection Response

From computations for each station within each subsystem, we estimated the probability that the station registered a positive response. These probability values are operated on to obtain a system response.

First, within each subsystem, we use the individual station response probabilities to compute the probability that exactly N (N is a positive integer) stations registered a positive response. The best way to explain the computation is with an example. Suppose that a subsystem consists of three stations: A, B, and C. For a given test scenario, the response probabilities for each station are 0.5, 0.7, and 0.9 respectively. There are eight possible responses for this system. The responses and probabilities associated with each response are shown in the table below, treating the three stations independently. A value of 0 implies that the station did not respond, and a value of 1 implies that it did.

A	B	C	Probability
0	0	0	(.5 x .3 x .1) = .015
1	0	0	(.5 x .3 x .1) = .015
0	1	0	(.5 x .7 x .1) = .035
0	0	1	(.5 x .3 x .9) = .135
1	1	0	(.5 x .7 x .1) = .035
1	0	1	(.5 x .3 x .9) = .135
0	1	1	(.5 x .7 x .9) = .315
1	1	1	(.5 x .7 x .9) = .315

The first case gives the probability, .015, that exactly 0 stations respond. There are three cases where 1 station responds, and the probability that exactly 1 station responds is the sum of the three probabilities, .015 + .035 + .135 = .185. There are three cases where 2 stations respond, and the probability that exactly 2 stations respond is the sum of the three probabilities, .035 + .135 + .315 = .485. The probability that exactly 3 stations respond is .315. In summary:

the probability of exactly 0 = 0.015 ,
the probability of exactly 1 = 0.185 ,
the probability of exactly 2 = 0.485 , and
the probability of exactly 3 = 0.315 .

If these were seismic stations, we could denote the probabilities as P(0S), P(1S), P(2S), and P(3S) respectively. Notice that they add to 1.00, as they should. The algorithm used by the model to find these probabilities works for any number of stations. To avoid problems associated with many stations, each having a very small response probability, we ignore stations

in all subsystems with a detection probability less than 0.2 in conformance to seismic network analysis practice.

Above, we combined individual station response probabilities to get subsystem response probabilities for exactly N stations. We call the probability that exactly N seismic stations respond P(NS). Note that this is really a set of probabilities: P(0S), P(1S), P(2S), P(3S), and etc. The probability that N infrasound stations respond is P(NI); the probability that N radionuclide stations respond is P(NR); and the probability that N hydroacoustic stations respond is P(NH). The system's response is the combination of subsystem responses; that is, 2 seismic plus 1 infrasound plus 1 radionuclide plus 0 hydroacoustic responses is a specific system response. We would designate this specific system response as (2S, 1I, 1R, 0H). The general system response (NS, NI, NR, NH) represents all possible system responses if we let NS, NI, NR, and NH include all numbers of stations up to the total number in their respective subsystems. The probability P(NS, NI, NR, NH) that we get system response (NS, NI, NR, NH) is equal to the product of the individual subsystem response probabilities since the subsystems operate independently. This joint probability is given by the following equation:

$$P(NS, NI, NR, NH) = P(NS) \times P(NI) \times P(NR) \times P(NH) \quad \text{(F1)}$$

P (NS, NI, NR, NH) is a four dimensional table or matrix which we call the system detection response table. This table is the model's description of a system's detection response to an event.

As an example, suppose the system consists of four seismic sensors and four infrasound sensors but no radionuclide or hydroacoustic sensors. There are twenty-five possible system responses:

0 seismic and 0, 1, 2, 3, or 4 infrasound responses,
1 seismic and 0, 1, 2, 3, or 4 infrasound responses,
2 seismic and 0, 1, 2, 3, or 4 infrasound responses,
3 seismic and 0, 1, 2, 3, or 4 infrasound responses, and
4 seismic and 0, 1, 2, 3, or 4 infrasound responses.

Assume that the probability for 0 seismic sensor responses is P(0S) = 0.015, P(1S) = 0.185, P(2S) = 0.485, P(3S) = 0.315, and that P(4S) = 0.0. Also assume that P(0I) = 0.008, P(1I) = 0.116, P(2I) = 0.444, P(3I) = 0.432, and that P(4I) = 0.0. The probability of getting 0 seismic and 0 infrasound responses is 0.015 x 0.008 = 0.00012; the probability for 2 seismic and 3 infrasound is 0.485 x 0.432 = 0.2095; and etc. The system detection response table would look like Table F1.

The model's table will have four dimensions (one for each technology), and the number of stations in each dimension will be equal to the number of stations used by that technology subsystem.

Table F1. Simplified (Two-Technology) Detection Response Table (Joint Probabilities)

Number of Responses					
Seismic	0S	1S	2S	3S	4S
Infrasound					
0I	.0001	.0015	.0039	.0025	.0000
1I	.0017	.0215	.0563	.0365	.0000
2I	.0067	.0821	.2153	.1399	.0000
3I	.0065	.0799	.2095	.1361	.0000
4I	.0000	.0000	.0000	.0000	.0000

System Detection Effectiveness

We define system detection effectiveness to be the measure of "how good" the system is at detecting an event. More specifically, it is a weighted probability of detection. The weights come from the detection effectiveness table and, in principle, reflect the "information content" in a detection by a specified number and combination of sensors. If the weights are exclusively values of 0.00 and 1.00, system detection effectiveness is specifically the probability of detection with detection defined by the detection effectiveness table as those system responses which get a value of 1.00.

The system detection response is denoted (NS, NI, NR, NH) where NS is the number of seismic stations which respond, NI is the number of infrasound stations which respond, NR is the number of radionuclide stations which respond, and NH is the number of hydroacoustic stations which respond. Associated with each possible system response is the probability of getting that response, P(NS, NI, NR, NH). Also associated with each possible system detection response is a system detection effectiveness E(NS, NI, NR, NH). This value, which we define to be between 0 and 1 inclusively, is a "goodness" of detection or a detection "figure of merit." It is represented by a four dimensional table or matrix and is currently specified in input by the user. It is a qualitative judgement, made by the user, which associates an effectiveness value with each possible system detection response. If the user gives a detection effectiveness value of either 1.00 or 0.00 to each specific system detection response, then he has defined some responses as detections and others as nondetections. In this case, the system detection effectiveness computed by the model will be the probability of detection. If values between 0.00 and 1.00 are used, detection effectiveness is a weighted probability of detection.

The model combines the system detection response table with the system detection effectiveness table to get a system detection effectiveness value. It does this by multiplying the system response probability by the system response effectiveness for each possible system response and adding the results. This is expressed in the following algorithm:

$$\text{System Detection Effectiveness} = \Sigma\,[E\,(NS, NI, NR, NH) \times P\,(NS, NI, NR, NH)] \qquad (F2)$$

The summation is done over all values of NS, NI, NR, and NH. The result is an expected value of detection effectiveness. To clarify this algorithm and the integration process, we will look at a two-dimensional example. Using the system which has four seismic and four infrasound sensors from the example above and the detection effectiveness table given in Table F2, we can find the system's detection effectiveness. System responses (0S,0I), (0S,1I), (1S,0I), (1S,1I), (2S,0I), and (2S,1I) all have probabilities greater than 0.0; but, they are assigned effectiveness values of 0.0 in the detection effectiveness table (Table F2); thus, they contribute nothing to detection effectiveness. System responses (4S,0I), (4S,1I), (4S,2I), (4S,3I), (4S,4I), (0S,4I), (1S,4I), (2S,4I), and (3S,4I), have effectiveness values of 1.0; but they all have 0.0 probability; thus, they contribute nothing to detection effectiveness. The contribution from each response is the response's probability multiplied by its effectiveness: (3S,0I)--0.0025x1.0; (3S,1I)--0.0365x1.0; (0S,2I)--.0067x1.0; (1S,2I)--0.0821x1.0; (2S,2I)--0.2153x1.0; (3S,2I)--0.1399x1.0; (0S,3I)--0.0065x1.0; (1S,3I)--0.0799x1.0; (2S,3I)--0.2095x1.0; and (3S,3I)--0.1361x1.0. These are added to get the overall system detection effectiveness value of 0.915.

Table F2. Two-Technology Detection Effectiveness Table Example

Number of Responses Seismic / Infrasound	0S	1S	2S	3S	4S
0I	.00	.00	.00	1.00	1.00
1I	.00	.00	.00	1.00	1.00
2I	1.00	1.00	1.00	1.00	1.00
3I	1.00	1.00	1.00	1.00	1.00
4I	1.00	1.00	1.00	1.00	1.00

System Detection Synergy

Table F2 indicates that 3 seismic station detections or 2 infrasound station detections are required to form a system detection. It does not allow mixed technology detection. It is theoretically possible that 2 seismic plus 1 infrasound detection (a mixed technology detection) can form an event because this case provides sufficient information for an event location estimate. In IVSEM we can allow mixed technology detection (detection synergy) using Table F3.

Table F3. Two-Technology Detection Effectiveness Table Example

Number of Responses Seismic Infrasound	0S	1S	2S	3S	4S
0I	.00	.00	.00	1.00	1.00
1I	.00	.00	1.00	1.00	1.00
2I	1.00	1.00	1.00	1.00	1.00
3I	1.00	1.00	1.00	1.00	1.00
4I	1.00	1.00	1.00	1.00	1.00

In the main body of this report and in Appendix A we described the mechanics of defining the system detection effectiveness table. We will now discuss the role that mixed technology synergy might play in defining the system detection effectiveness table. Notice that the examples use detection effectiveness values between 0 and 1 inclusively instead of being limited to either 0.0 or 1.0. Consider three definitions of synergy.

Definition # 1.--The **American Heritage Dictionary** defines synergy as the action of two or more substances, organs, or organisms to achieve an effect of which each is individually incapable. We can apply this definition to the CTBT monitoring system and define the desired effect to be detecting nudets in any medium. No individual technology can achieve this effect by itself, but a combination of technologies can. Thus, according to this definition, there is synergy in having a variety of monitoring technologies which operate independently in different media, and, to achieve synergy, it is not necessary to give special value if a nudet is detected by more than one technology. For example, infrasound technology will detect atmospheric detonations but not underground ones, and seismic technology will detect underground detonations but not atmospheric ones. It can be said that there is synergy between the two because they work together to cover both media while neither can cover both media by itself. (More accurately, it can be said that there is complementarity between the two subsystems.) If this is our definition, of synergy, and if NI infrasound and NS seismic stations detect a nudet with E(NI) and E(NS) as corresponding independent subsystem effectiveness values, system effectiveness, E(NI, NS), will be equal to the greatest of E(NI) and E(NS). Assuming that (0I)=E(0S)=0.0, E(1I)=E(1S)=0.1, E(2I)=E(2S)=0.3, E(3I)=E(3S)=0.7, E(4I)=E(4S)=0.9, and E(5I)=E(5S)=1.0, we will complete the infrasound-seismic detection effectiveness table.

Table F4. Two-Technology Detection Effectiveness Table
Definition #1

Number of Responses Seismic / Infrasound	0S	1S	2S	3S	4S	5S
0I	.0	.1	.3	.7	.9	1.
1I	.1	.1	.3	.7	.9	1.
2I	.3	.3	.3	.7	.9	1.
3I	.7	.7	.7	.7	.9	1.
4I	.9	.9	.9	.9	.9	1.
5I	1.	1.	1.	1.	1.	1.

Definition # 2--Webster's Third New International Dictionary defines synergy as follows: the combined action of two or more agents is greater than the sum of the action of one agent used alone. We do not know how one can take the sum of the action of one agent, but we interpret this definition to mean that the action of two or more agents is greater than the action of one agent acting alone. For our application, this definition means that if more than one subsystem detects an event, system effectiveness is greater than the highest individual subsystem effectiveness. This definition has a greater requirement for synergy than does definition #1. If this is our definition, then system effectiveness will be greater than both E(NI) and E(NS). An additive scheme, which adds E(NI) and E(NS), E(NI,NS) = E(NI)+ E(NS), is based on this kind of definition, and the resulting effectiveness table is shown below.

Table F5. Two-Technology Detection Effectiveness Table
Definition #2

Number of Responses Seismic / Infrasound	0S	1S	2S	3S	4S	5S
0I	.0	.1	.3	.7	.9	1.
1I	.1	.2	.4	.8	1.	1.
2I	.3	.4	.6	1.	1.	1.
3I	.7	.8	1.	1.	1.	1.
4I	.9	1.	1.	1.	1.	1.
5I	1.	1.	1.	1.	1.	1.

Definition # 3--Webster's New World Dictionary, College Edition definition is as follows: the simultaneous action of separate agencies which, together, have greater total effect than the sum of their individual effects. This definition requires that the combined effect be greater than the sum of the individual effects (E(NI ,NS) > E(NI) + E(NS)). Definition # 3 constitutes a more stringent concept of synergy than either #1 or #2. The requirement--if N total stations detect an event, then effectiveness is highest when N is divided among technologies-- satisfies this third definition. This scheme might lead to the following detection effectiveness table.

Table F6. Two-Technology Detection Effectiveness Table
Definition #3

Number of Responses Seismic Infrasound	0S	1S	2S	3S	4S	5S
0I	.0	.1	.3	.7	.9	1.
1	.1	.33	.77	.99	1.	1.
2I	.3	.77	1.	1.	1.	1.
3I	.7	.99	1.	1.	1.	1.
4I	.9	1.	1.	1.	1.	1.
5I	1.	1.	1.	1.	1.	1.

Notice that 1 infrasound plus 1 seismic is better than 2 infrasound stations alone or 2 seismic stations alone. This scheme satisfies all of the requirements for definition # 3 and can be used to develop a four dimensional table with radionuclide and hydroacoustic technologies added. All three of the above definitions are valid definitions of synergy, but none of them is completely adequate to define the synergy of a multi-technology sensor system based on a purely quantitative assessment.

The effectiveness values we have selected for each technology depend on our qualitative ideas about the possibility of a false alarm. We assign effectiveness values smaller than 1.0 to some responses because we believe that there is some probability that those responses are false alarms caused by extraneous events. If two or more independent subsystems respond, we assign a higher effectiveness value because we believe it less likely for an extraneous event to fool multiple technology subsystems simultaneously than to fool a single subsystem. We believe that the effectiveness measure should be related to the probability that the alarm was caused by an extraneous event. A more adequate definition of synergy would be: independent technologies working together to minimize the probability of a false alarm. A metric for synergy should be based on the probability of a false alarm. Unfortunately, we do not have enough information on false alarms (false positives) to use this definition of synergy.

Until we can develop the information needed to characterize a more comprehensive type of synergy, we need to pick one of the above three definitions or pick something else that we think is better. We favor the third definition of synergy because of the requirement that if N total stations detect an event, then effectiveness is highest when N is divided among technologies. We believe that this requirement comes closest to capturing the true sense of synergy for a sensor system made up of independent subsystems.

APPENDIX G. LOCATION ACCURACY ESTIMATION

Location Accuracy Introduction and Background

IVSEM estimates the accuracy with which the overall IMS can locate an event. It also estimates the location accuracy which can be attained by each individual IMS subsystem. When the IMS detects and estimates the location of an event, the estimated location will have an associated error. The size of the error will depend on where the event was located relative to the various types of sensors and which sensors responded.

To help understand what is meant by location accuracy, consider an event which is repeated thousands of times in an identical manner. The sensor system will make thousands of event location estimates. The estimates will not all be the same, even though the events are identical, because of variations in the stations responding, source strength, perturbations in propagation, random noise, and variations in sensor performance. These variations and perturbations will give rise to variations in station-to-event bearing angles and signal arrival times which are used to estimate event location. The location process is similar to taking thousands of shots at a bull's-eye target. Like holes in the target, the location estimates, considered as a group, will have a center, and individual estimates will be spread out around the center. If the center of the group is not at the true event location, then the location process has a bias. IVSEM assumes that the IMS will have only unbiased (random) location errors. The assumption of unbias means that the center of the group is at the true event location, not off to one side. Unbias will probably be realized only for a mature, well characterized system. The group of location estimates, centered on the true event location, will have an associated 90% confidence ellipse; that is, an ellipse can be found which contains 90% of the location estimates. In other words, if an event is repeated thousands of times in an identical manner, location estimates will be within the ellipse 90% of the time. IVSEM approximates the area of the described 90% percent confidence ellipse.

IVSEM estimates location accuracy employing a statistical location error. The statistical model considers two types of stations: bearing stations (infrasound) where each station estimates a station-to-event angular bearing; and signal arrival time stations (infrasound, seismic, and hydroacoustic) where each station records a signal arrival time. Each infrasound station records both bearing angle and signal arrival time. IVSEM does not make a radionuclide location error estimate.

Based on geometric considerations, a minimum number of detecting stations is required to obtain a location estimate. The IVSEM location estimate does not include altitude or depth; thus, the estimate is for a surface location. Bearing information from at least two stations or arrival time information from at least three stations is required to make a location estimate.

IVSEM estimates location accuracy using the following process. This process will be described in more detail later in this section. Stations with a detection probability greater than 20% are included in a 100 random trial probabilistic analysis to estimate the system's location accuracy. IVSEM estimates location accuracy as a 90% elliptical confidence area, in square kilometers.

The probability that a station participates in any specific random location trial is equal to its detection probability. Each station which participates in a trial is assigned a randomly generated "measured" signal arrival time or "measured" station-to-event bearing angle, or both, depending on the type of station and on the station's statistical error distribution. Each participating station provides a bearing or arrival time (or both) residual equation to the location analysis for the trial. A location estimate is made for each random trial by finding the event time and location which minimizes the sum of the weighted, squared residuals. The minimization process is described later in this appendix. The location estimates for the 100 random trials are used in a bivariate Gaussian analysis to find the elliptical area which has a 90% chance of including all location estimates. Location estimates are made for the integrated system and for each individual subsystem.

The statistical location error model assumes a planar Cartesian instead of a spherical coordinate system to reduce computation time. While the geometries of the two coordinate systems are significantly different, we have shown that location errors will be similar since typical errors are small compared to the Earth's radius. This will be confirmed later in the validation section. The statistical model assumes that an event is located at the origin (X=0, Y=0) of the coordinate system, where X+ represents east and Y+ represents north, and that the coordinates of all stations are given by values of X and Y relative to the origin. The orientation of each station relative to the event is first found in spherical coordinates then transformed into Cartesian coordinates keeping the direction of and distance to each station the same as they were in spherical coordinates.

We will begin describing the statistical model by considering combinations of stations which locate an event using the event's signal arrival time at each station (seismic, hydroacoustic, and infrasound stations). This will be followed by showing how the statistical model is applied to stations which get bearings on the event (infrasound stations) and locate the event by combining the bearing information from each station. We will complete the discussion of the statistical model by considering the location of an event using mixed types of sensor stations.

Seismic, Hydroacoustic, and Infrasound Stations--Signal Arrival Time

Each station which detects an event will provide a measured signal arrival time and an arrival time residual equation to the location analysis. The residual is given by Equation G1.

$$r_i = T_{i,measured} - T_{i,modeled} \qquad (G1)$$

Simply stated, the residual is the difference between measured arrival time and the arrival time computed from an event time and location estimate, $T_{i,modeled}$. If the estimate is accurate, the residual will tend to be small.

$T_{i,measured}$ is the measured signal arrival time at station "i". It depends on the time at which the event occurs (which is unknown), the time it takes the signal to travel from the event to the station (which is also unknown since event location is unknown), and errors associated with picking the arrival time from data. $T_{i,\ modeled}$ is an estimated signal arrival time based on an event time and location estimate. We can express $T_{i,modeled}$ as in Equation G3.

$$d_i = [(X_i - x)^2 + (Y_i - y)^2]^{1/2} \quad \text{(G2)}$$

$$T_{i,modeled} = t + f(d_i) \quad \text{(G3)}$$

X_i is the station's X position in a Cartesian coordinate system, and Y_i is its Y position. The values t, x, and y are possible (or estimated) event time and location (we assume z, the vertical dimension, is 0). d_i is the distance from the location estimate to the station. The function $f(d_i)$ is modeled signal travel time.

For IVSEM's seismic location model, $f(d_i)$ is based on empirical measurements made as a function of angular distance by the seismic community, see Figure 1. IVSEM uses a travel time table provided by John Claassen (SNL, January 1997) and converts between angle and distance using 111.3 km/degree.

Figure 1. Seismic Signal Travel Time Model

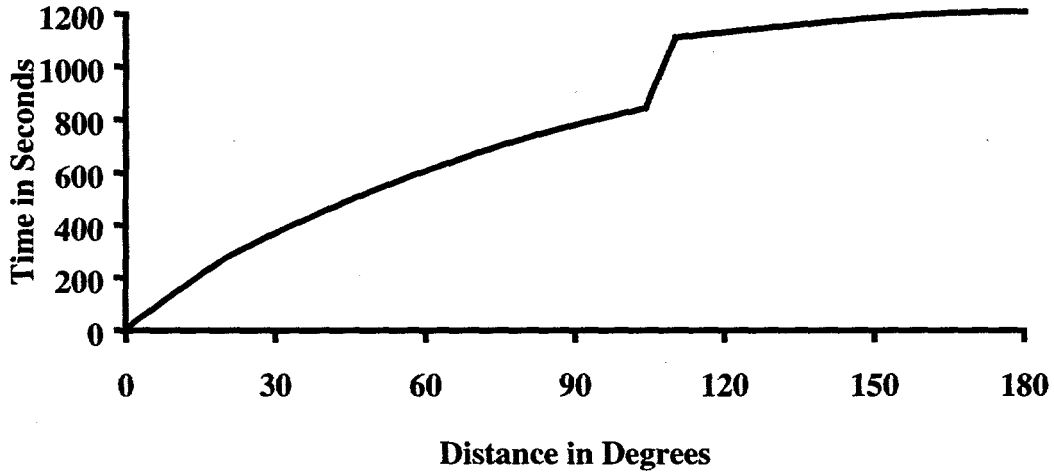

For IVSEM's hydroacoustic and infrasound location models, $f(d_i)$ is equal to d_i divided by a signal speed which is assumed to be 1.5 km/s for hydroacoustic signals and 0.3 km/s for infrasound signals.

If we select values of t, x, and y which make $T_{i,modeled}$ equal to $T_{i,measured}$, those values of t, x, and y satisfy (are a solution to) Equation G1 and the residual is equal to 0. In other words, the t, x, and y selected are a possible event time and location since the modeled arrival time agrees with the measured arrival time. The solution is not unique since there are an infinite number of t, x, y combinations which solve Equation G1. Three station detections (none of the three stations can be colinear with respect to the event) with their three residual equations are required to get a unique time and location estimate since we have three unknown variables: t, x, and y. This t, x, y solution will make the three residuals equal zero If more than three stations detect the event, we are unlikely to have a unique solution which makes all residuals equal to zero because arrival times are not exact, and the equations are unlikely to be consistent. Arrival time errors may arise from inaccuracy in interpreting which part of the signal constitutes arrival or from errors in the arrival time model due to variations in media or signal path. With three or more detections, the best method for locating the event is to select the event estimate t, x, and y which minimizes the sum of the weighted, squared residuals . The resulting x , y , and t is an estimate for the event's location and time, but it is not the true event location and time because of the errors discussed above.

If an event could be repeated in an identical manner for a large number of trials, we would get a different set of residual equations and a different time and location estimate for each trial. All of the location estimates could be used to get an idea of how accurate location estimates are. It is this multiple trial process which is modeled in IVSEM.

For each trial in IVSEM's statistical location model, we assume that "measured" arrival time for each station has a Gaussian statistical distribution with a mean arrival time, $T_{i\ ave}$ (which is an unbiased arrival time), and a standard deviation, σ_i. This σ_i is very important because it is the parameter which determines location accuracy. To generate random arrival times, one for each station, we select a set of random numbers, r_i , using a Gaussian random number generator, and we use Equations G4 through G6.

$$T_{i\ ave} = f(D_i) \tag{G4}$$

$$D_i = (X_i^{\ 2} + Y_i^{\ 2})^{1/2} \tag{G5}$$

$$T_{i,measured} = T_{i\ ave} + \sigma_i r_i \tag{G6}$$

D_i is the true distance from the event to the station, and we assume that true detonation time is 0.

For seismic location, IVSEM assumes that σ_i has two parts, a pick time error of 0.15s/(snr-1) and a model error of 0.75s, as suggested by John Claassen (SNL, April 1996), where snr is the signal-to-noise ratio. These two parts are combined as in Equation G7 to get the value used in IVSEM.

$$\sigma_i = \{0.75^2 + [.15/(snr-1)]^2\}^{1/2} \text{ sec} \quad \text{(G7)}$$

For hydroacoustic stations, IVSEM assumes σ_i has two parts, a pick time error of 1s for hydrophone stations (5s for T-phase stations) and a travel time error 0.02 multiplied by the square root of distance as suggested by Dave Harris (LLNL, May 1996)

$$\sigma_i = [1^2 + .02^2 D_i]^{1/2} \text{ sec} \quad \text{(G8)}$$

$$\sigma_{iT} = [25 + .0004 D_i]^{1/2} \text{ sec} \quad \text{(G9)}$$

For infrasound stations, IVSEM assumes σ_i is 2% of travel time.

$$\sigma_i = 0.02 D_i / 0.3 \text{ km/s} \quad \text{(G10)}$$

From the set of random arrival times, we calculate a location estimate which minimizes the sum of the weighted, squared residuals. The weighting factor for each squared residual is the reciprocal of variance, $1/\sigma_i^2$. The process is repeated for a large number of trials to find a statistical distribution for the location estimates. The distribution consists of the x, y location estimate coordinates for each trial. These coordinates are used in a covariance analysis to find the area of an ellipse which contains 90% of the location estimates. The statistical analysis assumes that the location coordinates are from a bivariate Gaussian distribution. If every trial were to use the same set of stations, the distribution would be a bivariate Gaussian; however, the stations used in the analysis change from trial to trial. Each station is randomly selected to participate in a trial in proportion to its detection probability. If a station has a detection probability of 1.0, it will be included in every trial. If its detection probability is 0.5, it will be included half of the trials. Because the stations included change from trial to trial, the location coordinates will not form a bivariate Gaussian distribution; thus, our 90% elliptical confidence area is an approximation.

Infrasound Stations--Station-to-Event Bearing Angle

If two stations which detect an event give us station-to-event bearing estimates, and if the two stations do not fall on the same line with the event, the point at which the two bearing lines intersect gives an estimate of the event's location. The intersection is only an estimate because bearings are never perfectly accurate. If we have bearings from only two stations, there is a

unique intersection and it is the event's location estimate. If more than two stations give us bearing estimates, we will rarely have a unique intersection. More than two bearing estimates may seem to complicate event location, but, in fact, more bearing estimates result in better location accuracy.

IVSEM uses the same process to estimate location accuracy using bearing measurements that it used with signal arrival time measurements except that the residual equations are based on bearing angle instead of signal arrival time. Each station which detects the event provides a "measured" bearing angle and a residual equation as in Equation G11.

$$r_i = \theta_{i,measured} - \theta_{i,modeled} \tag{G11}$$

$$\theta_{i,modeled} = \tan^{-1} [(y-Y_i)/(x-X_i)] \tag{G12}$$

X_i , Y_i defines the location of station "I." The point x, y is a location estimate.

In our statistical location model, we assume that a bearing angle has a Gaussian statistical distribution with a mean value $\theta_{i\ ave}$, (which is the true bearing angle since we assume unbias) and a standard deviation, σ_i. The mean bearing angle is calculated using Equation G13.

$$\theta_{i\ ave} = \tan^{-1} (- Y_i / -X_i) \tag{G13}$$

We randomly select "measured" bearing angles using a Gaussian random number generator to generate a random number r_i for each station. The randomly selected bearing angle for each station is found using Equation G14.

$$\theta_{i,measured} = \theta_{i\ ave} + \sigma_i r_i \tag{G14}$$

IVSEM uses the standard deviation values given in Equation G15 as provided by Dean Clauter (NDC, April 1996).

$$\sigma_i = 1.8^{o} \text{ from 0 to 3000 km;} \tag{G15}$$

increasing to 7^{o} at 4000 km;
7^{o} from 4000 to 10,000 km;
increasing to 27.5^{o} at 15,000 km;
27.5^{o} beyond 15,000 km.

The weighting factor we use for the squared residual is the reciprocal of variance, $\sigma_i^{\ 2}$.

System Integration for Location Accuracy

IVSEM estimates the location accuracy for each individual subsystem by including only the subsystem's stations and residual equations in the location accuracy analysis. To estimate an integrated system location accuracy, IVSEM combines the weighted residual equations of all detecting seismic, hydroacoustic, and infrasound stations in the analysis. Infrasound stations will each contribute two residual equations, one for arrival time and one for bearing angle. The process is the same as that described in the signal arrival time section above.

Minimization Method

To estimate location accuracy, IVSEM minimizes the sum of the weighted, squared residuals from each detecting station. The general form of a residual equation is given by Equation G16. In this equation r_i is the residual for station "i." The equation is specifically for stations which measure arrival time but can be generalized to stations which measure bearing as well.

$$r_i = T_{i,measured} - T_{i,modeled} \qquad \text{(G16)}$$

r_i is a function of x, y, and t since $T_{i,modeled}$ is a function of x, y, and t. The point (x,y,t) is an event location and time estimate. Our objective is to find the (x, y, t) that minimizes the sum (over all stations) of the weighted, squared residuals. This (x,y,t) value will be the model's best estimate for event time and location. If we call the sum of the weighted, squared residuals R, we can express R as in Equation G17.

$$R = \Sigma W_i r_i^2 \qquad \text{(G17)}$$

To accomplish the objective of minimizing R, IVSEM finds the value of (x,y,t) which sets the gradient of R to zero, that is, sets the partials of R with respect to x, y, and t equal to zero. If we denote the partial of R with respect to x as R_x with similar notations for other partials, then the equations to be solved can be written as in Equations G18.

$$R_x = \Sigma 2 W_i r_i r_{ix} = 0$$

$$R_y = \Sigma 2 W_i r_i r_{iy} = 0 \qquad \text{(G18)}$$

$$R_t = \Sigma 2 W_i r_i r_{it} = 0$$

We can linearize these equations by expanding r_i in a three dimensional, first order Taylor series around the point (x_0, y_0, t_0) which we will denote as p_0 which is a vector. We will denote the point (x,y,t) by p.

$$r_i(p) \approx r_i(p_0) + r_{ix}(p_0)(x-x_0) + r_{iy}(p_0)(y-y_0) + r_{it}(p_0)(t-t_0) \qquad \text{(G19)}$$

The partials of r_i are found using the specific functional relation between r_i and x, y, and t. This approximation to r_i is linear in x, y, and t and can be substituted into Equations (G18). The result of this substitution is given in equations G20.

$$\Sigma W_i r_{ix}(p_0)\, r_i(p_0) + (x-x_0)\Sigma W_i r_{ix}(p_0) r_{ix}(p_0) + (y-y_0)\Sigma W_i r_{ix}(p_0) r_{iy}(p_0) + (t-t_0)\Sigma W_i r_{ix}(p_0) r_{it}(p_0) = 0$$

$$\Sigma W_i r_{iy}(p_0) r_i(p_0) + (x-x_0)\Sigma W_i r_{iy}(p_0) r_{ix}(p_0) + (y-y_0)\Sigma W_i r_{iy}(p_0) r_{iy}(p_0) + (t-t_0)\Sigma W_i r_{iy}(p_0) r_{it}(p_0) = 0$$

$$\Sigma W_i r_{it}(p_0) r_i(p_0) + (x-x_0)\Sigma W_i r_{it}(p_0) r_{ix}(p_0) + (y-y_0)\Sigma W_i r_{it}(p_0) r_{iy}(p_0) + (t-t_0)\Sigma W_i r_{it}(p_0) r_{it}(p_0) = 0$$

(G20)

IVSEM uses an initial guess of $x_0=0$, $y_0=0$, $t_0=0$ and solves Equations G20 for (x,y,t) using Gaussian elimination. The new solution (x,y,t) replaces the old (x_0, y_0, t_0) and the process is repeated until the solution reaches a limit.

APPENDIX H. LOCATION ACCURACY MODEL VALIDATION

This section will present two areas of validation for IVSEM's location accuracy model:

1. Comparison of results from the Cartesian coordinates used in IVSEM with those from a spherical coordinate analysis.

2. Comparison of IVSEM location accuracy global contours with more comprehensive seismic, hydroacoustic, and infrasound models.

Spherical Vs. Cartesian Coordinates For Location Accuracy Analysis

IVSEM uses a two-dimensional approximation in its location error module to reduce computation time. A three-dimensional analysis in this high computation density module would be significantly more time consuming than the two dimensional analysis. The module, which computes the sum of the weighted residuals, is repeated roughly 30 million times depending on the number of responding stations and the number of iterations required to reach convergence; thus, we desire to keep computations in this module as simple as possible. IVSEM presently requires roughly seven minutes for a global coverage location accuracy computation on a 120 MHZ Pentium PC, and we do not want to significantly increase this computation time. Although we use two dimensions in the location module, we use three-dimensional spherical coordinates to find correct station distances and station orientations relative to the event. These distances and orientations are transferred into the two-dimensional location accuracy module.

To quantify the errors associated with using a two-dimensional instead of a three-dimensional location accuracy analysis, we developed a three-dimensional spherical location accuracy module for IVSEM which we will call the spherical module. This module uses the same basic location algorithms as IVSEM, but it uses three-dimensional spherical coordinates instead of two-dimensional Cartesian coordinates.

Figure H1 shows a global contour plot for seismic location accuracy generated using the two-dimensional location module. Figure H2 shows the same plot generated using the spherical module. Both are for magnitude 4.25 underground or underwater events. Results for the two are essentially the same. They vary in only very small details. From this comparison, we conclude that IVSEM's two-dimensional module is excellent for location analyses using stations which measure signal arrival time.

IVSEM Color Key

Blue --	**32 - 100 km^2**	**Green --**	**100 - 320**
Yellow --	**320 - 1000**	**Orange --**	**1000 - 3200**
Red --	**3200 - 10,000**	**Brown --**	**10,000 - 32,000**
Black --	**32,000+**		

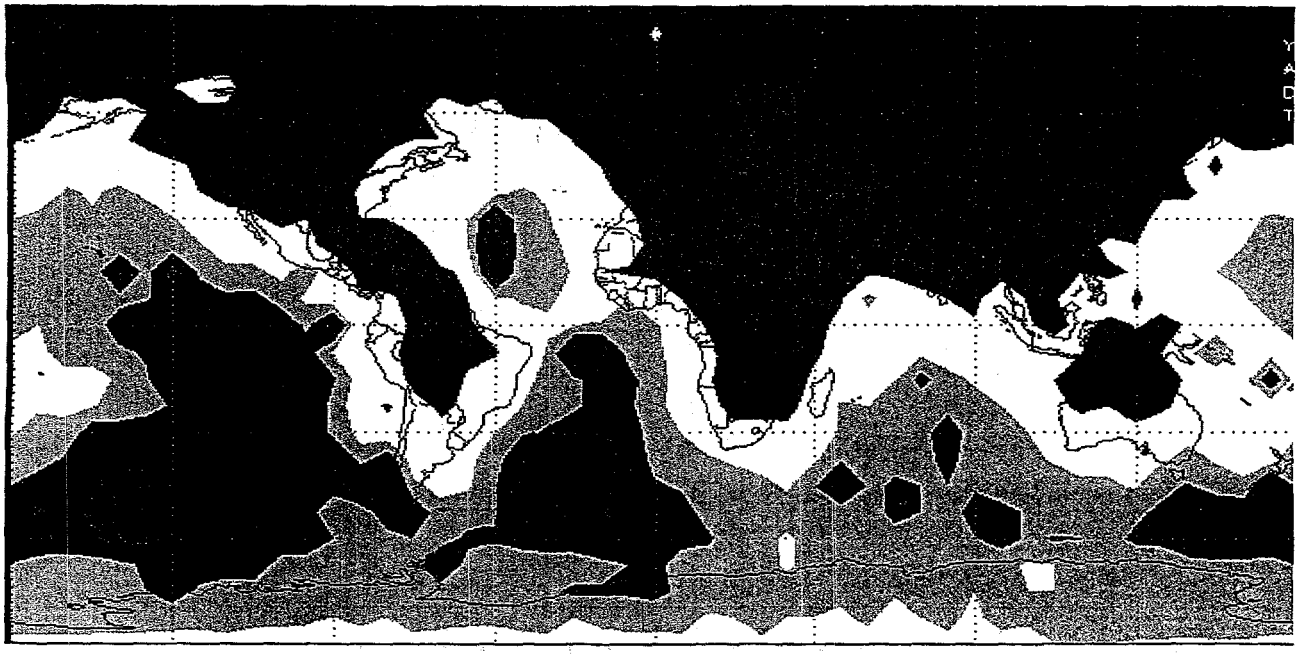

Figure H1. Seismic Location Accuracy Using IVSEM's Two-Dimensional Module

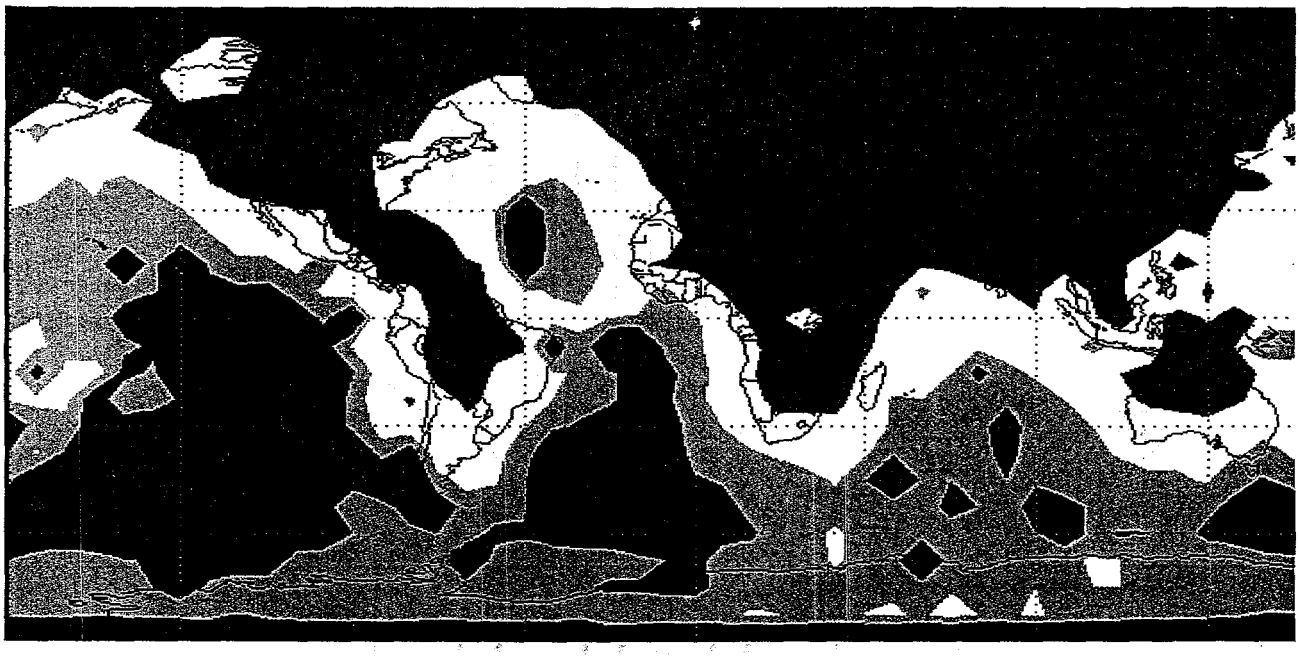

Figure H2. Seismic Location Accuracy Using Spherical Module

Figures H3 and H4 show results for two-dimensional and spherical infrasound location accuracy modules respectively. Both are for a small, atmospheric event. From these figures it appears that IVSEM's two-dimensional module underestimates location accuracy for infrasound stations by roughly 30%. We believe that the 30% location accuracy difference between the two models is acceptable considering the inherent uncertainty in location accuracy.

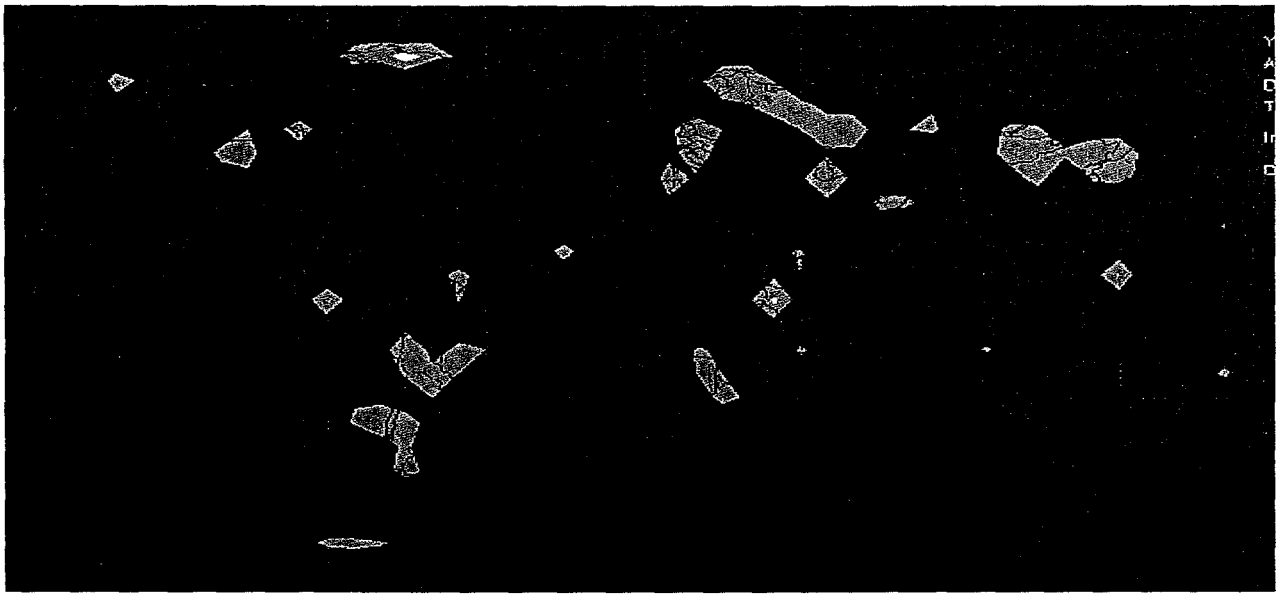

Figure H3. Infrasound Location Accuracy Using IVSEM's Two-Dimensional Module

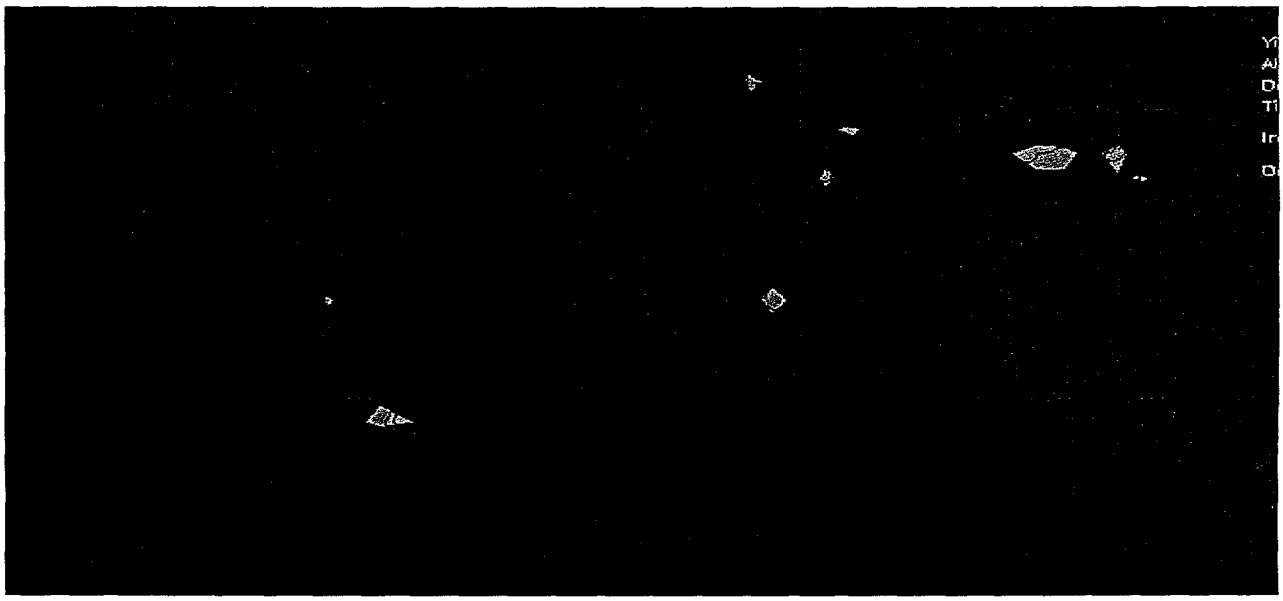

Figure H4. Infrasound Location Accuracy Using the Spherical Module

Comparison of IVSEM Location Accuracy Results With Those From More Comprehensive Models

Location accuracy results from IVSEM have been compared to those from more comprehensive models: NetSim (Sereno,1990), a comprehensive seismic network model, and HydroCAM, a comprehensive hydroacoustic model (Ferrell, 1996).

Figure H5 shows an IVSEM generated global contour plot for seismic network location accuracy. The plot is for a 4.25 magnitude event and a network which consists of 50 primary and 120 auxilliary stations as specified by WP330 (1996). Figure H6 shows the corresponding plot generated by NetSim.

The two plots are very similar. High and low values are in the same places and contours have the same shape. NetSim's 100 km^2 area, centered on Russia, is slightly larger than that of IVSEM. The 1000 km^3 contour lines for the two plots fall in almost exactly the same place. IVSEM estimates slightly larger location errors in the southern oceans. Agreement between the two models is very good, but not perfect. We have examined a few individual location errors to determine why the two models are not exactly the same. There are four main differences.

1. The two models get slightly different station detection probabilities because they use different noise values for some stations. This means that the stations which participate in location will be slightly different in one model than the other.
2. The two models use different interpretations of 90% confidence area. NetSim finds the 90% confidence elliptical area for each of many randomly generated station sets. (A station is selected to participate in a location set based on its detection probability.) The 90^{th} percentile elliptical area is selected. IVSEM randomly generates many station sets with a single randomly generated location estimate for each station set. A 90% confidence elliptical area is "fit" to the location estimates.
3. IVSEM uses only 100 random trials while NetSim uses 1000 randomly selected station sets. One-hundred random trials are nearly always sufficient, but there are exceptional cases.
4. IVSEM uses two-dimensional coordinates while NetSim uses spherical coordinates. For stations which measure signal arrival time, two-dimensional coordinates nearly always give accurate results, but there are a few cases we have seen where the error is 30%.

IVSEM Color Key

Blue -- 32 - 100 km^2	**Green -- 100 - 320**
Yellow -- 320 - 1000	**Orange -- 1000 - 3200**
Red -- 3200 - 10,000	**Brown -- 10,000 - 32,000**
Black -- 32,000+	

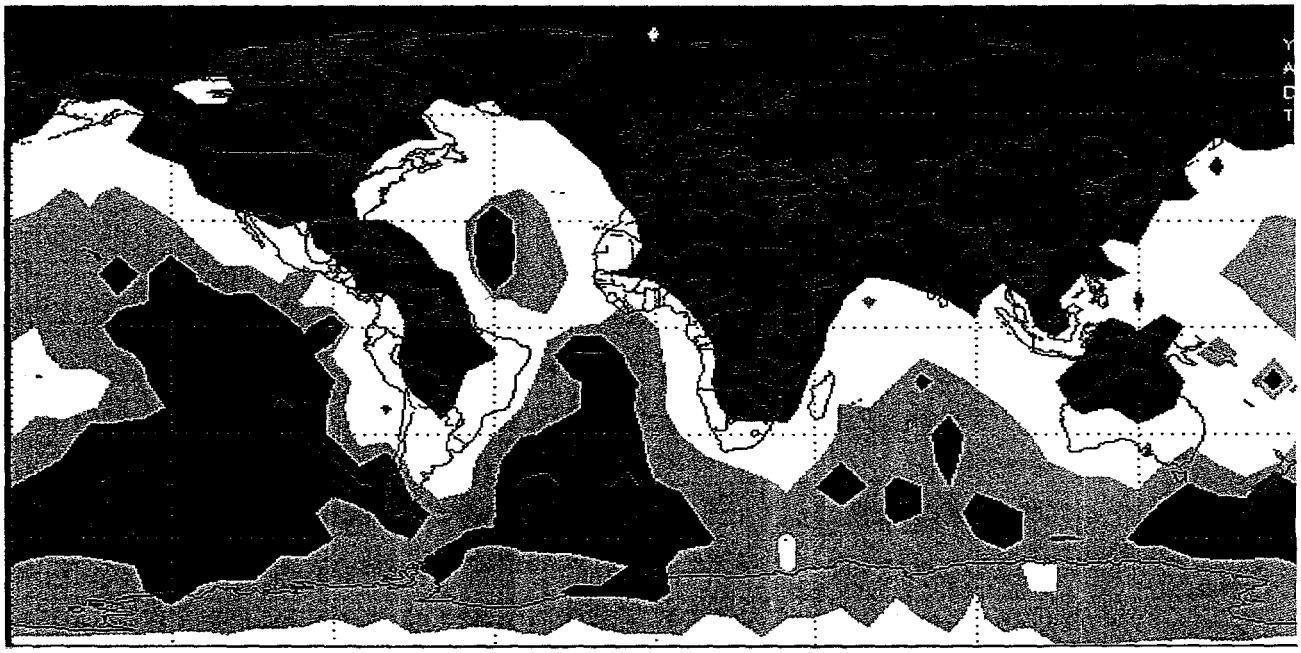

Figure H5. Global Seismic Location Accuracy Contour Map From IVSEM

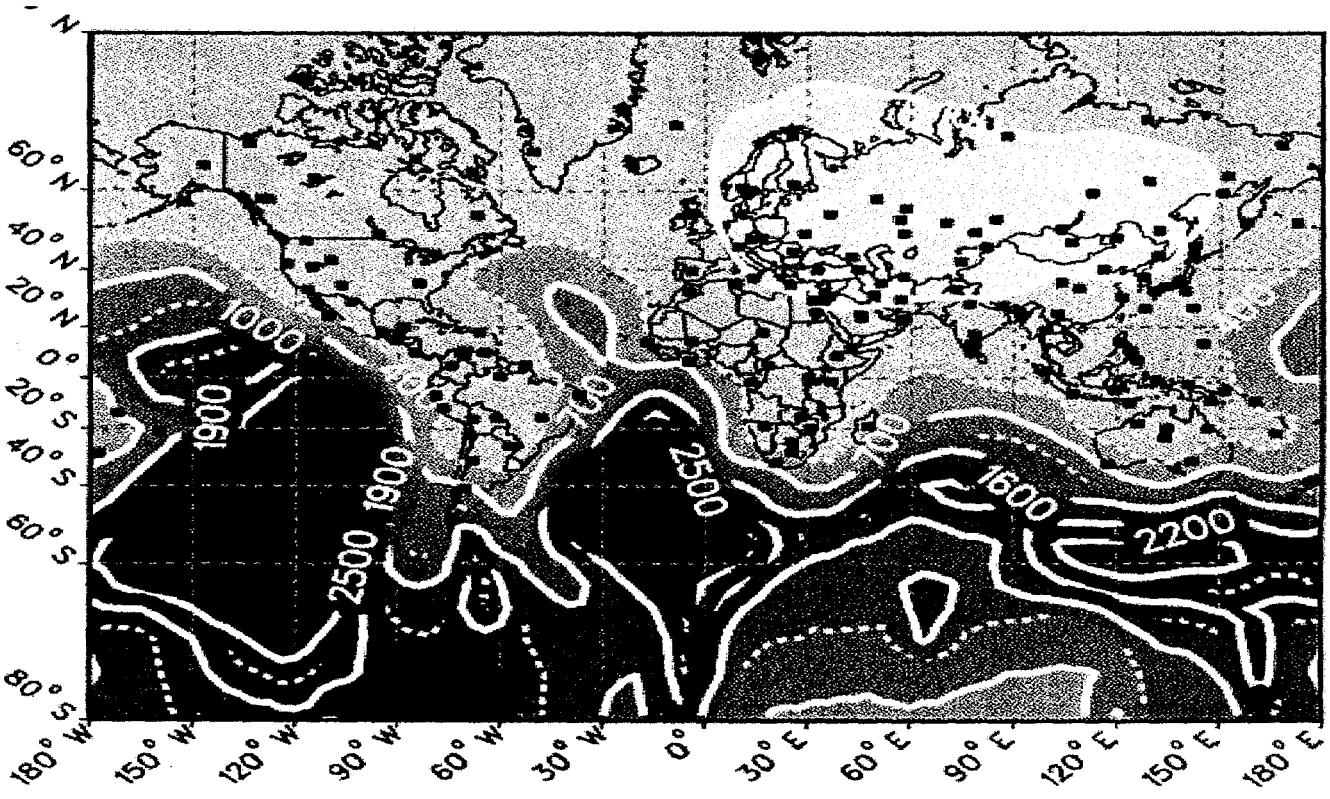

Figure H6. Global Seismic Location Accuracy Contour Map From NetSim

Figures H7 and H8 show global hydroacoustic contour maps from IVSEM and HydroCAM respectively. Both are for a small, underwater explosion, and both use a 16 station network: the 6 hydrophone station--5 island T-phase station network described in WP330 plus 4 seismic stations used as T-phase stations located at Tahiti, Rarotonga, Easter Island, and Jan Mayen Island. Color scales for the two are as follows with location accuracy in square km:

IVSEM		HydroCAM	
32 - 100	**blue**	**0 - 200**	**white**
100 - 320	**green**	**200 - 400**	**sky blue**
320 - 1000	**yellow**	**400 - 600**	**lavendar**
		600 - 800	**purple**
		800 - 1000	**gray**
1000 - 3200	**orange**	**1000 - 6000**	**blue to black**
3200 - 10,000	**red**		
10,000 - 32,000	**brown**		
32,000 +	**black**		

The HydroCAM colors may appear to progress from white to blue as different shades of blue. Bright blue is roughly 1000 km^2.

For both models, most ocean regions have location uncertainty areas of less than 1000 km^2. Both models show regions in the north Atlantic, off Argentina and Chile, east of southern Africa, west of Africa, and the Phillipine Sea to have location uncertainty areas greater than 1000 km^2. Both show areas in the the eastern Pacific and in the Indian Ocean where the uncertainty is less than 200 km^2.

There are two main differences in model results. HydroCAM shows more detail than IVSEM as expected, and IVSEM shows a weak region in the Indian Ocean not shown by HydroCAM. The reason for the weak area in the Indian Ocean is due to IVSEM's assumption that hydroacoustic stations have a 95% reliability. For an event in this region, four stations usually detect the event--the three Indian Ocean hydrophone stations and T-phase station Tristan da Cunha. IVSEM assigns a 95% reliability to each hydroacoustic station; thus, there is a roughly 14% chance that one of the three Indian Ocean stations is not operating. In this case, the two remaining Indian Ocean stations and the Tristan da Cunha station locate the event which could not have been located without the Tristan da Cunha station, but location accuracy is poor since the geometry is poor. The poor location accuracies are included in location statistics and cause a relatively large 90% confidence ellipse. One might ask why location accuracies are better in other regions of the Indian Ocean. In other regions, the Tristan da Cunha station will not detect the event. If only two hydro stations detect the event; an event cannot be formed; and no location accuracy is included in location statistics to increase the size of the 90% confidence ellipse.

In summary, results for the two models are very similar over nearly all ocean regions.

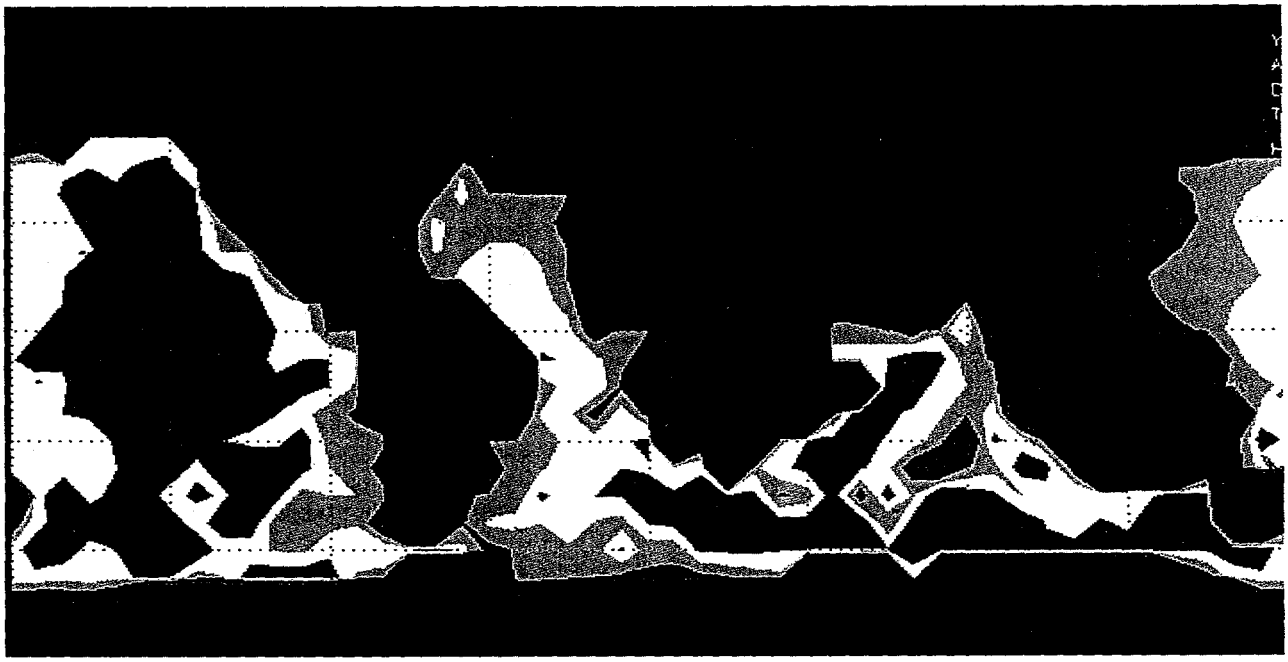

Figure H7. Global Hydroacoustic Location Accuracy Contour Map From IVSEM

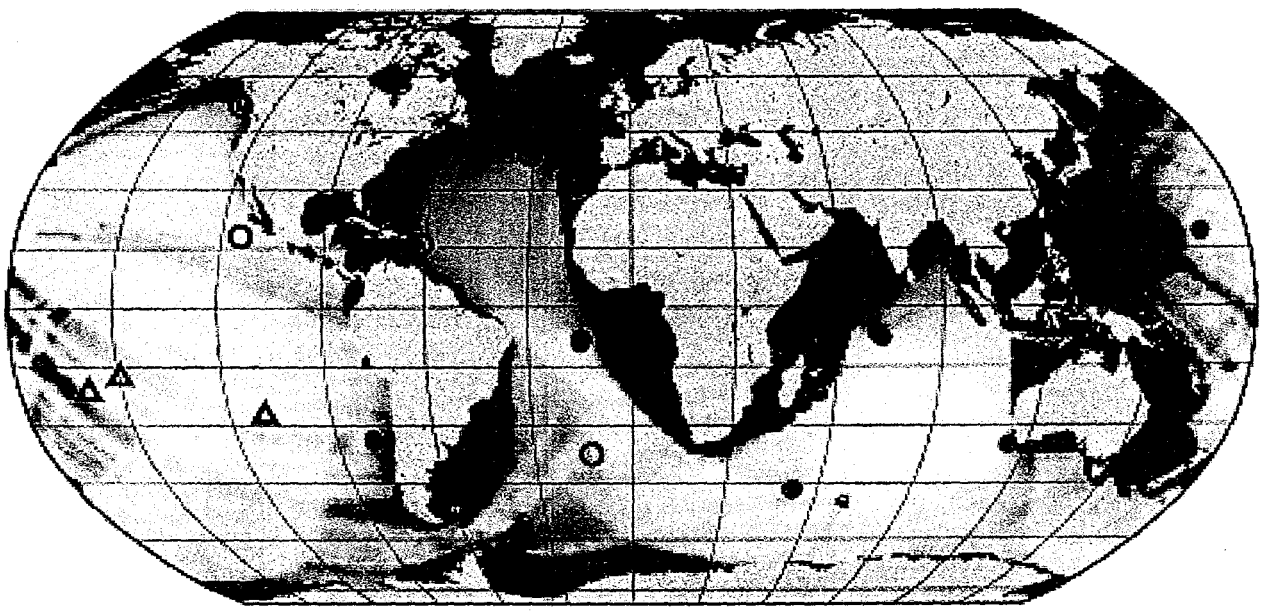

Figure H8. Global Hydroacoustic Location Accuracy Contour Map From HydroCAM

Figures H9 and H10 compare infrasound location accuracy for IVSEM and NetSim respectively for a small, atmospheric event. Both models used the 60 station infrasound network described in WP330. Both models used the same bearing errors and signal arrival time errors as specified earlier. IVSEM uses 50 km wind conditions typical of March. NetSim does not consider the effect of 50 km winds except to include their effect in the infrasound signal's variance. The NetSim results are given as a radius of uncertainty in km. IVSEM estimates location uncertainty area as a 90% conficence ellipse, so we converted IVSEM results to radius by dividing the uncertainty area by pi and taking the square root of the result. The following list describes IVSEM's color key with location accuracy in km.

IVSEM Color Key (km)

10 - 18	**yellow**
18 - 32	**orange**
32 - 56	**red**
56 - 100	**brown**
100 +	**black**

The NetSim results show the lowest location uncertainty in west Africa, Europe, Asia (except Siberia), western North America, most of South America, and Australia with a location uncertainty between 25 and 50 km. IVSEM results show the lowest location uncertainty in the same areas with values between 18 and 56 km. There are a few isolated places where IVSEM uncertainties go below 18 km. Features in the southern oceans are remarkably similar although, IVSEM appears to be estimating slightly lower uncertainty than NetSim. The areas enclosed by the 100 km contour are larger for NetSim than for IVSEM. In general, contour shapes are remarkably similar between the two models. Highs and lows fall in the same places, and details agree very well. As an overall average, it appears that IVSEM uncertainties are roughly 75% of those estimated by NetSim. We consider this to be very good agreement considering differences in the detection models and considering that IVSEM's two-dimensional location accuracy module projects areas that are roughly 30% low.

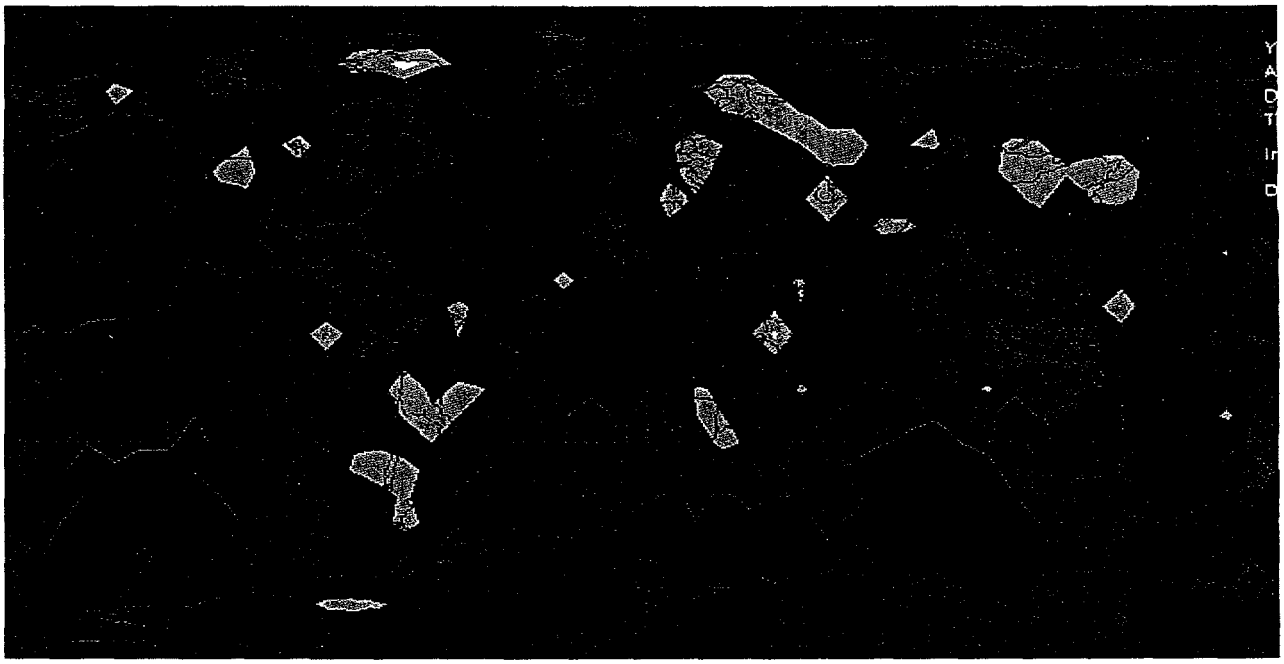

Figure H9. Global Infrasound Location Accuracy Contour Map From IVSEM

Figure H10. Global Infrasound Location Accuracy Contour Map From NetSim

REFERENCES

Farrell, 1996: Development of a Comprehensive Hydroacoustic Coverage Assessment Model, HydroCAM, Phillips Laboratory Report PL-TR-96-2248, T. Farrell, K. LePage, BBN Systems and Technologies, September 1996.

Sereno, 1990: NetSim: A Computer Program for Simulating Detection and Location Performance of Regional Seismic Networks, SAIC Report 90/1163, T.J. Sereno Jr., S.R. Bratt, and G. Yee, Science Applications International Corp., March 1990.

WP.330, 1996: Draft comprehensive Nuclear Test Ban Treaty, CD/NTB/WP.330, May 28, 1996.

Distribution for IVSEM Report

8 Department of Energy
1000 Independence Ave. SW
Washington, DC 20585

Dorothy Donnelly	DOE/NN-1
Leslie Casey	DOE/NN-20
Stan Rudnick	DOE/NN-20
Bob Waldron	DOE/NN-20
Cherie Fitzgerald	DOE/NN-40
Jay Norman	DOE/NN-42
John Wolcott	DOE/NN-42
Daria Antonucci	DOE/NN-42

3 Office of the Secretary of Defense
1901 N. Moore Street, Suite 609
Arlington, VA 22209

Ralph Alewine	OATSD/NCB
Gus Gustafson	OSD/NTPO
Todd Main	OSD/NTPO

1 AFTAC
1300 N. 17th Street
Suite 1450
Arlington, VA 22209-2308

Bob Blandford	AFTAC/TTR/CMR

11 AFTAC
1030 South Highway A1A
Patrick AFB, FL 32925-3002

Dean Clauter	AFTAC/TT
Carol Finn	AFTAC/TTR
Robert C. Kemerait	AFTAC/TTR
Maj. Lou Larson	AFTAC
John Lucas	AFTAC/TMAT
Joe Marshall	AFTAC/TTA
Dr. Dave O'Brien	AFTAC/CC
Dr. Frank Pilotte	AFTAC/TT
Dave Russell	AFTAC/TTR
Rick Schult	AFTAC/TT
Bruce Varnum	AFTAC/TTD

1 JAYCOR
PO Box 8154
San Diego, CA 92186-5154

Michael Treadway	JAYCOR

7 Arms Control and Disarmament Agency
320 21st Street NW
Washington, DC 20451

Nicholas Carrera	ACDA/MA
Robert Cockerham	ACDA/IVI
Pierce Corden	ACDA/MA
Mona Dreicer	ACDA/IVI
Ed Lacey	ACDA/IVI
Dick Morrow	ACDA/IVI
Terrill Ray	ACDA/MA

3 ACIS
Washington, DC 20505

Sean Doran	ACIS
Tim Murphy	ACIS
Larry Turnbull	ACIS

4 Battelle Pacific Northwest National Laboratory
PO Box 999
Richland, WA 99352

Kevin Anderson	PNNL K5-12
Dan Hagedorn	PNNL K5-12
Dick Perkins	PNNL K6-48
Ray Warner	PNNL K6-48

5 Lawrence Livermore National Laboratory
PO Box 808
Livermore, CA 94550

Marv Denny	LLNL L-205
Bill Dunlop	LLNL L-175
David Harris	LLNL L-205
Albert Smith	LLNL L-205
Jay Zucca	LLNL L-205

8 Los Alamos National Laboratory
PO Box 1663
Los Alamos, NM 87545

Wendee Brunish	LANL F659
Allen Cogbill	LANL C335
Paul Mutschlecner	LANL F659
Howard J. Patton	LANL C335
D. Craig Pearson	LANL C335
David J. Simons	LANL D460
Steve Taylor	LANL C335
Rod Whitaker	LANL F665

1 Pacific Sierra Research
1400 Key Boulevard, Suite 700
Arlington, VA 22209

Roger Mason	PSR

1	MS-0463	Roger Hagengruber, 5000
1	MS-0473	Tom Sellers, 5300
1	MS-0473	John Taylor, 5335
1	MS-1215	Rich Preston, 5336
1	MS-1215	Bob Gough, 5336
1	MS-0467	Clyde Layne, 5337
1	MS-1373	Arian Pregenzer, 5341
1	MS-1373	George Baldwin, 5341
1	MS-1373	Kent Biringer, 5341
1	MS-0421	Curtis Hines, 5401
1	MS-0421	Tommy Woodall, 5402
1	MS-0415	Keith Almquist, 5411
1	MS-0419	Rob Easterling, 5412
1	MS-0417	Bill Ling, 5413
1	MS-0417	Marcus Bunting, 5413
1	MS-0425	Stan Fraley, 5415
1	MS-0425	Art Payne, 5415
1	MS-0425	Larry Trost, 5415
10	MS-0425	Mike Edenburn, 5415
1	MS-0423	Garry Brown, 5417
1	MS-0970	James Kelsey, 5700
1	MS-0979	Larry Walker, 5704
1	MS-0979	Dale Breding, 5704
2	MS-0979	Don Shuster, 5704
1	MS-0965	Richard Hunt, 5715
1	MS-0980	Luba Kmetyk, 5725
1	MS-0655	Preston Herrington, 5736
1	MS-0655	Eric Chael, 5736
1	MS-0655	John Claassen, 5736
1	MS-0655	Chris Young, 5736
1	MS-1138	Ralph Keyser, 6531
5	MS-0889	Technical Library, 4114
1	MS-0619	Review and Approval, 12690